



NAM

Full-Scale Shaking Table Test on a Dutch URM Cavity Wall Terraced House end-unit - – EUC-BUILD-6

M. Miglietta, L. Mazzella, L. Grottoli, G. Guerrini, F. Graziotti

EUCENTRE Italy, University of Pavia and IUSS Pavia

European Centre for Training and Research in Earthquake Engineering, Italy

Università degli studi di Pavia (University of Pavia)

L'Istituto Universitario di Studi Superiori di Pavia (University School for Advanced Studies Pavia)

Date October 2018

Editors Jan van Elk & Dirk Doornhof

General Introduction

Many of the buildings in the Groningen field area are unreinforced masonry buildings. A program to assess the response of these building to earthquakes was therefore initiated. This program built on the experimental and modelling program into the properties of URM building materials, wall elements and wall units.

A typical Groningen terraced house, built using materials from the Groningen area by builders from the Groningen area, was tested at the shake-table of Eucentre in Pavia, Italy (Ref. 1). Although at the end of this test program the building was seriously damaged, the building had not collapsed. This left questions on the remaining capacity of the structure and its ability to resist larger seismic movements before (partially) collapsing. The test in Eucentre was therefore followed-up with further tests at the laboratory of LNEC in Lisbon, Portugal (Ref. 2 to 5). Here the upper floors of the building tested in Eucentre were re-built in the LNEC laboratory and subjected to movements measured at the base of the upper floors in Eucentre. Additionally, the roof structure was tested separately.

Next, a detached house was tested in EUCentre at the shake-table (Ref. 6 and 7). This detached house represents a typical pre-1940 Dutch single-storey residential building constructed of double wythe clay brick masonry walls with timber floor diaphragms and a timber roof supported by timber trusses.

The third masonry building tested (Ref. 8) was a house with a typical Dutch gambrel roof that allowed for living space above the attic floor. These high gables are potentially vulnerable to out-of-plane excitation. The floor was made of timber joists and planks, resulting in a flexible diaphragm. This building also had two chimneys.

A study was also initiated into falling objects like chimneys, gables and parapets (Ref. 9 and 10), using a very practical approach. To investigate the performance of falling non-structural masonry elements in earthquakes, two clay-brick chimneys were included in the detached house to be tested.

This report describes the result for a shake-table test of a URM cavity-wall terraced house end-unit with large openings on the front and back façades, especially at the ground floor. The first floor consists of precast reinforced concrete panels, completed by a structural topping slab, which provide a rigid diaphragm. The roof and the second-floor framing instead consist of timber joists and planks, resulting in highly flexible diaphragms. Masonry gables support the roof joists at the ends of each structural unit.

It is planned to build the same house again and test the house after building strengthening measures have been implemented. The combination of the test described in the current report, of a house without strengthening measures, and the same house with strengthening measures implemented will provide information on the effectiveness of the strengthening measures applied.

References

1. Eucentre Shake-table Test of Terraced House Modelling Predictions and Analysis Cross Validation, staff from ARUP, Eucentre (Pavia) and TU Delft, November 2015 [this document also includes; (1) Instruments full-scale test-house Eucentre Laboratory, (2) Protocol for Shaking Table Test on Full Scale Building (Eucentre) V_1, and (3) Selection of Acceleration Time-Series for Shake Table Testing of Groningen Masonry Building at the EUCENTRE, Pavia, all three by staff from Eucentre (Pavia)],
2. Collapse shake-table testing of terraced house (LNEC-BUILD1), Eucentre and LNEC (U. Tomassetti, A. A. Correia, F. Graziotti, A.I. Marques, M. Mandirola, P.X. Candeias), 1st September 2017.
3. LNEC-BUILD1: Modelling predictions and analysis cross-validation, ARUP, TU Delft, Eucentre and Mosayk (several staff members from all four institutions), 8th September 2017.
4. Using the Applied Element Method to model the collapse shake-table testing of a URM cavity wall structure (LNEC-BUILD1), Mosayk (D. Malomo, R. Pinho), 31st October 2017.
5. Using the Applied Element Method to model the collapse shake-table testing of a terraced house roof substructure (LNEC-BUILD2), Mosayk (D. Malomo, R. Pinho), 31st October 2017.
6. Experimental campaign on a clay URM full-scale specimen representative of the Groningen building stock (EUC-BUILD2), Eucentre (F. Graziotti, U. Tomassetti, A. Rossi, B. Marchesi, S. Kallioras, M. Mandirola, A. Fragomeli, E. Mellia, S. Peloso, F. Cuppari, G. Guerrini, A. Penna, G. Magenes, G), 20th July 2016.
7. EUC-BUILD2: Modelling predictions and analysis cross-validation of detached single-storey URM Building, ARUP, TU Delft, Eucentre and Arcadis (several staff members from all four institutions), 30th September 2016
8. LNEC-BUILD-3 - An incremental shake-table test on a Dutch URM detached house with Chimneys, IUSS Pavia, LNEC Portugal, EUCENTRE Italy, University of Pavia, Stylianos Kallioras, António Araújo Correia, Ana Isabel Marques, Vasco Bernardo, Paulo Xavier Candeias and Francesco Graziotti, October 2018
9. Risk Assessment of Falling Hazards in Earthquakes in the Groningen region, Tony Taig and Florence Pickup (TTAC Ltd.), March 2016.
10. Risk Assessment of Falling Hazards in Earthquakes in the Groningen region (Appendices), Tony Taig and Florence Pickup (TTAC Ltd.), March 2016.



NAM

Title	Full-Scale Shaking Table Test on a Dutch URM Cavity Wall Terraced House end-unit -- EUC-BUILD-6		Date	October 2018
			Initiator	NAM
Autor(s)	M. Miglietta, L. Mazzella, L. Grottole, G. Guerrini, F. Graziotti	Editors	Jan van Elk and Dirk Doornhof	
Organisation	EUCENTRE Italy, University of Pavia and IUSS Pavia European Centre for Training and Research in Earthquake Engineering, Italy Università degli studi di Pavia (University of Pavia) L'Istituto Universitario di Studi Superiori di Pavia (University School for Advanced Studies Pavia)	Organisation	NAM	
Place in the Study and Data Acquisition Plan	Study Theme: Seismic Response of Buildings (URM)			
	Comment: Many of the buildings in the Groningen field area are unreinforced masonry buildings. A program to assess the response of these building to earthquakes was therefore initiated. This program built on the experimental and modelling program into the properties of URM building materials, wall elements and wall units. A typical Groningen terraced house, built using materials from the Groningen area by builders from the Groningen area, was tested at the shake-table of Eucentre in Pavia, Italy (Ref. 1). Although at the end of this test program the building was seriously damaged, the building had not collapsed. This left questions on the remaining capacity of the structure and its ability to resist larger seismic movements before (partially) collapsing. The test in Eucentre was therefore followed-up with further tests at the laboratory of LNEC in Lisbon, Portugal (Ref. 2 to 5). Here the upper floors of the building tested in Eucentre were re-built in the LNEC laboratory and subjected to movements measured at the base of the upper floors in Eucentre. Additionally, the roof structure was tested separately. Next, a detached house was tested in EUCentre at the shake-table (Ref. 6 and 7). This detached house represents a typical pre-1940 Dutch single-storey residential building constructed of double wythe clay brick masonry walls with timber floor diaphragms and a timber roof supported by timber trusses. The third masonry building tested (Ref. 8) was a house with a typical Dutch gambrel roof that allowed for living space above the attic floor. These high gables are potentially vulnerable to out-of-plane excitation. The floor was made of timber joists and planks, resulting in a flexible diaphragm. This building also had two chimneys. A study was also initiated into falling objects like chimneys, gables and parapets (Ref. 9 and 10), using a very practical approach. To investigate the performance of falling non-structural masonry elements in earthquakes, two clay-brick chimneys were included in the detached house to be tested.			

	<p>This report describes the result for a shake-table test of a URM cavity-wall terraced house end-unit with large openings on the front and back façades, especially at the ground floor. The first floor consists of precast reinforced concrete panels, completed by a structural topping slab, which provide a rigid diaphragm. The roof and the second-floor framing instead consist of timber joists and planks, resulting in highly flexible diaphragms. Masonry gables support the roof joists at the ends of each structural unit.</p> <p>It is planned to build the same house again and test the house after building strengthening measures have been implemented. The combination of the test described in the current report, of a house without strengthening measures, and the same house with strengthening measures implemented will provide information on the effectiveness of the strengthening measures applied.</p>
Directly linked research	<ul style="list-style-type: none"> (1) Shake table tests (2) Fragility curves for building typologies (URM) (3) Falling Objects (4) Risk Assessment
Used data	Experiments
Associated organisation	NAM
Assurance	Eucentre

FULL-SCALE SHAKING TABLE TEST ON A DUTCH URM CAVITY-WALL TERRACED-HOUSE END UNIT – EUC-BUILD-6

October 19, 2018

Document authors

M. Miglietta^{1,3}, L. Mazzella^{1,2}, L. Grottoli¹, G. Guerrini^{1,2}, F. Graziotti^{1,2}

¹*EUCENTRE*

²*University of Pavia*

³*IUSS Pavia*

Research Report

Protocol number: EUC160/2018U



FULL-SCALE SHAKING TABLE TEST ON A DUTCH URM CAVITY-WALL TERRACED-HOUSE END UNIT – EUC-BUILD-6

M. Miglietta^{1,3}, L. Mazzella^{1,2}, L. Grottoli¹, G. Guerrini^{1,2}, F. Graziotti^{1,2}

¹*EUCENTRE*

²*University of Pavia*

³*IUSS Pavia*



According to law, EUCENTRE Foundation trademark cannot be reproduced, copied or utilized, without the written permission of the EUCENTRE Foundation, which is the owner, except in accordance with established contract conditions pertaining to the production of this document.

October 19, 2018

Pavia

Nessuna parte di questa pubblicazione può essere riprodotta o trasmessa in qualsiasi forma o con qualsiasi mezzo elettronico, meccanico o altro senza l'autorizzazione scritta dei proprietari dei diritti e dell'editore.

No parts of this publication may be copied or transmitted in any shape or form, and by any type of electronic, mechanical or different means, without the prior written permission of the copyright holder and the publisher.

© Copyright 2018 – **EUCENTRE**

prodotto e distribuito da:

produced and distributed by:

EUCENTRE Foundation

Via Adolfo Ferrata, 1 - 27100 Pavia, Italy

Phone (+39) 0382.5169811 - Fax (+39) 0382.529131

E-mail: info@eucentrepress.it - Web: www.eucentrepress.it

TABLE OF CONTENTS

TABLE OF CONTENTS	VI
LIST OF TABLES.....	VIII
LIST OF FIGURES	IX
1. FULL SCALE BUILDING PROTOTYPE.....	1
1.1 GEOMETRY AND GENERAL FEATURES OF THE PROTOTYPE	1
1.2 BUILDING CONSTRUCTION DETAILS.....	19
1.2.1 Inner-to-outer leaf connection	19
1.2.2 First-floor reinforced concrete diaphragm and floor-to-wall connections.....	19
1.2.3 Reinforced concrete lintels.....	24
1.2.4 Second-floor timber diaphragm and floor-to-wall connections	27
1.2.5 Roof timber diaphragm and roof-to-wall connections	30
1.2.6 North-gable opening	32
1.2.7 North-gable beam cover plates	34
1.2.8 Window timber frames	35
1.3 PROTOTYPE MASSES	37
2. MECHANICAL PROPERTIES OF MATERIALS	39
2.1 TENSILE AND COMPRESSIVE STRENGTH OF MASONRY UNITS	39
2.1.1 Test procedure	39
2.1.2 Test results	41
2.2 TENSILE AND COMPRESSIVE STRENGTH OF MORTAR.....	43
2.2.1 Test procedure	43
2.2.2 Test results	44
2.3 COMPRESSIVE STRENGTH OF MASONRY	53
2.3.1 Test procedure	53
2.3.2 Test results	55
2.4 BOND STRENGTH OF MASONRY	67
2.4.1 Test procedure	67
2.4.2 Test results	69
2.5 DIRECT SHEAR STRENGTH OF MASONRY	72
2.5.1 Test procedure	72
2.5.2 Test results	73
2.6 TORSIONAL SHEAR STRENGTH OF MORTAR	76
2.6.1 Test procedure	76
2.6.2 Test results	78

2.7	SUMMARY OF MECHANICAL PROPERTIES.....	80
3.	INSTRUMENTATION AND ACQUISITION SYSTEM	81
3.1	ACCELEROMETERS.....	81
3.2	DISPLACEMENT TRANSDUCERS	90
3.3	3D OPTICAL MOTION ACQUISITION SYSTEM.....	100
4.	TEST PROCEDURE	104
4.1	SHAKE-TABLE INPUT SIGNALS	104
4.2	APPLIED INPUT DYNAMIC SEQUENCE.....	105
5.	TEST RESULTS	108
5.1	DAMAGE PATTERN EVOLUTION	108
5.1.1	Observed damage after Test #2, EQ-NPR 20%, PGA = 0.06 g	109
5.1.2	Observed damage after Test #3, EQ-NPR 33%, PGA = 0.1 g	112
5.1.3	Observed damage after Test #8, EQ-NPR 50%, PGA = 0.15 g	115
5.1.4	Observed damage after Test #10, EQ-NPR 66%, PGA = 0.20 g.....	118
5.1.5	Observed damage after Test #15, EQ-NPR 85%, PGA = 0.25 g.....	122
5.1.6	Observed damage after Test #21, EQ-NPR 100%, PGA = 0.30 g.....	126
5.1.7	Observed damage after Test #24, EQ-NPR IS 100%, PGA = 0.30 g (inverted sign) 131	
5.1.8	Observed damage after Test #25, EQ-NPR IS 133%, PGA = 0.40 g (inverted sign) 131	
5.1.9	Crack width evolution.....	136
5.2	ANALYSIS OF THE BUILDING RESPONSE	143
5.2.1	Test #2 EQ-NPR 20%, PGA = 0.06 g	144
5.2.2	Test #3 EQ-NPR 33%, PGA = 0.1 g	147
5.2.3	Test #8 EQ-NPR 50%, PGA = 0.15 g	150
5.2.4	Test #10 EQ-NPR 66%, PGA = 0.20 g.....	153
5.2.5	Test #15 EQ-NPR 85%, PGA = 0.25 g.....	156
5.2.6	Test #21 EQ-NPR 100%, PGA = 0.30 g.....	159
5.2.7	Test #24 EQ-NPR IS 100%, PGA = 0.30 g (inverted sign).....	162
5.2.8	Test #25 EQ-NPR IS 133%, PGA = 0.40 g (inverted sign).....	165
5.3	SUMMARY OF THE RESULTS	169
	REFERENCES	171
	APPENDIX	172
	A1. RESULTS FILE FORMAT	172
	A2. ORGANIZATION OF THE INSTRUMENTATION: ACCELEROMETERS	177
	A3. ORGANIZATION OF THE INSTRUMENTATION: POTENTIOMETERS	193

LIST OF TABLES

Table 1 Prototype mass breakdown.....	37
Table 2 Compressive strength of bricks.	41
Table 3 Flexural strength of bricks loaded in the X and Y directions.....	42
Table 4 Mortar mix design.....	43
Table 5 Test results for mortar for CS masonry.....	45
Table 6 Test results for mortar for CL masonry.	47
Table 7 CS masonry compressive strength (f_m) and Young's modulus (E_m).	64
Table 8 CL specimens CL_2 and CL_3 compressive strength (f_m) and Young's modulus (E_m).....	65
Table 9 CL specimens CL_4, CL_5, CL_6 and CL_7 compressive strength (f_m) and Young's modulus (E_m).	66
Table 10 CL masonry compressive strength (f_m) and Young's modulus (E_m).....	66
Table 11 Bond strength of CS specimens.	69
Table 12 Bond strength of CL specimens.	70
Table 13 Shear tests results for CS masonry specimens.	74
Table 14 Shear tests results for CL masonry specimens.....	75
Table 15 Values of cohesion and friction coefficient for CS and CL masonry under direct shear...	75
Table 16 Torsion tests results.	78
Table 17 Values of cohesion and friction coefficient for CS and CL masonry under torsion.	80
Table 18 Masonry mechanical properties.....	80
Table 19 Accelerometer list.....	81
Table 20 Wire potentiometer list.....	90
Table 21 Linear potentiometer list.	93
Table 22 Characteristics of the input signals.	104
Table 23 Testing sequence.	106
Table 24 Summary of the main-shock input parameters.	107
Table 25 Crack widths evolution	137
Table 26 Results file format: accelerometers	172
Table 27 Results file format: wire potentiometers.....	174
Table 28 Results file format: linear potentiometers.....	174
Table 29 Results file format: derived data.	176

LIST OF FIGURES

Figure 1 Typical terraced house in Groningen: (a) front façade with end unit highlighted; (b) plan view.	1
Figure 2 Plan view of the EUCENTRE Lab. and position of the shake-table and the walls of the test-house.	3
Figure 3 Foundation system: (a) composite steel-concrete beams; (b) calcium silicate walls during construction over the concrete layer.	4
Figure 4 Prototype construction phases: (a) first-storey West elevation; (b) first-storey East elevation.	4
Figure 5 Prototype construction phases: (a) first-storey rigid steel frame; (b) placement of the first-floor reinforced concrete slab.	5
Figure 6 Prototype construction phases: second-floor timber structure.	5
Figure 7 Completed prototype: a) North and West façades; b) West and South façades.	6
Figure 8 Completed prototype: a) South and East façades; b) South and East façades.	6
Figure 9 Plan view of the ground floor. The red arrow indicates the shaking direction. Units of cm.	7
Figure 10 Plan view of the first floor. The red arrow indicates the shaking direction. Units of cm.	8
Figure 11 Plan view of the second floor. The red arrow indicates the shaking direction. Units of cm.	9
Figure 12 Plan view of the roof. Units of cm.	10
Figure 13 Vertical section looking at the West CS inner leaf from outside. Units of cm.	11
Figure 14 Vertical section looking at the East CS inner leaf from outside. Units of cm.	12
Figure 15 Vertical section looking at the North CS inner leaf from outside. Units of cm.	13
Figure 16 Vertical section looking at the North CS inner leaf from inside. Units of cm.	14
Figure 17 South elevation of the specimen CS inner leaf. Units of cm.	15
Figure 18 West elevation of the specimen Clay outer leaf. Units of cm.	16
Figure 19 East elevation of the specimen Clay outer leaf. Units of cm.	17
Figure 20 North elevation of the specimen Clay outer leaf. Units of cm.	18
Figure 21 Steel ties positioning: (a) length from CS wall; (b) embedment into clay walls.	19
Figure 22 Reinforced concrete slab: a, b) concrete casting and finishing; c) edge detail. Units of mm.	20
Figure 23 Reinforced concrete slab positioning: a) North-East corner; b) unsupported East side.	20
Figure 24 Reinforced concrete slab plan view. Units of cm.	21
Figure 25 Reinforced concrete slab-to-wall connection detail. Units of cm.	21
Figure 26 Reinforced concrete slab: North-South top and bottom reinforcement plan view.	22
Figure 27 Reinforced concrete slab: East-West top and bottom reinforcement plan view.	23
Figure 28 Reinforced concrete slab: perimeter reinforcement plan view. Units of cm.	24
Figure 29 Reinforced concrete lintel details: West façade inner leaf. Units of cm.	25

Figure 30 Reinforced concrete lintel details: East facade inner leaf. Units of cm.	25
Figure 31 Reinforced concrete lintel details: West facade outer leaf. Units of cm.	26
Figure 32 Reinforced concrete lintel details: East facade outer leaf. Units of cm.	26
Figure 33 Lintels positioning details.	27
Figure 34 Timber floor framing plan view. Units of cm.	28
Figure 35 Timber floor framing: timber-to-timber connection at staircase hole.	29
Figure 36 Timber floor framing: timber-to-timber details at staircase hole.	29
Figure 37 Timber floor framing: a, b, c) joist-to-wall connection; b) steel anchor details. Units of mm.	30
Figure 38 Timber roof framing: (a) structural layout; (b) ridge beam, joists, and spreader beam details; (c) joist-to-wall connection at South gable; (d) joist-to-wall connection at North gable. Units of mm.	31
Figure 39 Timber roof framing: (a) joists at South gable; (b) joists at North gable.	31
Figure 40 Roof finishes: a, b) counter and tile battens; c) steel rods restraint system.	32
Figure 41 Roof finishes: a) tiles positioning; (b) roof end-construction.	32
Figure 42 North gable opening: a) section looking from inside; b) timber lintel connections plan view; c) internal view of timber lintel connections; d) steel hanger; e) external view with timber stub. Units of cm.	33
Figure 43 Beam cover plates: a) at the roof ridge; b) at the outer-leaf spreader beam.	34
Figure 44 Detail of the cover plate connection to the outer-leaf spreader beam.	34
Figure 45 Ground-floor window frame external views: a) during construction, without side cover plates; b) screw locations; c) at the end of construction, with side cover plates and glass.	35
Figure 46 Ground-floor window frame internal views: a) during construction, without side cover plates; b) at the end of construction, with side cover plates.	36
Figure 47 North gable window frame: a) internal view with screw locations; b) external view.	36
Figure 48 Window frame-to-clay masonry leaf connections: a) during construction, without side cover plates; b) screw; c) at the end of construction, with side cover plates.	37
Figure 49 Position of the additional masses. Units of cm.	38
Figure 50 Brick dimensions: a) calcium silicate; b) clay.	40
Figure 51 Compressive test on bricks in the Y direction: a) calcium silicate; b) clay.	40
Figure 52 Flexural test on bricks: a) CS loaded in the Y direction; b) CS loaded in the X direction; c) CL loaded in the Y direction; b) CL loaded in the X direction.	40
Figure 53 Compressive strength of bricks: a) calcium silicate; b) clay.	41
Figure 54 Flexural strength of bricks in the X and Y direction: a) calcium silicate; b) clay.	42
Figure 55 Pre-mixed mortar bags: a) for CS masonry; b) for CL masonry.	43
Figure 56 Mould for the mortar specimens.	44
Figure 57 Setup of the mortar three-point bending test.	44
Figure 58 Tensile strength of mortar for CS masonry.	49
Figure 59 Compressive strength of mortar for CS masonry.	50
Figure 60 Tensile strength of mortar for CL masonry.	51
Figure 61 Compressive strength of mortar for CL masonry.	52

Figure 62 Geometry and instrumentation of test specimen, CS wallettes.....	53
Figure 63 Geometry and instrumentation of test specimen, CL wallettes.	54
Figure 64 Example of loading history used for the axial compression test on: a) CS masonry wallettes; b) CL masonry wallettes.....	54
Figure 65 CS_1 compression test results: a) vertical strain time histories; b) vertical stress vs. vertical and horizontal strains.....	55
Figure 66 CS_2 compression test results: a) vertical strain time histories; b) vertical stress vs. vertical and horizontal strains.....	56
Figure 67 CS_3 compression test results: a) vertical strain time histories; b) vertical stress vs. vertical and horizontal strains.....	56
Figure 68 CS_4 compression test results: a) vertical strain time histories; b) vertical stress vs. vertical and horizontal strains.....	57
Figure 69 CS_5 compression test results: a) vertical strain time histories; b) vertical stress vs. vertical and horizontal strains.....	57
Figure 70 CS_6 compression test results: a) vertical strain time histories; b) vertical stress vs. vertical and horizontal strains.....	58
Figure 71 CS_7 compression test results: a) vertical strain time histories; b) vertical stress vs. vertical and horizontal strains.....	58
Figure 72 CL_1 compression test results: a) vertical strain time histories; b) vertical stress vs. vertical and horizontal strains.....	59
Figure 73 CL_2 compression test results: a) vertical strain time histories; b) vertical stress vs. vertical and horizontal strains.....	59
Figure 74 CL_3 compression test results: a) vertical strain time histories; b) vertical stress vs. vertical and horizontal strains.....	60
Figure 75 CL_4 compression test results: a) vertical strain time histories; b) vertical stress vs. vertical and horizontal strains.....	60
Figure 76 CL_5 compression test results: a) vertical strain time histories; b) vertical stress vs. vertical and horizontal strains.....	61
Figure 77 CL_6 compression test results: a) vertical strain time histories; b) vertical stress vs. vertical and horizontal strains.....	61
Figure 78 CL_7 compression test results: a) vertical strain time histories; b) vertical stress vs. vertical and horizontal strains.....	62
Figure 79 CL masonry courses built with weak mortar: West façade.....	62
Figure 80 CL masonry courses built with weak mortar: East façade.....	63
Figure 81 CL masonry courses built with weak mortar: North façade.	64
Figure 82 CS masonry mechanical properties: (a) compressive strength; (b) Young's modulus....	65
Figure 83 CL specimens CL_2 and CL_3 mechanical properties: (a) compressive strength; (b) Young's modulus.	65
Figure 84 CL specimens CL_4, CL_5, CL_6, and CL_7 mechanical properties: (a) compressive strength; (b) Young's modulus.	66
Figure 85 Geometry of the specimens: a) CS masonry; b) CL masonry.....	67
Figure 86 Examples of the tested specimens: a) CS masonry; b) CL masonry.	67
Figure 87 Layout of the bond-wrench test (EN 1052-5).....	68

Figure 88 Possible failure modes in the bond wrench test (EN 1052-5).	68
Figure 89 Bond strength: a) CS specimens; b) CL specimens.	71
Figure 90 Shear test: a) CS specimen; b) CL specimen.....	72
Figure 91 Shear test specimen geometry.....	72
Figure 92 Shear test setup.	73
Figure 93 Shear test results for CS specimens: shear strength (τ) vs. normal compressive stress (σ).....	74
Figure 94 Shear test results for CL specimens: shear strength (τ) vs. normal compressive stress (σ).....	75
Figure 95 Torsion test: a) CS specimen; b) CL specimen.	76
Figure 96 Torsion test set-up: a) overview; b) loading setup; c) instrumentation; d) photo.	77
Figure 97 Torsion test results for CS specimens: torsional shear strength (τ) vs. normal compressive stress (σ).....	79
Figure 98 Torsion test results for CL specimens: torsional shear strength (τ) vs. normal compressive stress (σ).....	79
Figure 99 Accelerometer 3D view: foundation, first floor, second floor and roof diaphragms.	83
Figure 100 Accelerometer 3D view: calcium silicate inner leaves.....	84
Figure 101 Accelerometer 3D view: clay outer leaves.	85
Figure 102 Accelerometer plan views: a) foundation level; b) first-floor level (R.C. diaphragm).....	86
Figure 103 Accelerometer plan views: a) second-floor level (timber diaphragm); b) roof level.....	86
Figure 104 Accelerometer elevation: North calcium silicate inner leaf - Section A-A.	87
Figure 105 Accelerometer elevation: South calcium silicate inner leaf - Section B-B.....	87
Figure 106 Accelerometer elevation: West calcium silicate inner leaf - Section C-C.	88
Figure 107 Accelerometer elevation: East calcium silicate inner leaf - Section D-D.	88
Figure 108 Accelerometer elevation: a) North clay outer leaf; b) West clay outer leaf.	89
Figure 109 Accelerometer elevation: East clay outer leaf.....	89
Figure 110 Wire potentiometer 3D view.	91
Figure 111 Wire potentiometer elevation: Section A-A.	92
Figure 112 Wire potentiometer elevation: Section B-B.	92
Figure 113 Linear potentiometer 3D view: foundation, first floor, second floor and roof diaphragms.	94
Figure 114 Linear potentiometer 3D view: calcium silicate inner leaves.	95
Figure 115 Linear potentiometer 3D view: clay outer leaves.	96
Figure 116 Linear potentiometer plan views: a) foundation level; b) ground-floor level.....	97
Figure 117 Linear potentiometer plan views: a) first-floor level (R.C. diaphragm); b) second-floor level (timber diaphragm).	97
Figure 118 Linear potentiometer plan view: roof level.	98
Figure 119 Linear potentiometer elevation: West calcium silicate inner leaf - Section C-C.....	98
Figure 120 Linear potentiometer elevation: East calcium silicate inner leaf - Section D-D.....	99
Figure 121 Linear potentiometer elevation: West clay outer leaf.	99

Figure 122 Linear potentiometer elevation: East clay outer leaf.	100
Figure 123 Reflective markers: a) North and West façades; b) West façade; c) West and South façades.	100
Figure 124 Reflective marker distribution: North façade.	101
Figure 125 Reflective marker distribution: South façade.	102
Figure 126 Reflective marker distribution: West façade.....	103
Figure 127 EQ-NPR acceleration time history (PTA = Peak table acceleration).	104
Figure 128 EQ-NPR elastic response spectra: acceleration (left), and displacement (right).	105
Figure 129 Damage evolution legend: a) location of the vertical sections to show inner calcium silicate walls; b) crack notations.	108
Figure 130 EQ-NPR 20% cracks - Calcium silicate longitudinal walls.	109
Figure 131 EQ-NPR 20% cracks - Calcium Silicate transversal walls.	109
Figure 132 EQ-NPR 20% cracks – West and East clay façades.	110
Figure 133 EQ-NPR 20% cracks – North clay façade.	110
Figure 134 EQ-NPR 20% Cracks view: a) South façade roof joist-to-wall connection; b) plank-to-wall interface.....	111
Figure 135 EQ-NPR 20% Cracks on the West facade: a) overall view; b) window corner.	111
Figure 136 EQ-NPR 33% cracks - Calcium silicate longitudinal walls.	112
Figure 137 EQ-NPR 33% cracks - Calcium Silicate transverse walls.	112
Figure 138 EQ-NPR 33% cracks – West and East clay façades.	113
Figure 139 EQ-NPR 33% cracks – North clay façade.	113
Figure 140 EQ-NPR 33% - Overall view of the cracks on the South gable wall: a) West side; b) East side.....	114
Figure 141 EQ-NPR 33% - Zoom-in on the cracks of the South gable wall: a) West side; b) East side.....	114
Figure 142 EQ-NPR 33% - West facade sliding cracks: a) overall view of the North side; b) zoom-in on the South side.	114
Figure 143 EQ-NPR 50% cracks - Calcium silicate longitudinal walls.	115
Figure 144 EQ-NPR 50% cracks - Calcium silicate transverse walls.....	116
Figure 145 EQ-NPR 50% cracks – West and East clay façades.	116
Figure 146 EQ-NPR 50% cracks – North clay façade.	117
Figure 147 EQ-NPR 50% pier base cracks on the inner leaf: a) C8; b) C9.....	117
Figure 148 EQ-NPR 50% pier base cracks: C9 on the inner leaf and corresponding crack on the outer leaf.....	117
Figure 149 EQ-NPR 50% sliding cracks: between timber spreader beam and West façade outer leaf: a) North end; b) mid-span.....	118
Figure 150 EQ-NPR 66% cracks - Calcium silicate longitudinal walls.	119
Figure 151 EQ-NPR 66% cracks - Calcium silicate transverse walls.....	119
Figure 152 EQ-NPR 66% cracks – West and East clay façade.....	120
Figure 153 EQ-NPR 66% cracks – North clay façade.	120

Figure 154 EQ-NPR 66% cracks: a) C20 overview; b) C20 zoom in.	121
Figure 155 EQ-NPR 66% cracks: a) C6 overview; b) C6 zoom in.	121
Figure 156 EQ-NPR 66% cracks: C10 overview.	121
Figure 157 EQ-NPR 66% cracks: a) C23; b) C25.....	122
Figure 158 EQ-NPR 85% cracks - Calcium silicate longitudinal walls.	123
Figure 159 EQ-NPR 85% cracks - Calcium silicate transversal walls.	123
Figure 160 EQ-NPR 85% cracks – West and East clay façades.	124
Figure 161 EQ-NPR 85% cracks – North clay façade.	124
Figure 162 EQ-NPR 85% cracks: a) C9 and C17 overview ; b) C9 and C17 Zoom in.	125
Figure 163 EQ-NPR 85% cracks: a) C12 and C15; b) C13.	125
Figure 164 EQ-NPR 85% cracks: a) C24; b) C31.....	125
Figure 165 EQ-NPR 85% cracks: a) C25; b) C22.....	126
Figure 166 EQ-NPR 100% cracks - Calcium silicate longitudinal walls.	127
Figure 167 EQ-NPR 100% cracks - Calcium silicate transversal walls.	127
Figure 168 EQ-NPR 100% cracks – West and East clay façades	128
Figure 169 EQ-NPR 100% cracks – North clay façade.	128
Figure 170 EQ-NPR 100% cracks: a) C8, C11, C13 and C14 overview; b) C13 zoom in.	129
Figure 171 EQ-NPR 100% cracks: a) C4, C11, C12 and C15 overview; b) C4 and C15 zoom in.	129
Figure 172 EQ-NPR 100% cracks: a) C33; b) C34.....	130
Figure 173 EQ-NPR 100% cracks: a) C34; b) C31.....	130
Figure 174 EQ-NPR 100% cracks: a) C29, C31 overview; b) C29 zoom in.	130
Figure 175 EQ-NPR IS 133% cracks - Calcium silicate longitudinal walls.	131
Figure 176 EQ-NPR IS 133% cracks - Calcium silicate transversal walls.....	132
Figure 177 EQ-NPR IS 133% cracks - West and East clay façades.....	132
Figure 178 EQ-NPR IS 133% cracks - North clay façade.....	133
Figure 179 EQ-NPR IS 133% cracks: a) C4 and C15 overview; b) C4 zoom in.....	133
Figure 180 EQ-NPR IS 133% cracks: a) C9 and C17 overview; b) C9 zoom in.....	134
Figure 181 EQ-NPR IS 133% cracks: a) C8, C11 and C14; b) C13.	134
Figure 182 EQ-NPR IS 133% cracks: a) C13; b) C13 zoom-in.....	134
Figure 183 EQ-NPR IS 133% cracks: a) C11 and C14 overview; b) C11 zoom in.....	135
Figure 184 EQ-NPR IS 133% cracks: a) C22 overview; b) C22 zoom in.	135
Figure 185 EQ-NPR IS 133% cracks: a) C24; b) C25.	135
Figure 186 EQ-NPR IS 133% cracks: a) C29 and C31 overview; b) C31 zoom in.....	136
Figure 187 EQ-NPR IS 133% cracks: a) C29, C31 overview; b) C29 zoom in.....	136
Figure 188 Crack C4 evolution: a) location; b) in-plane residual widths.....	138
Figure 189 Crack C4 after EQ-NPR 100%: a) overview; b) zoom in.....	138
Figure 190 Crack C4 after EQ-NPR IS 133%: a) looking North; b) looking West.....	138

Figure 191 Cracks C4, C13 evolution: a) location; b) in-plane residual widths.	139
Figure 192 Crack C13 after EQ-NPR 100%: a) overview; b) North-East walls intersection.	139
Figure 193 Crack C13 after EQ-NPR IS 133%: a) looking North; b) North-East walls intersection.	140
Figure 194 Cracks C13 after EQ-NPR IS 133%: a) looking East; b) Out-of-plane residual width zoom in.	140
Figure 195 Cracks C24 evolution: a) location; b) in-plane residual widths.	141
Figure 196 Crack C24: a) after EQ-NPR 85%; b) after EQ-NPR IS 133%.	141
Figure 197 Crack C31 evolution: a) location; b) in-plane residual widths.	142
Figure 198 Crack C31: a) after EQ-NPR 85%; b) after EQ-NPR 100%.	142
Figure 199 Crack C31 after EQ-NPR IS 133%: a) overview; b) zoom in.	142
Figure 200 Test #2 EQ-NPR 20% - Target and experimental elastic response spectra.	144
Figure 201 Test #2 EQ-NPR 20% - Hysteretic force-displacement response.	145
Figure 202 Test #2 EQ-NPR 20% - Displacement profile at maximum second-floor displacement.	145
Figure 203 Test #2 EQ-NPR 20% - Interstorey drift ratio envelope.	146
Figure 204 Test #2 EQ-NPR 20% - First-floor diaphragm deformed shapes: a) at maximum first-floor displacement; b) at maximum average second-floor displacement.	146
Figure 205 Test #2 EQ-NPR 20% - Second-floor diaphragm deformed shape at maximum average second-floor displacement.	147
Figure 206 Test #3 EQ-NPR 33% - Target and experimental elastic response spectra.	147
Figure 207 Test #3 EQ-NPR 33% - Hysteretic force-displacement response.	148
Figure 208 Test #3 EQ-NPR 33% - Displacement profile at maximum second-floor displacement.	148
Figure 209 Test #3 EQ-NPR 33% - Interstorey drift ratio envelope.	149
Figure 210 Test #3 EQ-NPR 33% - First-floor diaphragm deformed shapes: a) at maximum first-floor displacement; b) at maximum average second-floor displacement.	149
Figure 211 Test #3 EQ-NPR 33% - Second-floor diaphragm deformed shape at maximum average second-floor displacement.	150
Figure 212 Test #8 EQ-NPR 50% - Target and experimental elastic response spectra.	150
Figure 213 EQ-NPR 50% - Hysteretic force-displacement response.	151
Figure 214 Test #8 EQ-NPR 50% - Displacement profile at maximum second-floor displacement.	151
Figure 215 Test #8 EQ-NPR 50% - Interstorey drift ratio envelope.	152
Figure 216 Test #8 EQ-NPR 50% - First-floor diaphragm deformed shapes: a) at maximum first-floor displacement; b) at maximum average second-floor displacement.	152
Figure 217 Test #8 EQ-NPR 50% - Second-floor diaphragm deformed shape at maximum average second-floor displacement.	153
Figure 218 Test #10 EQ-NPR 66% - Target and experimental elastic response spectra.	153
Figure 219 Test #10 EQ-NPR 66% - Hysteretic force-displacement response.	154

Figure 220 Test #10 EQ-NPR 66% - Displacement profile at maximum second-floor displacement.	154
Figure 221 Test #10 EQ-NPR 66% - Interstorey drift ratio envelope.	155
Figure 222 Test #10 EQ-NPR 66% - First-floor diaphragm deformed shapes: a) at maximum first-floor displacement; b) at maximum average second-floor displacement.	155
Figure 223 Test #10 EQ-NPR 66% - Second-floor diaphragm deformed shape at maximum average second-floor displacement.	156
Figure 224 Test #15 EQ-NPR 85% - Target and experimental elastic response spectra.	156
Figure 225 Test #15 EQ-NPR 85% - Hysteretic force-displacement response.	157
Figure 226 Test #15 EQ-NPR 85% - Displacement profile at maximum second-floor displacement.	157
Figure 227 Test #15 EQ-NPR 85% - Interstorey drift ratio envelope.	158
Figure 228 Test #15 EQ-NPR 85% - First-floor diaphragm deformed shapes: a) at maximum first-floor displacement; b) at maximum average second-floor displacement.	158
Figure 229 Test #15 EQ-NPR 85% - Second-floor diaphragm deformed shape at maximum average second-floor displacement.	159
Figure 230 Test #21 EQ-NPR 100% - Target and experimental elastic response spectra.	159
Figure 231 Test #21 EQ-NPR 100% - Hysteretic force-displacement response.	160
Figure 232 Test #21 EQ-NPR 100% - Displacement profile at maximum second-floor displacement.	160
Figure 233 Test #21 EQ-NPR 100% - Interstorey drift ratio envelope.	161
Figure 234 Test #21 EQ-NPR 100% - First-floor diaphragm deformed shapes: a) at maximum first-floor displacement; b) at maximum average second-floor displacement.	161
Figure 235 Test #21 EQ-NPR 100% - Second-floor diaphragm deformed shape at maximum average second-floor displacement.	162
Figure 236 Test #24 EQ-NPR IS 100% - Target and experimental elastic response spectra.	162
Figure 237 Test #24 EQ-NPR IS 100% - Hysteretic force-displacement response.	163
Figure 238 Test #24 EQ-NPR IS 100% - Displacement profile at maximum second-floor displacement.	163
Figure 239 Test #24 EQ-NPR IS 100% - Interstorey drift ratio envelope.	164
Figure 240 Test #24 EQ-NPR IS 100% - First-floor diaphragm deformed shapes: a) at maximum first-floor displacement; b) at maximum average second-floor displacement.	164
Figure 241 Test #24 EQ-NPR IS 100% - Second-floor diaphragm deformed shape at maximum average second-floor displacement.	165
Figure 242 Test #25 EQ-NPR IS 133% - Target and experimental elastic response spectra.	165
Figure 243 Test #25 EQ-NPR IS 133% - Hysteretic force-displacement response.	166
Figure 244 Test #25 EQ-NPR IS 133% - Displacement profile at maximum second-floor displacement.	166
Figure 245 Test #25 EQ-NPR IS 133% - Interstorey drift ratio envelope.	167
Figure 246 Test #25 EQ-NPR IS 133% - First-floor diaphragm deformed shapes: a) at maximum first-floor displacement; b) at maximum average second-floor displacement.	167
Figure 247 Test #25 EQ-NPR IS 133% - Second-floor diaphragm deformed shape at maximum average second-floor displacement.	168

Figure 248 Backbone force-displacement curve. 169

Figure 249 Evolution of the building specimen response..... 170

1. FULL SCALE BUILDING PROTOTYPE

This experimental campaign aims at investigating the vulnerability of terraced houses, built with unreinforced masonry (URM) cavity walls and a combination of rigid reinforced concrete and flexible timber diaphragms. This is a residential building typology commonly found in the Groningen region of the Netherlands. A unidirectional incremental shake-table test was carried out on a full-scale, two-storey building prototype at the EUCENTRE laboratory in Pavia, Italy, within a comprehensive research programme on the seismic vulnerability of existing Dutch URM structures.

The building specimen was representative of the end unit of a two-storey URM cavity-wall terraced house of the late 1970s (Figure 1). This residential typology consists of adjacent units, structurally independent from each other, and is characterised by large openings on the front and back façades, especially at the ground floor. The first floor is typically built with precast reinforced concrete panels, completed by a structural topping slab, which provide a rigid diaphragm. The roof and the second-floor framing instead consist of timber joists and planks, resulting in highly flexible diaphragms. Masonry gables support the roof joists at the ends of each structural unit. Figure 1 shows the front view of a classic terraced house and its plan view.

The unidirectional dynamic shake-table test was performed applying ground motions of increasing intensity up to the near-collapse limit state of the specimen. The input motions were selected to be representative of the dynamic characteristics of induced seismicity for the area.

1.1 Geometry and general features of the prototype

Cavity-walls typically consist of two masonry leaves spaced by an air-gap of approximately 8 cm: the inner leaf, made of calcium-silicate (CS) bricks, has vertical load-bearing function; the outer leaf, built with clay (CL) bricks, has no intended structural function. Steel ties provide connections between the two leaves. The transverse walls of terraced houses, which separate individual units, are generally 7- to 8-m long without openings: therefore, they can resist significant in-plane lateral forces. Considering the high amount of openings in the longitudinal front and back façades, terraced houses are generally more flexible and vulnerable in the longitudinal direction.

Floor systems are discontinuous between adjacent units and rest only on transverse CS walls, which consequently carry most of the vertical loads. Intermediate transverse walls consist of two independent CS leaves, making each unit structurally separated from the adjacent ones. The only continuous walls shared among adjacent units are the outer non-structural CL veneers.

For these reasons, a prototype representative of a sub-volume of a terraced house (Figure 1), namely an end-unit, was extracted and tested in the longitudinal direction, as already investigated in [1] and [2]. However, as opposed to the cited work, this prototype was characterized by large irregular openings, a flexible timber diaphragm at the second floor instead of a concrete slab, and staircase openings in both floors, adding complexity to the study.

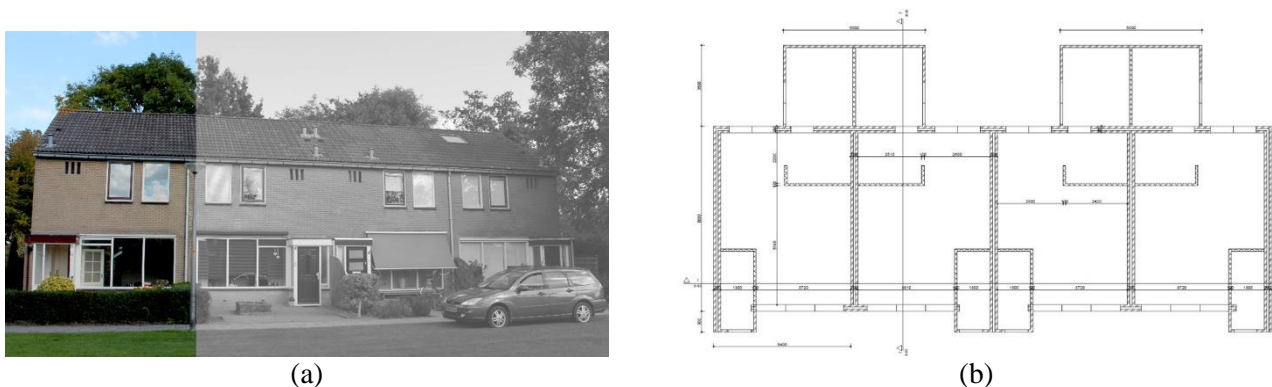


Figure 1 Typical terraced house in Groningen: (a) front façade with end unit highlighted; (b) plan view.

The full-scale two-storey prototype was adapted to the shake-table dimensional limitations: the typical one-storey storage room on the back of the units (Figure 1 b) was removed, while the transverse dimension was reduced down to 5.58 m from common lengths of 7 to 8 m. The plan dimensions were 5.95 m in the longitudinal shaking direction, and 5.58 m in the transverse direction, with a total height of about 7.83 m.

The specimen was built directly on the shake-table of the EUCENTRE laboratory (Figure 2), supported by a composite steel-concrete foundation. The walls were all founded on a 110-mm-thick concrete layer (Mapei Mapefill 50 with gravel), contained in UPN 400 steel profiles (Figure 3). These were bolted to HE 300B beams, connected to the table and stiffened by steel plates approximately every 250 mm.

The masonry cavity walls included a 100-mm-thick CL outer leaf and a 102-mm-thick CS inner leaf, both with 10-mm mortar joints, mechanically connected through L-shape steel ties with a density of approximately 1 tie/m². The CS bricks had dimensions of 212 x 102 x 71 mm while the CL ones of 210 x 100 x 50 mm. Only the inner leaf was continuous along the entire perimeter of the house. The outer CL leaf was not present on the South side, as in reality the adjacent residential unit would border with it.

The first-floor concrete slab and the second-floor and roof timber joists spanned in the North-South direction between the two transverse inner CS walls. Staircase openings were provided to both floors in proximity of the North wall. Two gable walls atop the transverse (North and South) façades supported a 39° pitched timber roof. The North gable included an opening.

A 2 mm-thick plaster layer was applied to half of the ground floor as shown in Figure 9. With the adopted configuration, non-structural damage to squat and slender piers in the longitudinal East and West walls could be captured, as well as damage to the transverse South wall. The roof was finished with counter and tile battens and clay tiles. Two window timber frames were also installed: one in the large opening at the ground floor of the West façade and one in the North gable wall. These finishes allowed studying damage to non-structural elements.

A very stiff steel frame was mounted on the shaking table inside the building prototype with two main goals. First, it provided a safety restraint in the event of a partial or global collapse that may occur during the dynamic tests, a scenario that would create significant damage to the testing apparatus. Second, it provided reference points to measure displacements of the specimen with respect to the shaking table surface, to which the nearly rigid structure is firmly bolted. The steel frame columns passed through four holes provided in both floor diaphragms. Gaps of at least ±20 cm were left in the shaking direction, and of ±10 cm in the perpendicular one, to allow floor lateral displacements without engaging the frame.

Figure 4 shows the first floor of the specimen under construction. Figure 5 illustrates the rigid steel frame at the ground floor and the placement of the first-floor concrete slab. Figure 6 depicts the second-floor timber structure. Figure 7 and Figure 8 show overviews of the building prototype after completion. Figure 9 through Figure 12 show plan view dimensions of ground, first, and second floors and roof, respectively. Figure 13 through Figure 20 illustrate vertical sections and elevations of the specimen, where blue dots indicate the location of the steel ties connecting inner and outer masonry leaves.

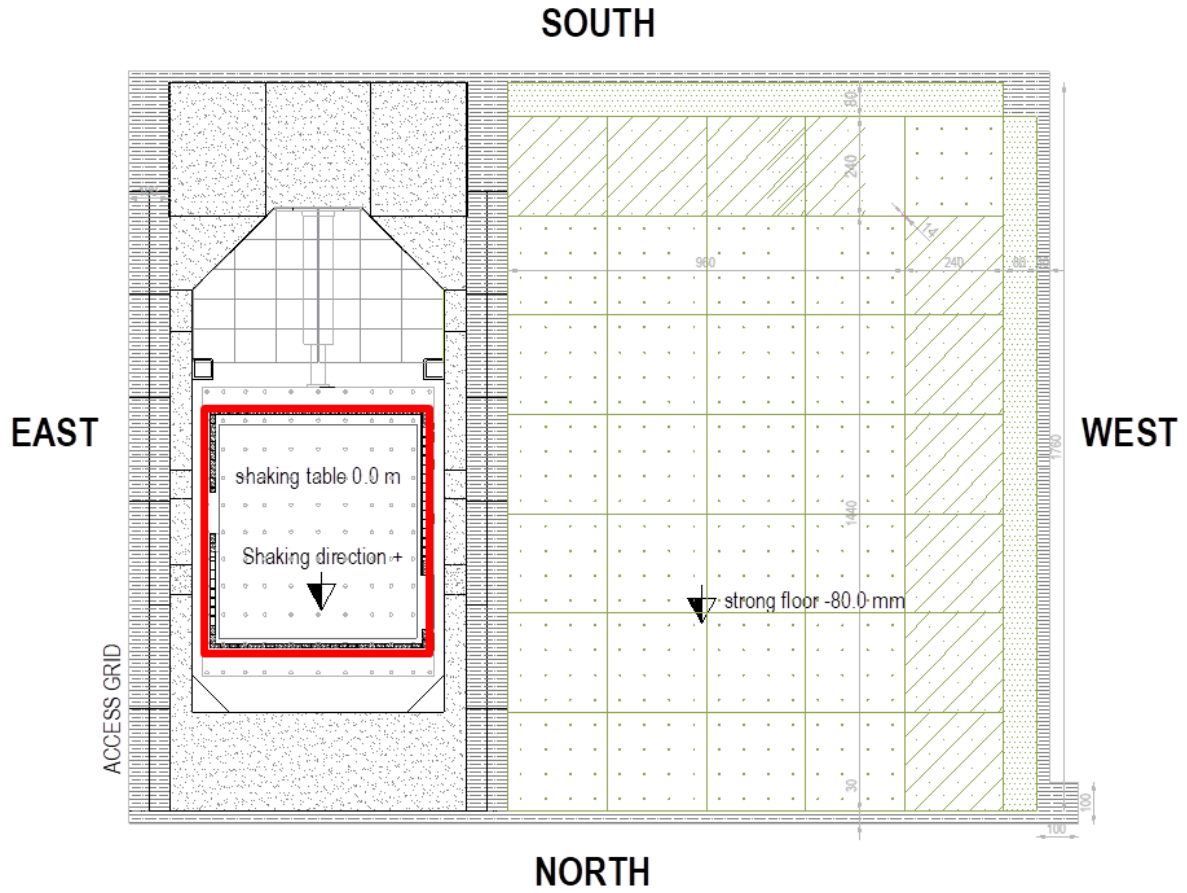


Figure 2 Plan view of the EUCENTRE Lab. and position of the shake-table and the walls of the test-house.



a)



b)

Figure 3 Foundation system: (a) composite steel-concrete beams; (b) calcium silicate walls during construction over the concrete layer.

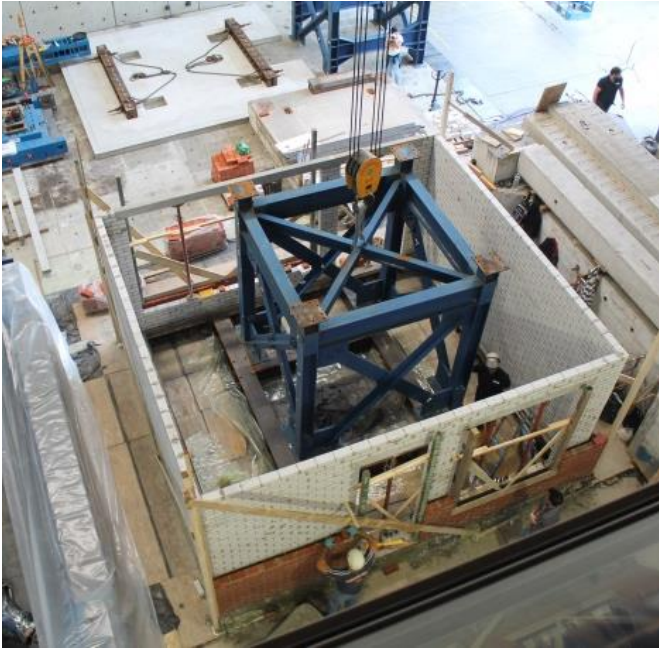


a)

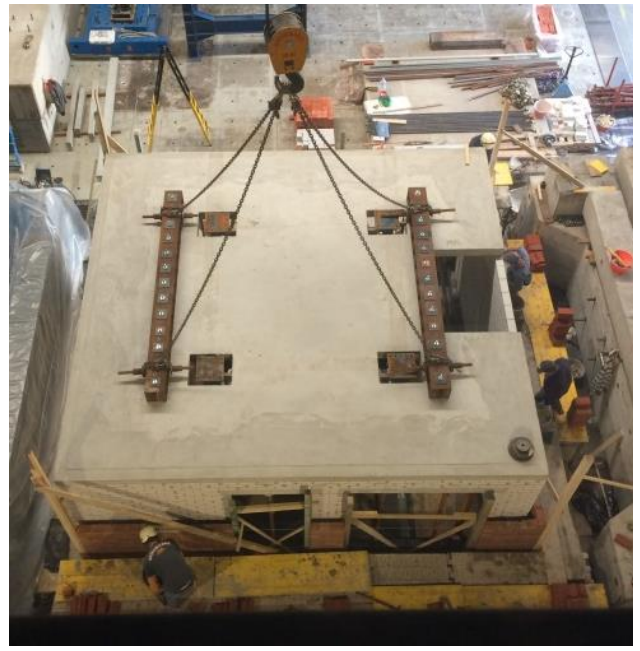


b)

Figure 4 Prototype construction phases: (a) first-storey West elevation; (b) first-storey East elevation.



a)



b)

Figure 5 Prototype construction phases: (a) first-storey rigid steel frame; (b) placement of the first-floor reinforced concrete slab.



Figure 6 Prototype construction phases: second-floor timber structure.



a)



b)

Figure 7 Completed prototype: a) North and West façades; b) West and South façades.



a)



b)

Figure 8 Completed prototype: a) South and East façades; b) South and East façades.

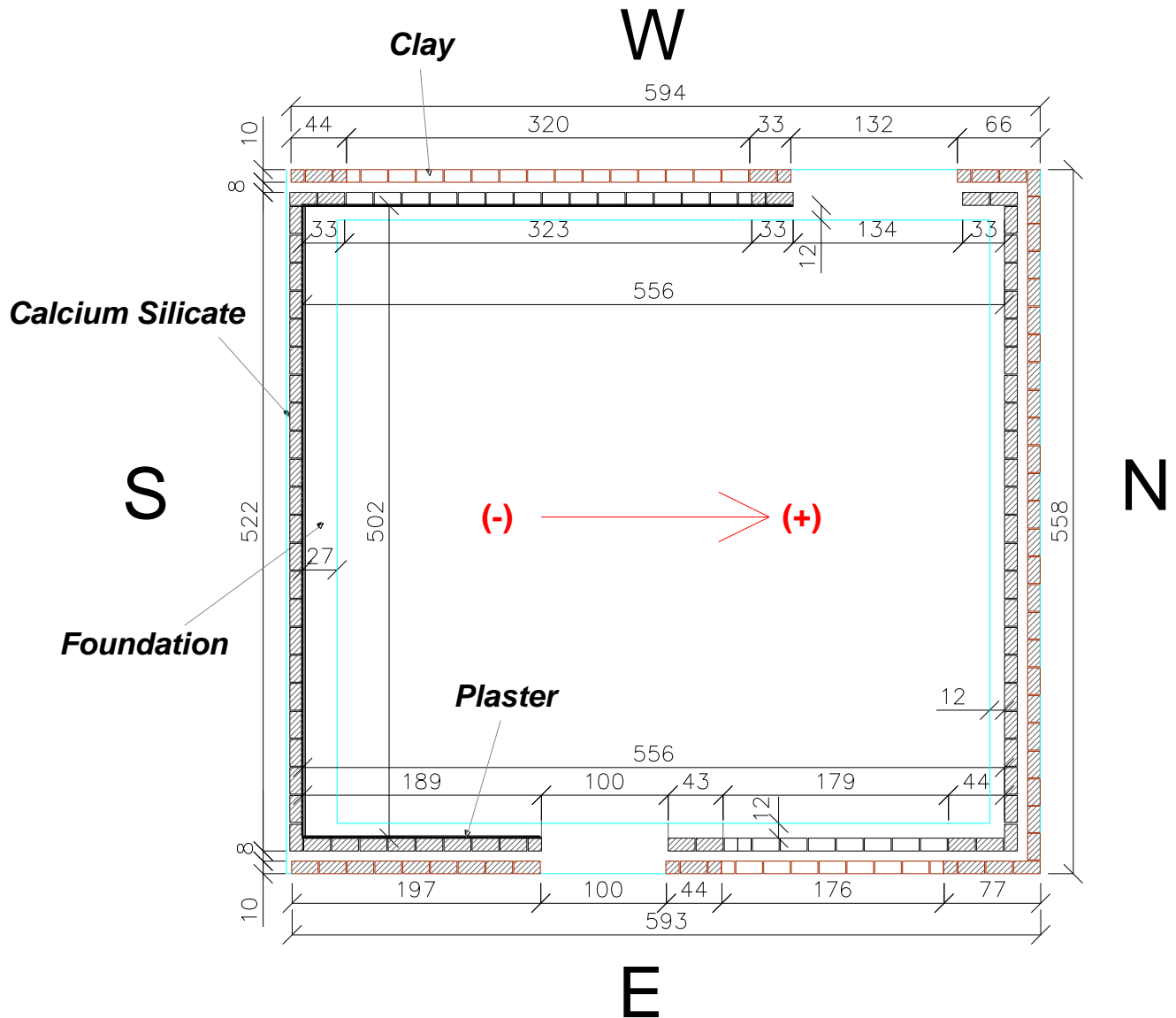


Figure 9 Plan view of the ground floor. The red arrow indicates the shaking direction. Units of cm.



Figure 10 Plan view of the first floor. The red arrow indicates the shaking direction. Units of cm.

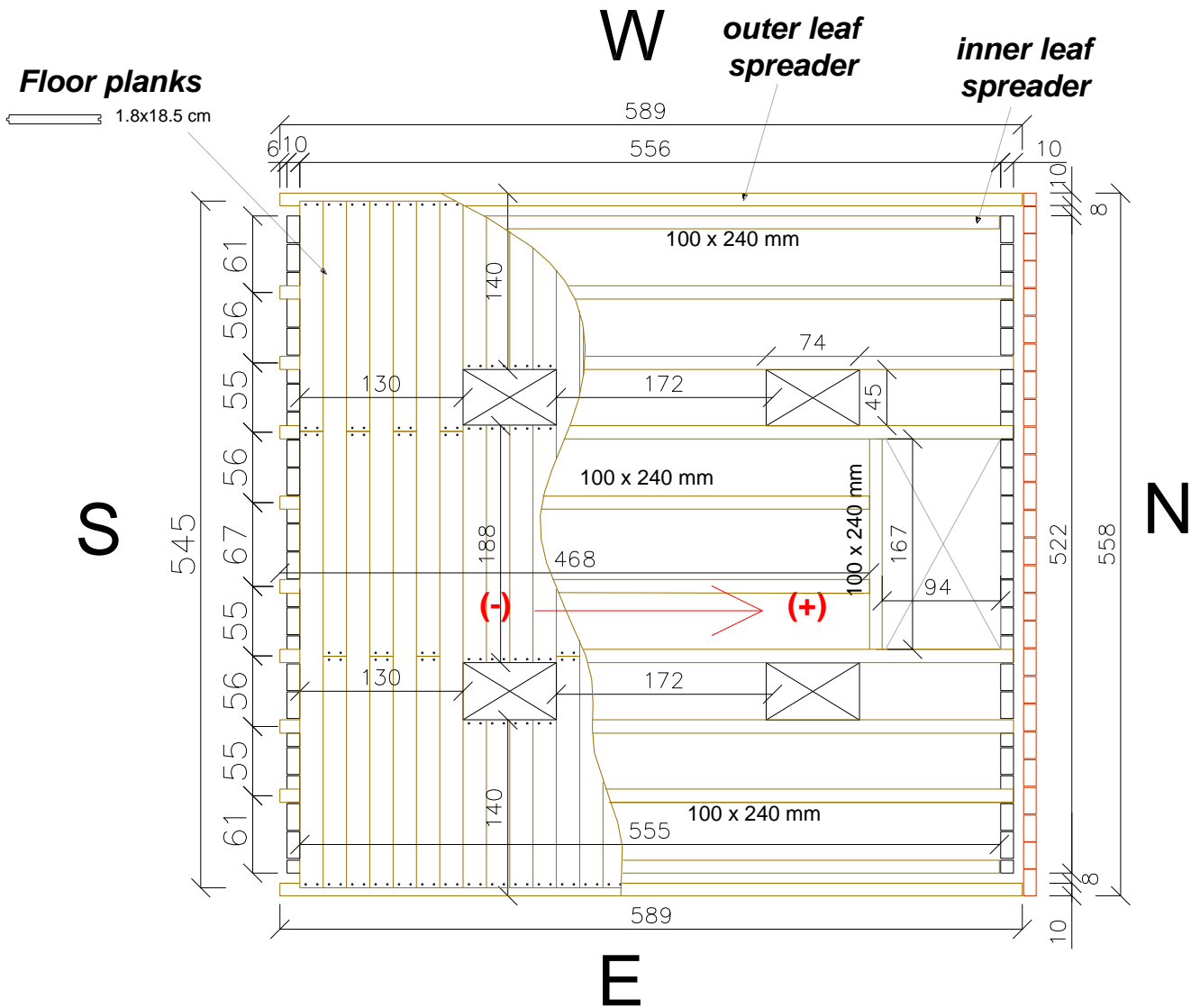


Figure 11 Plan view of the second floor. The red arrow indicates the shaking direction. Units of cm.

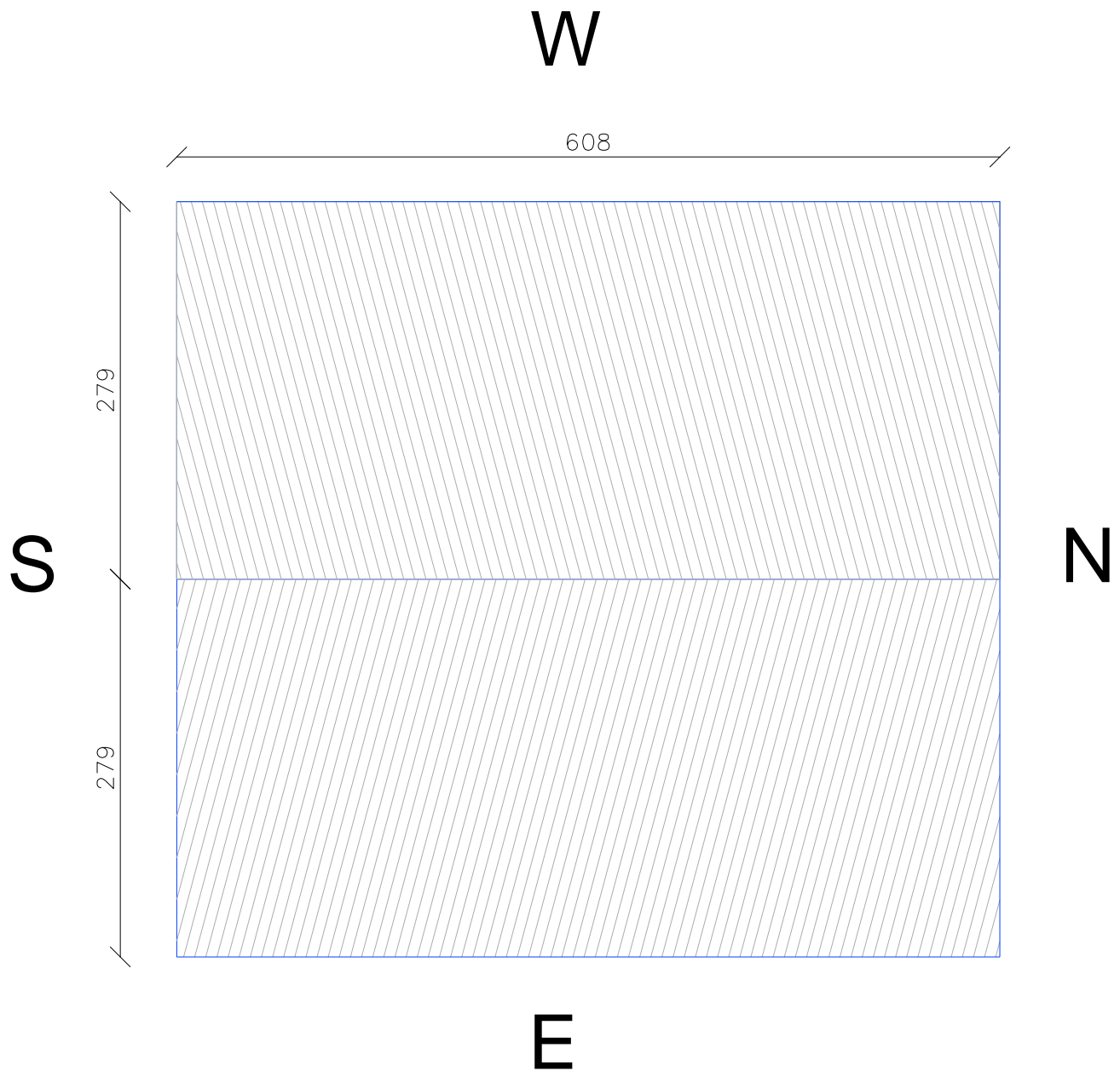


Figure 12 Plan view of the roof. Units of cm.

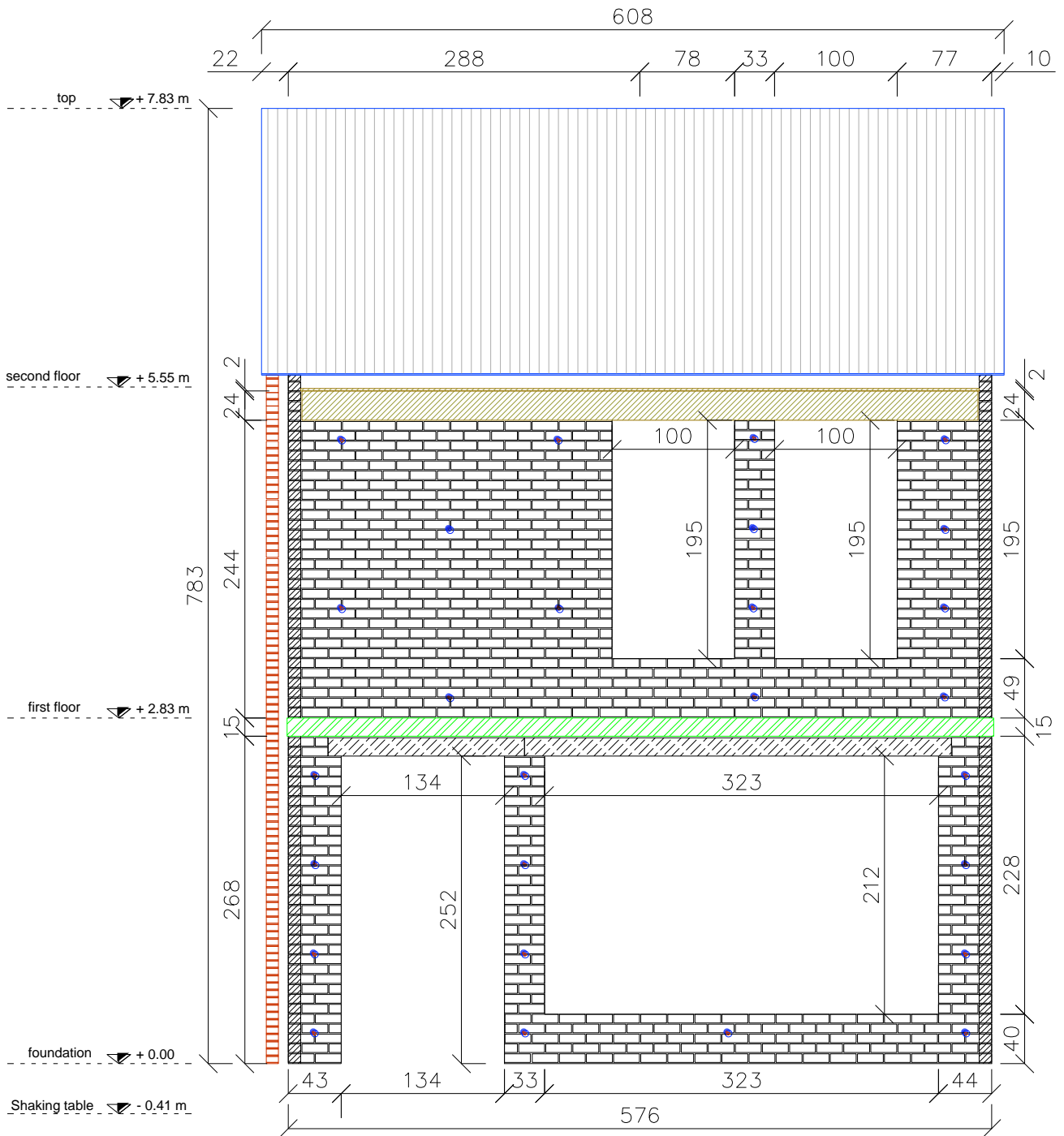
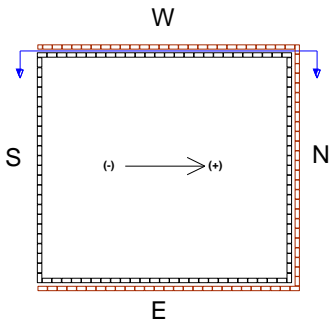


Figure 13 Vertical section looking at the West CS inner leaf from outside. Units of cm.

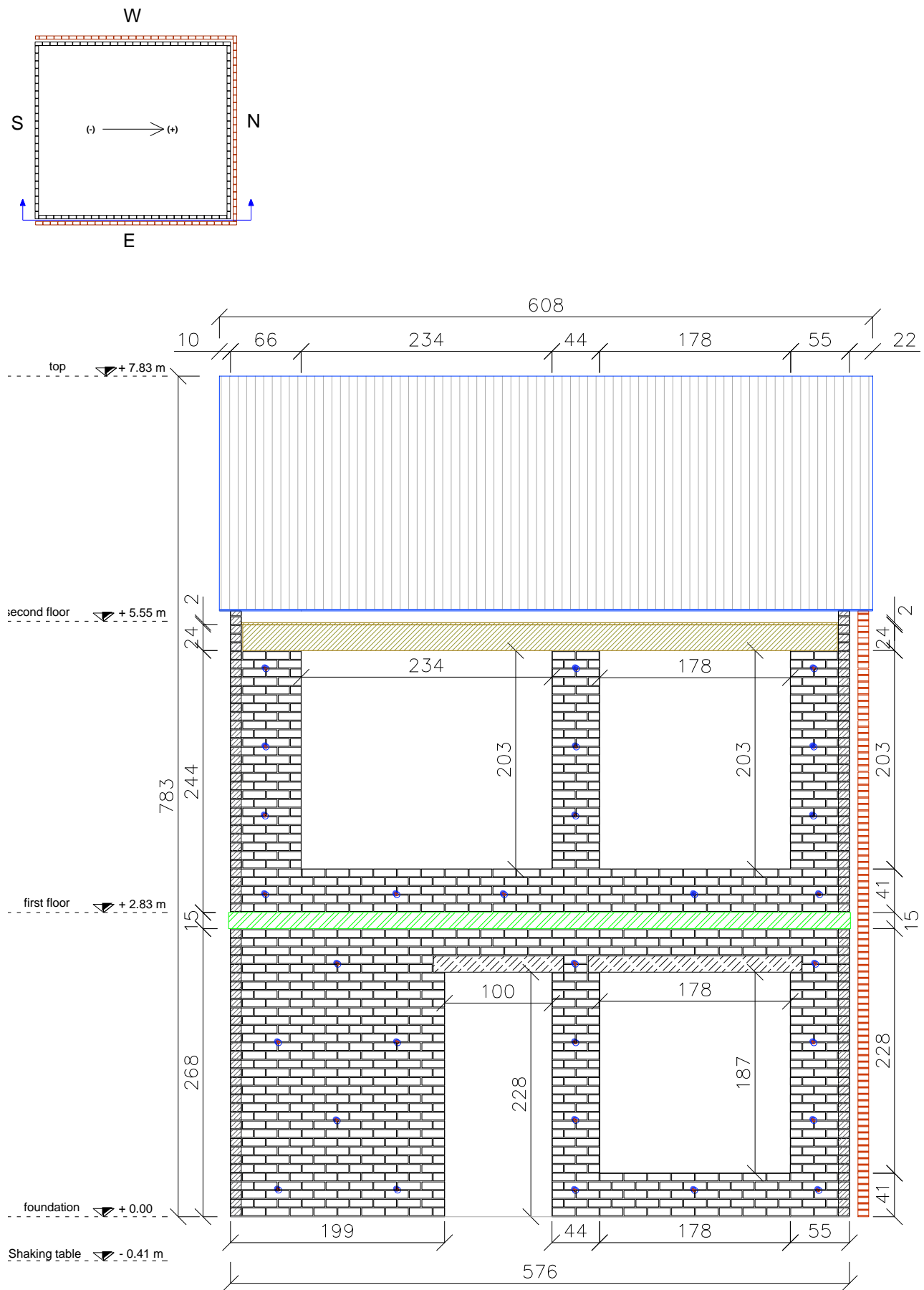


Figure 14 Vertical section looking at the East CS inner leaf from outside. Units of cm.

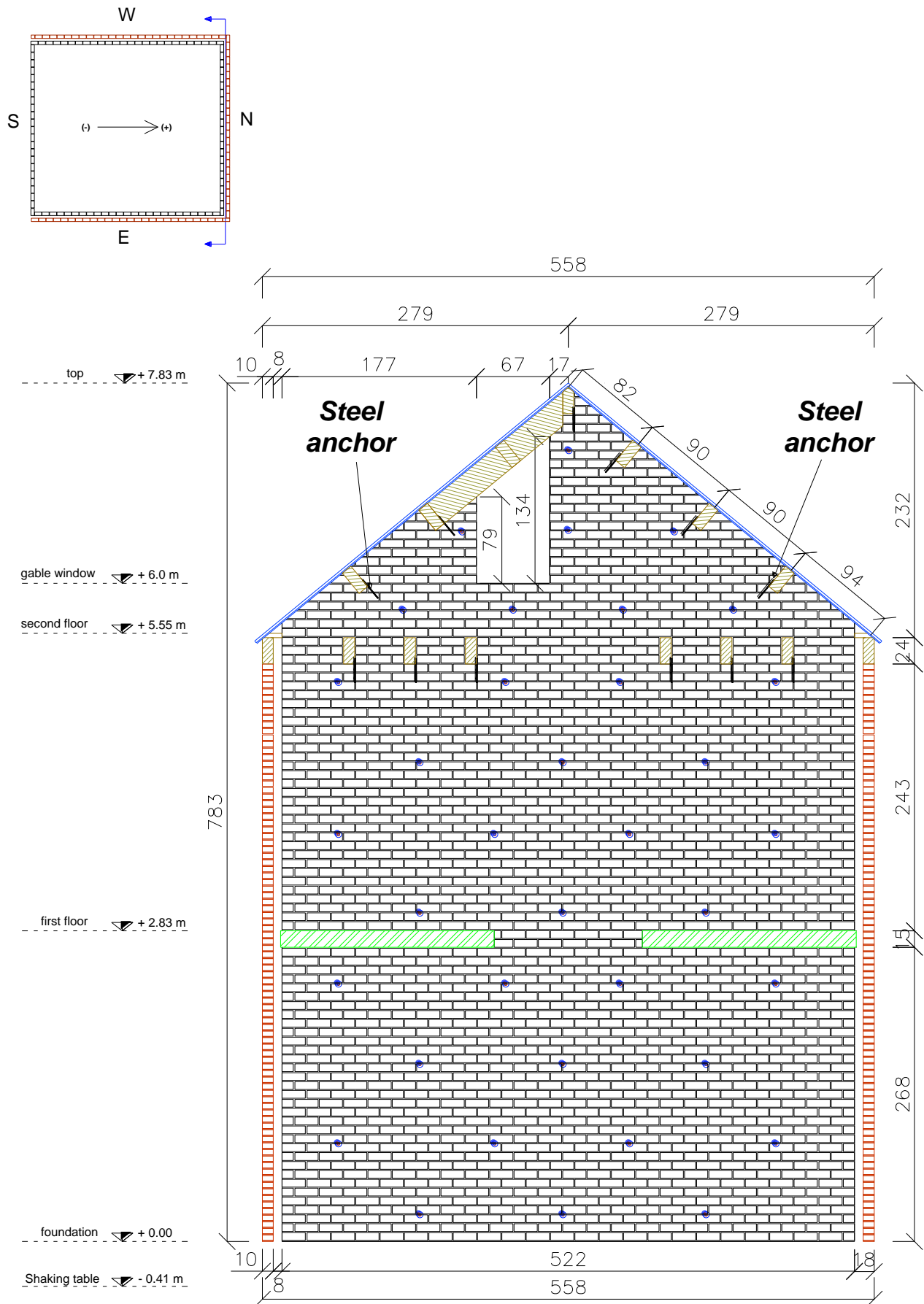


Figure 15 Vertical section looking at the North CS inner leaf from outside. Units of cm.

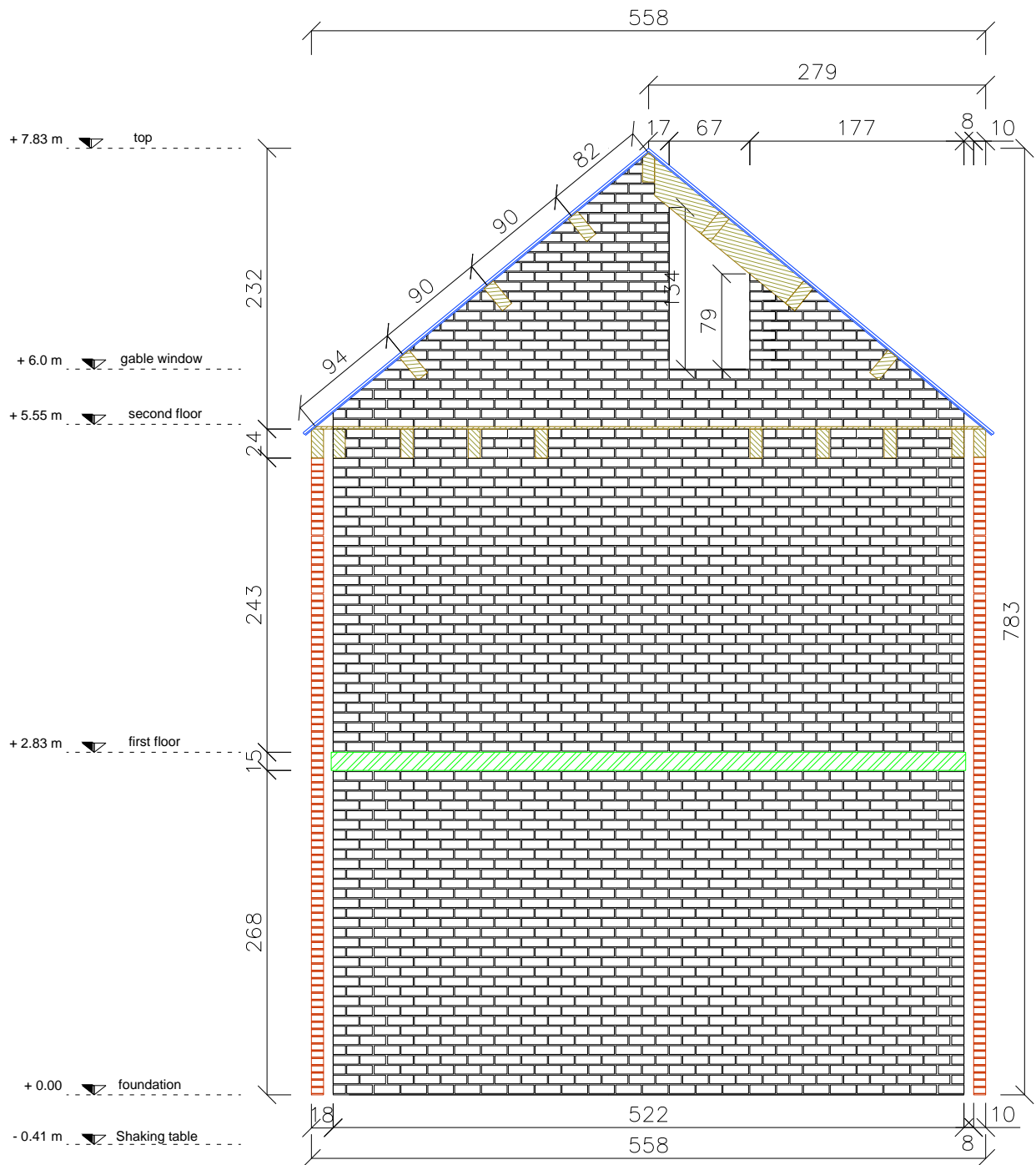
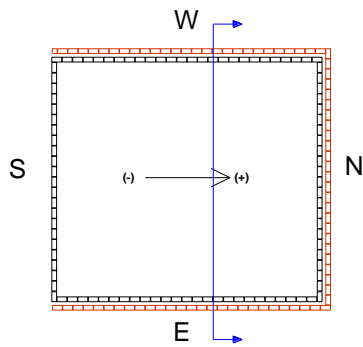


Figure 16 Vertical section looking at the North CS inner leaf from inside. Units of cm.

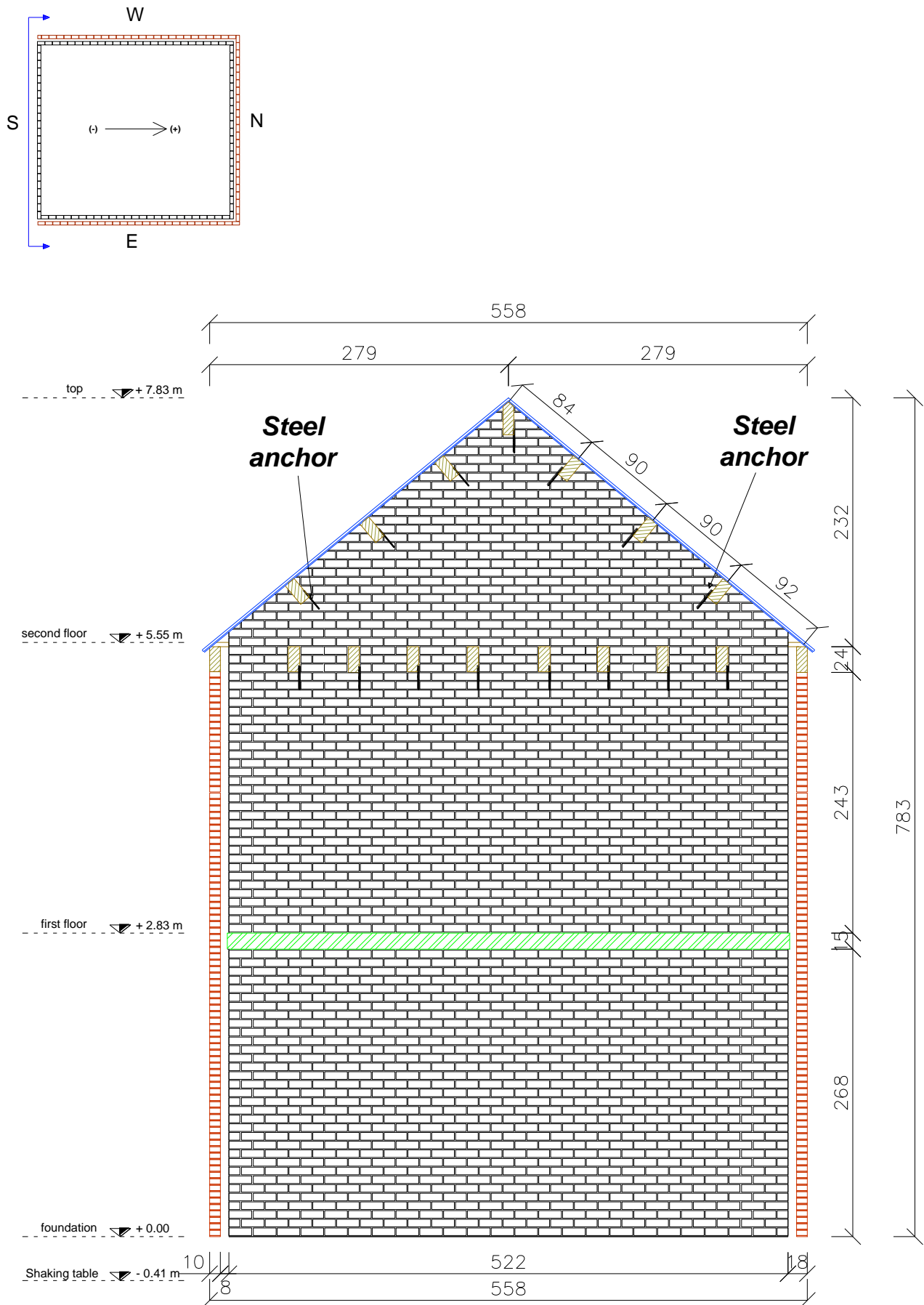


Figure 17 South elevation of the specimen CS inner leaf. Units of cm.

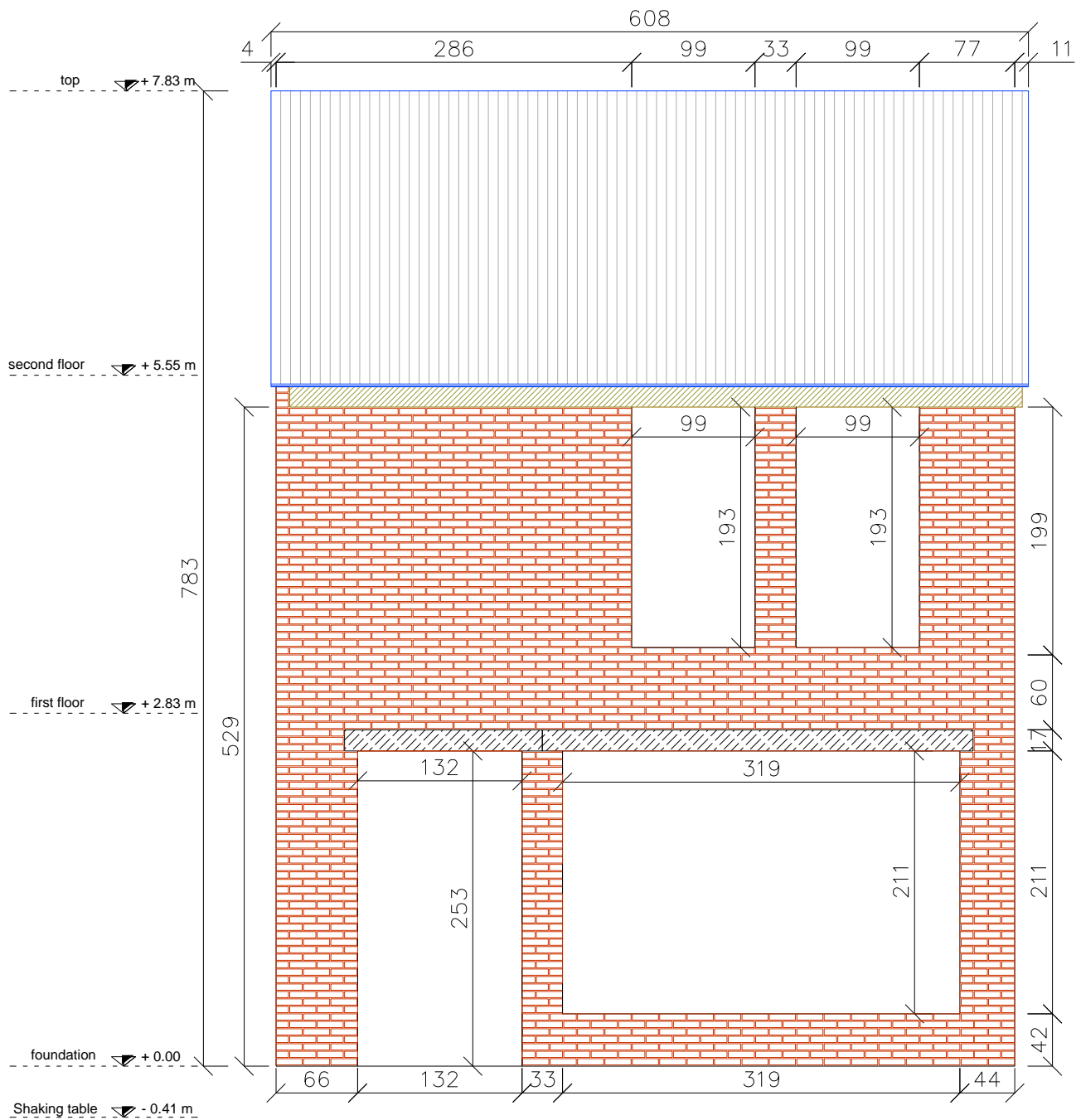
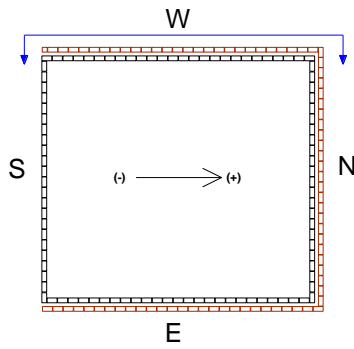


Figure 18 West elevation of the specimen Clay outer leaf. Units of cm.

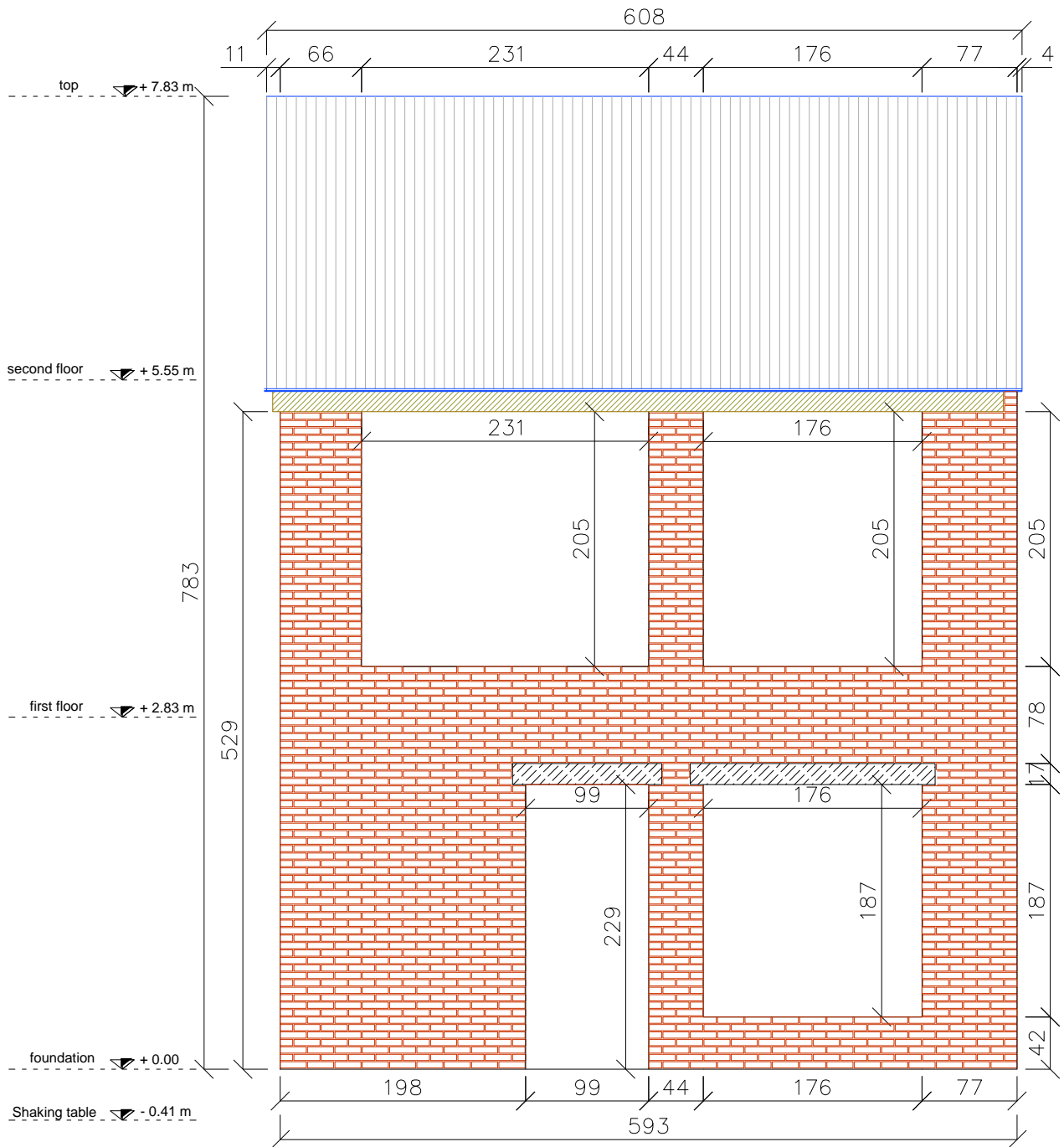
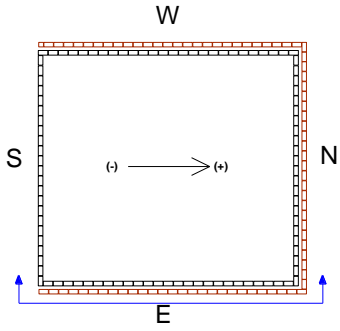


Figure 19 East elevation of the specimen Clay outer leaf. Units of cm.

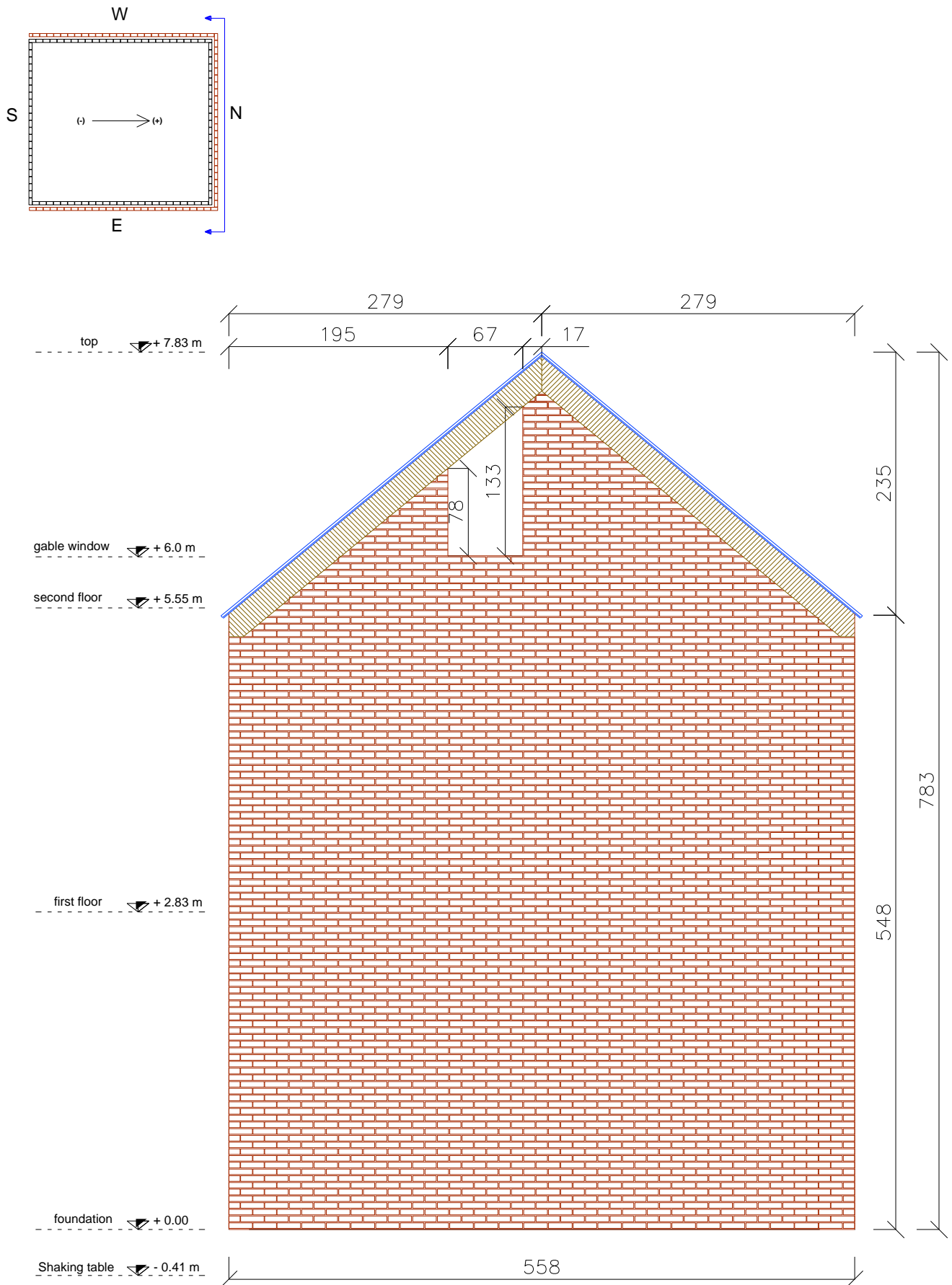


Figure 20 North elevation of the specimen Clay outer leaf. Units of cm.

1.2 Building construction details

The construction details of the specimen were representative of the Dutch common practice of the 1960s and 1970s. The following sections provide extensive description of the construction details of the building prototype.

1.2.1 Inner-to-outer leaf connection

As mentioned in par. 1.1, the connection between inner and outer leaves was granted by steel ties, with a diameter of 3.4 mm and a length of 200 mm. They were embedded in the 10-mm-thick mortar bed-joints during construction of the walls. The L-hook side was embedded in the inner CS walls for a length of 60 mm, while the “zig-zag” extremity was embedded in the CL veneers for a length of 60 mm as shown in Figure 21. They were distributed as shown on the CS inner leaf walls section views (Figure 13, Figure 14 and Figure 15) with a density of approximately 1 tie/m². This density was intended to represent the worst condition that could be found in the Groningen area, excluding cases of very severe corrosion.

1.2.2 First-floor reinforced concrete diaphragm and floor-to-wall connections

The first floor consisted of a 160-mm-thick reinforced concrete slab, monolithically precast aside (Figure 22 a and b) and subsequently placed above the CS masonry leaves (Figure 23). The monolithic slab was deemed equivalent to precast panels completed with a topping slab in providing a rigid diaphragm. The 160-mm thickness was selected to include the mass of the floor structure, as well as the one coming from superimposed dead and live loads. The floor slab thickness was reduced to 150 mm along the perimeter for the first 140 mm from each edge (Figure 22), to keep it consistent with the height of two bricks with a 10-mm horizontal mortar joint.

A 1.35 x 1.03 m staircase opening was provided on the North side of the slab (Figure 24), leaving that portion of the North wall horizontally unrestrained and free from any vertical overburden (see Figure 5). Because a similar detail was adopted for the second floor timber framing, the inner CS wall was continuous from the base through the roof. Four additional 0.45 x 0.55 m holes accommodated the rigid steel frame inside the building (Figure 24). Their dimensions assured no interference between the steel structure and the specimen during the test.

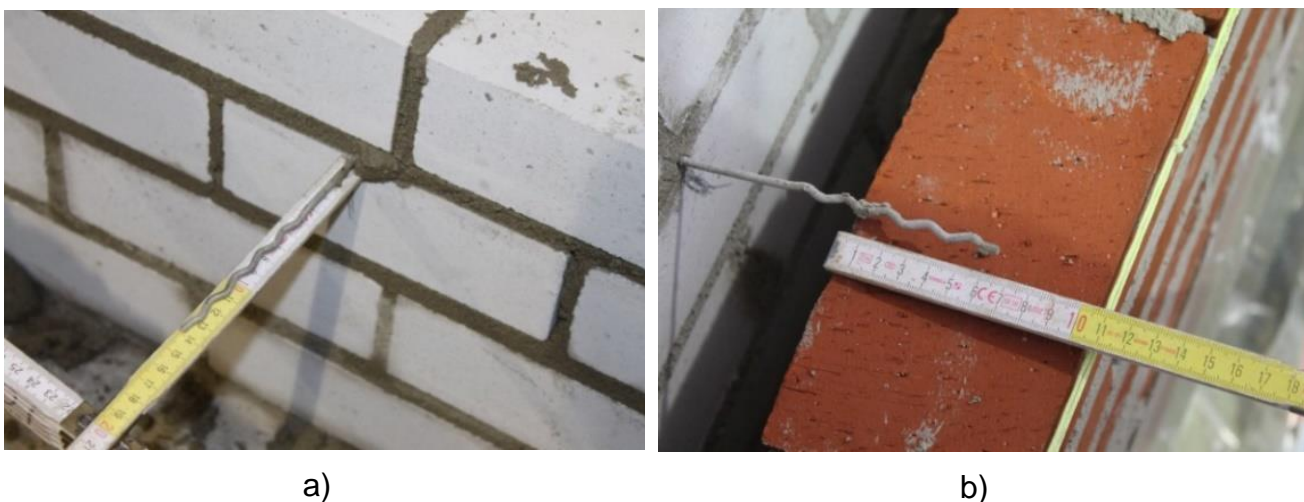


Figure 21 Steel ties positioning: (a) length from CS wall; (b) embedment into clay walls.

The slab was laid down on the North and South load-bearing CS inner leaves, leaving a gap atop the East and West walls (Figure 23): this operation intended to load only the transverse walls, leaving the longitudinal ones unloaded in static conditions. The gap was then filled with mortar after creep deformations of the concrete were exhausted. The connection of the concrete slab with the load-bearing CS walls relied only on the mortar layers below and above the slab (Figure 25).

Figure 26 through Figure 28 show the slab reinforcement, consisting of:

- 54 top and bottom $\phi 12$ in the North-South direction;
- 36 top and bottom $\phi 12$ in the East-West direction;
- 1 $\phi 12$ along the perimeter of the slab;
- 1 $\phi 12$ along the sides of each hole.

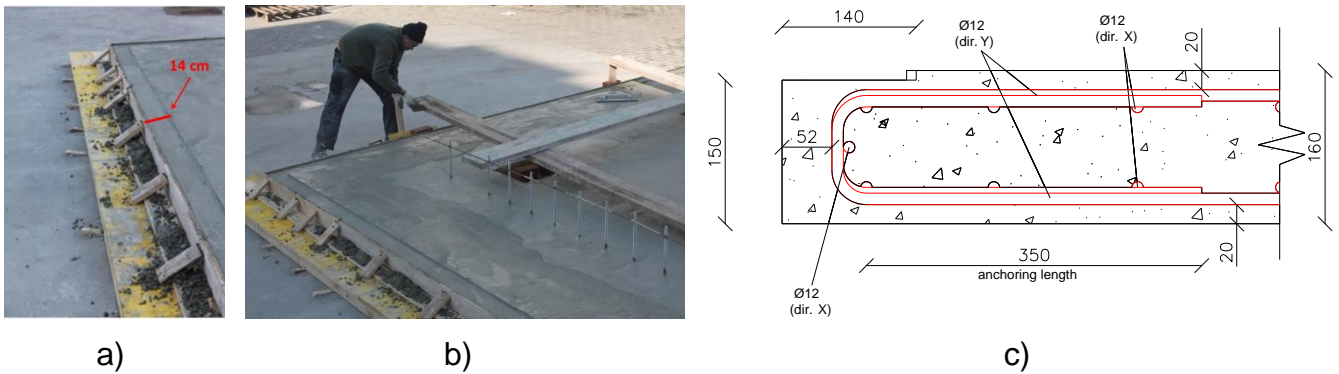


Figure 22 Reinforced concrete slab: a, b) concrete casting and finishing; c) edge detail. Units of mm.

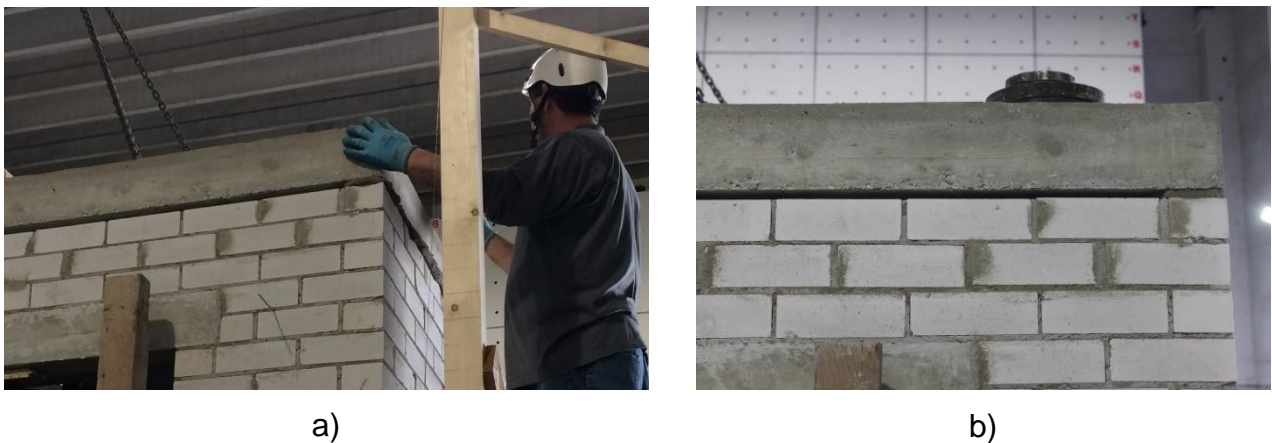


Figure 23 Reinforced concrete slab positioning: a) North-East corner; b) unsupported East side.

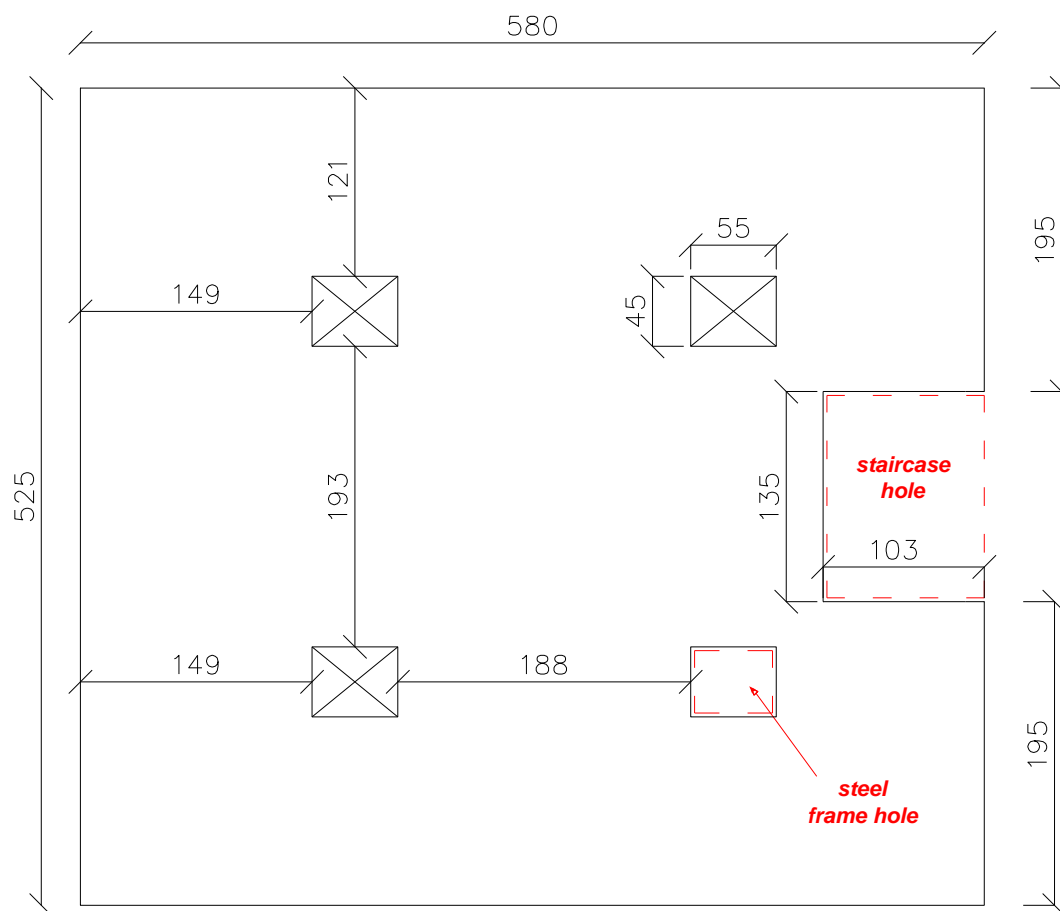


Figure 24 Reinforced concrete slab plan view. Units of cm.

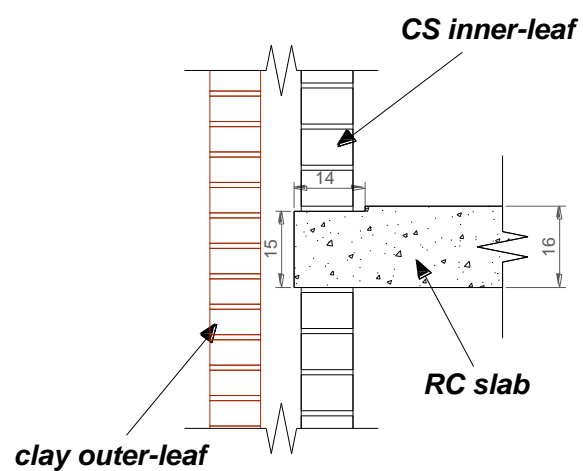


Figure 25 Reinforced concrete slab-to-wall connection detail. Units of cm.

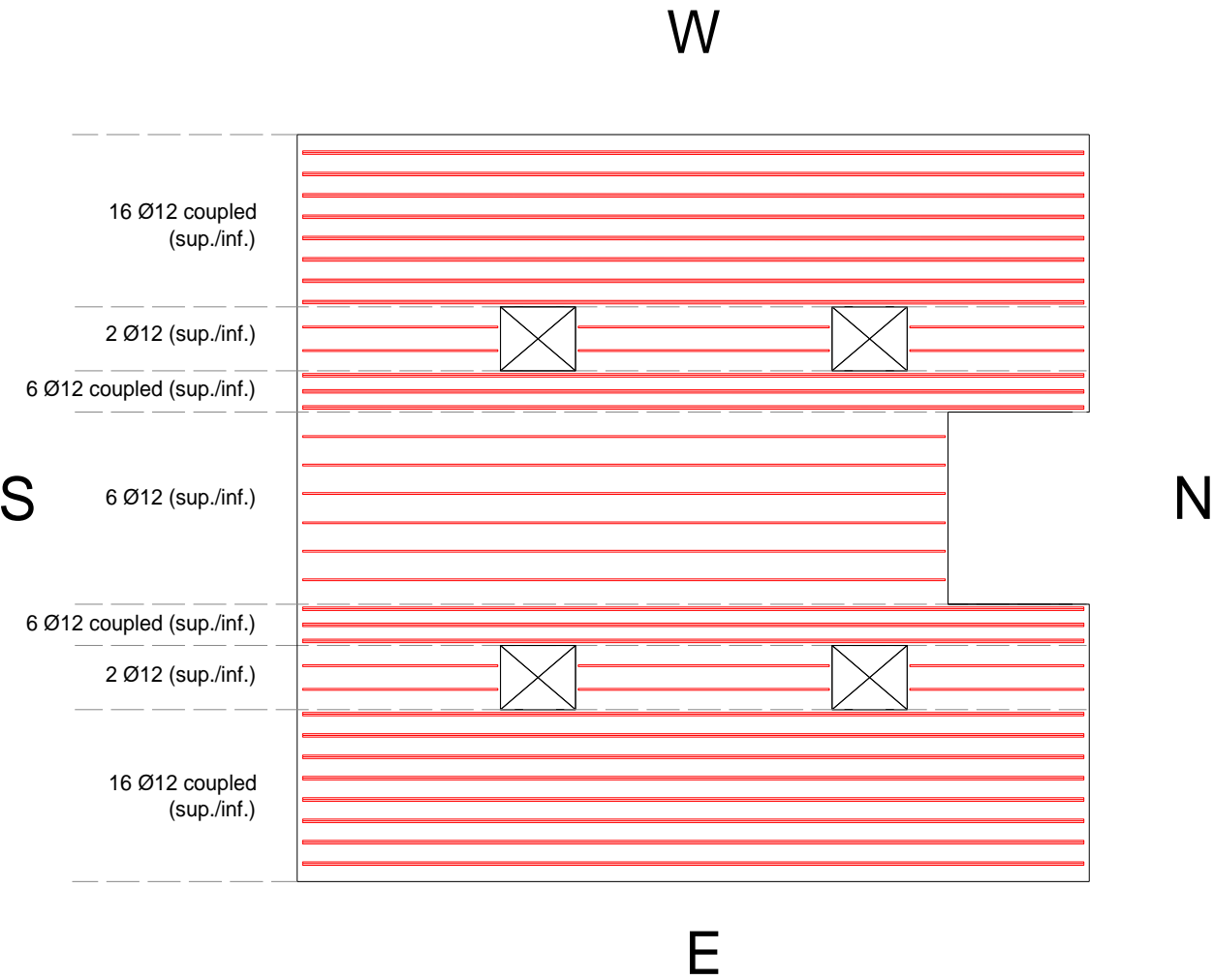


Figure 26 Reinforced concrete slab: North-South top and bottom reinforcement plan view.

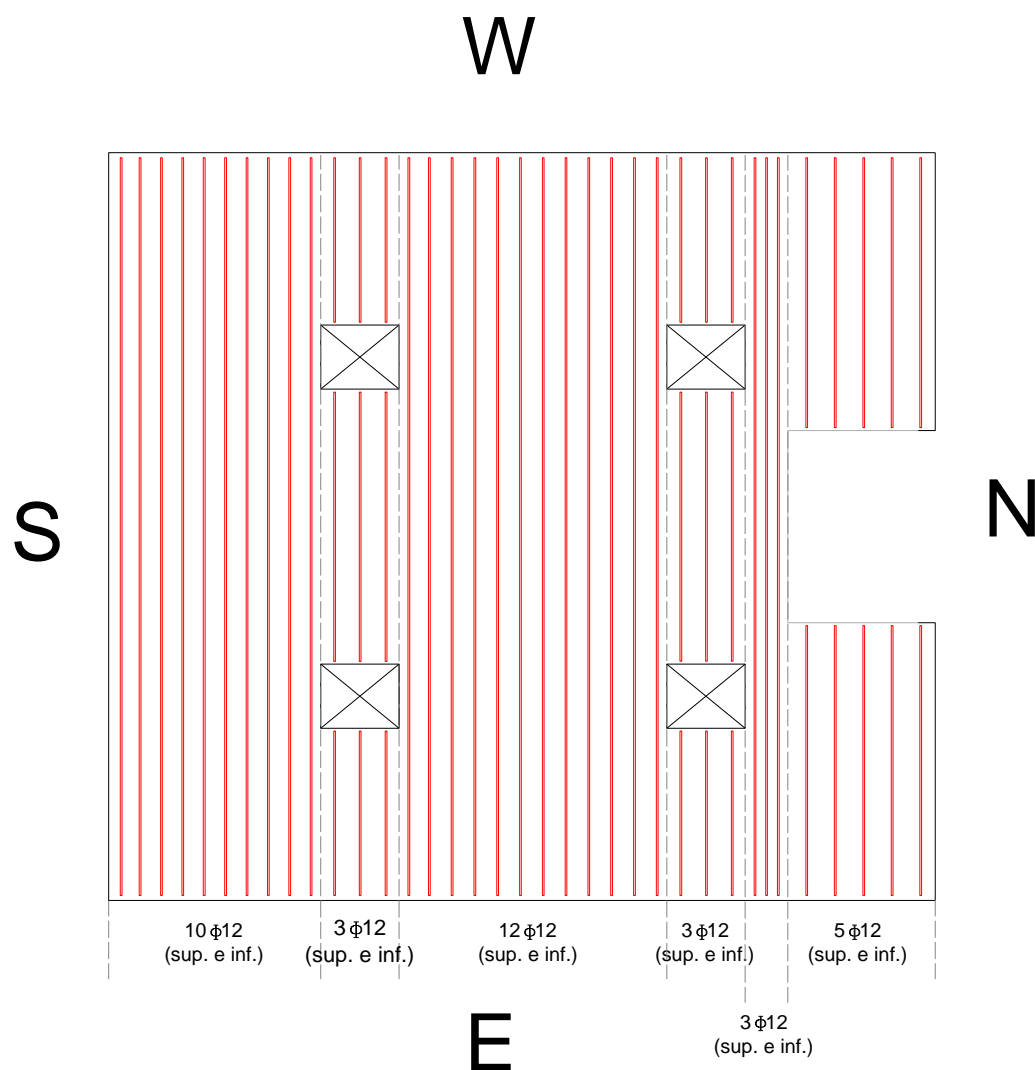


Figure 27 Reinforced concrete slab: East-West top and bottom reinforcement plan view.

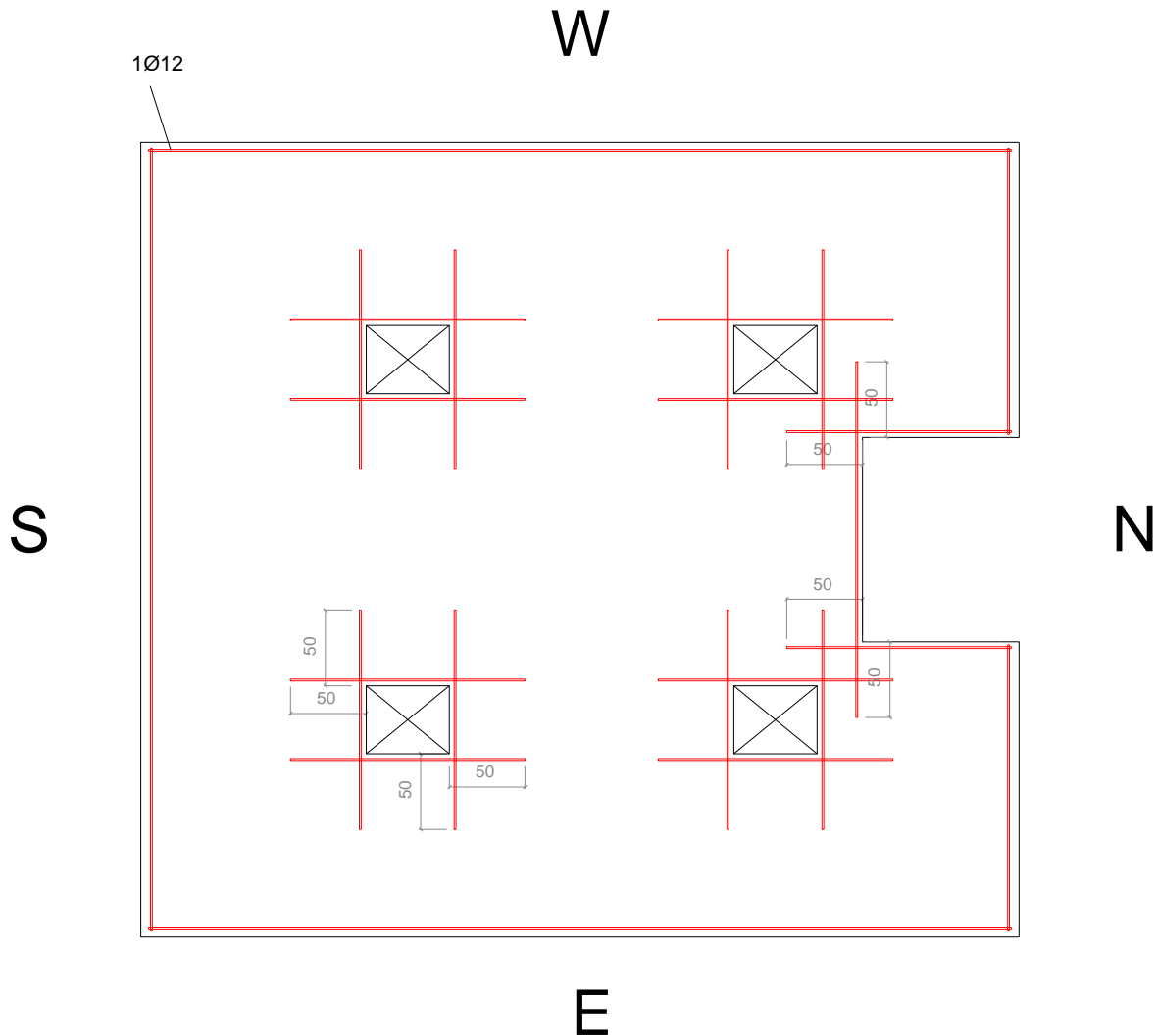


Figure 28 Reinforced concrete slab: perimeter reinforcement plan view. Units of cm.

1.2.3 Reinforced concrete lintels

Eight reinforced concrete lintels were placed above the openings of the first storey (Figure 29 through Figure 32). They were precast aside and subsequently laid on the walls for a length of 100 mm at both ends (Figure 33). Their section was 100 x 150 mm for the calcium silicate walls (height of two brick courses plus one mortar joint) and 100 x 170 mm for the clay walls (height of three brick courses height plus two mortar joints). The reinforcement was designed with a high safety factor to avoid failure of the lintels:

- Longitudinal reinforcement: 8 ϕ 14;
- Transverse reinforcement: ϕ 6/100 mm.

**West facade
Inner leaf (calcium silicate)**

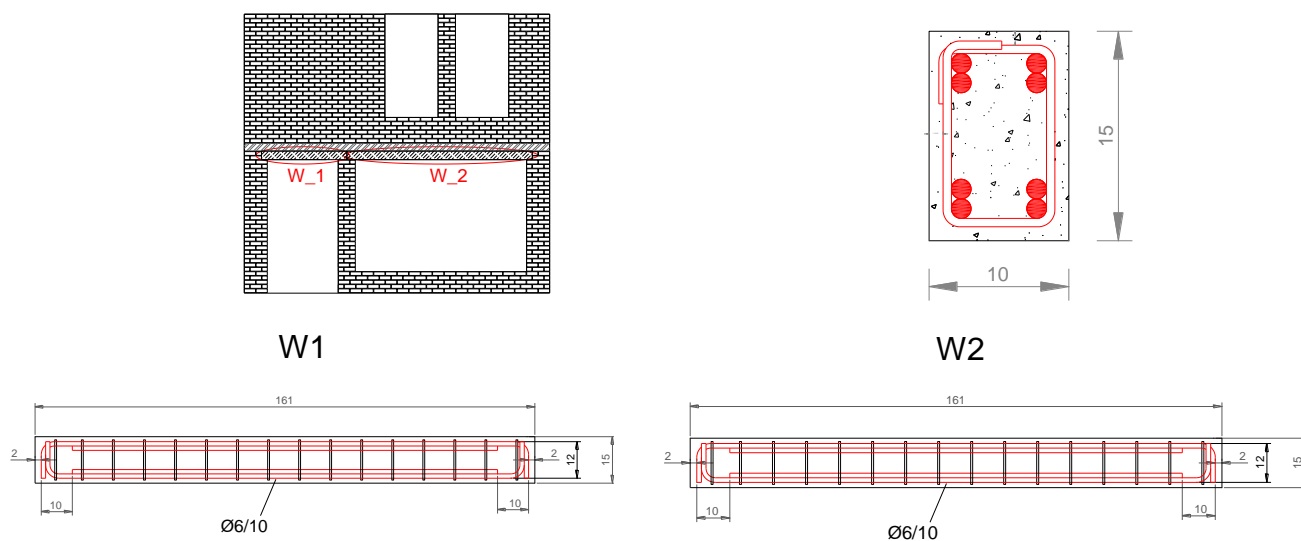


Figure 29 Reinforced concrete lintel details: West façade inner leaf. Units of cm.

**East facade
Inner leaf (calcium silicate)**

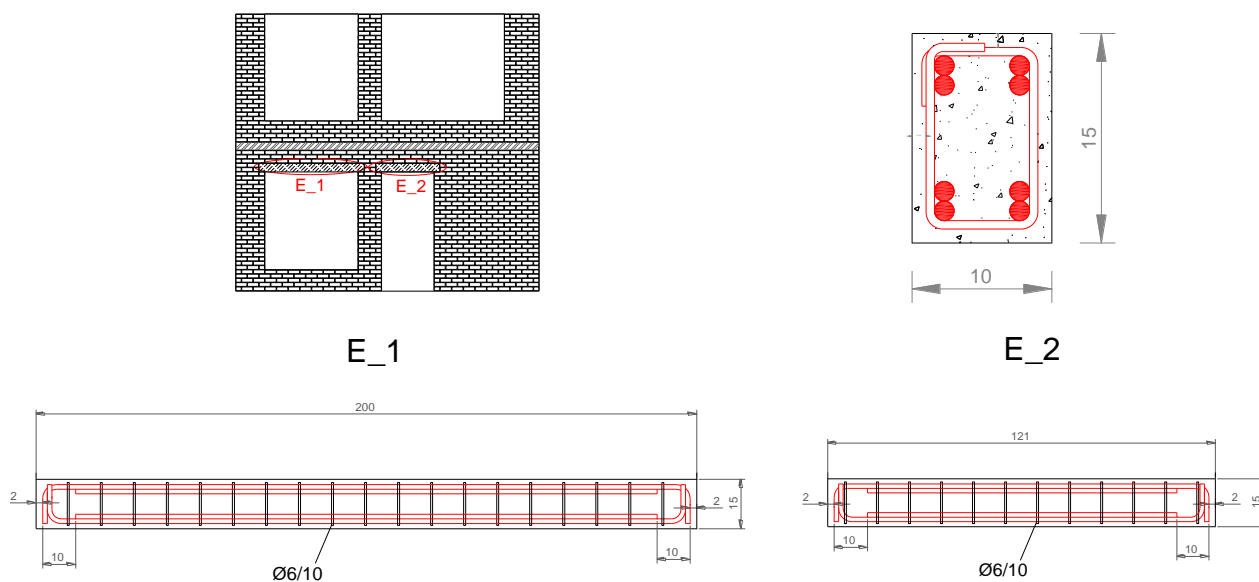


Figure 30 Reinforced concrete lintel details: East façade inner leaf. Units of cm.

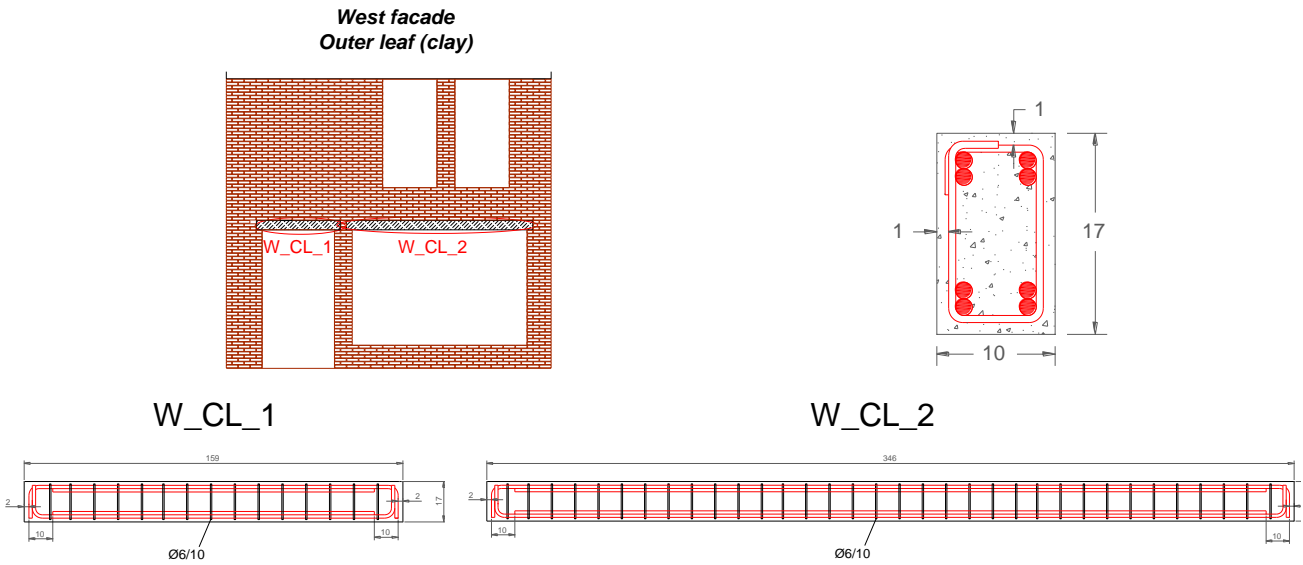


Figure 31 Reinforced concrete lintel details: West facade outer leaf. Units of cm.

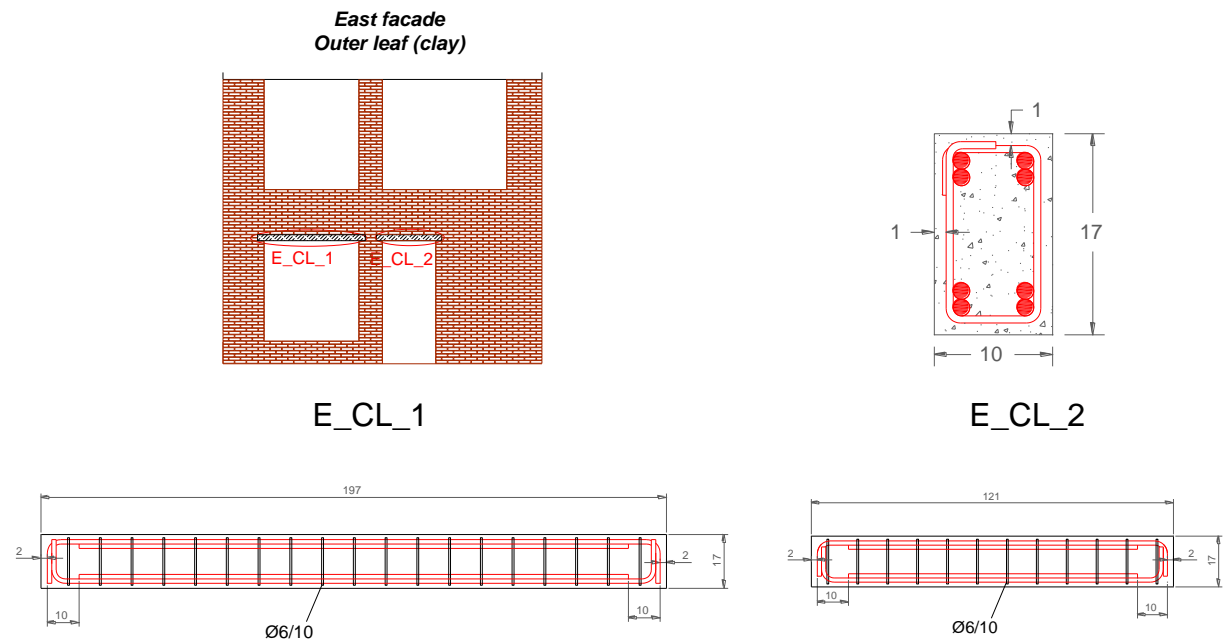


Figure 32 Reinforced concrete lintel details: East facade outer leaf. Units of cm.



a)



b)

Figure 33 Lintels positioning details.

1.2.4 Second-floor timber diaphragm and floor-to-wall connections

The second floor (Figure 34 and Figure 35) was made of 185 mm x 18 mm tongue and groove planks supported by eight 100 x 240 mm timber joists, spanning continuously between the North and South CS walls with an average centre-to-centre spacing of 600-mm. A total of four 100 x 240 mm timber spreader beams were placed above the CS inner leaf and the CL outer leaf of East and West façades, serving also as lintels for the second-storey openings. The planks were connected to the joists by two 60 x 2 mm nails at every intersection.

As for the concrete slab, a 1.67 x 0.94 m staircase opening was provided on the North side of the slab. Four 0.45 x 0.74 m holes were created to accommodate the steel frame columns (Figure 6), allowing displacement of the floor diaphragm with respect to the steel frame during shaking.

A transverse 1.67-m-long 100 x 240 mm timber beam was provided along the South edge of the staircase hole, to support the joists interrupted by the opening; this beam was then connected to two longitudinal joists as shown in Figure 35 and Figure 36. The timber-to-timber connections were obtained with steel hangers, fastened to the supporting joist by 12 nails and to the supported element by 5 screws per side. Steel Anker nails (by Wurth) with a characteristic strength of 1.25 kN (EN 1995:2009 – 8.2.3) were used for these connections.

235 x 245 mm L-shaped steel anchors, with a diameter of 14 mm, were provided at each joist end at the North and South CS walls (Figure 37). They were fastened to the timber joists by 3 screws and passed through the CS wall, bearing against the exterior surface of the CS leaf. Their locations are highlighted on the section views of the North and South CS walls (Figure 15 and Figure 17).

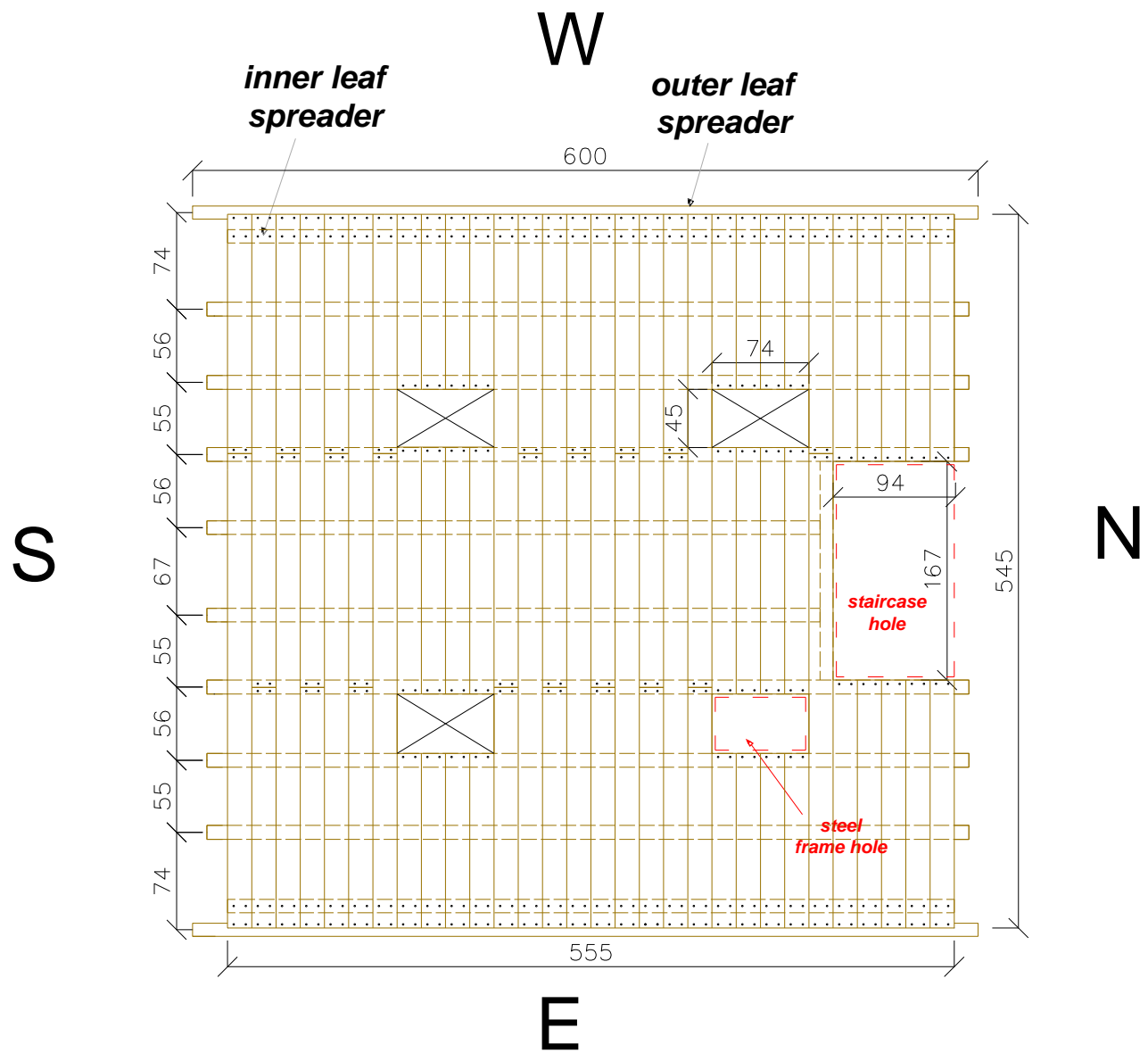


Figure 34 Timber floor framing plan view. Units of cm.

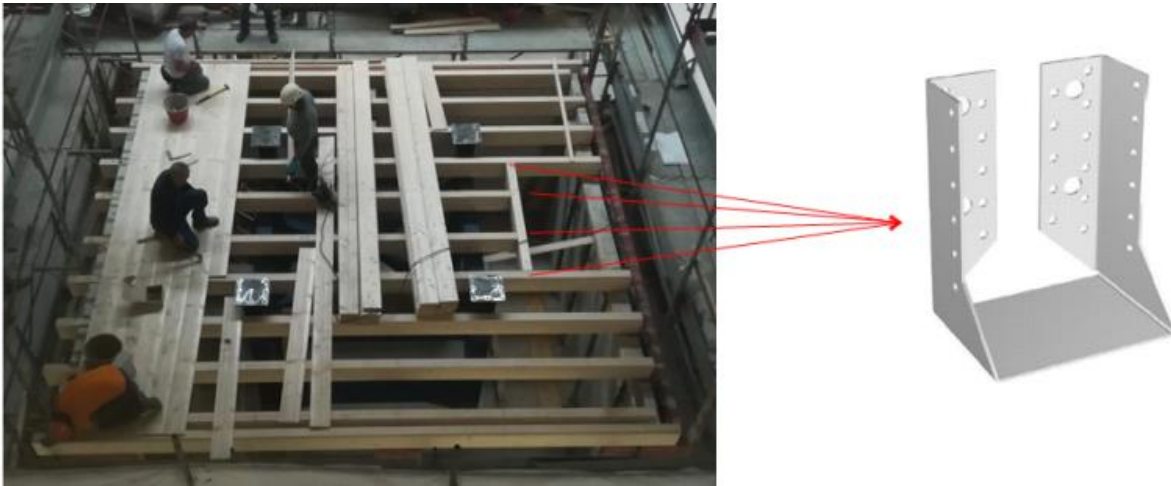


Figure 35 Timber floor framing: timber-to-timber connection at staircase hole.



a)



b)

Figure 36 Timber floor framing: timber-to-timber details at staircase hole.



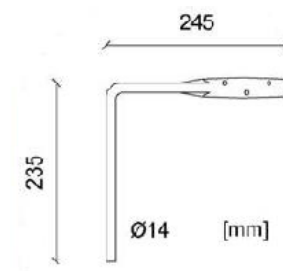
a)



b)



c)



d)

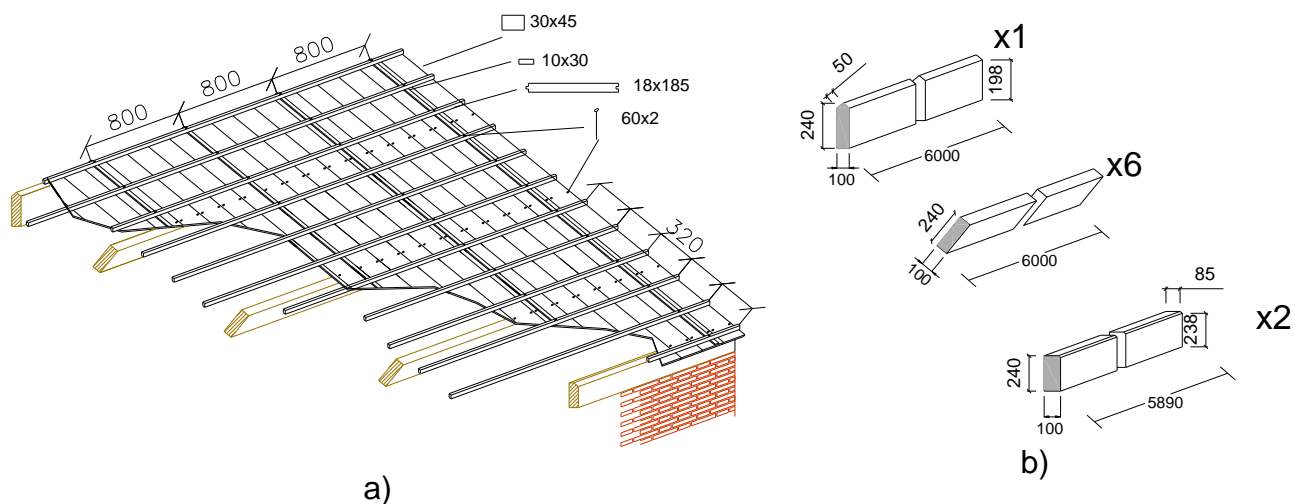
Figure 37 Timber floor framing: a, b, c) joist-to-wall connection; b) steel anchor details. Units of mm.

1.2.5 Roof timber diaphragm and roof-to-wall connections

The roof structure consisted of a timber ridge beam, two timber spreader beams on top of the longitudinal outer leaves (the same mentioned in the second floor description), and three additional timber joists per side, spaced at approximately 0.9 m. Tongue and groove 185 mm x 18 mm planks were nailed with two 60 x 2 mm nails at each intersection with the roof joists and beams (Figure 38 a). The inner CS leaves of the North and South gables supported joists and ridge beam (Figure 39). The same 235 x 245 mm L-shaped steel anchors used for the second-floor joists improved this connection (Figure 38 c). Differently from the second-floor joists, ridge beam and roof joists extended all the way through the North façade CL outer leaf (Figure 38 d).

Counter and tile battens were placed above the planks (Figure 38 a; Figure 40 a and b). Clay tiles completed the roof (Figure 41).

A restraint system made of steel cables, connecting the ridge beam to the internal steel frame, provided safety against collapse of the roof, which could result in a severe damage to the test equipment (Figure 40 c). This cable system allowed horizontal out-of-plane gable displacements up to about 200 mm without interfering with the prototype response.



c)

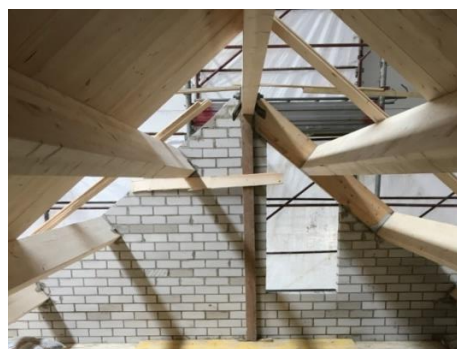


d)

Figure 38 Timber roof framing: (a) structural layout; (b) ridge beam, joists, and spreader beam details; (c) joist-to-wall connection at South gable; (d) joist-to-wall connection at North gable. Units of mm.



a)



b)

Figure 39 Timber roof framing: (a) joists at South gable; (b) joists at North gable.

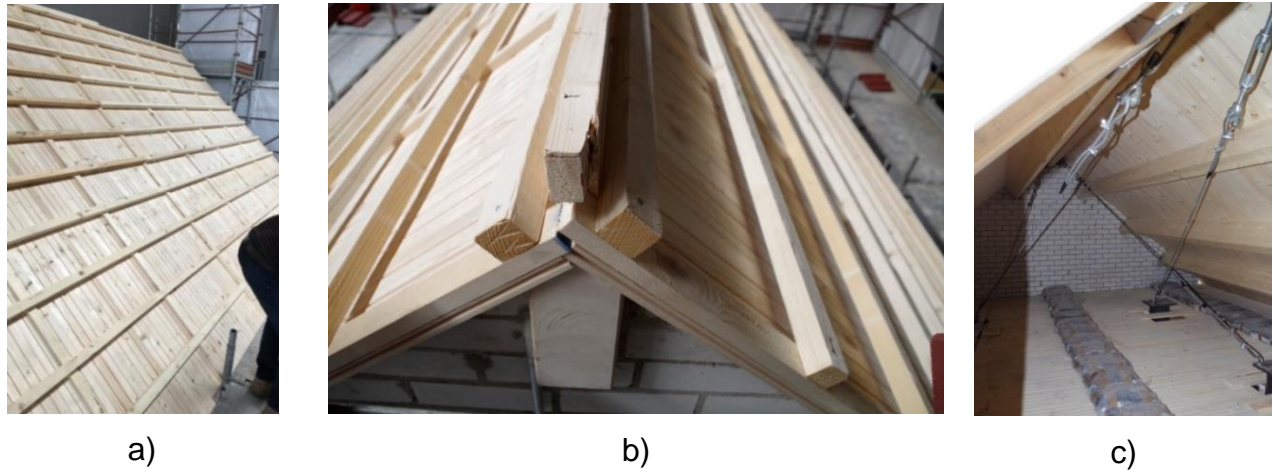


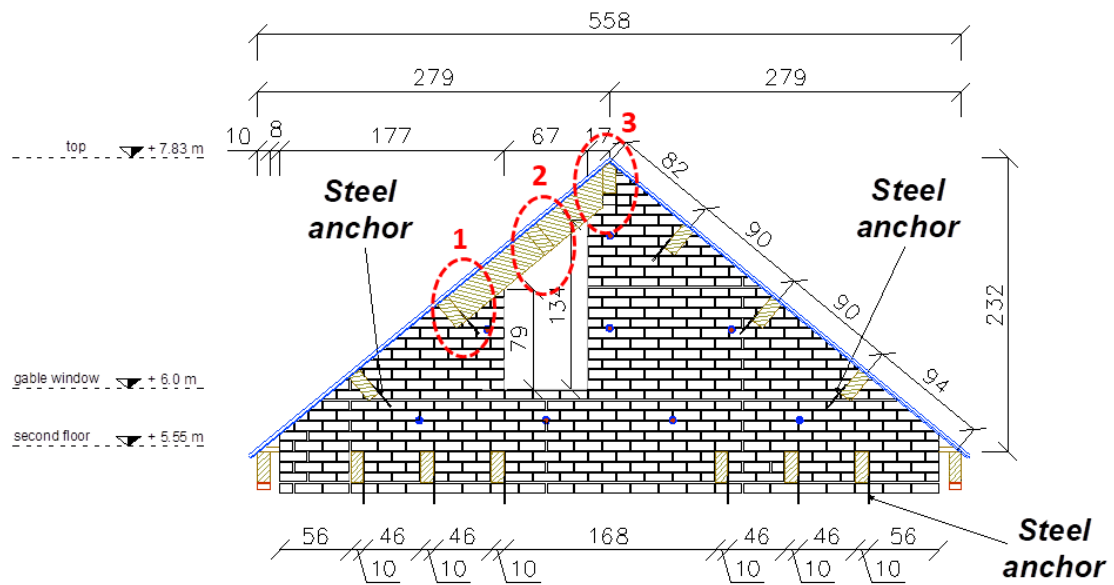
Figure 40 Roof finishes: a, b) counter and tile battens; c) steel rods restraint system.



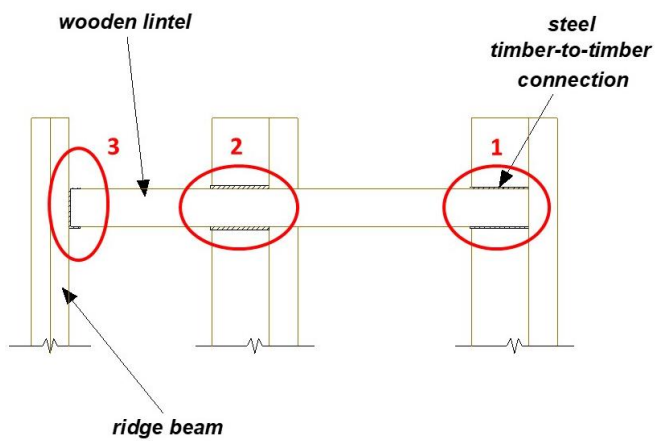
Figure 41 Roof finishes: a) tiles positioning; (b) roof end-construction.

1.2.6 North-gable opening

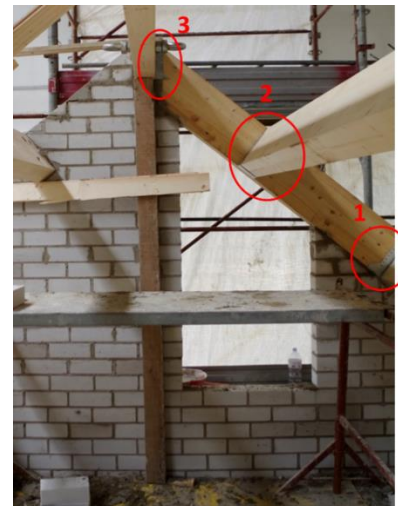
An opening at the top of an end-unit gable can be frequently observed in typical terraced house of the Groningen region. For this reason, the building prototype presented a trapezoidal window on the North gable (Figure 42). A timber lintel, inclined as the roof pitches, provided support for the joist landing above the opening and was connected to the adjacent joists; the same steel hangers used for the staircase hole at the second floor (par. 1.2.4) connected the timber elements. On the exterior surface of the lintel a short timber stub, with the same section of the joists, was mounted, cantilevering to the exterior surface of the CL masonry leaf (Figure 42).



(a)



b)



c)



d)



e)

Figure 42 North gable opening: a) section looking from inside; b) timber lintel connections plan view; c) internal view of timber lintel connections; d) steel hanger; e) external view with timber stub. Units of cm.

1.2.7 North-gable beam cover plates

Two timber cover plates were placed at the top of the North CL façade (Figure 7, Figure 20 and Figure 43) to cover the ends of the roof joists and ridge beam. They had thickness of 20 mm, height of 240 mm (as the joists), and were tailored to match the spreader beams at their bottom ends. These plates were connected to all roof timber joists with two 60 x 2 mm nails each. Two 6.5 x 240 mm screws, passing through the masonry leaf, provided connections with the spreader beams on top of the East and West CL façades (Figure 44).



a)



b)

Figure 43 Beam cover plates: a) at the roof ridge; b) at the outer-leaf spreader beam.



Figure 44 Detail of the cover plate connection to the outer-leaf spreader beam.

1.2.8 Window timber frames

Two window timber frames were installed. The first one was provided at the large 3.22 x 2.12 m ground-floor opening of the west façade (Figure 45 and Figure 46). The second one was mounted at the North gable trapezoidal opening, as shown in Figure 47.

Both window frames were connected to the CL outer leaf by 6-mm diameter, 110-mm long screws (Figure 48), which penetrated the CL walls by 55 mm. The ground-floor frame was connected to the masonry by 2 screws along its bottom side and 2 screws per vertical side, spaced at 100 cm (Figure 45 b). The gable window had 2 screws on each vertical side, spaced at 55 cm (Figure 47 a). Cover plates, connected to each other by screws but mechanically disconnected from the masonry, completed the window frames. Finally, a 6-mm-thick layered anti-burst glass, with dimensions of 88 x 185 cm, was installed on the southern shutter of the ground-floor window as shown in Figure 45 c.



Figure 45 Ground-floor window frame external views: a) during construction, without side cover plates; b) screw locations; c) at the end of construction, with side cover plates and glass.



a)



b)

Figure 46 Ground-floor window frame internal views: a) during construction, without side cover plates; b) at the end of construction, with side cover plates.



a)



b)

Figure 47 North gable window frame: a) internal view with screw locations; b) external view.

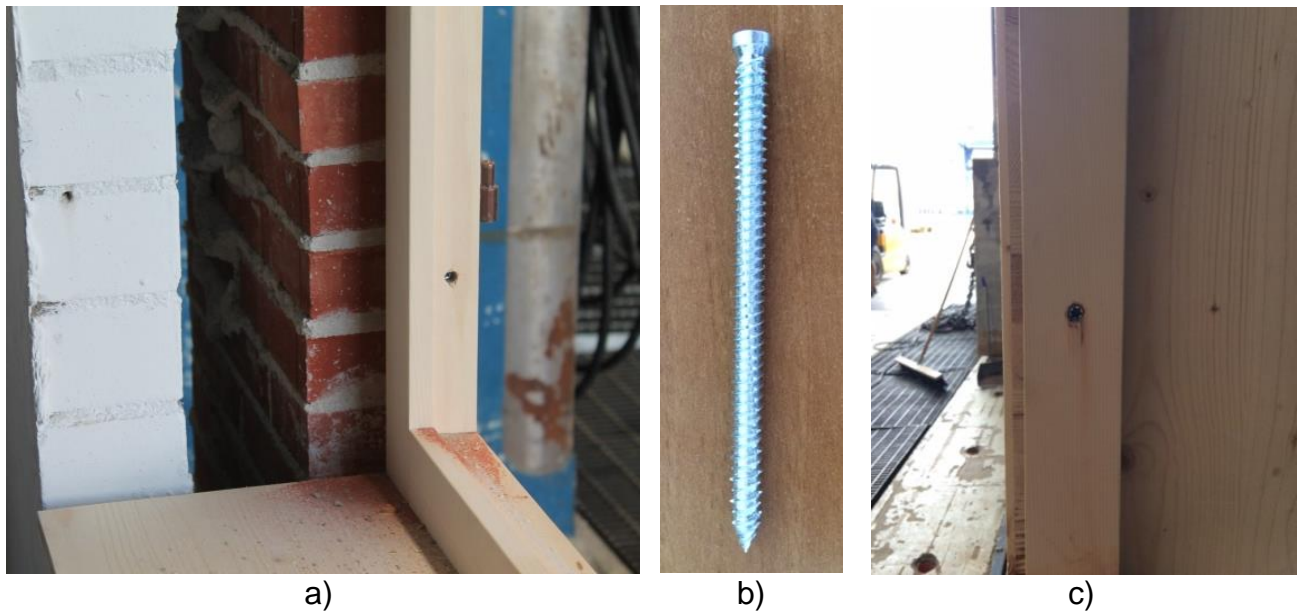


Figure 48 Window frame-to-clay masonry leaf connections: a) during construction, without side cover plates; b) screw; c) at the end of construction, with side cover plates.

1.3 Prototype masses

The prototype total mass was 47.5 t. To calculate this value, the density of calcium-silicate masonry was taken equal to 1837 kg/m^3 , the one of clay masonry equal to 1967 kg/m^3 , and the one of timber equal to 480 kg/m^3 .

The total value of 47.5 t includes an additional mass of 1.2 t which was added to the second-floor diaphragm by 48 mortar bags (25 kg each), representing superimposed dead and live loads. The bag distribution is shown in Figure 49: 16 bags were placed on the centre line of the floor, 16 along the East line, and 16 along the West line.

Table 1 specifies the masses of each structural element.

Table 1 Prototype mass breakdown.

Side	CS wall [t]	CL wall [t]	1 st floor [t]	2 nd floor [t]	Roof [t]
North	6.0	7.1	11.2	1.90 (0.7 timber + 1.2 additional mass)	2.77 (0.70 timber + 2.07 tiles)
South	6.2	-			
West	2.8	3.4			
East	2.7	3.4			

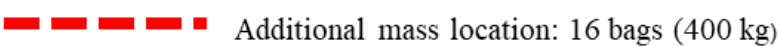


Figure 49 Position of the additional masses. Units of cm.

2. MECHANICAL PROPERTIES OF MATERIALS

The experimental campaign included characterization tests to determine the mechanical properties of the materials employed for the construction of the specimen, similar to those performed by [1] and [2]. It comprised bending and compression tests on bricks and mortar samples, as well as compression, bond wrench, direct shear, and torsion tests on small masonry assemblages.

Calcium silicate (CS) and clay (CL) bricks were tested in compression according to EN 772-1 (2011) [3] and bending, to obtain their compressive (f_b) and tensile (f_{bt}) strengths. The tensile (f_t) and compressive (f_c) strengths of the two corresponding types of mortar were determined according to the prescriptions of EN 1015-11 (2006) [4].

Seven masonry wallettes made of CS and CL bricks were tested in compression in the direction perpendicular to the horizontal bed-joints, according to EN 1052-1 (1998) [5]; these tests allowed the determination of the masonry compressive strength (f_m), as well as the masonry secant elastic modulus at 33% of its compressive strength (E_m). Bond wrench tests on twenty CS and twenty CL masonry samples were performed in order to determine the bond strength of masonry, according to EN 1052-5 (2005) [6]. Specimens of both types of masonry were also subjected to the shear test for the determination of the initial shear strength (f_{vo}) and the friction coefficient (μ), according to the guidelines given by EN 1052-3 (2007) [7]. Additional tests were carried out to characterize the torsional strengths of both types of masonry.

A series of wallettes of both types of masonry was also built for future tests to evaluate the horizontal out-of-plane flexural strength.

The materials characterization tests were performed on specimens that reached 28 days of maturation.

2.1 Tensile and compressive strength of masonry units

2.1.1 Test procedure

The mechanical properties of calcium silicate and clay bricks were evaluated by compressive and flexural tests in accordance with EN 772-1 [3] at the laboratory of the Department of Civil Engineering and Architecture (DICAr) of the University of Pavia. Figure 50 shows the brick dimensions. The X axis is parallel to the intermediate side, the Y axis to the shortest one, and the Z axis to the longest one. Four series of test were performed:

- Compression test on 6 CS bricks in the Y direction (Figure 51 a);
- Compression test on 6 CL bricks in the Y direction (Figure 51 b);
- Flexural test on 6 CS bricks loaded in the Y direction (Figure 52 a) and on 6 CS bricks loaded in the X direction (Figure 52 b);
- Flexural test on 6 CL bricks loaded in the Y direction (Figure 52 c) and on 6 CL bricks loaded in the X direction (Figure 52 d).

The brick compressive strength (f_b) was computed as:

$$f_b = \frac{F}{B \cdot L} \quad [\text{MPa}]$$

where:

- F is the maximum load applied to the specimen (N);
- B is the X-dimension of the specimen (102 mm for CS bricks and 100 mm for clay bricks);
- L is the Z-dimension of the specimen (212 mm for CS bricks and 210 mm for clay bricks).



Figure 50 Brick dimensions: a) calcium silicate; b) clay.

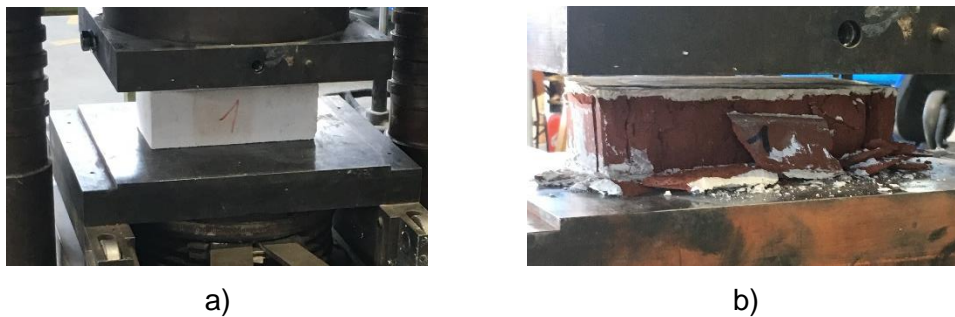


Figure 51 Compressive test on bricks in the Y direction: a) calcium silicate; b) clay.

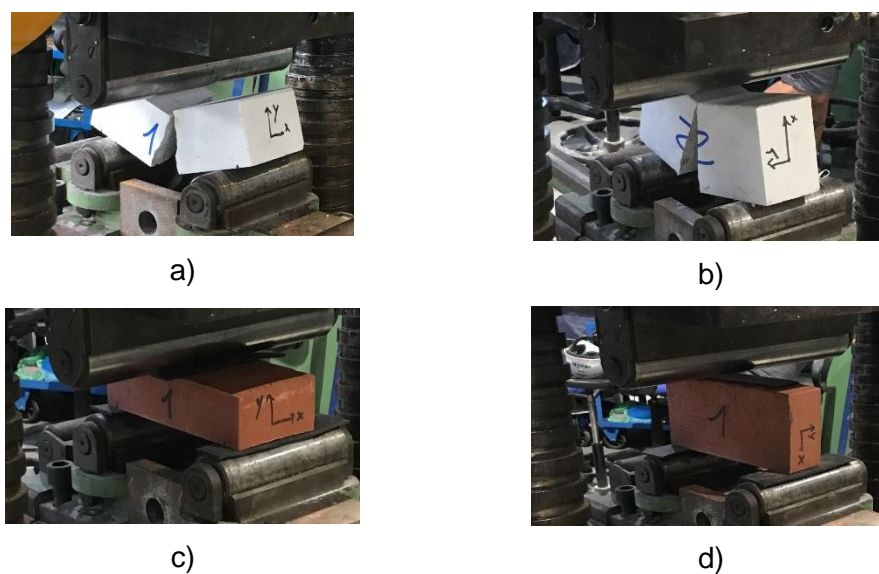


Figure 52 Flexural test on bricks: a) CS loaded in the Y direction; b) CS loaded in the X direction; c) CL loaded in the Y direction; d) CL loaded in the X direction.

The brick tensile strengths were computed from the three-point flexural test in the Y direction ($f_{bt,y}$) and in the X direction ($f_{bt,x}$) as:

$$f_{bt,y} = 1.5 \cdot \frac{F \cdot d}{B \cdot H^2} \quad [\text{MPa}]$$

$$f_{bt,x} = 1.5 \cdot \frac{F \cdot d}{H \cdot B^2} \quad [\text{MPa}]$$

where:

- F is the maximum load applied to the specimen (N);
- d is the distance between the supporting rollers (172 mm);
- B is the X-dimension of the specimen (102 mm for CS bricks and 100 mm for CL bricks);
- H is the Y-dimension of the specimen (71 mm for CS bricks and 50 mm for CL bricks).

2.1.2 Test results

Table 2 and Table 3 summarize the test results in terms of compressive and tensile strengths for CS and CL bricks. Results are graphically represented in Figure 53 and Figure 54.

Table 2 Compressive strength of bricks.

Specimen	CS	CL
	f_b [MPa]	f_b [MPa]
1	18.06	56.06
2	25.18	53.44
3	19.28	51.01
4	19.51	42.04
5	22.00	51.76
6	14.83	45.87
Average	19.81	50.03
St. Dev.	3.52	5.16
C.o.V.	0.18	0.10

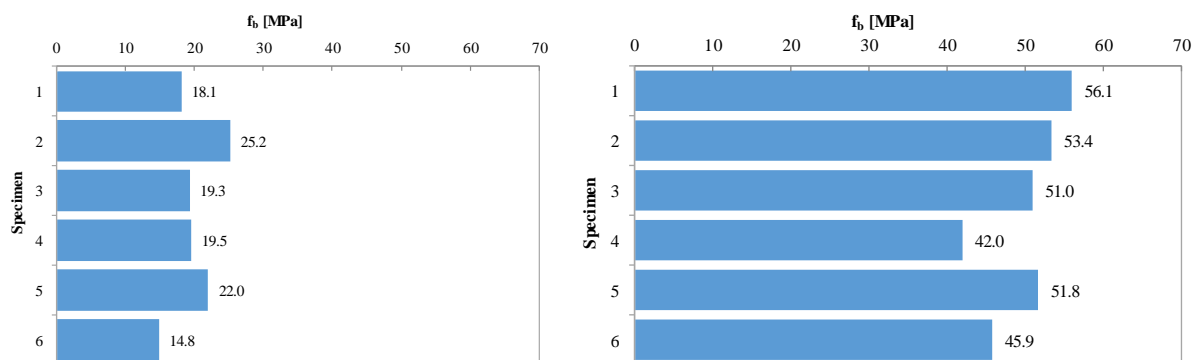
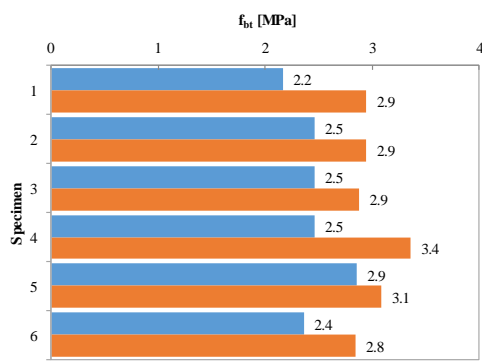


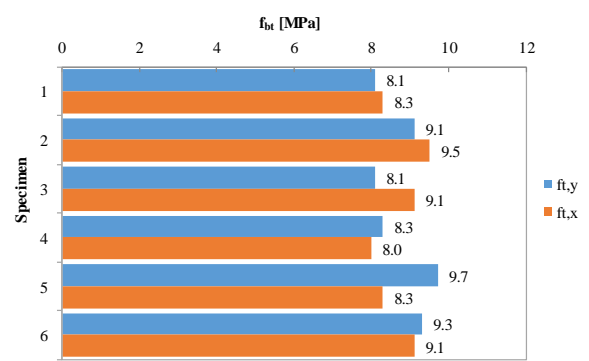
Figure 53 Compressive strength of bricks: a) calcium silicate; b) clay.

Table 3 Flexural strength of bricks loaded in the X and Y directions.

Specimen	CS		CL	
	$f_{bt,y}$ [MPa]	$f_{bt,x}$ [MPa]	$f_{bt,y}$ [MPa]	$f_{bt,x}$ [MPa]
1	2.17	2.95	8.10	8.30
2	2.46	2.95	9.11	9.52
3	2.46	2.88	8.10	9.11
4	2.46	3.36	8.30	8.00
5	2.85	3.08	9.72	8.30
6	2.36	2.84	9.31	9.11
Average	2.46	3.01	8.77	8.72
St. Dev.	0.22	0.19	0.70	0.60
C.o.V.	0.09	0.06	0.08	0.07



a)



b)

Figure 54 Flexural strength of bricks in the X and Y direction: a) calcium silicate; b) clay.

2.2 Tensile and compressive strength of mortar

The mortar used for CS masonry differs from the one used for CL masonry: the pre-mixed material (Figure 55), the water ratio, and the additional sand proportion are not the same.

Table 5 shows the two mortar mix designs referred to one bag of pre-mixed product. Sand was added only to the mortar for CS masonry, with the objective of reducing its strength to values more compatible with existing structures from the 1970s.

2.2.1 Test procedure

The mechanical properties of mortar are fundamental to evaluate the overall behaviour of masonry structural elements. Hence, the mortar used to build both the full-scale prototype building and the companion characterization specimens was tested in order to define its flexural and compressive strength.

The tests were performed in accordance with EN 1015-11 [4] at the laboratory of the Department of Civil Engineering and Architecture (DICAr) of the University of Pavia. Prismatic test specimens with dimensions 160 x 40 x 40 mm were cast in moulds with three slots (Figure 56), and were closed in plastic bags for 48 hours. After 48 hours, the specimens were extracted from the moulds and placed again in plastic bags for 5 other days. Finally, they were removed from the bags and left in ambient atmosphere until they reached the age of 28 days.

Each specimen was first tested in three-point bending, and the two resulting stubs were subsequently tested in compression. Consequently, each sample of three specimens yielded three values of tensile strength and three average values of compressive strength.

Figure 57 shows the bending test setup, where the transverse load was applied with a constant velocity within 100 N/s and 50 N/s, in order to obtain failure after about 30÷90 seconds [4]. The compressive load was instead applied at a constant velocity within 50 N/s and 500 N/s, in order to reach failure after about 30÷90 seconds [4].



Figure 55 Pre-mixed mortar bags: a) for CS masonry; b) for CL masonry.

Table 4 Mortar mix design.

	Dry mortar (M)		Water (W)		Sand (S)		W/M		S/M	
	[kg]	[lt]	[kg]	[lt]	[kg]	[lt]	Weight	Volume	Weight	Volume
Mortar for CS masonry	25	13.5	3.5	3.5	3.25	2.2	14%	26%	13%	16%
Mortar for CL masonry	25	15.7	3.4	3.4	0	0	14%	22%	0	0

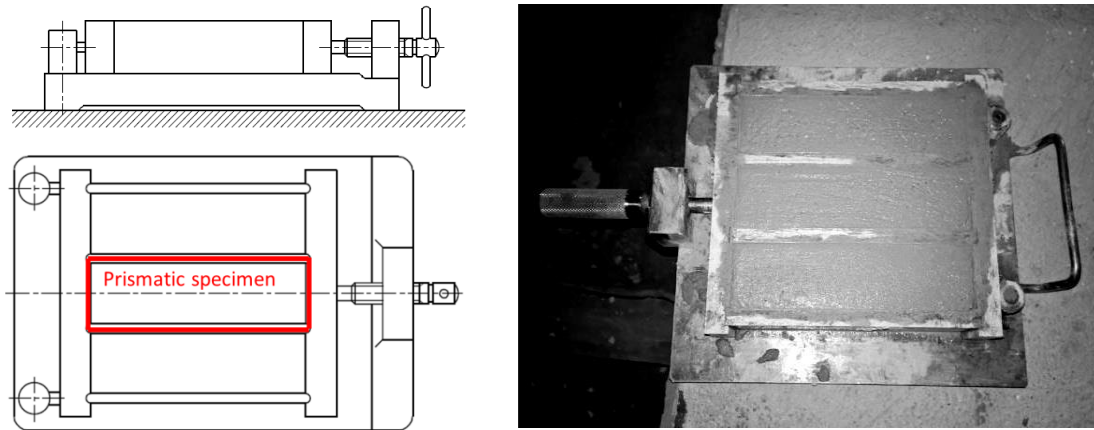


Figure 56 Mould for the mortar specimens.

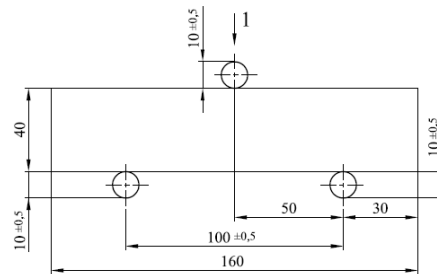


Figure 57 Setup of the mortar three-point bending test.

The mortar flexural strength (f_t) was computed as:

$$f_t = 1.5 \cdot \frac{F \cdot d}{B \cdot H^2} \quad [\text{MPa}]$$

where:

- F is the maximum load applied to the specimen (N);
- d is the distance between the rollers (100 mm);
- B is the width of the specimen (40 mm);
- H is the depth of the specimen (40 mm).

The mortar compressive strength (f_c) was computed as:

$$f_c = \frac{F}{a^2} \quad [\text{MPa}]$$

where:

- F is the maximum load applied to the specimen (N);
- a is the size of the square contact area of the test setup (40 mm);

2.2.2 Test results

Table 5 and Table 6 show the tests results on mortar specimens after 28 days of maturation; following them, results are graphically displayed from Figure 58 to Figure 61.

Table 5 Test results for mortar for CS masonry.

Sample	Cast date	Test date	Age [days]	f_t [MPa]	f_c [MPa]
1	05/04/2018	03/05/2018	28	2.12	5.77
				2.16	5.68
				1.79	5.10
2	06/04/2018	04/05/2018	28	2.16	6.05
				2.21	5.30
				2.21	4.72
3	06/04/2018	04/05/2018	28	1.98	4.89
				2.16	5.92
				1.75	4.54
4	10/04/2018	08/05/2018	28	1.43	3.46
				0.97	5.73
				0.41	3.73
5	11/04/2018	09/05/2018	28	1.43	7.60
				1.89	6.93
				1.93	7.46
6	11/04/2018	09/05/2018	28	1.75	4.92
				1.79	4.89
				2.12	5.21
7	12/04/2018	10/05/2018	28	1.45	5.17
				1.52	3.95
				1.52	4.80
8	12/04/2018	10/05/2018	28	0.78	3.23
				0.87	2.46
				1.24	3.35
9	13/04/2018	11/05/2018	28	1.06	3.05
				1.20	3.79
				1.06	3.54
10	13/04/2018	11/05/2018	28	0.92	2.58
				1.01	3.53
				1.24	2.82
11	16/04/2018	14/05/2018	28	2.67	5.26
				2.48	5.30
				1.98	4.42
12	16/04/2018	14/05/2018	28	1.52	4.80
				1.61	4.51
				1.24	4.46
13	18/04/2018	16/05/2018	28	2.58	7.17
				2.30	6.01
				2.35	5.69

Sample	Cast date	Test date	Age [days]	f_t [MPa]	f_c [MPa]
14	23/04/2018	21/05/2018	28	1.61	4.79
				1.93	5.35
				2.02	4.51
15	23/04/2018	21/05/2018	28	1.15	3.63
				1.20	3.75
				1.29	3.38
16	24/04/2018	22/05/2018	28	2.25	5.38
				2.18	5.98
				2.25	5.11
17	02/05/2018	30/05/2018	28	1.98	4.89
				2.12	5.13
				2.14	5.44
18	03/05/2018	30/05/2018	28	1.56	5.18
				1.89	5.35
				2.02	5.27
19	03/05/2018	01/06/2018	29	2.25	7.11
				2.21	7.48
				2.12	6.62
20	04/05/2018	01/06/2018	28	1.93	6.30
				1.84	6.62
				1.89	6.70
21	04/05/2018	01/06/2018	28	1.75	5.64
				1.47	5.64
				1.61	5.53
Average				1.74	5.06
St. Dev.				0.49	1.24
C.o.V.				0.28	0.24

Table 6 Test results for mortar for CL masonry.

Sample	Cast date	Test date	Age [days]	f_t [MPa]	f_c [MPa]
1	16/04/2018	14/05/2018	28	0.92	3.68
				0.97	3.53
				1.06	4.19
2	17/04/2018	16/05/2018	29	1.06	2.96
				0.97	3.52
				0.97	3.08
3	17/04/2018	16/05/2018	29	0.46	1.39
				0.46	1.31
				0.55	1.39
4	18/04/2018	16/05/2018	28	0.28	1.47
				0.64	1.50
				0.69	1.48
5	19/04/2018	17/05/2018	28	0.46	1.42
				0.55	1.33
				0.41	1.23
6	19/04/2018	17/05/2018	28	0.28	1.28
				0.32	1.24
				0.32	1.35
7	20/04/2018	18/05/2018	28	0.87	3.42
				1.10	3.42
				1.06	3.46
8	20/04/2018	18/05/2018	28	0.18	1.14
				0.14	1.12
				0.25	1.28
9	24/04/2018	22/05/2018	28	0.37	2.31
				0.78	2.39
				0.60	2.07
10	26/04/2018	24/05/2018	28	0.41	0.67
				0.37	0.46
				0.09	0.56
11	26/04/2018	24/05/2018	28	0.46	1.87
				0.51	1.71
				0.46	1.78
12	27/04/2018	28/05/2018	31	1.24	2.79
				1.20	2.89
				1.24	2.73
13	27/04/2018	28/05/2018	31	0.41	1.12
				0.41	1.10
				0.37	1.10

Sample	Cast date	Test date	Age [days]	f_t [MPa]	f_c [MPa]
14	02/05/2018	30/05/2018	28	1.15	3.76
				1.33	3.66
				0.97	2.96
15	05/05/2018	04/06/2018	30	1.15	3.26
				1.20	2.63
				0.83	2.77
16	05/05/2018	04/06/2018	30	1.29	3.53
				1.43	4.09
				1.15	4.22
17	07/05/2018	04/06/2018	28	1.01	3.94
				1.20	3.79
				0.97	3.77
18	07/05/2018	04/06/2018	28	0.69	2.77
				1.15	3.18
				0.78	3.19
Average				0.74	2.38
St. Dev.				0.37	1.11
C.o.V.				0.50	0.47

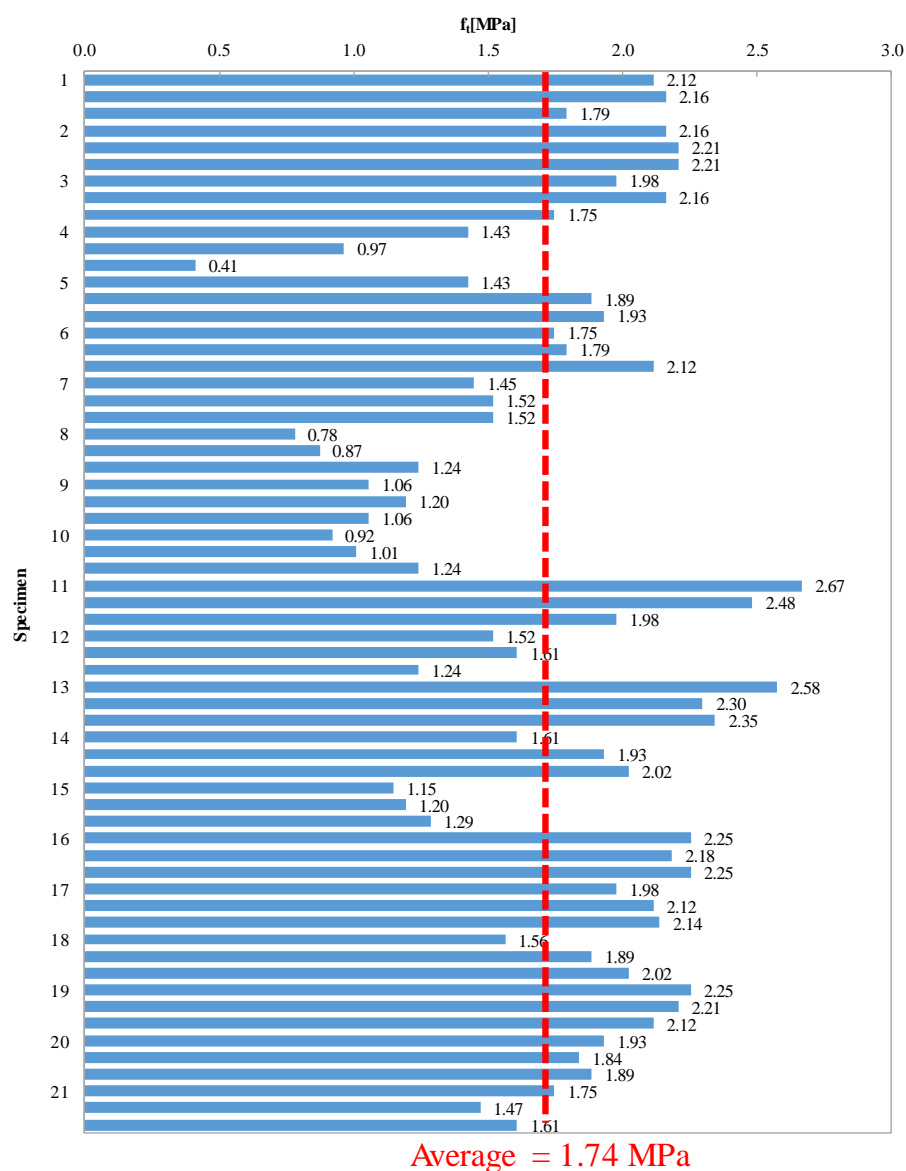


Figure 58 Tensile strength of mortar for CS masonry.

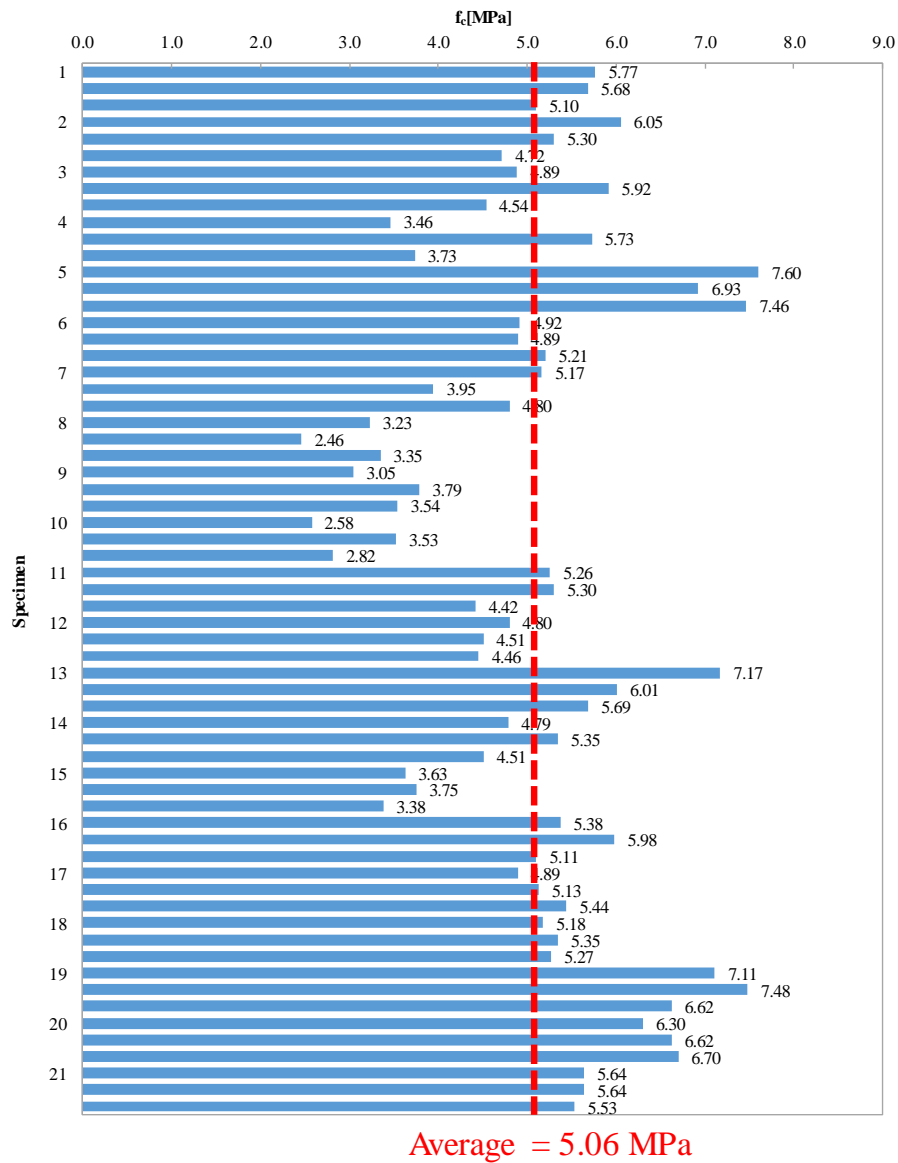


Figure 59 Compressive strength of mortar for CS masonry.

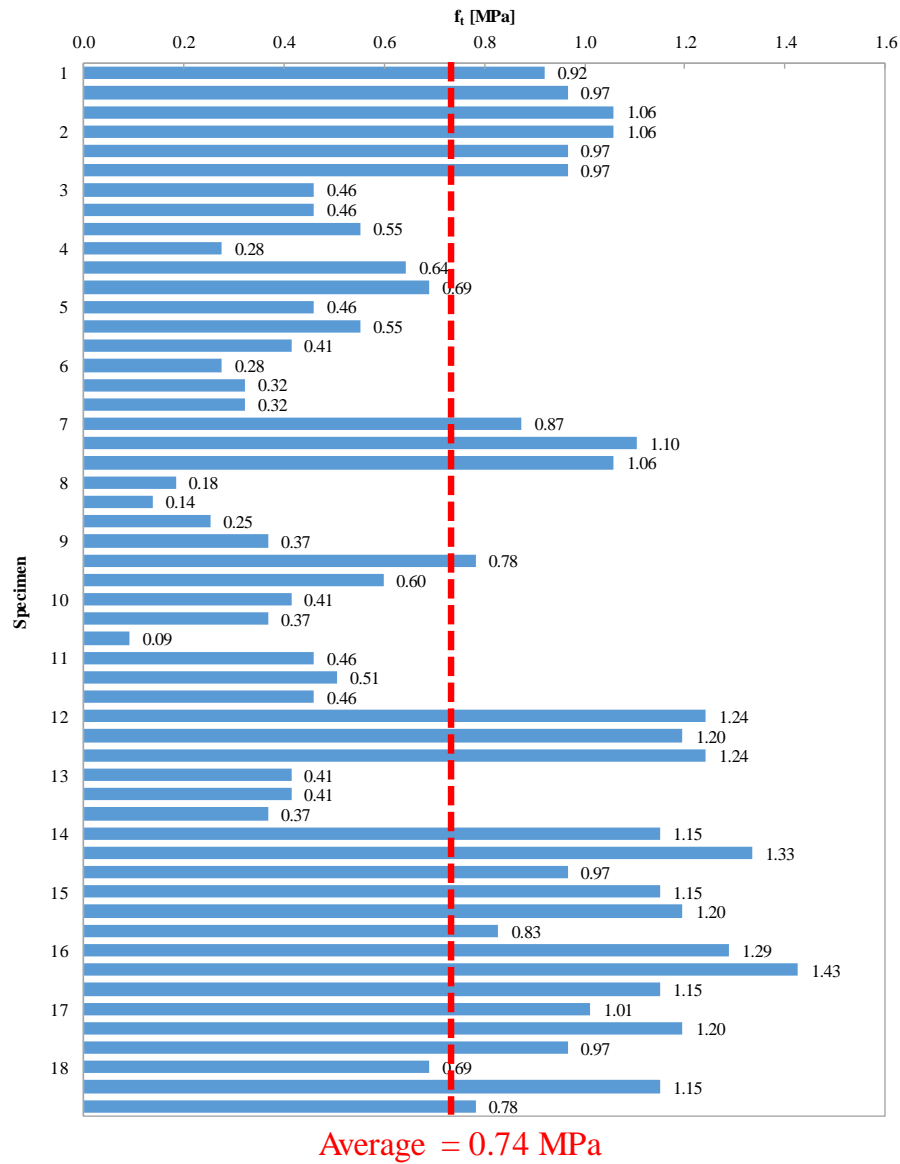


Figure 60 Tensile strength of mortar for CL masonry.

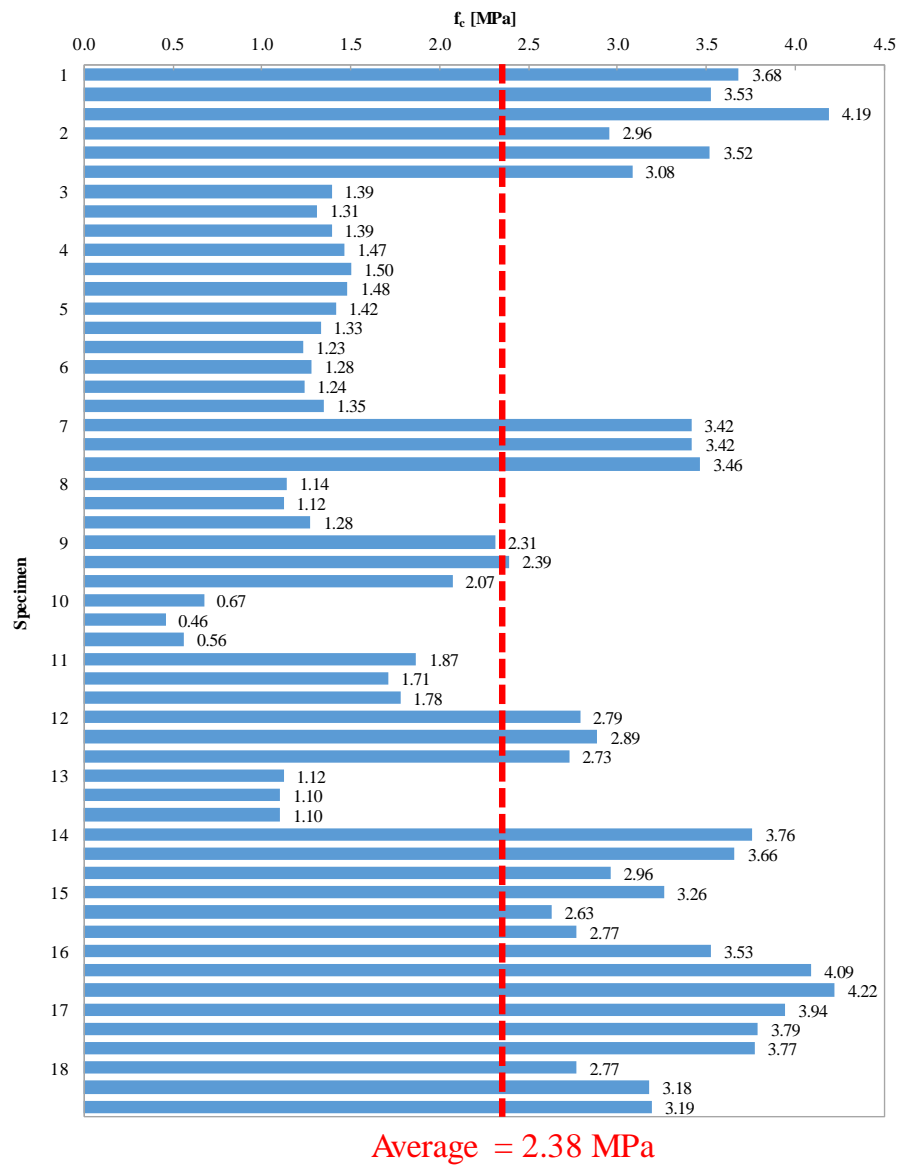


Figure 61 Compressive strength of mortar for CL masonry.

2.3 Compressive strength of masonry

2.3.1 Test procedure

The tests were performed in accordance with EN 1052-1 [5] at the laboratory of the Department of Civil Engineering and Architecture (DICAr) of the University of Pavia. The specimens were made with the same materials used to build the full-scale prototype; the compressive strength refers to the direction perpendicular to specimens bed-joints. Two series of axial compression test were performed:

- 6 CS wallettes (Figure 62);
- 6 CL wallettes (Figure 63).

The specimen dimensions were chosen according to the EN-1052-1 [5] prescriptions (section 7.1). The instrumentation on the front-side of the CS masonry wallettes included: two vertical potentiometers of length equal to 243 mm, spaced at 333 mm, and one 298-mm-long horizontal potentiometer, located at mid-height of the fourth layer of bricks. Similar instrumentation was applied to the back side: two vertical potentiometers with length equal to 243 mm, spaced at 333 mm and one 298 mm long horizontal potentiometer at the mid-height of the third layer of bricks (Figure 62).

The CL masonry wallettes were instrumented on the front side with two vertical potentiometers of length equal to 300 mm, spaced at 330 mm, and one 300 mm long horizontal potentiometer at the mid-height of the fifth layer of bricks. On the back side two vertical potentiometers of length equal to 300 mm, spaced at 330 mm, and one 300 mm long horizontal potentiometer at the mid-height of the fourth layer of bricks (Figure 63) were installed.

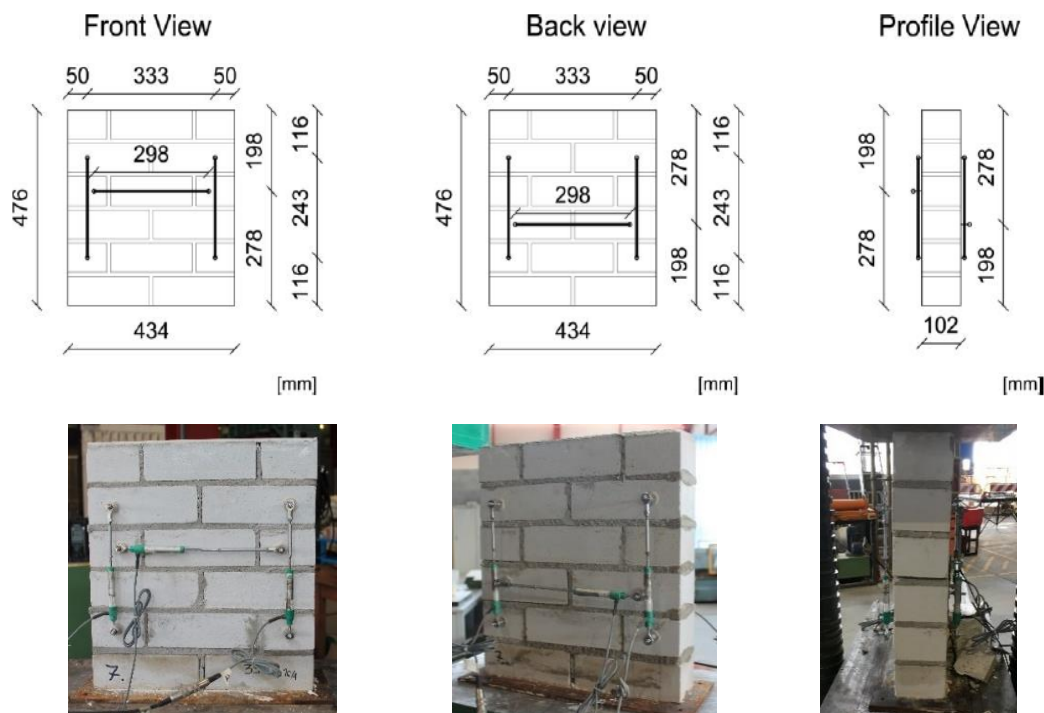


Figure 62 Geometry and instrumentation of test specimen, CS wallettes

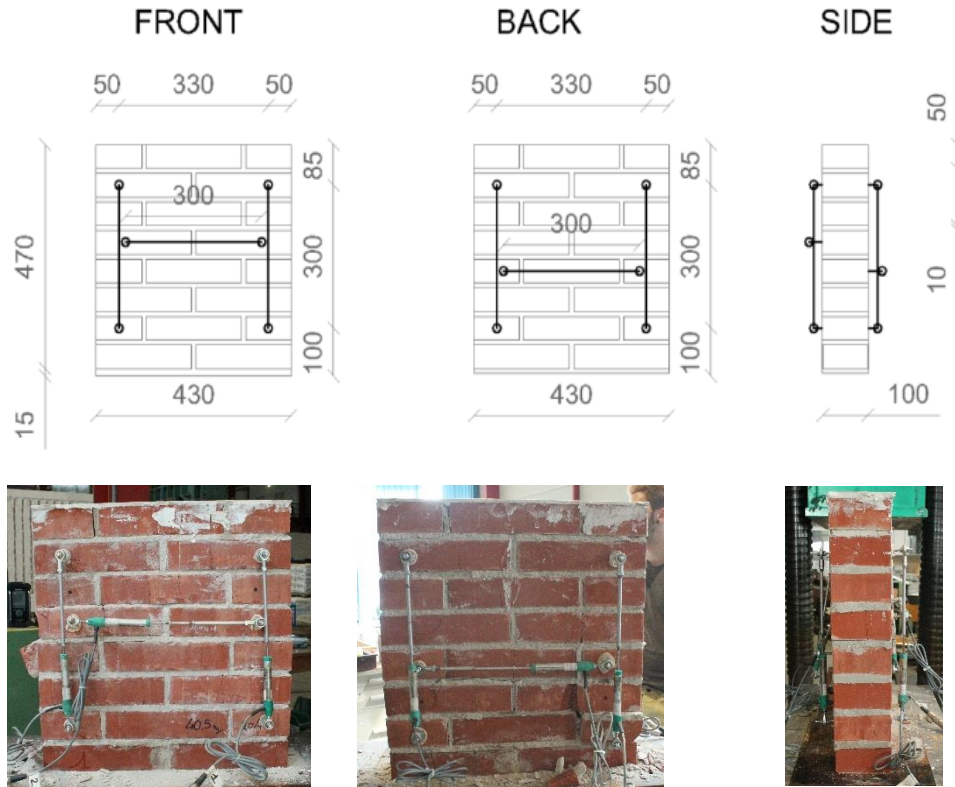


Figure 63 Geometry and instrumentation of test specimen, CL wallettes.

The test aimed at reaching failure of the specimens by means of a vertical axial compression load. The loading protocol consisted of three series of three cycles of loading and unloading at equal maximum force (Figure 64). After the three series, the specimen was monotonically brought to failure, if not yet occurred. The loading velocity was kept constant and consistent with the prescriptions [5].

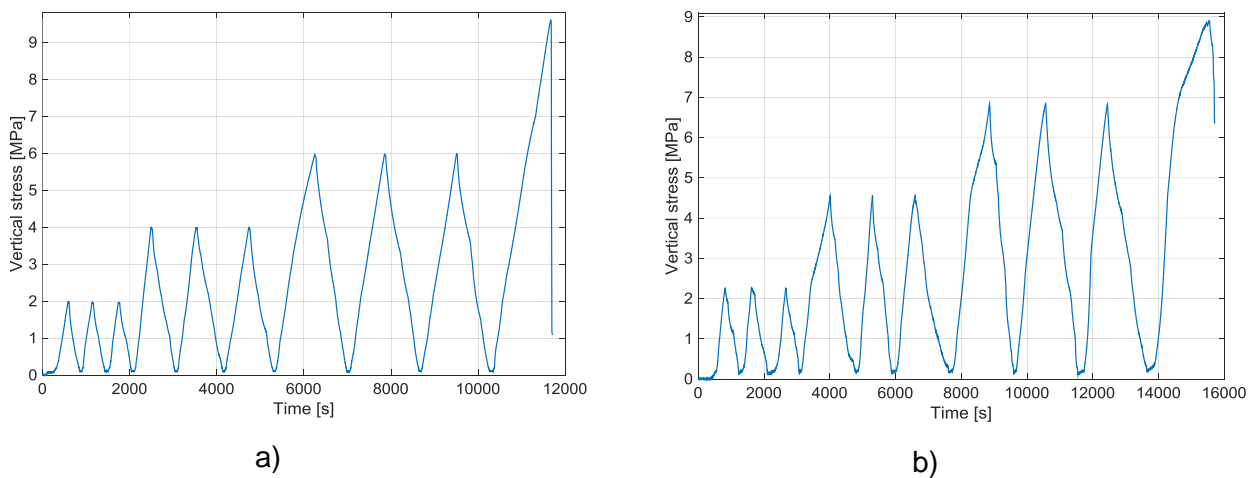


Figure 64 Example of loading history used for the axial compression test on: a) CS masonry wallettes; b) CL masonry wallettes.

The vertical and horizontal deformations were obtained averaging the displacements (normalised by the gauge length) recorded by each vertical and horizontal potentiometer. In particular, the vertical deformation was obtained averaging the readings of vertical potentiometers 0-1-3-4, while the horizontal deformation was obtained averaging the measurements of horizontal potentiometers 2 and 5.

The Young modulus (E_m) was taken as the secant elastic modulus through the point at 33% of the recorded compressive strength (f_m) and the origin (0,0).

2.3.2 Test results

The recorded displacement time histories and stress-strain curves are reported for each compression test in the following figures. For both materials, the first tested specimen served as calibration for the following ones.

Focusing on the CS wallettes (from Figure 65 to Figure 71), it can be seen that all the specimens behave similarly, with small accumulation of residual deformation in each cycle and similar values of compressive strength. The same conclusions cannot be extended to the clay specimens, which showed mainly two different behaviours (from Figure 72 to Figure 78). Excluding the first specimen, the results obtained for CL_2 and CL_3 are significantly higher than the other ones, showing a very small accumulation of deformation. By correlating such information with the characterization tests of mortar, it was found that the mortar cast in the afternoon of the CL specimens construction day had worse mechanical properties compared to the one cast in the morning (Figure 61). In light of this observation, the results of CL_2 and CL_3 are presented separately (Table 8 and Figure 83). Moreover, referring to Figure 61, also other mortar specimens showed lower compressive strengths compared to the average (specimens #3, 4, 5, 6, 8, 10 and 13). The prototype portions built with those mortars are highlighted in Figure 79 through Figure 81.

Table 7 through Table 10 summarize the compressive strength (f_m) and the Young's modulus (E_m) of each specimen.

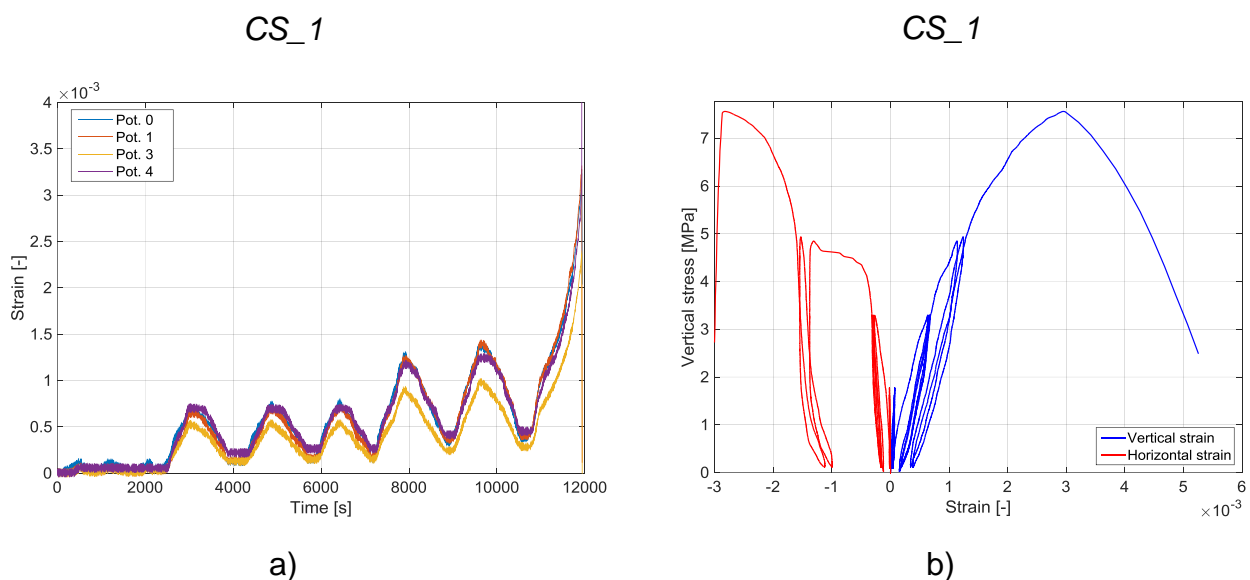


Figure 65 CS_1 compression test results: a) vertical strain time histories; b) vertical stress vs. vertical and horizontal strains.

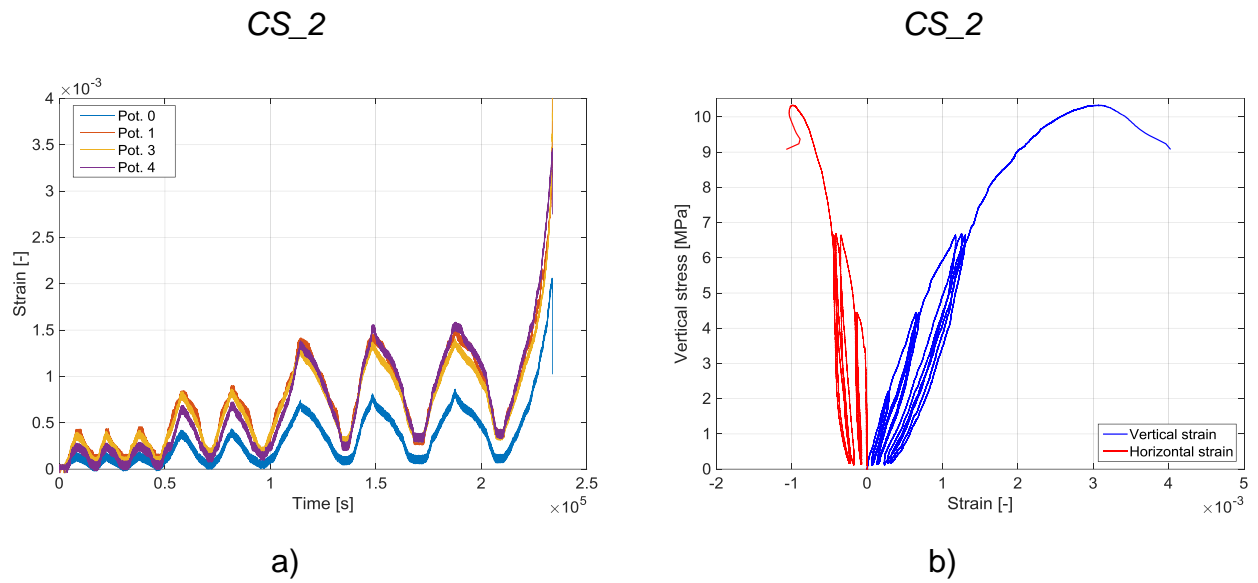


Figure 66 CS_2 compression test results: a) vertical strain time histories; b) vertical stress vs. vertical and horizontal strains.

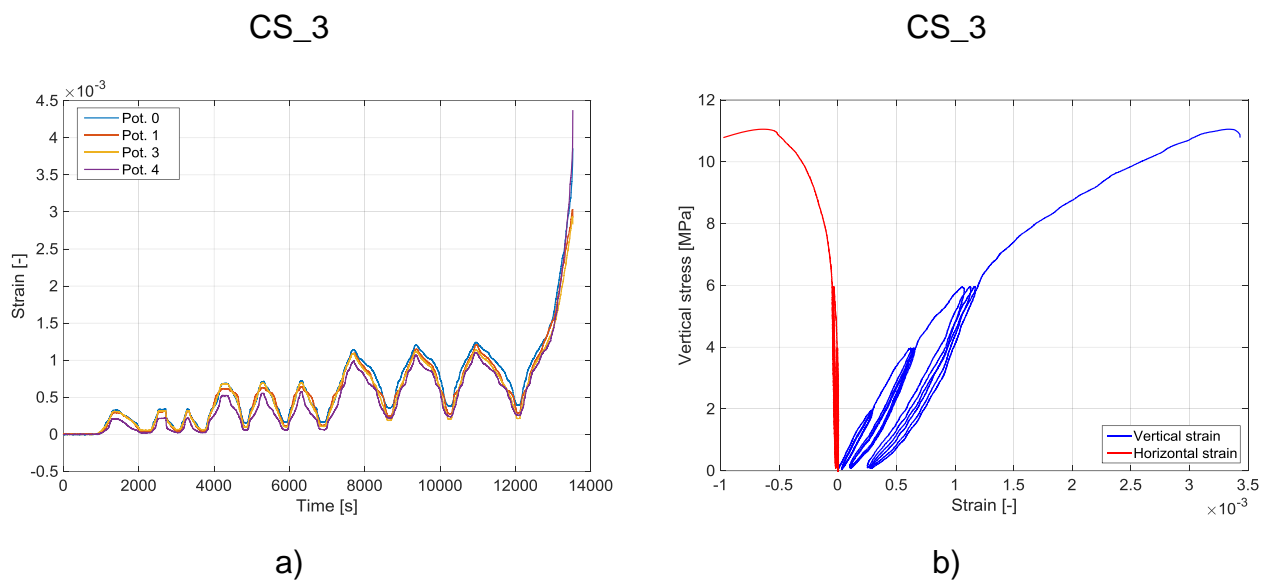
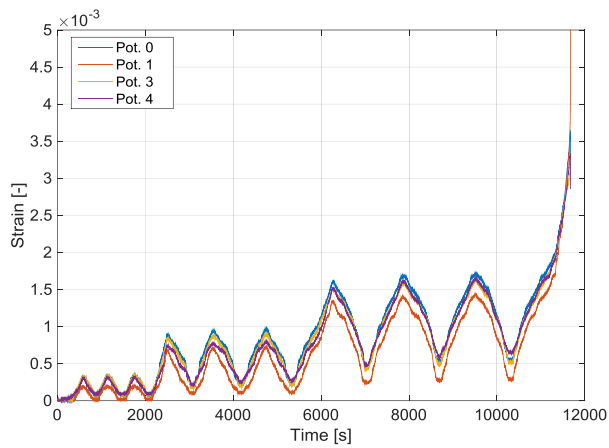


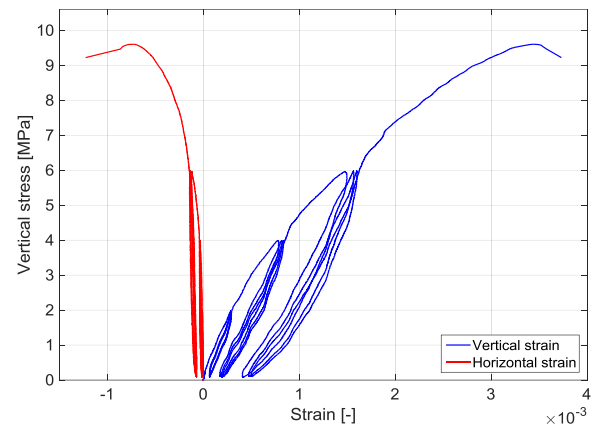
Figure 67 CS_3 compression test results: a) vertical strain time histories; b) vertical stress vs. vertical and horizontal strains.

CS_4



a)

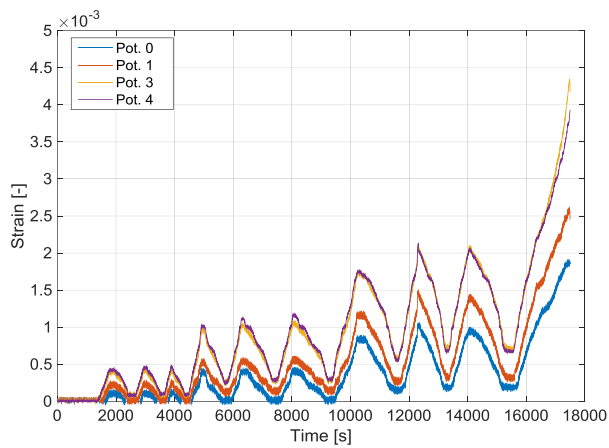
CS_4



b)

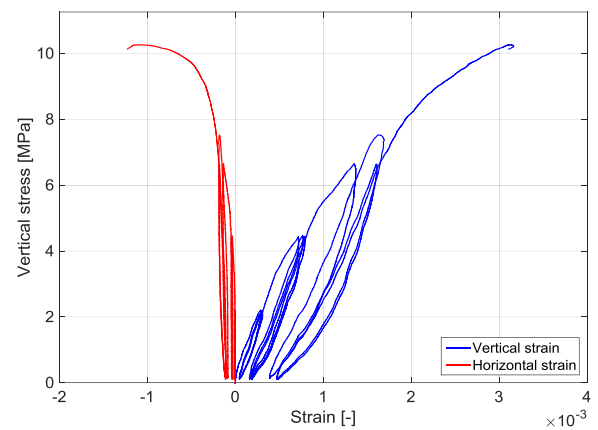
Figure 68 CS_4 compression test results: a) vertical strain time histories; b) vertical stress vs. vertical and horizontal strains.

CS_5



a)

CS_5



b)

Figure 69 CS_5 compression test results: a) vertical strain time histories; b) vertical stress vs. vertical and horizontal strains.

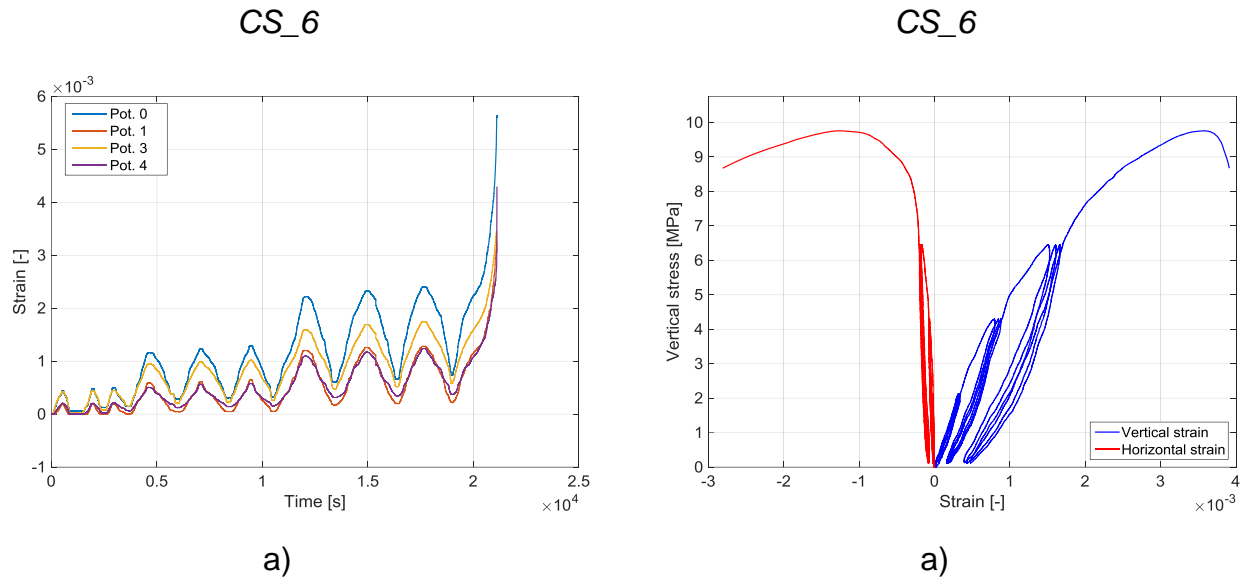


Figure 70 CS_6 compression test results: a) vertical strain time histories; b) vertical stress vs. vertical and horizontal strains.

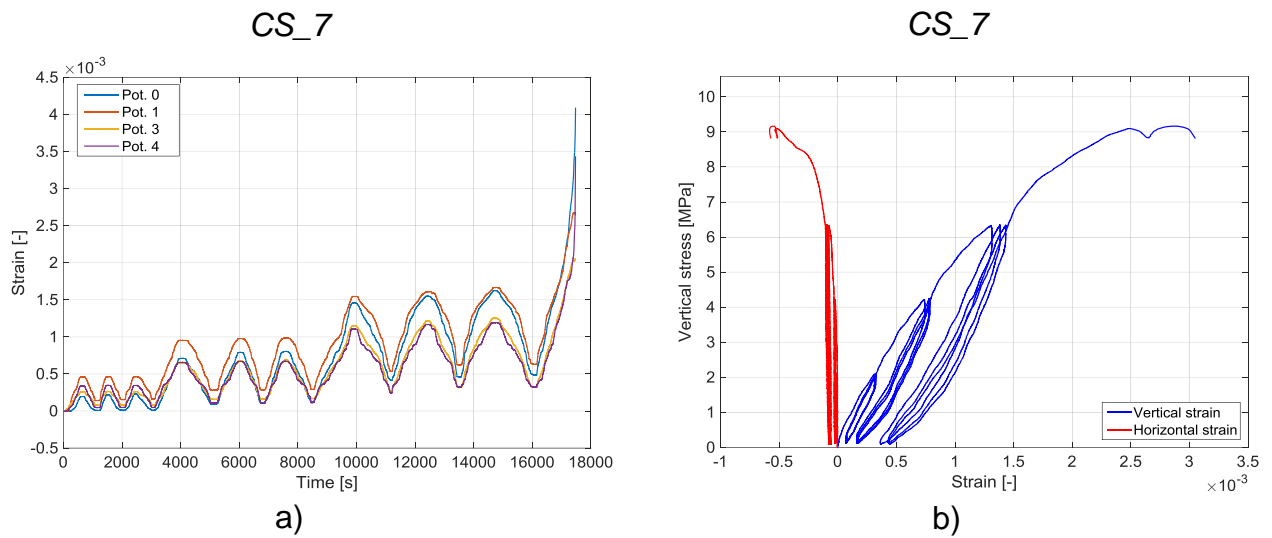
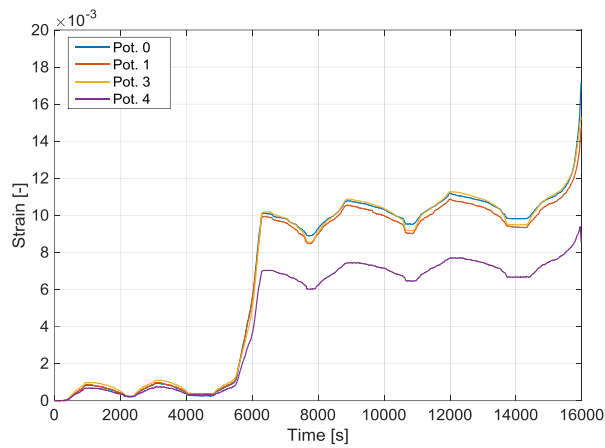


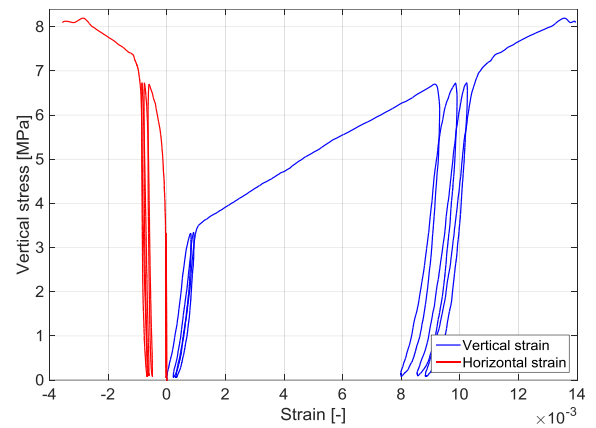
Figure 71 CS_7 compression test results: a) vertical strain time histories; b) vertical stress vs. vertical and horizontal strains.

CL_1



a)

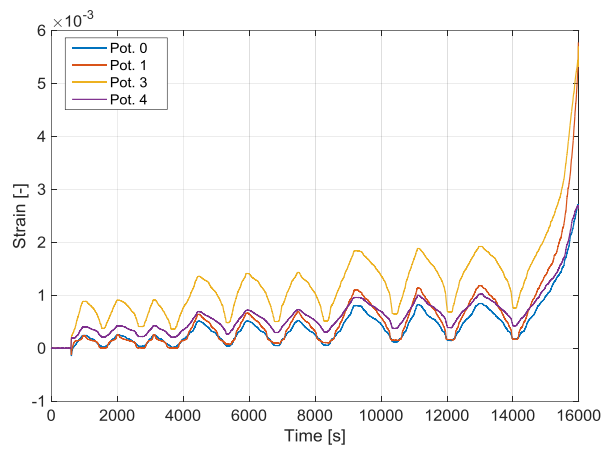
CL_1



b)

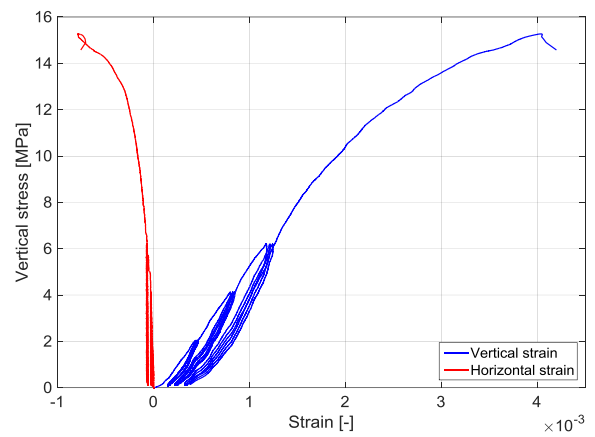
Figure 72 CL_1 compression test results: a) vertical strain time histories; b) vertical stress vs. vertical and horizontal strains.

CL_2



a)

CL_2



b)

Figure 73 CL_2 compression test results: a) vertical strain time histories; b) vertical stress vs. vertical and horizontal strains.

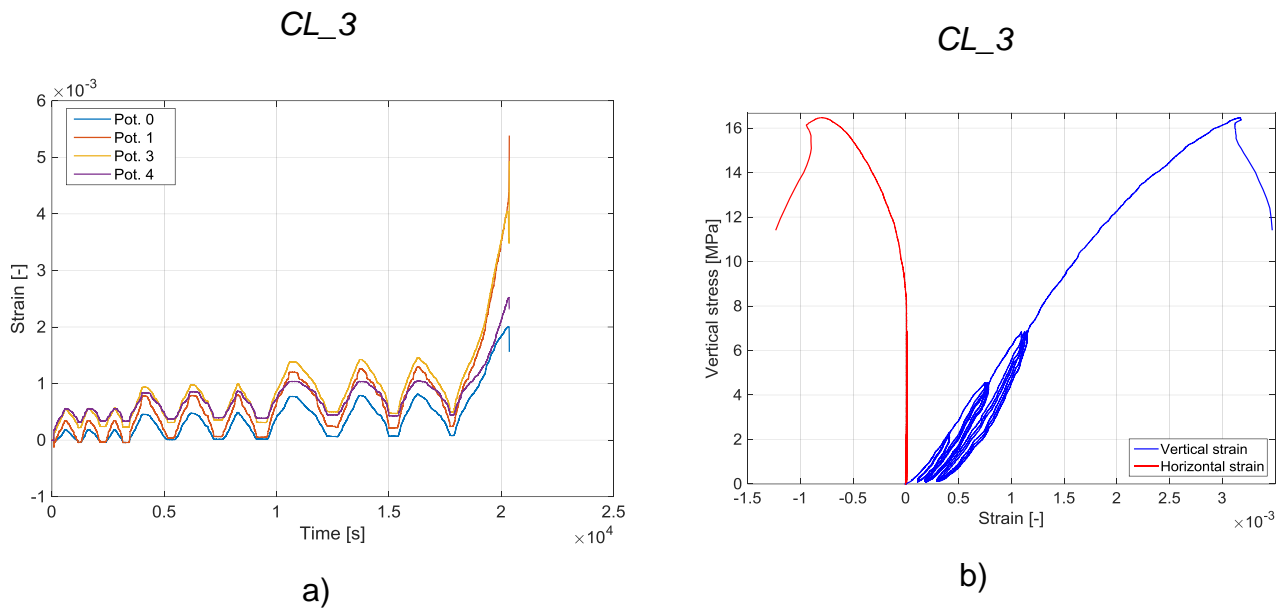


Figure 74 CL_3 compression test results: a) vertical strain time histories; b) vertical stress vs. vertical and horizontal strains.

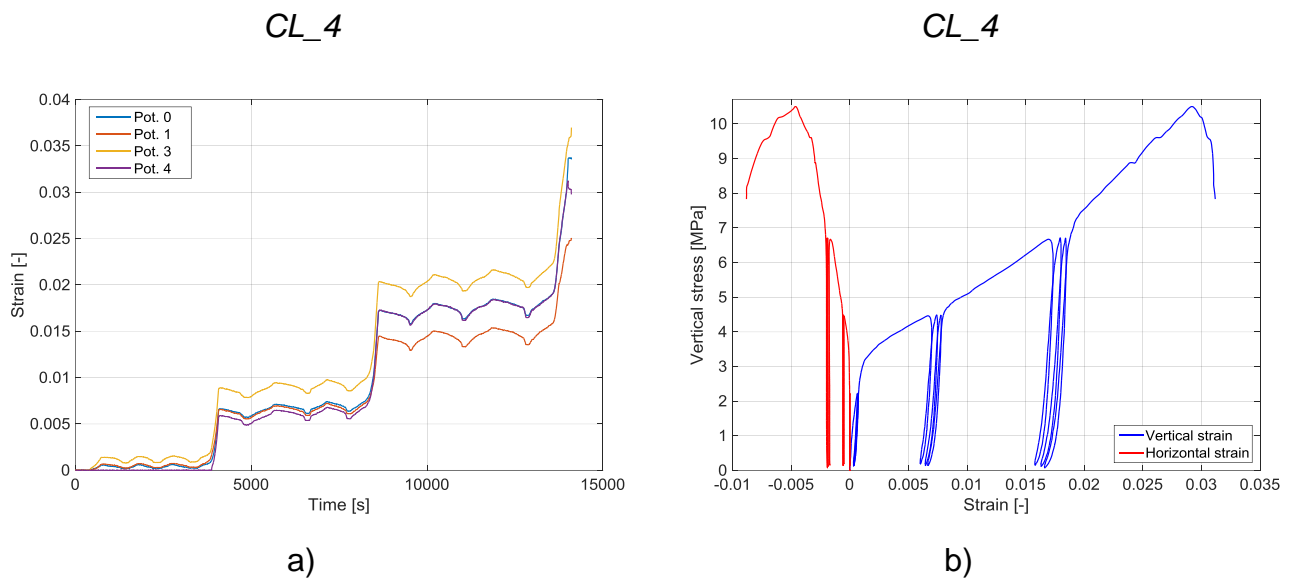
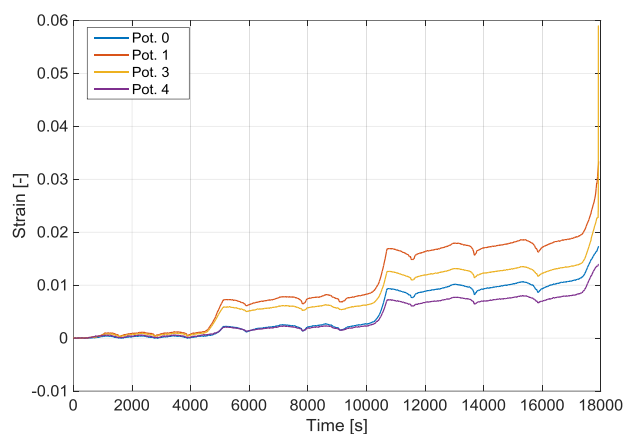


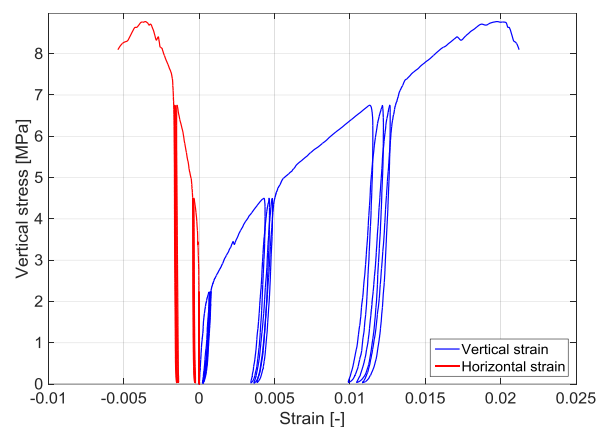
Figure 75 CL_4 compression test results: a) vertical strain time histories; b) vertical stress vs. vertical and horizontal strains.

CL_5



a)

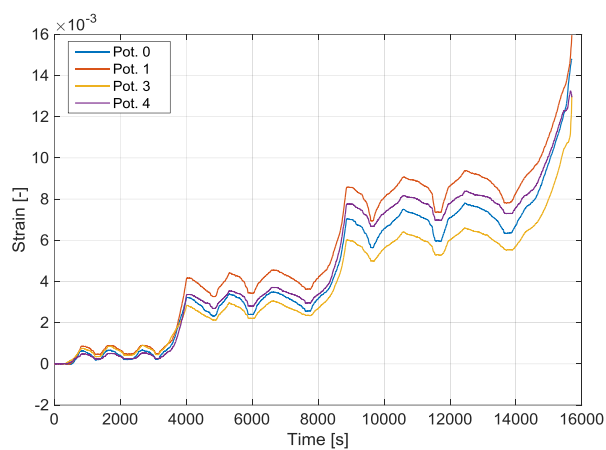
CL_5



b)

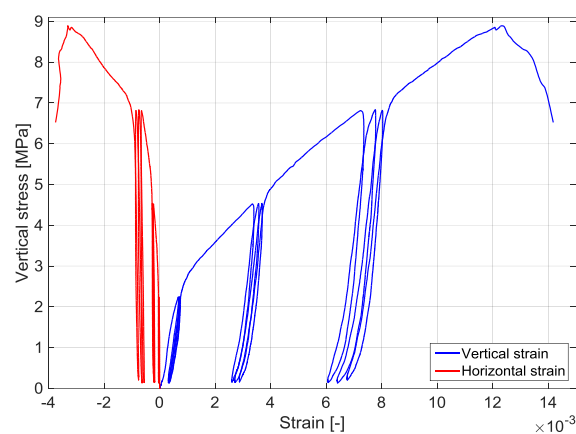
Figure 76 CL_5 compression test results: a) vertical strain time histories; b) vertical stress vs. vertical and horizontal strains.

CL_6



a)

CL_6



b)

Figure 77 CL_6 compression test results: a) vertical strain time histories; b) vertical stress vs. vertical and horizontal strains.

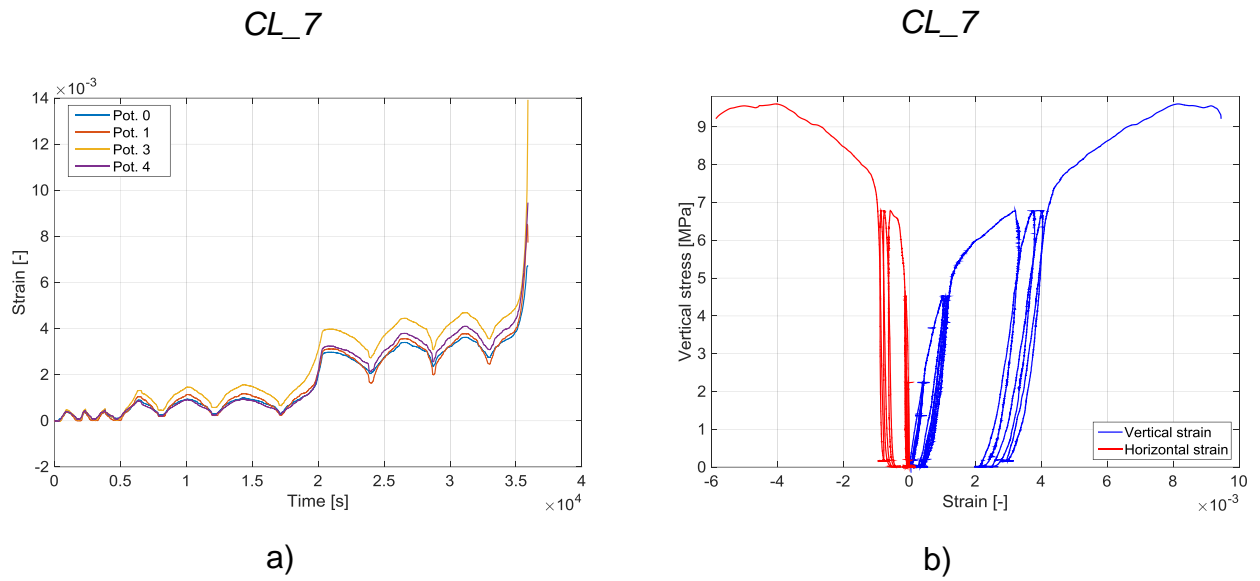


Figure 78 *CL_7* compression test results: a) vertical strain time histories; b) vertical stress vs. vertical and horizontal strains.

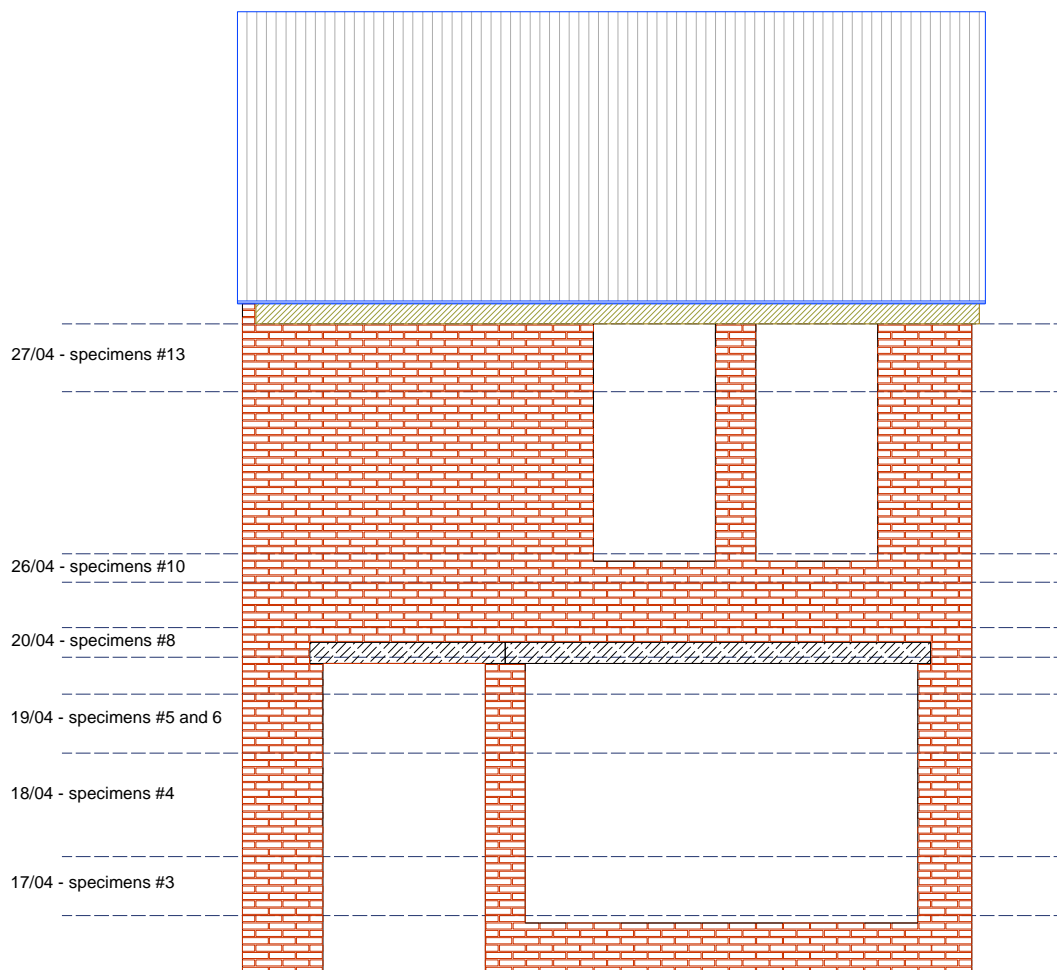


Figure 79 CL masonry courses built with weak mortar: West façade.

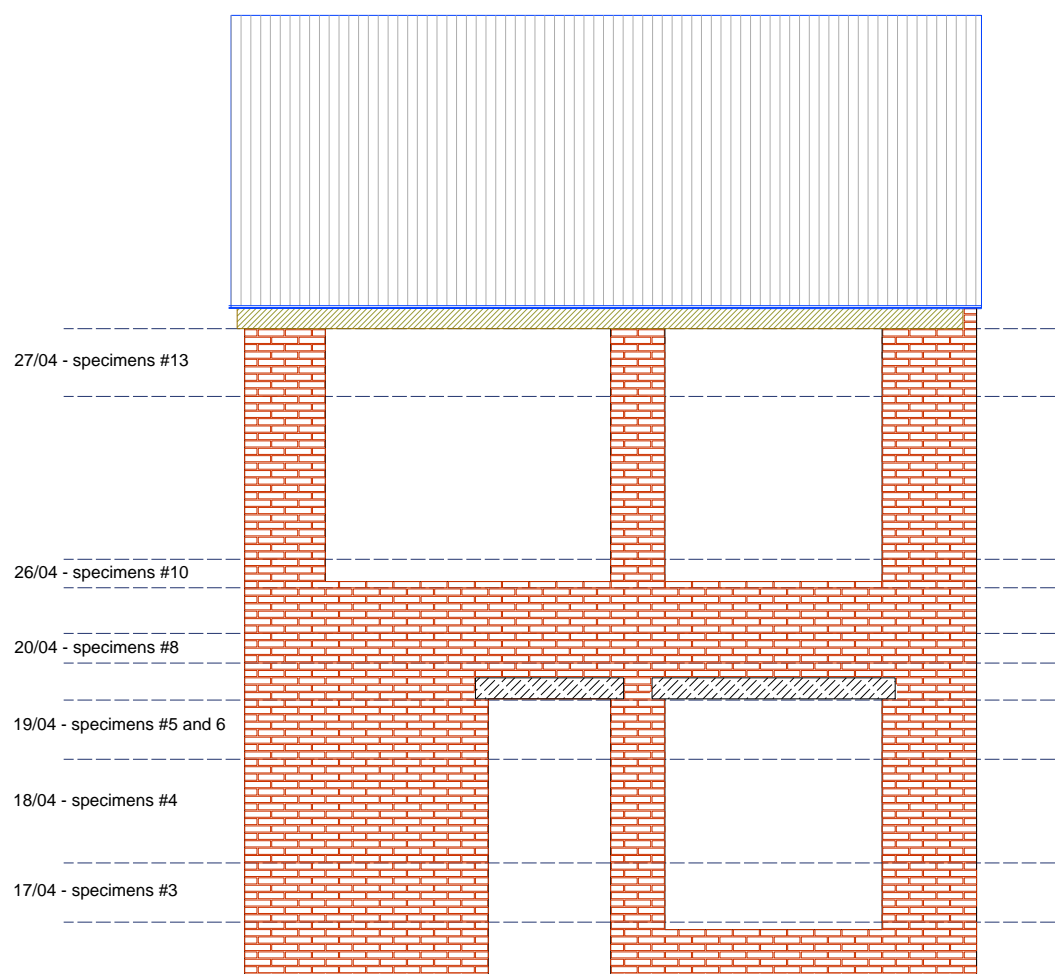


Figure 80 CL masonry courses built with weak mortar: East façade.

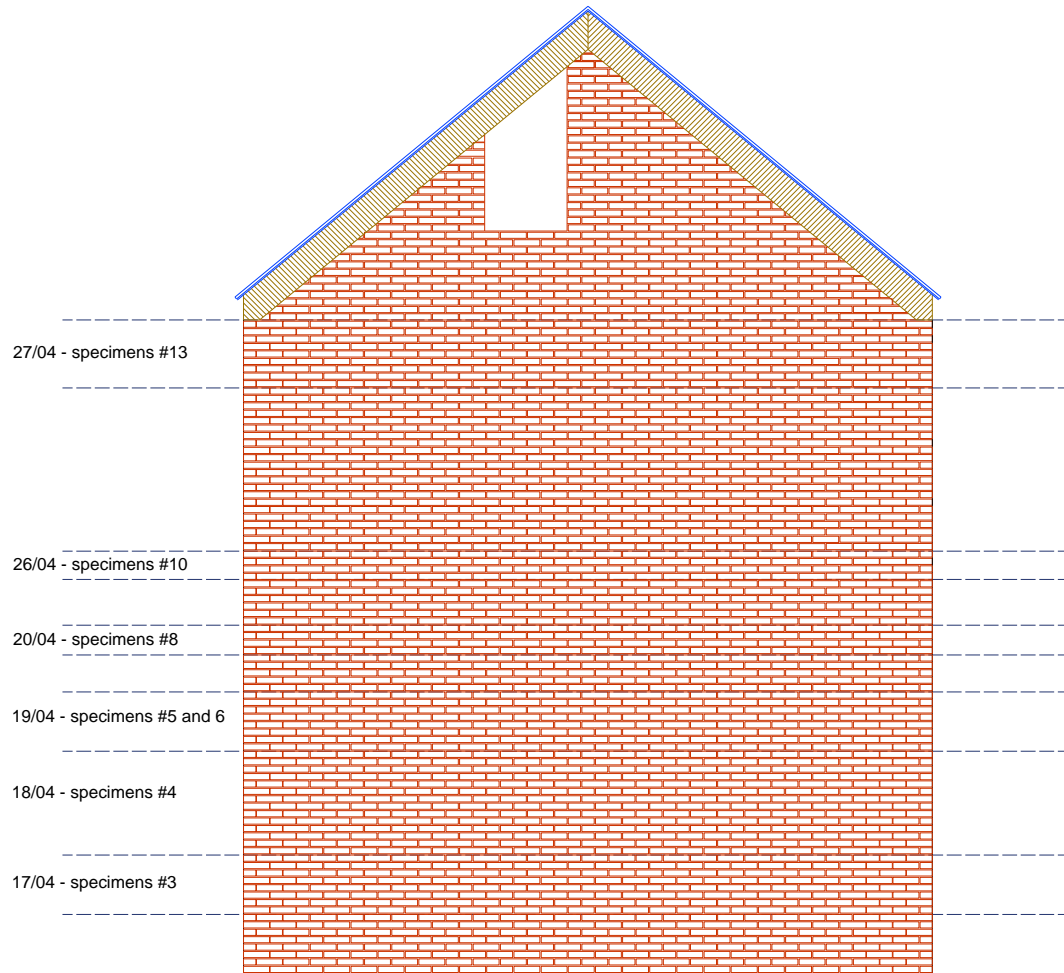


Figure 81 CL masonry courses built with weak mortar: North façade.

Table 7 CS masonry compressive strength (f_m) and Young's modulus (E_m).

Specimen	f_m [MPa]	E_m [MPa]
CS_2	10.32	6022
CS_3	11.05	7242
CS_4	9.60	6700
CS_5	10.25	6044
CS_6	9.76	7384
CS_7	9.57	6164
Average	10.1	6593
St. Dev.	0.57	611.50
C.o.V.	0.06	0.09

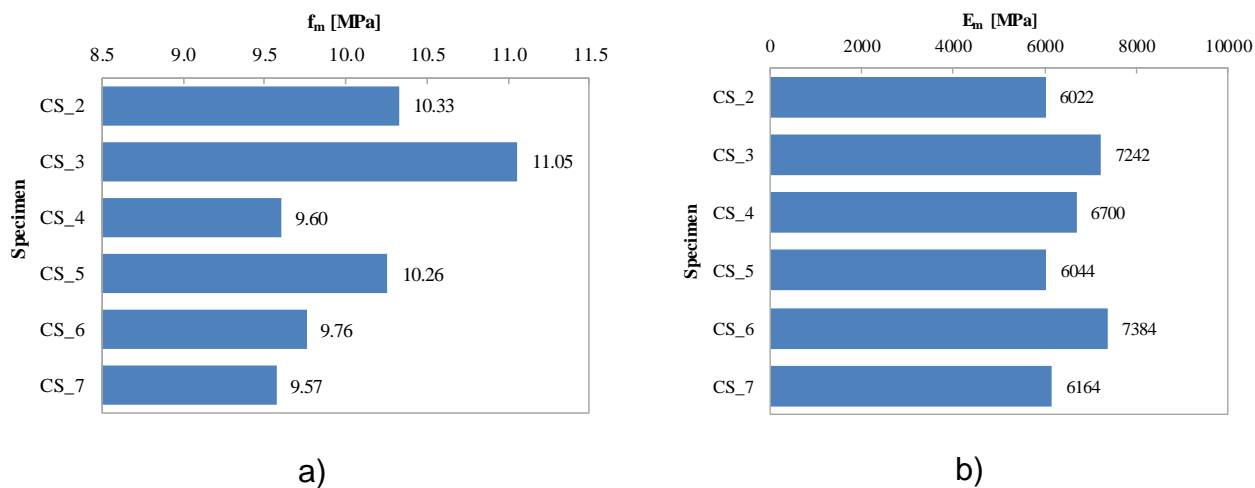


Figure 82 CS masonry mechanical properties: (a) compressive strength; (b) Young's modulus.

Table 8 CL specimens CL_2 and CL_3 compressive strength (f_m) and Young's modulus (E_m).

Specimen	f_m [MPa]	E_m [MPa]
CL_2	15.27	5240
CL_3	16.47	6135
Average	15.87	5687

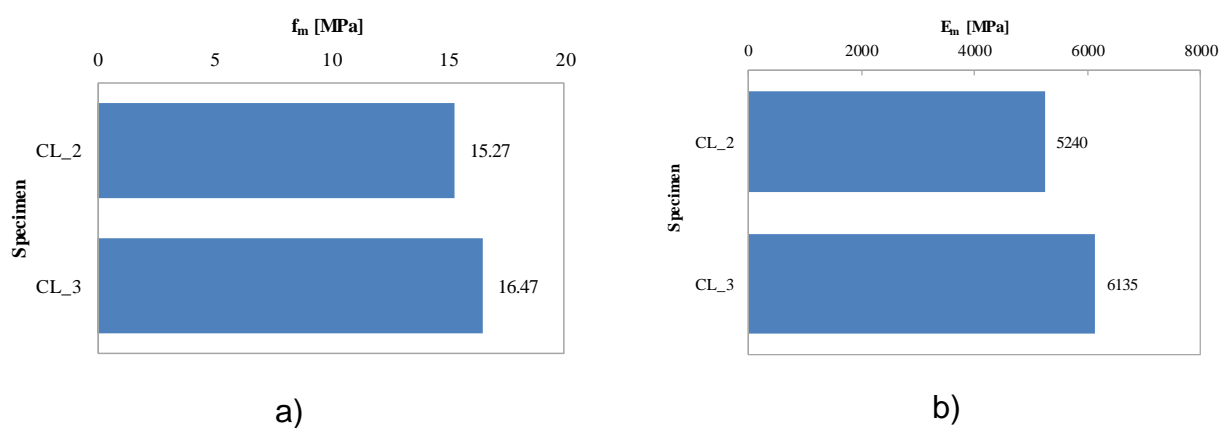
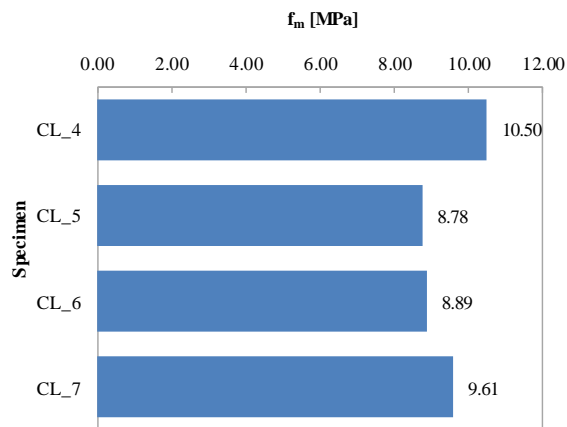


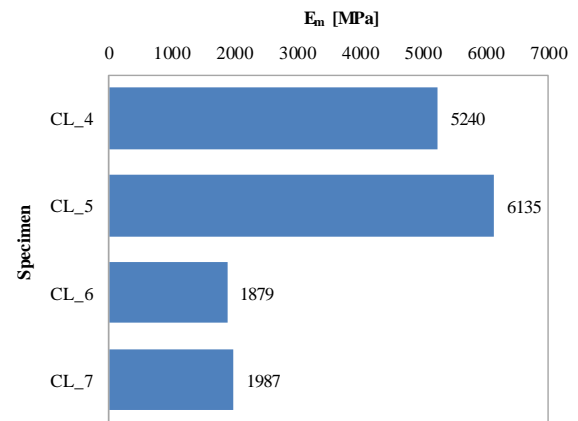
Figure 83 CL specimens CL_2 and CL_3 mechanical properties: (a) compressive strength; (b) Young's modulus.

Table 9 CL specimens CL_4, CL_5, CL_6 and CL_7 compressive strength (f_m) and Young's modulus (E_m).

Specimen	f_m [MPa]	E_m [MPa]
CL_4	10.50	5240
CL_5	8.78	6135
CL_6	8.89	1879
CL_7	9.61	1987
Average	9.44	3810



a)



b)

Figure 84 CL specimens CL_4, CL_5, CL_6, and CL_7 mechanical properties: (a) compressive strength; (b) Young's modulus.

Table 10 CL masonry compressive strength (f_m) and Young's modulus (E_m).

Specimen	f_m [Mpa]	E_m [MPa]
CL_2	15.27	5240
CL_3	16.47	6135
CL_4	10.50	5240
CL_5	8.78	6135
CL_6	8.89	1879
CL_7	9.61	1987
Average	11.59	4436
St. Dev.	3.40	1980
C.o.V.	0.29	0.44

2.4 Bond strength of masonry

2.4.1 Test procedure

Bond wrench test on 60 masonry specimens were performed in order to characterize the bond strength of the horizontal bed-joint of CS and CL masonry. The tests were carried out in accordance with EN 1052-5 [6] at the laboratory of the Department of Civil Engineering and Architecture (DICAr) of the University of Pavia. Two series of tests were performed:

- 30 specimens made of calcium silicate masonry (Figure 86 a);
- 30 specimens made of clay masonry (Figure 86 b).

The specimens were composed by 2 bricks and 1 mortar joint as shown in Figure 85. Figure 87 shows the test setup: the top brick was subjected to a moment and a compressive force, while the bottom one was clamped. Torsional effects were accurately avoided, either from the weight of the lever or the applied force: The bond strength (f_w) was computed for each specimen as:

$$f_w = \frac{F_1 e_1 + F_2 e_2 - \frac{2}{3} d (F_1 + F_2 + W/4)}{bd^2/6} \quad [MPa]$$

where:

- e_1 is the distance from the applied load to the tension face of the specimen [mm];
- e_2 is the distance from the centre of gravity of the lever and upper clamp to the tension face of the specimen [mm];
- W is the weight of the masonry unit pulled off the specimen plus any adherent mortar [N];
- F_1 is the applied load [N];
- F_2 is the weight of the bond wrench [N];
- d is the mean depth of the bed-joint [mm];
- b is the mean width of the bed-joint [mm].

According to EN 1052-5 [6], Figure 88 shows all possible types of bed-joint failure, where only the first 3 types are acceptable (A,B and C).



Figure 85 Geometry of the specimens: a) CS masonry; b) CL masonry.



Figure 86 Examples of the tested specimens: a) CS masonry; b) CL masonry.

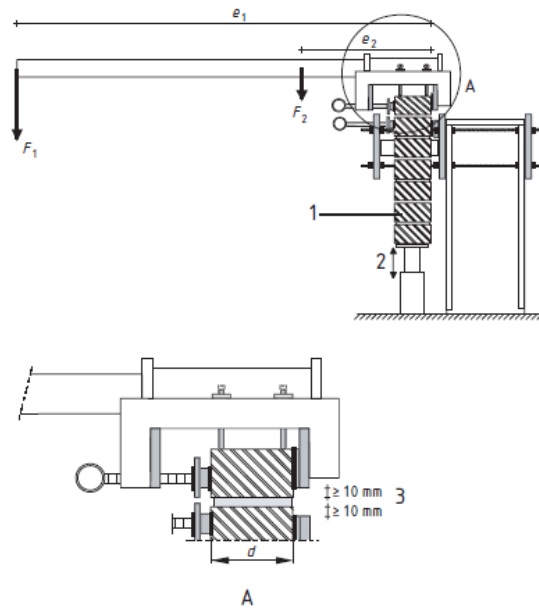


Figure 87 Layout of the bond-wrench test (EN 1052-5).

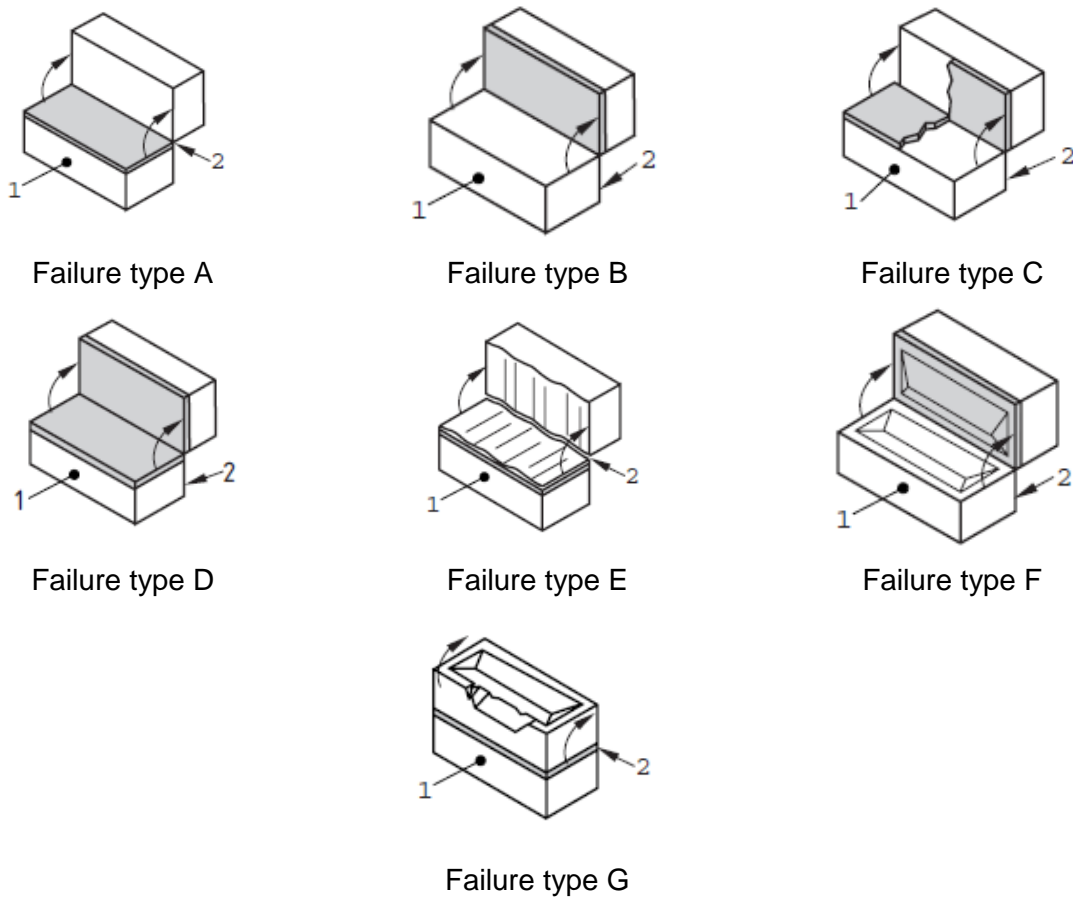


Figure 88 Possible failure modes in the bond wrench test (EN 1052-5).

2.4.2 Test results

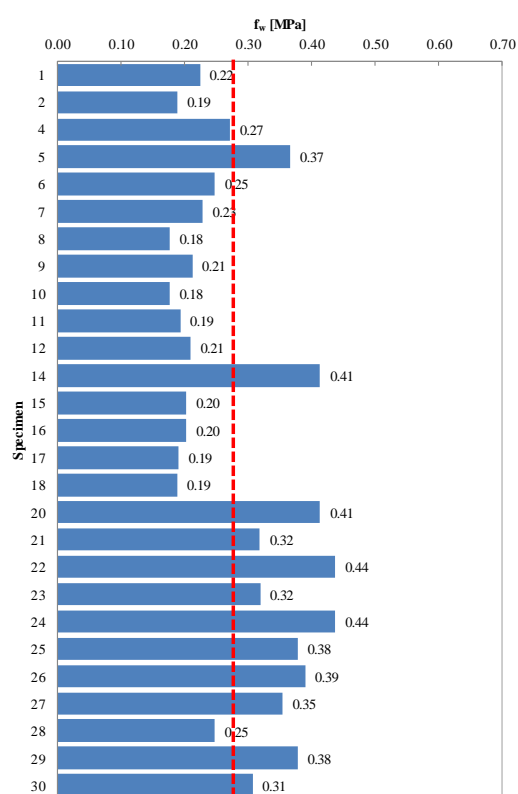
Table 11 and Table 12 report the results of performed bond-wrench tests. All of them concern specimens tested after, at least, 28 days of maturation.

Table 11 Bond strength of CS specimens.

Specimen	Weight [N]	M_{max} [Nm]	f_w [MPa]	Type of failure
1	27.3	90	0.22	A.1
2	27.4	75	0.19	A.1
3	-	-	-	Unacceptable
4	27.9	110	0.27	A.1
5	28.3	150	0.37	A.1
6	26.9	100	0.25	A.1
7	27.3	92	0.23	A.1
8	28.3	70	0.18	A.1
9	30.8	85	0.21	A.3
10	30.8	70	0.18	A.2
11	28.3	77	0.19	A.1
12	33.5	84	0.21	A.2
13	-	-	-	Unacceptable
14	27.1	170	0.41	A.1
15	28.4	81	0.20	A.1
16	26.8	81	0.20	A.1
17	27.2	76	0.19	A.1
18	28.7	75	0.19	A.1
19	-	-	-	Unacceptable
20	28.6	170	0.41	A.1
21	32.5	130	0.32	A.2
22	-	-	-	Unacceptable
23	27.3	130	0.32	A.1
24	28.3	180	0.44	A.1
25	29.6	155	0.38	A.1
26	27.6	160	0.39	A.1
27	29	145	0.35	A.1
28	29.8	100	0.25	A.1
29	27.6	155	0.38	A.1
30	28.1	125	0.31	A.1
Average			0.28	
St. Dev.			0.09	
COV			0.32	

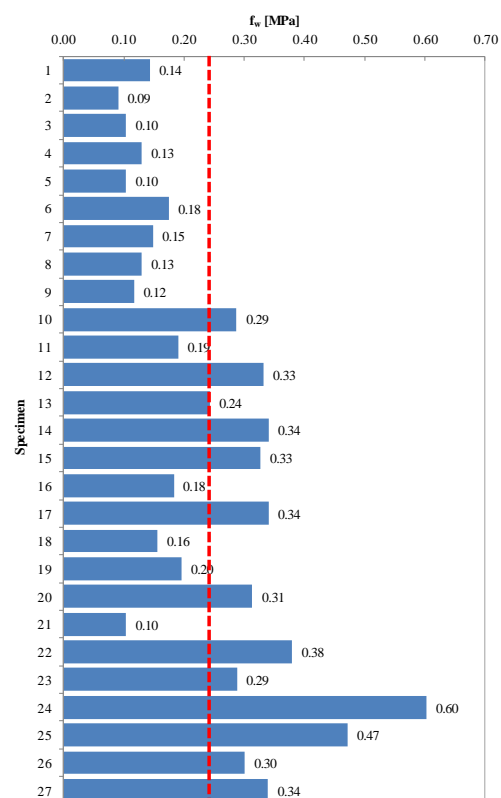
Table 12 Bond strength of CL specimens.

Specimen	Weight [N]	M_{max} [Nm]	f_{wi} [MPa]	Type of failure
1	21.6	50	0.14	A.1
2	21.6	30	0.09	A.1
3	23.5	35	0.10	A.3
4	21.8	45	0.13	A.1
5	21.9	35	0.10	A.1
6	20.8	62	0.18	A.1
7	25.5	52	0.15	A.2
8	22.1	45	0.13	A.1
9	22.5	40	0.12	A.1
10	22.9	105	0.29	A.1
11	25.4	68	0.19	A.2
12	21.6	122	0.33	A.1
13	-	-	-	Unacceptable
14	21.3	125	0.34	A.1
15	22.4	120	0.33	A.3
16	21.3	65	0.18	A.3
17	21.4	125	0.34	A.1
18	24.7	55	0.16	A.3
19	21.6	70	0.20	A.1
20	-	-	-	Unacceptable
21	21.1	35	0.10	A.1
22	23.5	140	0.38	A.1
23	20.7	105	0.29	A.1
24	22	225	0.60	A.4
25	-	-	-	Unacceptable
26	21.2	110	0.30	A.1
27	24.4	125	0.34	A.2
Average			0.24	
St. Dev.			0.13	
COV			0.52	



Average = 0.28

a)



Average = 0.24

b)

Figure 89 Bond strength: a) CS specimens; b) CL specimens.

2.5 Direct shear strength of masonry

2.5.1 Test procedure

The test purpose is to evaluate the shear resistance of two horizontal bed-joints bounding a single brick. The tests were performed in accordance with EN 1052-5 [7] at the laboratory of the Department of Civil Engineering and Architecture (DICAr) of the University of Pavia. Two series of tests were performed:

- 15 triplets made of CS masonry (Figure 90 a);
- 15 triplets made of CL masonry (Figure 90 b).

The specimens were type “I” (Figure 91) according to [7]: three bricks bonded with two layers of mortar. Procedure “A” was chosen: at least three specimens must be tested at three different level of pre-compression (0.2 MPa, 0.6 MPa, and 1.0 MPa).

Referring to Figure 92, a layer of gypsum was applied to the external faces of the specimens in order to obtain even surfaces. The specimen was rotated by 90 degrees with the bed-joints vertically oriented, and positioned between two steel plates in the testing apparatus. The two exterior bricks were vertically supported by roller bearings. A normal compressive force was applied to the two lateral faces of the specimen and maintained constant during the test. After that, an incremental shear force was applied vertically to the central brick up to sliding over the mortar bed-joints.

During each test the maximum shear force F_{max} and the constant compressive load F_p were recorded. Once the joint cracked and sliding initiated, the same specimen was subjected to additional tests with different levels of normal force. The additional tests allowed determining the frictional shear strength after cohesion had been overcome.



Figure 90 Shear test: a) CS specimen; b) CL specimen.

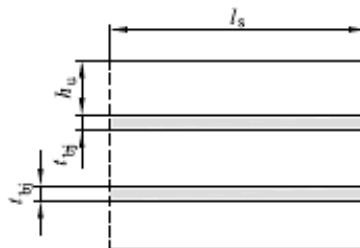


Figure 91 Shear test specimen geometry.

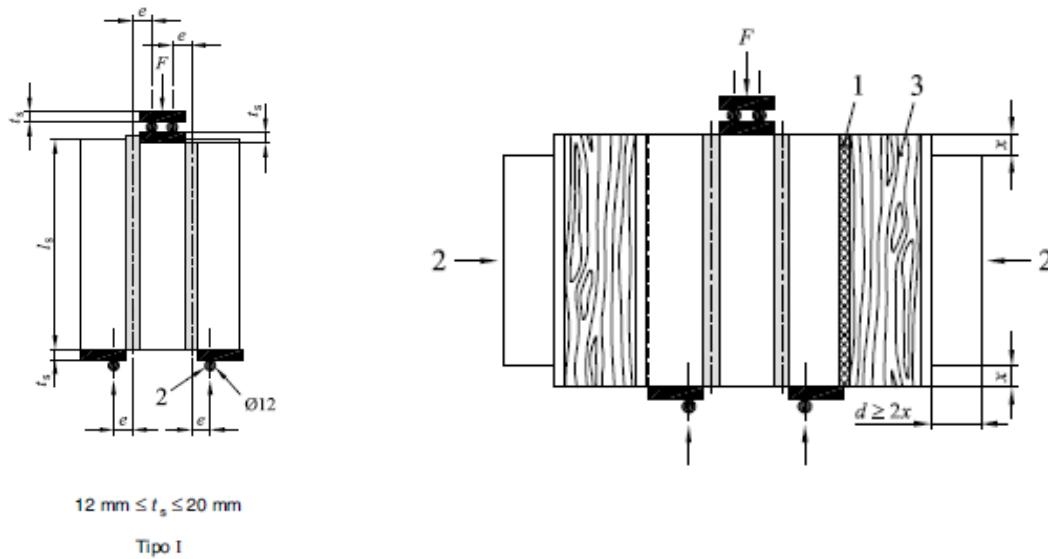


Figure 92 Shear test setup.

The shear strength τ and the corresponding compressive stress σ were computed as:

$$\tau = \frac{F_{max}}{2 A}$$

$$\sigma = \frac{F_p}{A}$$

where A is the bed-joint area normal to the compressive force.

By plotting each pair (σ, τ) it is possible to obtain a dispersion as shown by Figure 93 and Figure 94. A Coulomb-type law can be used to fit the results:

$$\tau = f_{v0} + \mu \sigma$$

where:

- f_{v0} is the cohesion [MPa];
- μ is the friction coefficient.

Cohesion contributes to the strength only if the mortar bed-joints are intact, while friction acts also after cracking, provided there is contact between the two materials.

2.5.2 Test results

Table 13 and Table 14 report the tests results. For each value of compressive stress σ a peak or residual value of shear strength τ was found. By plotting all pairs (σ, τ) obtained at peak strength, the values of cohesion f_{v0} and friction coefficient μ were determined as the Y-intercept and the slope of the linear regression line. (Figure 93 and Figure 94).

Considering the pairs (σ, τ) obtained at residual strength another line was obtained, with (nearly) zero-cohesion, as the joints were now cracked, and the same slope, since friction is not significantly affected by cracking. Table 15 summarizes the cohesion and friction coefficient for CS and CL masonry.

Table 13 Shear tests results for CS masonry specimens.

Specimen	Peak		Residual 1		Residual 2		Residual 3		Failure mode
	σ [MPa]	τ [MPa]	σ [MPa]	τ [MPa]	σ [MPa]	τ [MPa]	σ [MPa]	τ [MPa]	
1	0.96	1.16	1.01	0.95	0.60	0.24	0.60	0.30	Right joint
2	0.57	0.99	0.60	0.36	0.98	0.55	0.20	0.14	Left joint
3	0.18	0.62	0.19	0.17	0.59	0.35	0.99	0.52	Left joint
4	0.93	1.20	0.99	0.86	0.61	0.54	0.23	0.21	Left joint
5	0.57	1.30	0.60	0.54	0.21	0.19	0.99	0.86	Right joint
6	0.21	0.69	0.22	0.20	0.98	0.66	0.61	0.41	Right joint
7	0.92	1.32	0.97	0.57	0.21	0.15	0.58	0.31	Left joint
8	0.55	1.13	0.59	0.43	0.98	0.58	0.23	0.16	Left joint
9	0.19	0.60	0.20	0.18	0.59	0.39	0.98	0.59	Right joint
10	0.92	1.08	0.98	0.57	0.22	0.18	0.60	0.37	Left joint
11	0.58	1.10	0.20	0.09	0.62	0.13	0.96	0.61	Left joint
12	0.19	0.76	0.20	0.003	0.58	0.40	0.97	0.58	Left joint
13	0.93	0.75	0.99	0.57	0.61	0.33	0.23	0.15	Left joint
15	0.57	0.71	0.60	0.18	0.21	0.17	0.98	0.52	Left joint

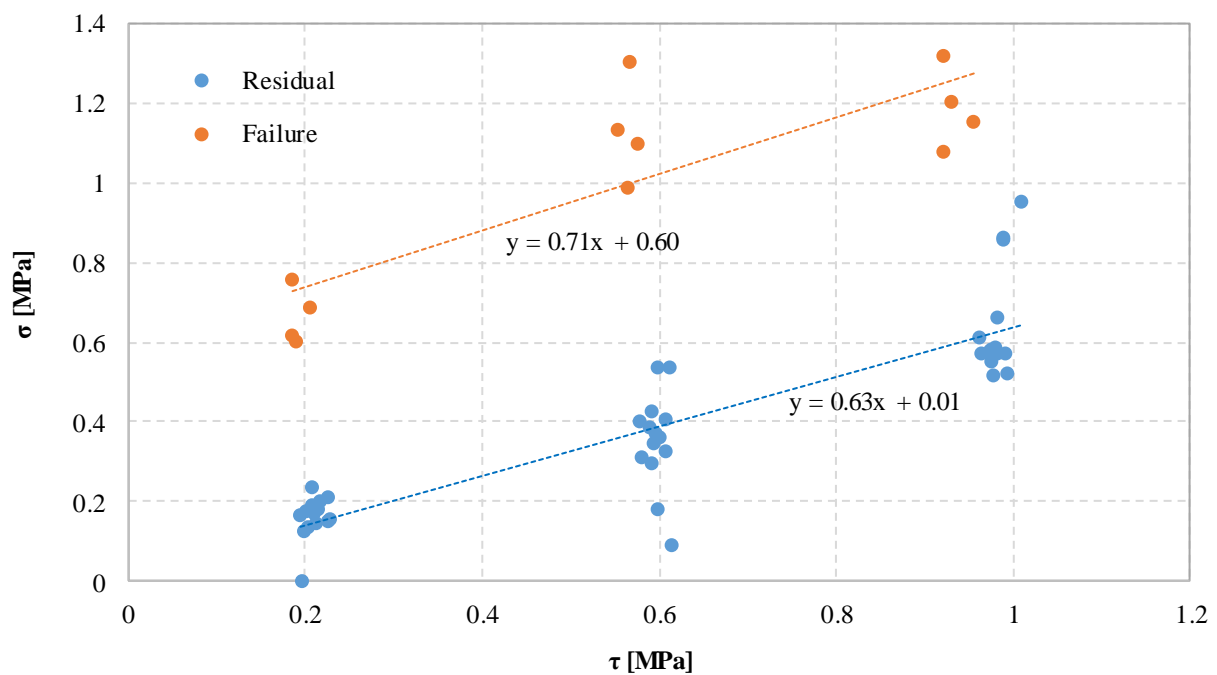
Figure 93 Shear test results for CS specimens: shear strength (τ) vs. normal compressive stress (σ).

Table 14 Shear tests results for CL masonry specimens.

Specimen	Peak		Residual 1		Residual 2		Residual 3		Failure mode
	σ [MPa]	τ [MPa]	σ [MPa]	τ [MPa]	σ [MPa]	τ [MPa]	σ [MPa]	τ [MPa]	
2	0.58	0.65	0.58	0.30	0.99	0.25	0.21	0.10	Left joint
4	0.21	0.37	0.21	0.23	1.00	0.74	0.62	0.46	Left joint
5	0.95	0.81	0.96	0.51	0.61	0.32	0.21	0.14	Left joint
6	0.57	0.45	0.59	0.28	0.21	0.14	-	-	Left joint
7	0.20	0.52	0.21	0.26	0.60	0.43	0.96	0.63	Left joint
8	0.95	0.88	0.98	0.79	0.22	0.18	0.60	0.40	Left joint
9	0.60	0.57	0.59	0.40	0.98	0.55	0.20	0.14	Left joint
10	0.19	0.55	0.20	0.15	0.61	0.36	0.98	0.59	Both joints
11	0.96	1.14	0.99	0.72	0.22	0.15	0.59	0.40	Both joints

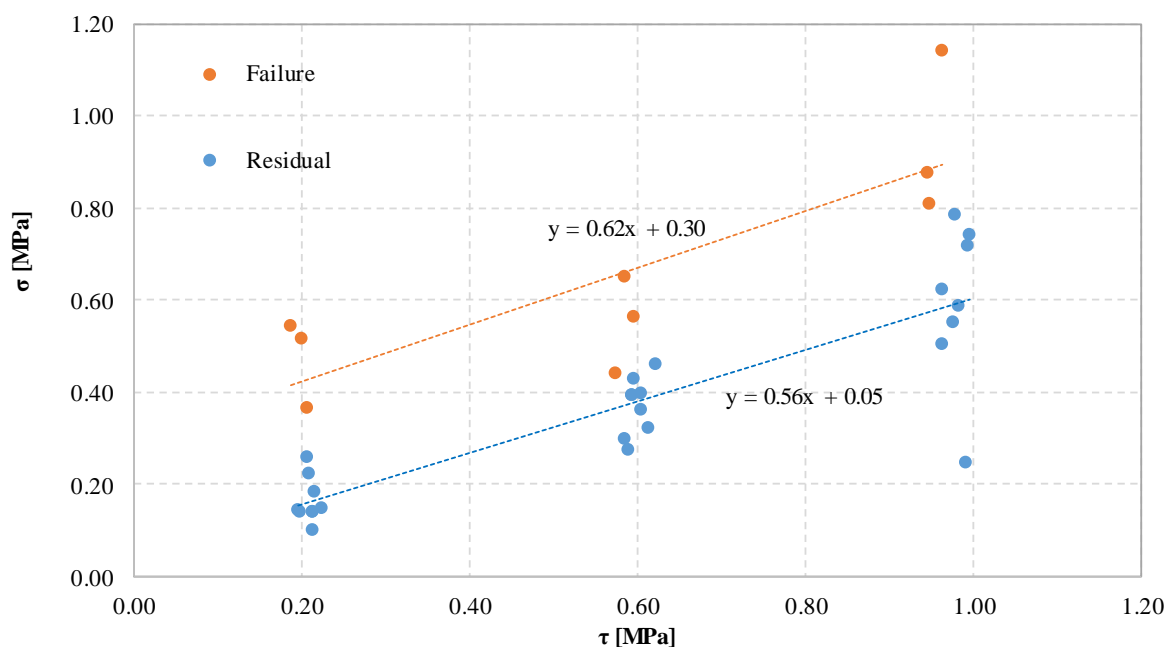
Figure 94 Shear test results for CL specimens: shear strength (τ) vs. normal compressive stress (σ).

Table 15 Values of cohesion and friction coefficient for CS and CL masonry under direct shear.

	Cohesion (f_{v0}) [MPa]	Friction coefficient (μ) [-]
CS masonry	0.60	0.71
CL masonry	0.30	0.62

2.6 Torsional shear strength of mortar

2.6.1 Test procedure

Two series of torsion tests were performed at the laboratory of the Department of Civil Engineering and Architecture (DICAr) of the University of Pavia:

- 20 specimens made of CS masonry (Figure 95 a);
- 20 specimens made of CL masonry (Figure 95 b).

Specimens consisted on two bricks joined by a square mortar bed-joint to reproduce the actual contact area within walls; polystyrene was placed in the remaining parts of the bed-joint to block out the square mortar area.

The bed-joint was horizontally oriented. A hydraulic jack applied a constant vertical compression to the top brick. A sheet of flexible elastomer was placed between the brick and the jack steel plate to allow dilatancy to occur. A torque was applied by two horizontal hydraulic jacks placed at a distance of 20 mm from the edge of the top brick (Figure 96 a and b). The torque was gradually increased up to sliding of the bed joint. The instrumentation is shown on Figure 96 c.

During each test the maximum torque T_{max} and the constant compressive load F_p were recorded. The elastic shear stress τ and the corresponding compressive stress σ were computed as:

$$\sigma = \frac{F_p}{a^2}$$

$$\tau = \frac{4.8 T_{max}}{a^3}$$

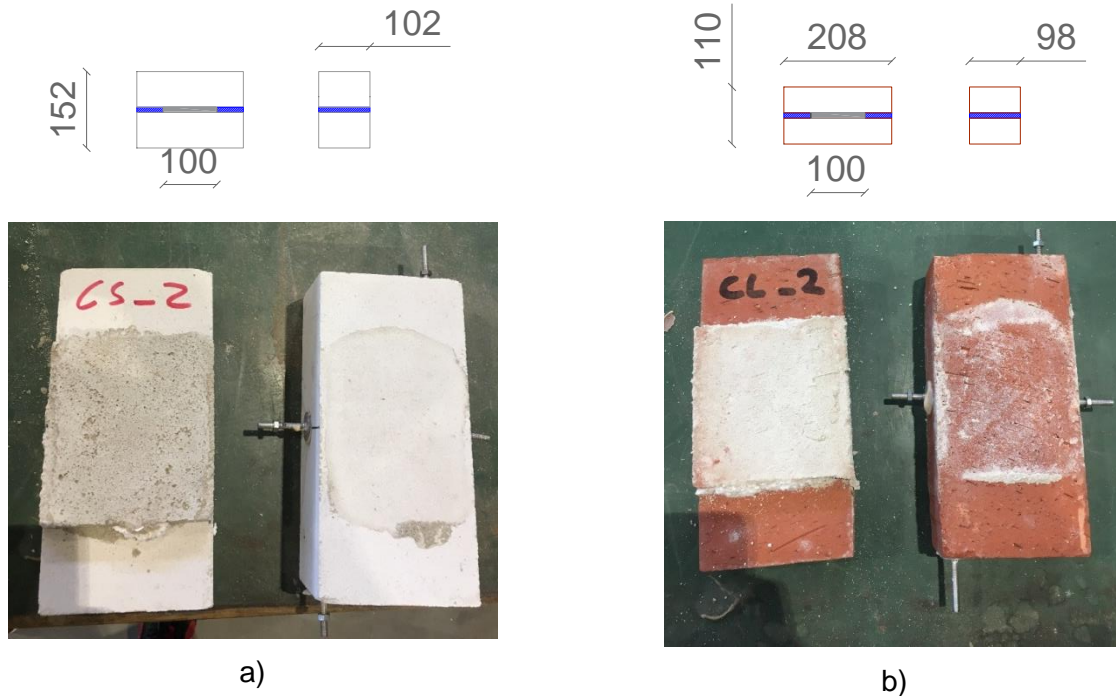
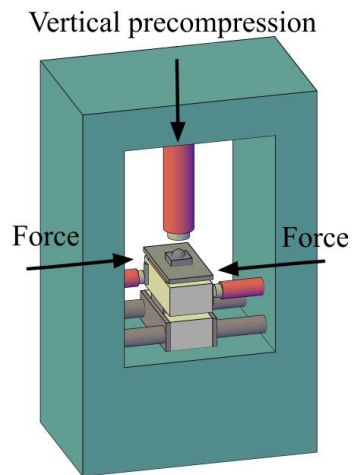
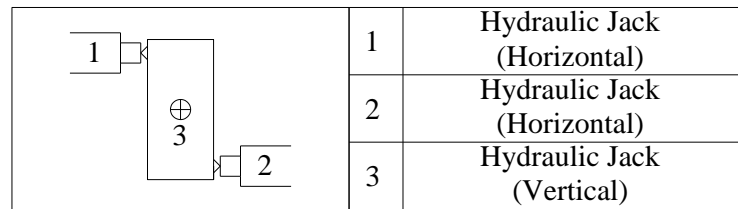


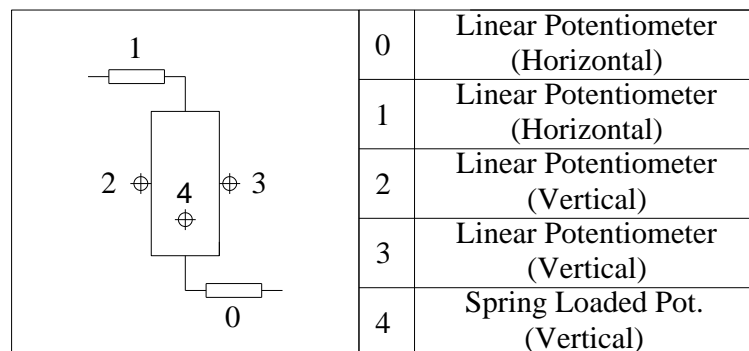
Figure 95 Torsion test: a) CS specimen; b) CL specimen.



a)



b)



c)



(d)

Figure 96 Torsion test set-up: a) overview; b) loading setup; c) instrumentation; d) photo.

where a is the dimension of the square mortar joint, equal to 100 mm for both CS and CL specimens.

The tests allowed the determination of the torsional shear strength of masonry bed joints. By plotting each pair (σ , τ) it is possible to obtain a dispersion as shown by Figure 97 and Figure 98. A Coulomb-type law can be used to fit the results:

$$\tau = f_{v0,tor} + \mu_{tor} \sigma$$

where:

- $f_{v0,tor}$ is the cohesion [MPa];
- μ_{tor} is the friction coefficient.

Cohesion contributes to the strength only if the mortar bed-joints are intact, while friction acts also after cracking, provided there is contact between the two materials.

2.6.2 Test results

Table 16 reports the tests results. For each value of compressive stress σ a peak or residual value of shear strength τ was found. By plotting all pairs (σ - τ) obtained at peak strength, the values of cohesion $f_{v0,tor}$ and friction coefficient μ_{tor} were determined as the Y-intercept and the slope of the linear regression line. (Figure 97 and Figure 98). Table 17 summarizes the cohesion and friction coefficient for CS and Clay masonry.

It should be noted that 1 out of 20 CS specimen broke before testing, as well as 6 out of 20 CL specimens. In order to give the same weight to each applied normal compression, the final values of torsional cohesion and friction coefficient were obtained by selecting 15 tests for CS masonry (5 per level of compression) and 12 tests for CL masonry (4 per level of compression).

Table 16 Torsion tests results.

Specimen	CS		CL	
	σ [MPa]	τ [MPa]	σ [MPa]	τ [MPa]
1	0.60	2.22	0.11	0.68
2	0.41	2.81	0.20	0.73
3	0.21	0.84	0.43	1.12
4	0.61	2.06	0.12	0.50
5	0.41	1.57	0.21	0.91
6	0.22	0.81	0.40	1.16
7	0.59	1.96	0.12	0.55
8	0.39	1.80	0.22	1.05
9	0.21	1.41	0.42	1.25
10	0.60	2.55	0.19	0.67
11	0.41	1.87	0.38	0.67
12	0.22	1.92	0.11	0.43
13	0.60	1.98	-	-
14	0.39	1.69	-	-
15	0.20	0.86	-	-
16	0.58	1.78	-	-
17	0.41	1.07	-	-
18	0.19	0.73	-	-

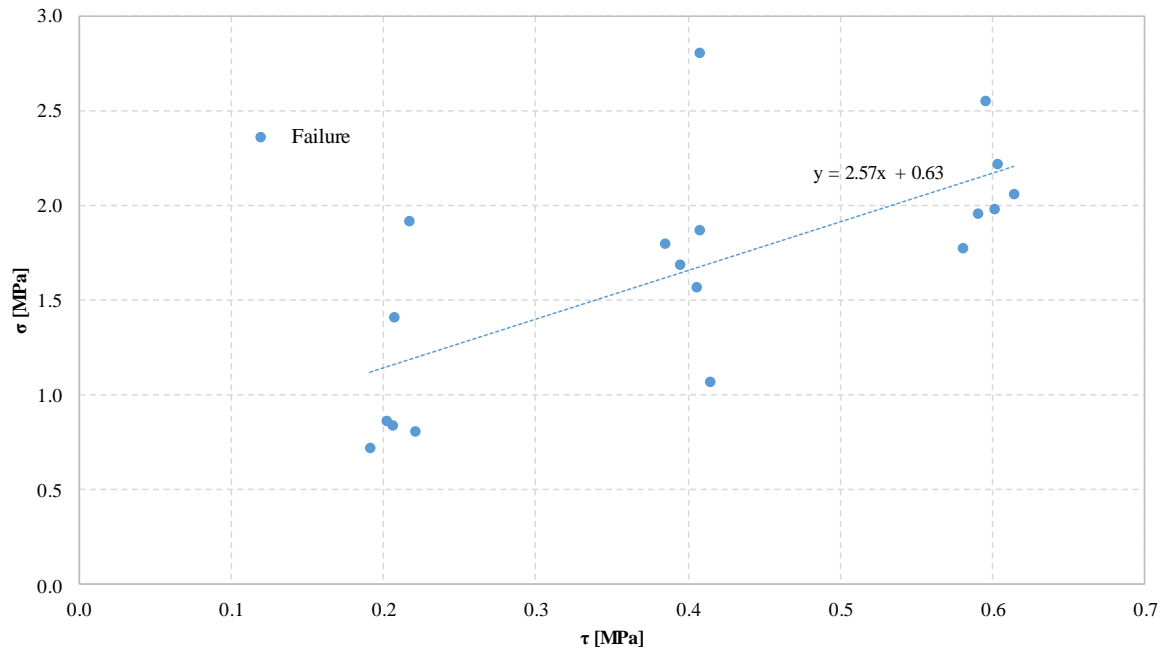


Figure 97 Torsion test results for CS specimens: torsional shear strength (τ) vs. normal compressive stress (σ).

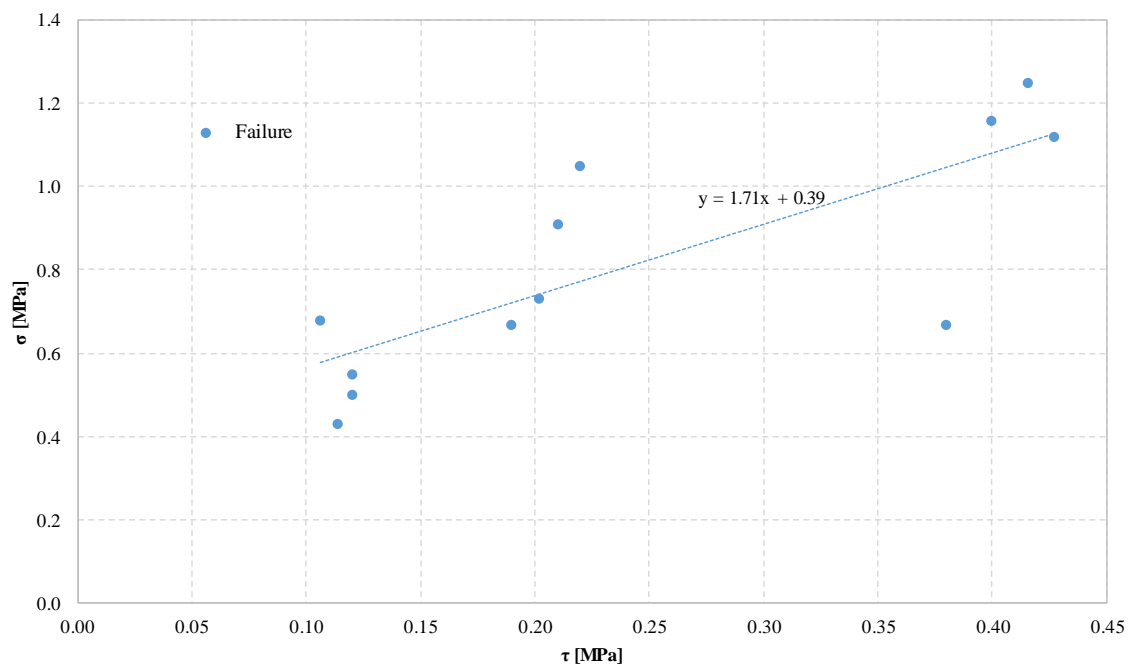


Figure 98 Torsion test results for CL specimens: torsional shear strength (τ) vs. normal compressive stress (σ).

Table 17 Values of cohesion and friction coefficient for CS and CL masonry under torsion.

	Cohesion ($f_{v0,tor}$) [MPa]	Friction coefficient (μ_{tor}) [-]
CS masonry	0.63	2.57
CL masonry	0.39	1.71

2.7 Summary of mechanical properties

Table 18 summarises the results of the material characterization tests.

Table 18 Masonry mechanical properties.

Material property	Symbol	Units	CS		CL	
			Avg.	C.o.V.	Avg.	C.o.V.
Density of bricks	ρ_b	kg/m ³	1756	-	1994	-
Density of masonry	ρ	kg/m ³	1837	-	1967	-
Brick compressive strength	f_b	MPa	19.8	0.18	50.0	0.10
Brick tensile strength	$f_{t,y}$	MPa	2.5	0.09	8.8	0.08
Mortar compressive strength	f_c	MPa	5.06	0.24	2.38	0.47
Mortar tensile strength	f_t	MPa	1.74	0.28	0.74	0.5
Masonry compressive strength	f_m	MPa	10.1	0.06	11.59*	0.29
Masonry Young's modulus (at 33% of f_m)	E_m	MPa	6593	0.09	4436*	0.44
Masonry bond strength	f_w	MPa	0.28	0.32	0.24	0.52
Masonry (bed joint) initial shear strength	f_{v0}	MPa	0.62	-	0.30	-
Masonry (bed joint) shear friction coefficient	μ_{shear}	-	0.71	-	0.62	-
Masonry (bed-joint) torsional initial shear strength	$f_{v0,tor}$	MPa	0.63	-	0.39	-
Masonry (bed-joint) torsional friction coefficient	μ_{tor}	-	2.57	-	1.71	-

* values are the mean values of all tested specimens, see par. 2.3.2.

3. INSTRUMENTATION AND ACQUISITION SYSTEM

The building specimen was subjected to an incremental dynamic tests applying a sequence of seismic excitations to its base in the North-South direction.

In order to monitor the structural response, several sensors were placed inside and outside the building. The instrumentation layout consisted of accelerometers and displacement transducers. A 3D optical motion acquisition system was also employed: passive reflective markers were densely attached to the external surface of the North, South and West clay walls, while high-definition cameras monitored their trajectories.

3.1 Accelerometers

Accelerometers allowed measuring the total acceleration of the following elements:

- Shake-table acceleration;
- Wall accelerations along the building height;
- Acceleration of 1st and 2nd floor and of the roof;
- Acceleration of the internal steel frame.

Table 19 lists all installed accelerometers, specifying their ID number, position, and associated mass.

Some accelerometers were removed during the last two runs of the incremental sequence (tests #24 and #25 of Table 23), to preserve the instrumentation in case of partial collapses. Accordingly, the masses initially associated with these accelerometers were redistributed to nearby sensors. Referring to the table below, the removed accelerometers are indicated with an asterisk in the Sensor ID column.

Table 19 Accelerometer list

Sensor ID	Location	Direction	Mass (X dir.) [kg]	Mass after test #21 (X dir.) [kg]
2	Foundation beam (West side)	Acceleration X	2928	2928
3	Foundation beam (East side)	Acceleration X	3572	3572
4	R.C. diaphragm (centre)	Acceleration Z	0	0
5	R.C. diaphragm (North-East corner)	Acceleration X	3363	3363
6	R.C. diaphragm (North-East corner)	Acceleration Y	0	0
7	R.C. diaphragm (North-East corner)	Acceleration Z	0	0
8	R.C. diaphragm (South-East corner)	Acceleration X	3242	3242
9	R.C. diaphragm (South-East corner)	Acceleration Y	0.0	0
10	R.C. diaphragm (South-East corner)	Acceleration Z	0.0	0
11	R.C. diaphragm (South-West corner)	Acceleration X	3760	3760
12	R.C. diaphragm (South-West corner)	Acceleration Y	0	0.0
13	R.C. diaphragm (South-West corner)	Acceleration Z	0	0
14	Timber diaphragm (North-West corner)	Acceleration X	651	651
15	Timber diaphragm (North-West corner)	Acceleration Y	0	0
16	Timber diaphragm (North-West corner)	Acceleration Z	0	0
17	Timber diaphragm (North-East corner)	Acceleration X	958	958

Sensor ID	Location	Measured parameter	Mass (X dir.) [kg]	Mass after test #21 (X dir.) [kg]
18	Timber diaphragm (North-East corner)	Acceleration Y	0	0
19	Timber diaphragm (North-East corner)	Acceleration Z	0	0
20	Timber diaphragm (South-East corner)	Acceleration X	888	888
21	Timber diaphragm (South-East corner)	Accelerations Y	0	0
22	Timber diaphragm (South-East corner)	Acceleration Z	0	0
23	Timber diaphragm (South-West corner)	Acceleration X	1071	1337
24	Timber diaphragm (South-West corner)	Acceleration Y	0	0
25	Timber diaphragm (South-West corner)	Acceleration Z	0	0
26	Timber diaphragm (centre)	Acceleration X	455	455
27	Timber diaphragm (centre)	Acceleration Z	0	0
28	North outer leaf (top of gable)	Acceleration X	136	392
29	Ridge beam (South end)	Acceleration X	692	692
30	Ridge beam (South end)	Acceleration Y	0	0
31	Ridge beam (South end)	Acceleration Z	0	0
32	Ridge beam (midspan)	Acceleration Z	0	0
33	North inner leaf (centre of gable)	Acceleration X	571	571
34	North inner leaf (second storey mid-height)	Acceleration X	1131	1131
35	North inner leaf (first storey mid-height)	Acceleration X	709	709
36	South inner leaf (centre of gable)	Acceleration X	1106	1106
37	South inner leaf (second-floor level)	Acceleration X	668	668
38	South inner leaf (second storey mid-height)	Acceleration X	1628	1628
39	South inner leaf (first storey mid-height)	Acceleration X	1274	1274
40	West inner leaf (top of second-storey squat pier)	Acceleration X	535	535
41	East inner leaf (top of first-storey squat pier)	Acceleration X	560	560
42*	North outer leaf (centre of gable)	Acceleration X	390	0
43	North outer leaf (second-floor level)	Acceleration X	615	1015
44	North-East outer leaf corner (second-floor level, North side)	Acceleration X	501	1442
45	North-West outer leaf corner (second-floor level)	Acceleration X	501	576
46*	North outer leaf (second storey mid-height)	Acceleration X	744	0.0
47	North outer leaf (first-floor level)	Acceleration X	664	4292
48*	North-East outer leaf corner (first-floor level, North side)	Acceleration X	1079	0
49*	North-West outer leaf corner (first-floor level)	Acceleration X	1338	0
50*	North outer leaf (first storey mid-height)	Acceleration X	1135	0
51*	South-West outer leaf corner (second-floor level)	Acceleration X	187	0
52	South-West outer leaf corner (first-floor level)	Acceleration X	728	728
53	West outer leaf (top of second-storey squat pier)	Acceleration X	611	611
54	West outer leaf (bott. of second-storey squat pier)	Acceleration X	780	1163
55	South-East outer leaf corner (second-floor level)	Acceleration X	160	160
56	South-East outer leaf corner (first-floor level)	Acceleration X	1042	1042
57	North inner leaf (first-floor level)	Acceleration X	1148	1148
58	Shaking table	Acceleration X	0	0

Sensor ID	Location	Measured parameter	Mass (X dir.) [kg]	Mass after test #21 (X dir.) [kg]
59	R.C. diaphragm (North-West corner)	Acceleration X	3245	3245
60	R.C. diaphragm (North-West corner)	Acceleration Y	0	0
61	R.C. diaphragm (North-West corner)	Acceleration Z	0	0
62	Rigid frame (second-floor level)	Acceleration X	0	0
63	Ridge beam (North end)	Acceleration X	692	692
64	Ridge beam (North end)	Acceleration Y	0	0
65	Ridge beam (North end)	Acceleration Z	0	0
66	North inner leaf (second-floor level)	Acceleration X	957	957
67*	North-East outer leaf corner (second-floor level, East side)	Acceleration X	159	0
68*	North-East outer leaf corner (first-floor level, East side)	Acceleration X	878	0

*removed after test #21.

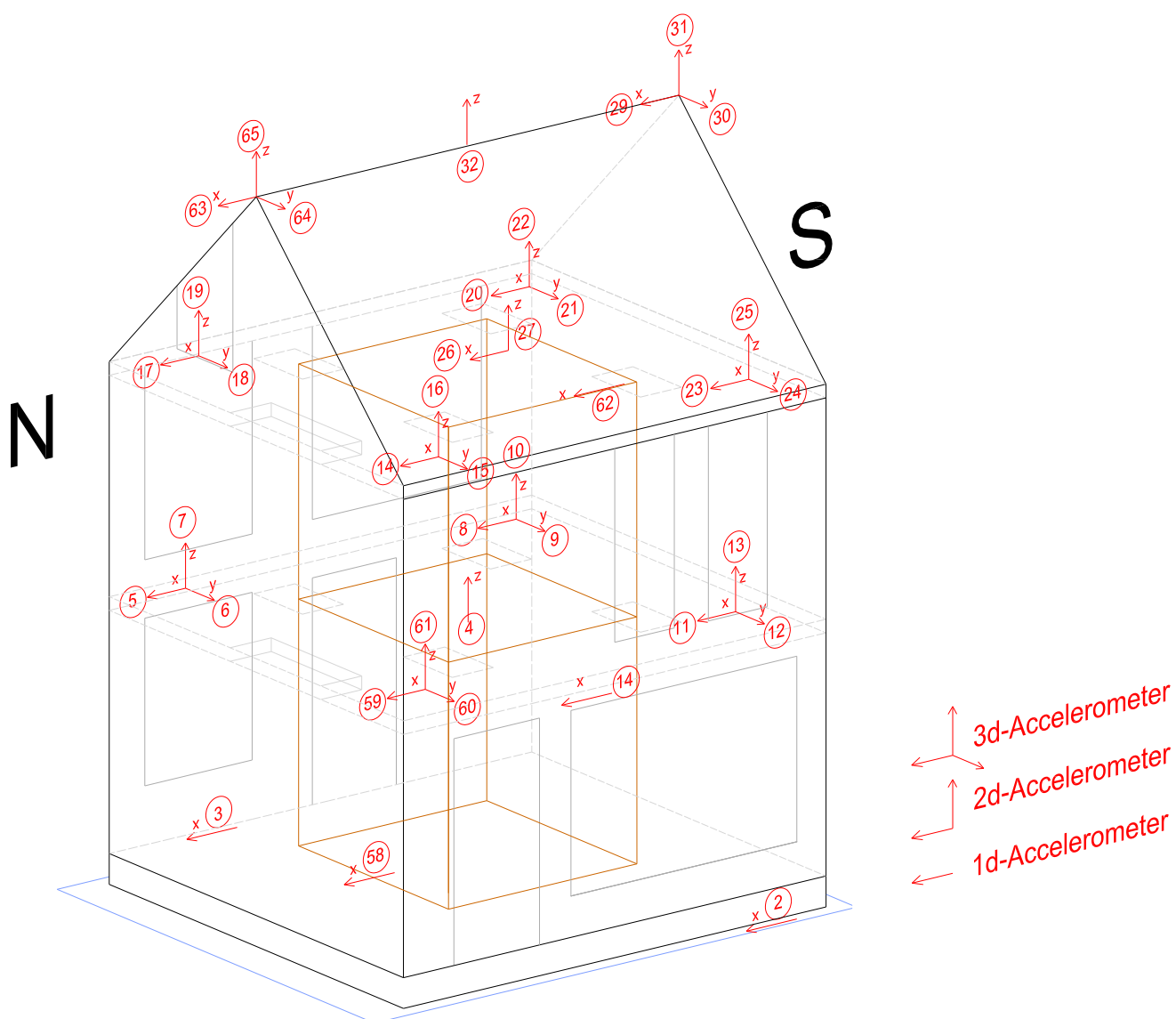


Figure 99 Accelerometer 3D view: foundation, first floor, second floor and roof diaphragms.

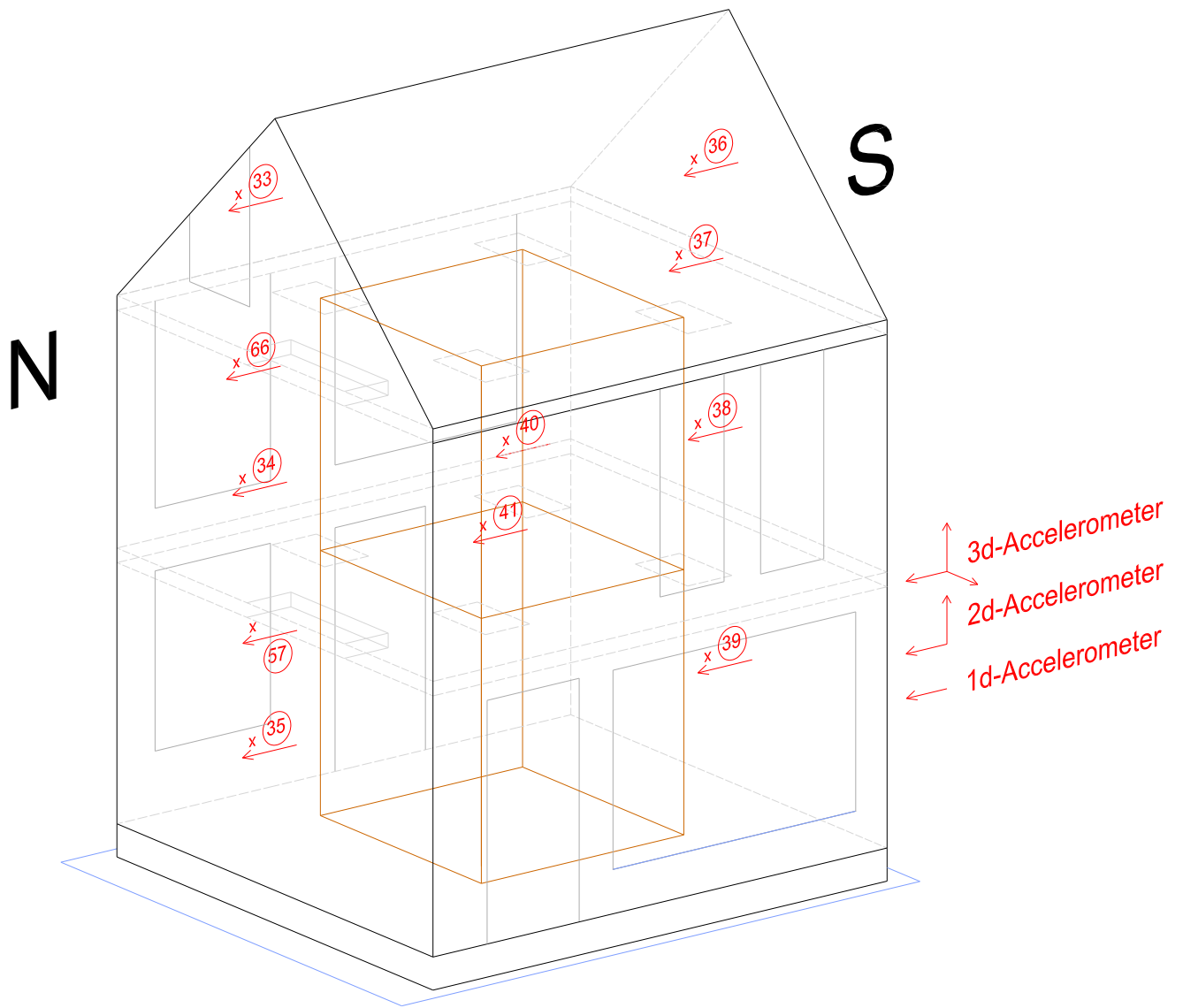


Figure 100 Accelerometer 3D view: calcium silicate inner leaves.

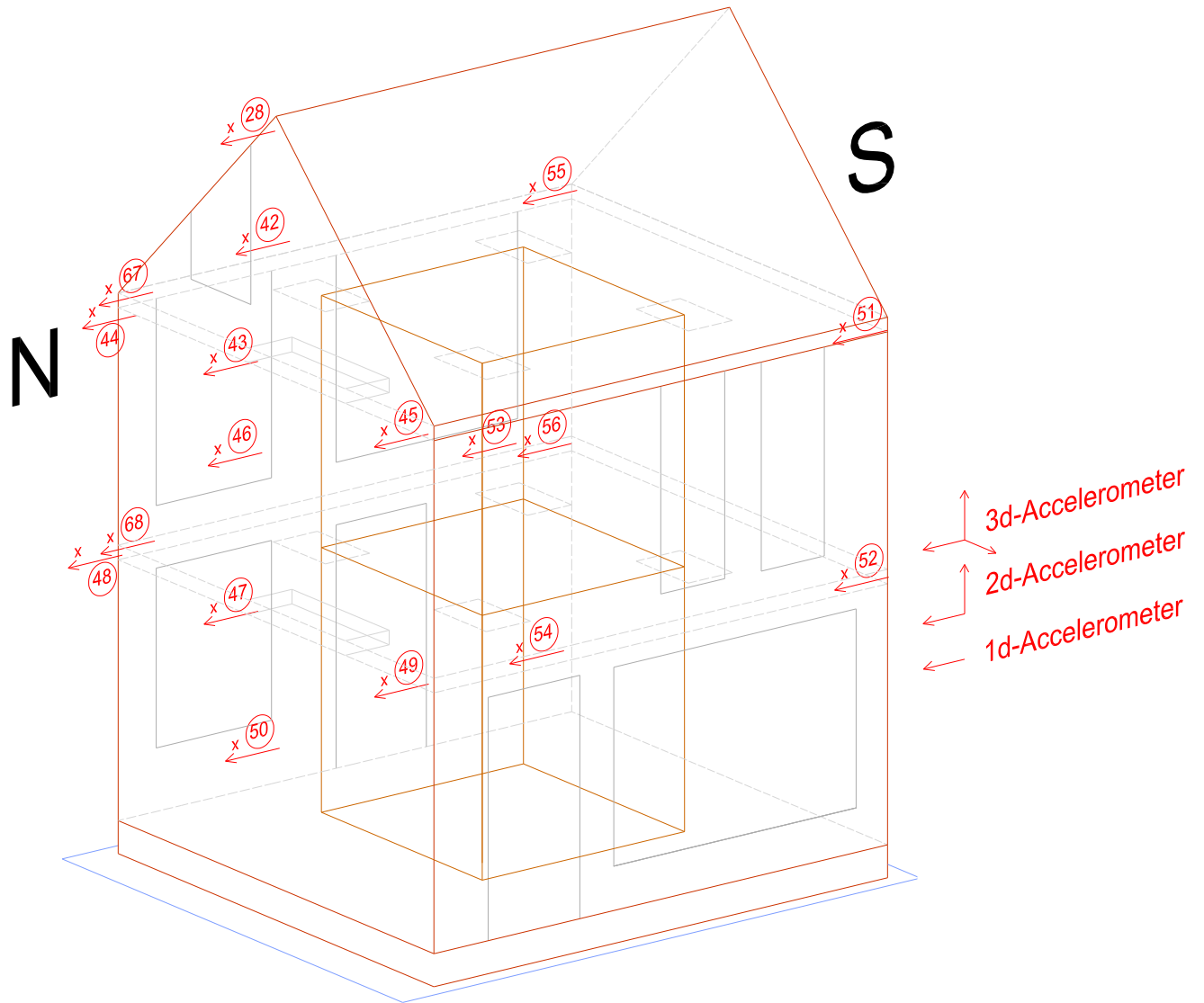


Figure 101 Accelerometer 3D view: clay outer leaves.

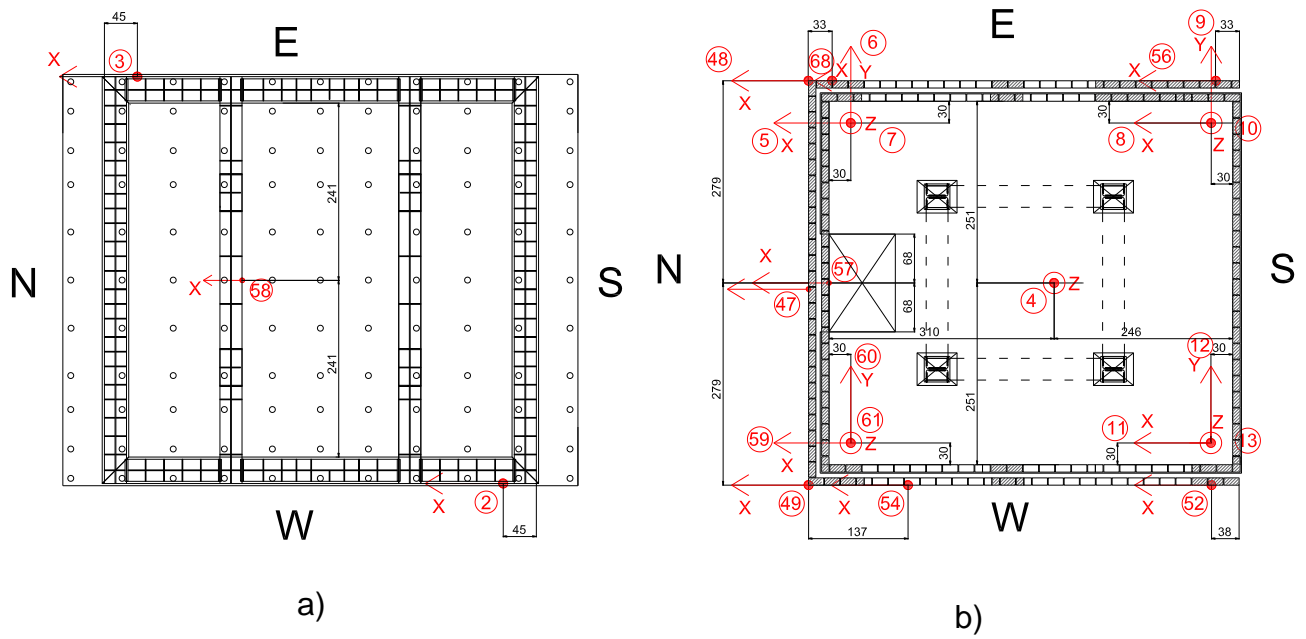


Figure 102 Accelerometer plan views: a) foundation level; b) first-floor level (R.C. diaphragm).

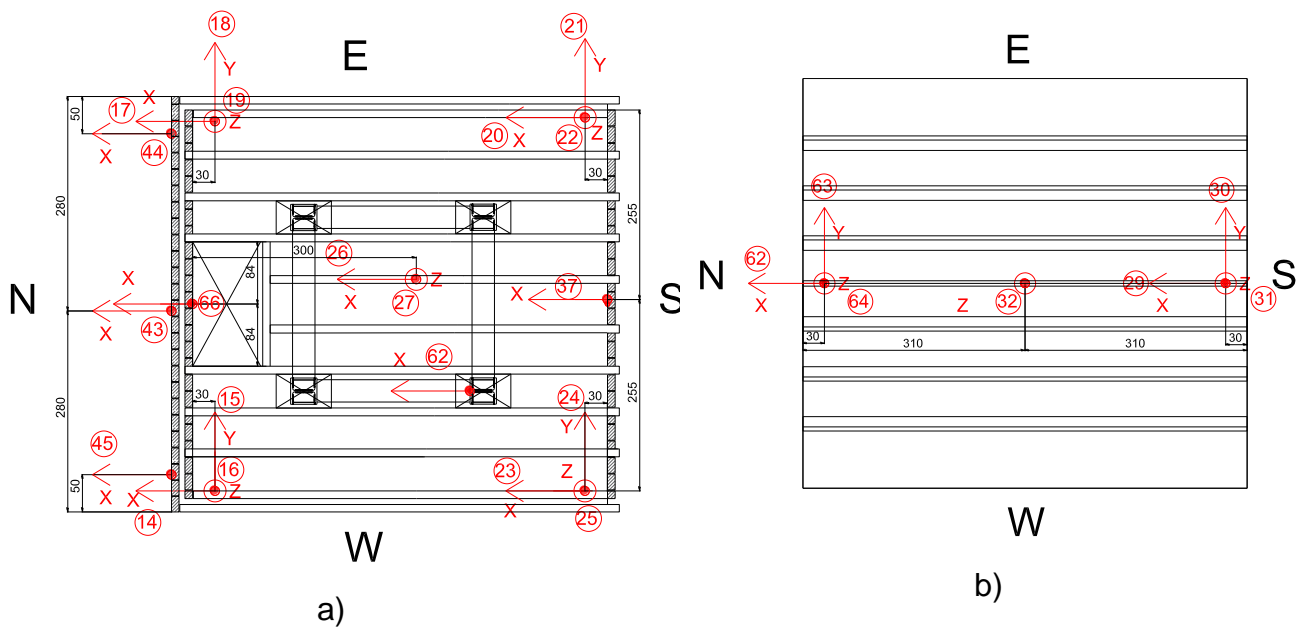


Figure 103 Accelerometer plan views: a) second-floor level (timber diaphragm); b) roof level.

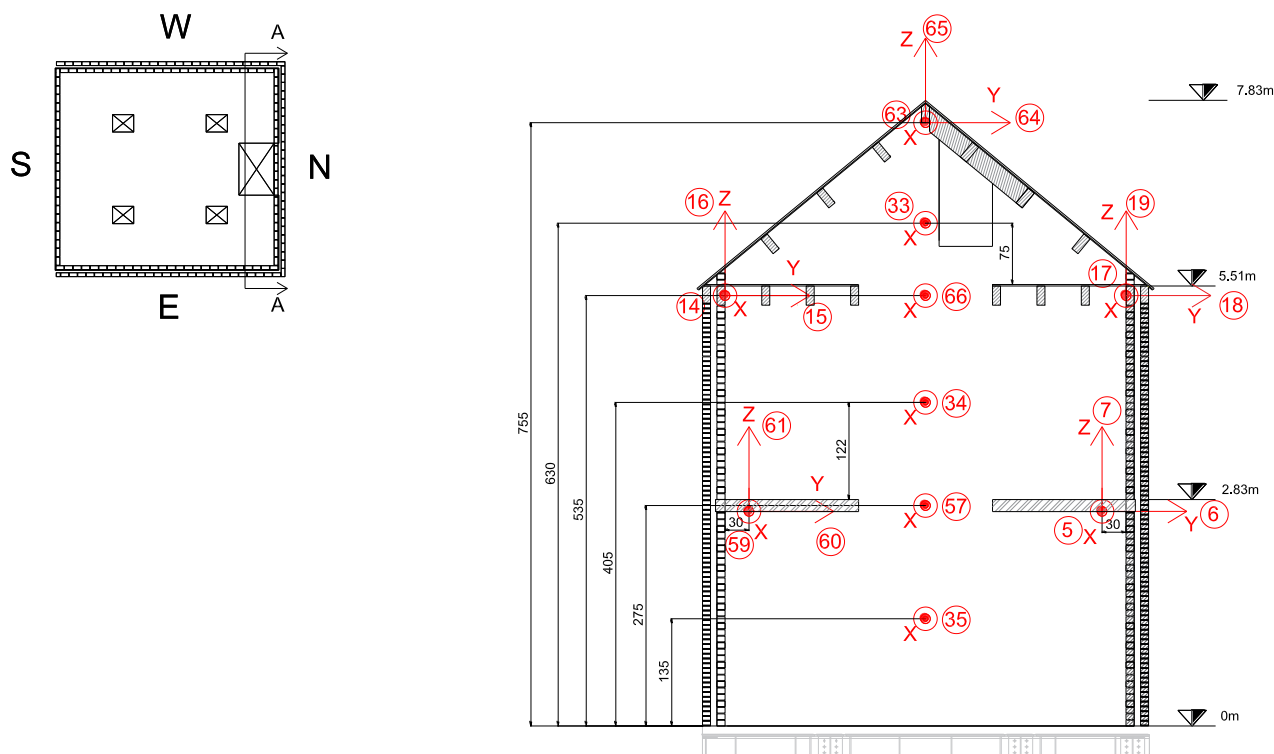


Figure 104 Accelerometer elevation: North calcium silicate inner leaf - Section A-A.

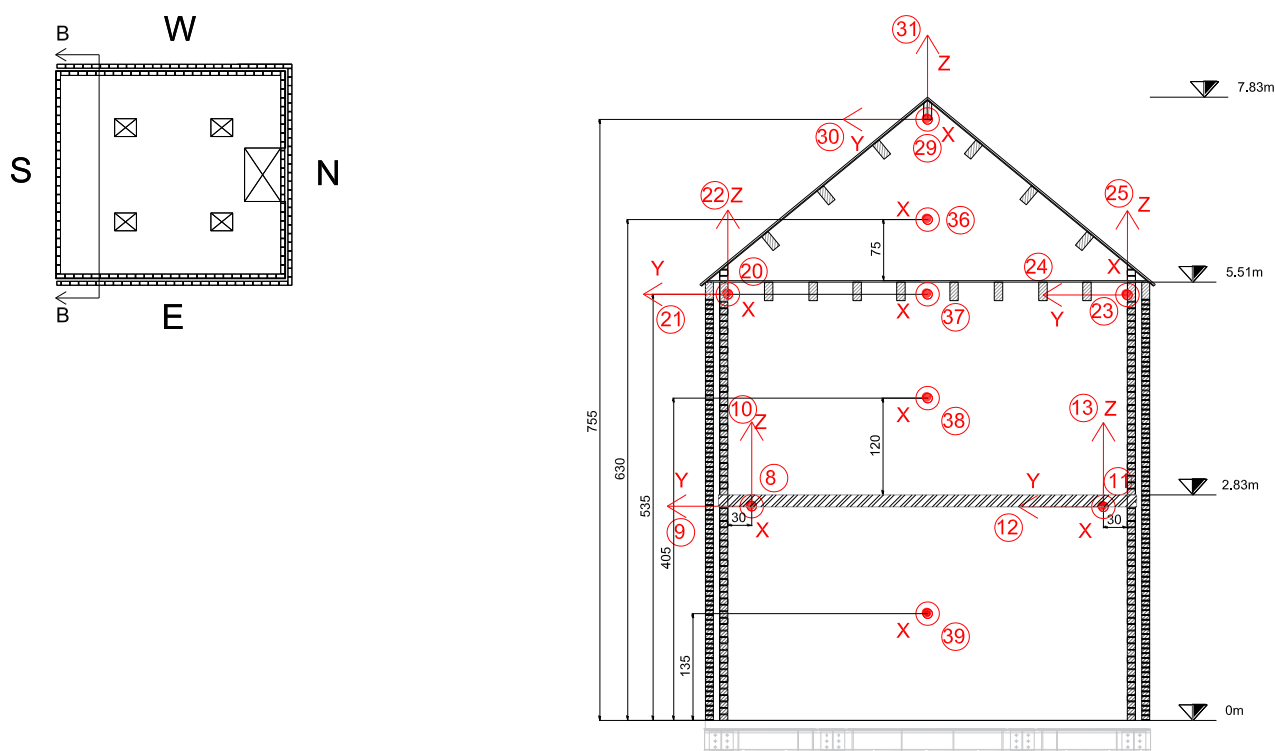


Figure 105 Accelerometer elevation: South calcium silicate inner leaf - Section B-B.

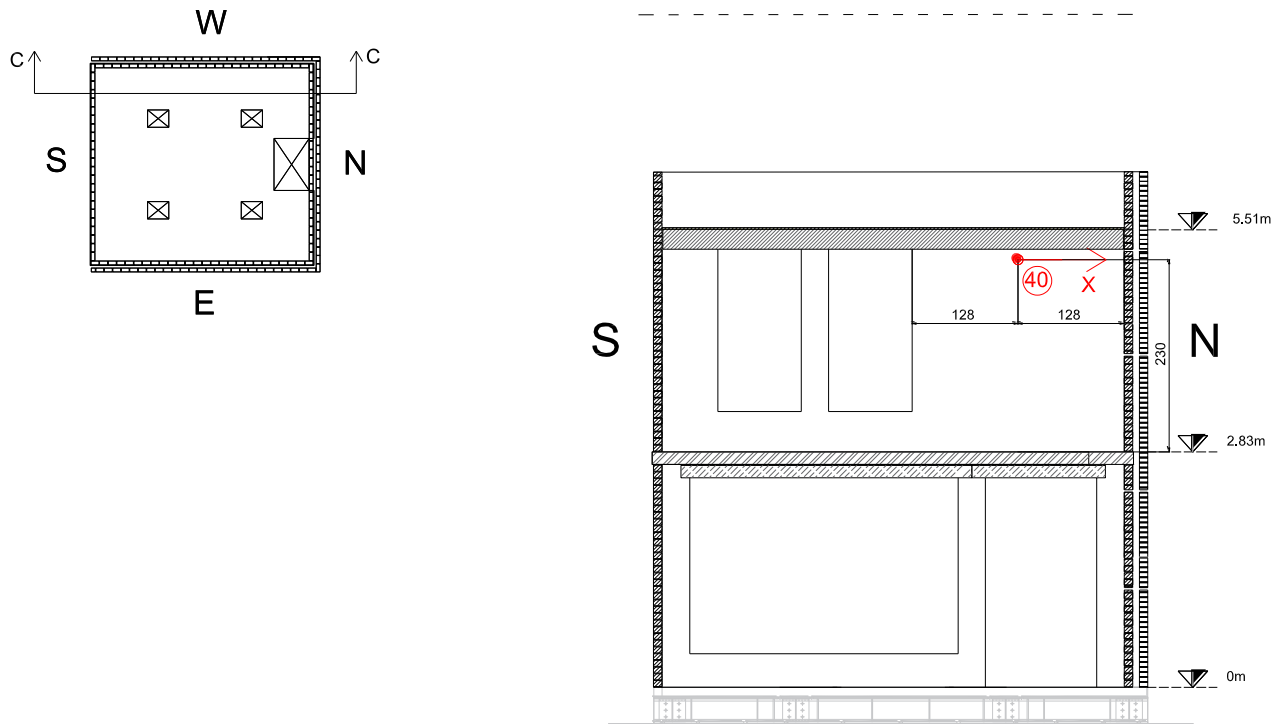


Figure 106 Accelerometer elevation: West calcium silicate inner leaf - Section C-C.

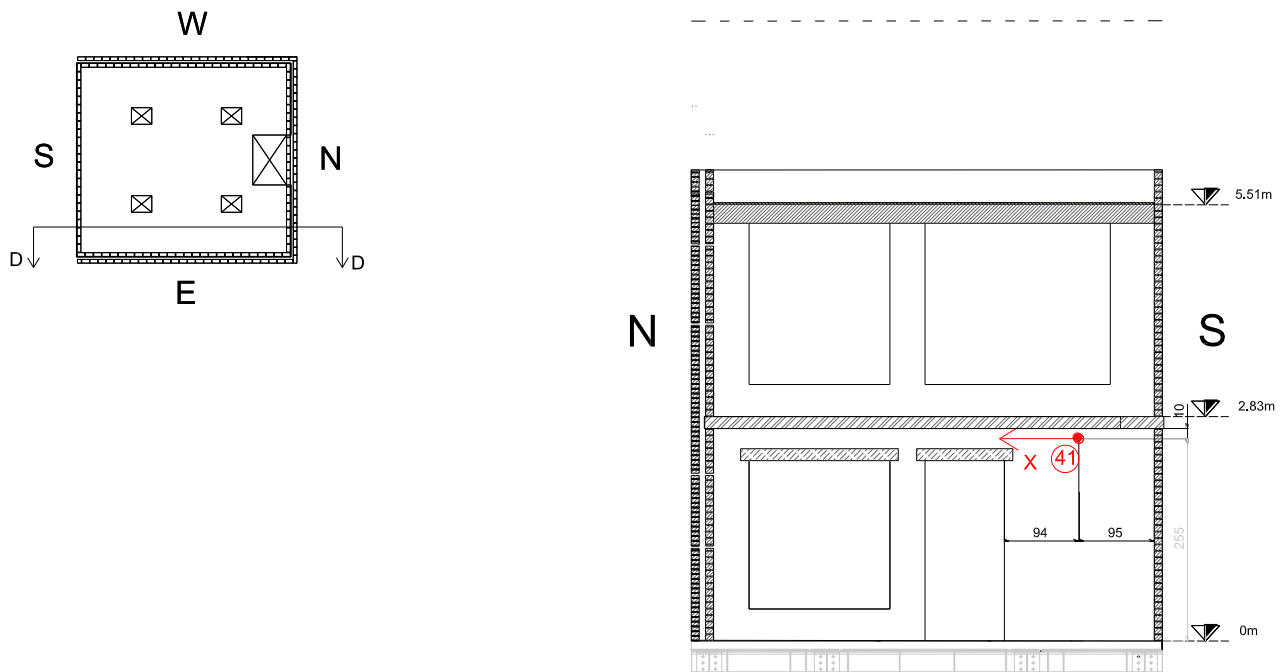


Figure 107 Accelerometer elevation: East calcium silicate inner leaf - Section D-D.

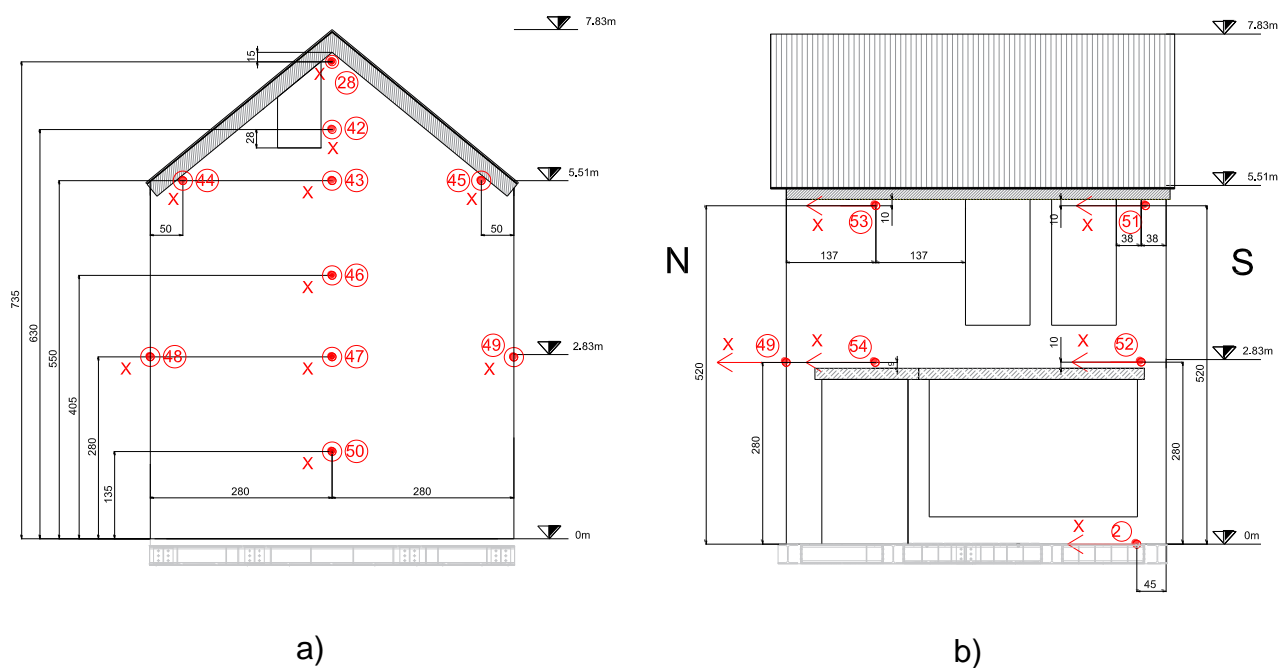


Figure 108 Accelerometer elevation: a) North clay outer leaf; b) West clay outer leaf.

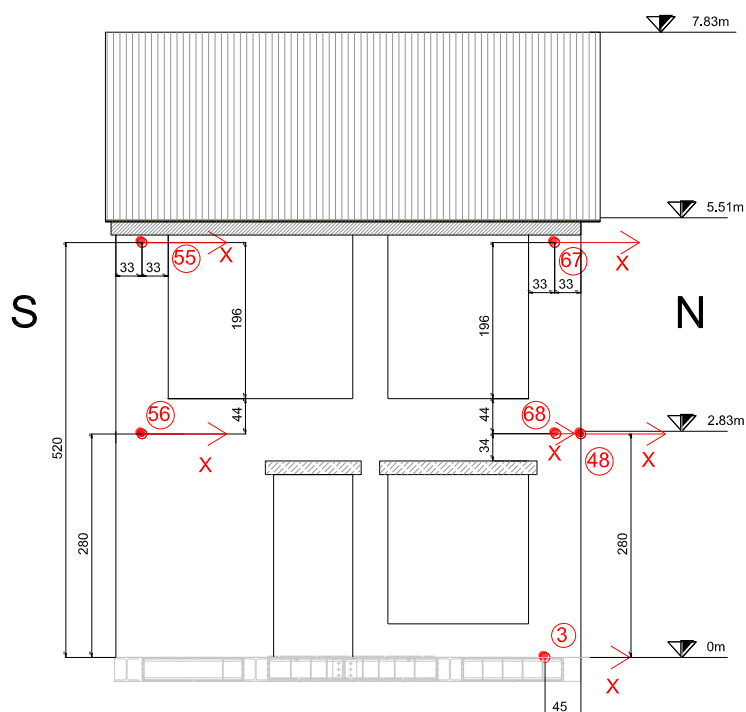


Figure 109 Accelerometer elevation: East clay outer leaf.

3.2 Displacement transducers

Displacement transducers allowed measuring displacements of the structural elements and their deformations.

A series of wire potentiometers recorded out-of-plane displacements of the North and South facades (CS and Clay) with respect to the rigid frame, while four wire potentiometers monitored in-plane deformations of the CS squat wall at the ground floor of the East façade. All wire potentiometers are listed in Table 20 and shown in Figure 110 through Figure 112.

Linear potentiometers were used to monitor the X and Y displacements of floor diaphragms with respect to the rigid frame, and to record possible uplifts and relative sliding of structural elements. All potentiometers are listed in Table 21 and shown in Figure 113 through Figure 122.

A text code is used to specify the structural elements connected to each linear or wire potentiometer, as specified on the 3D views of the transducers layout.

Some displacement transducers were removed during the last two runs of the incremental sequence (tests #24 and #25 of Table 23), to preserve the instrumentation in case of partial collapses. Specifically, all wire potentiometers connected to the outer leaf were removed as well as two potentiometers connected to the calcium silicate North façade. Referring to the following tables, the removed transducers are indicated with an asterisk in the Sensor ID column.

Table 20 Wire potentiometer list.

Sensor ID	Location	Measured parameter
73*	Ridge beam - North outer leaf (top of gable)	Displacement X
74	Ridge beam - Rigid frame	Displacement X
75	North inner leaf (centre of gable) - Rigid frame	Displacement X
76*	North outer leaf (centre of gable) - Rigid frame	Displacement X
77	South outer leaf (centre of gable) - Rigid frame	Displacement X
78*	North outer leaf (second-floor level) - Rigid frame	Displacement X
79	North inner leaf (second-floor level) - Rigid frame	Displacement X
80	North inner leaf (second storey mid-height) - Rigid frame	Displacement X
81*	North outer leaf (second storey mid-height) - Rigid frame	Displacement X
82	South inner leaf (second storey mid-height) - Rigid frame	Displacement X
83	North inner leaf (first-floor level) - Rigid frame	Displacement X
84*	North outer leaf (first-floor level) - Rigid frame	Displacement X
85	North inner leaf (first storey mid-height) - Rigid frame	Displacement X
86*	North outer leaf (first storey mid-height) - Rigid frame	Displacement X
87	South inner leaf (first storey mid-height) - Rigid frame	Displacement X
88	East inner leaf (first-storey squat pier)	Displacement Z
89	East inner leaf (first-storey squat pier)	Displacement Z
90	East inner leaf (first-storey squat pier)	Displacement along the diagonal
91	East inner leaf (first-storey squat pier)	Displacement along the diagonal

*removed after test #21.

IL → inner leaf;
OL → outer leaf;
FB → foundation beam;
T → shaking table;
LAB → laboratory floor;
RC → reinforced concrete diaphragm;
TD → timber diaphragm;
R → ridge beam;
IS → inner spreader beam;
OS → outer spreader beam;
F → internal rigid frame

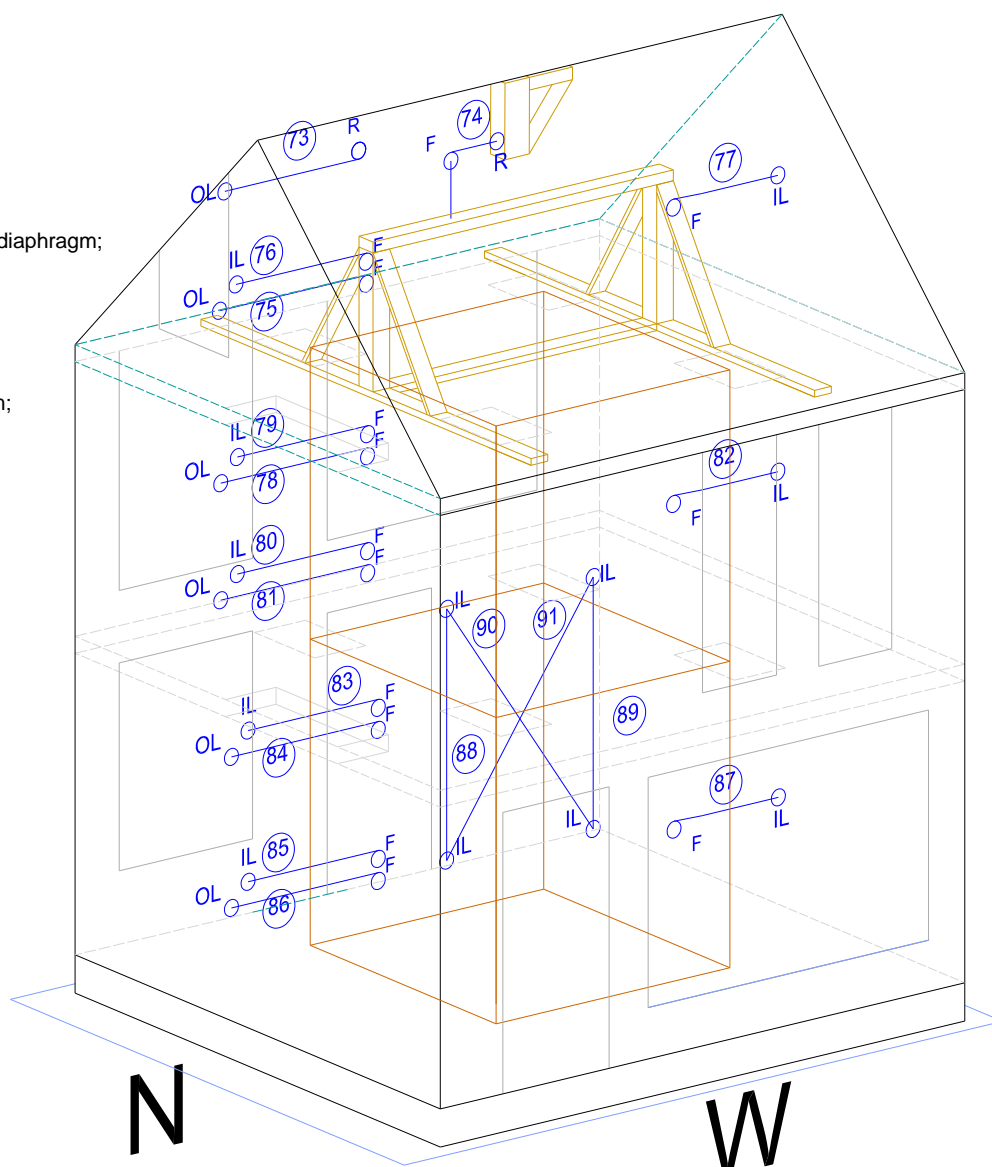


Figure 110 Wire potentiometer 3D view.

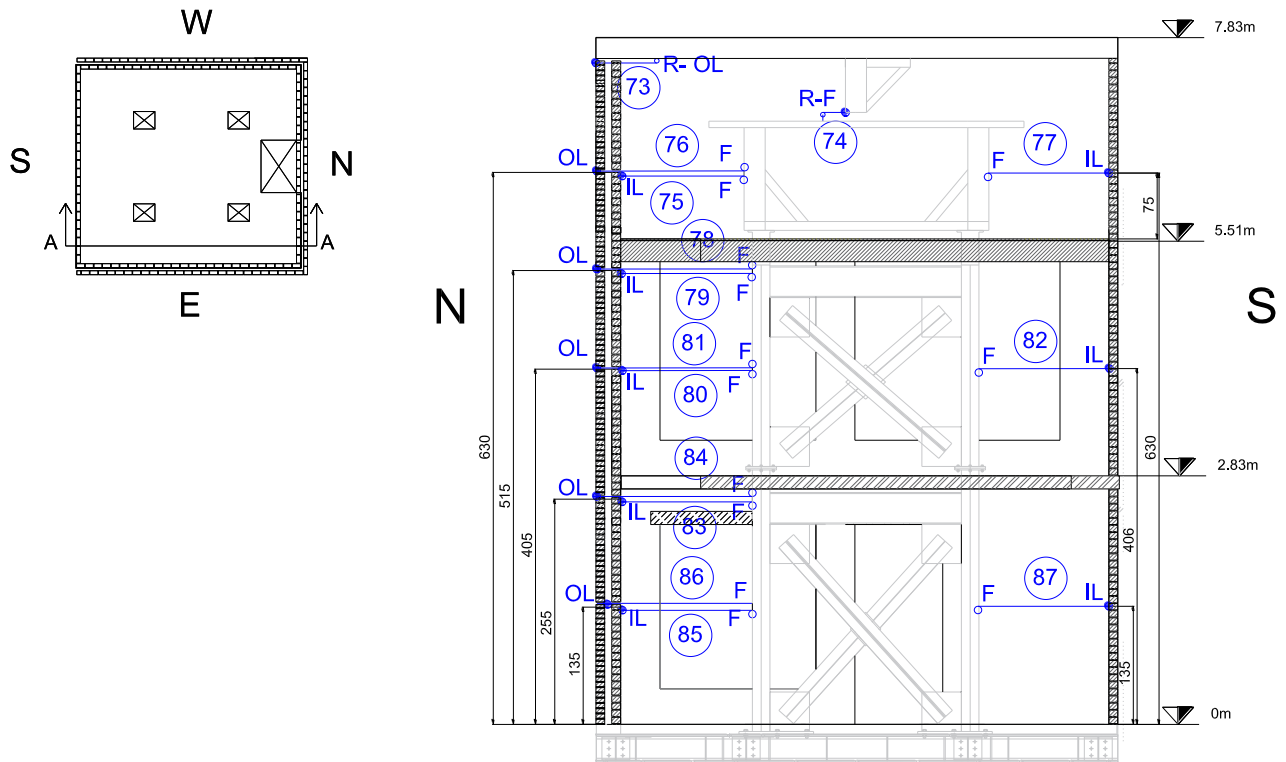


Figure 111 Wire potentiometer elevation: Section A-A.

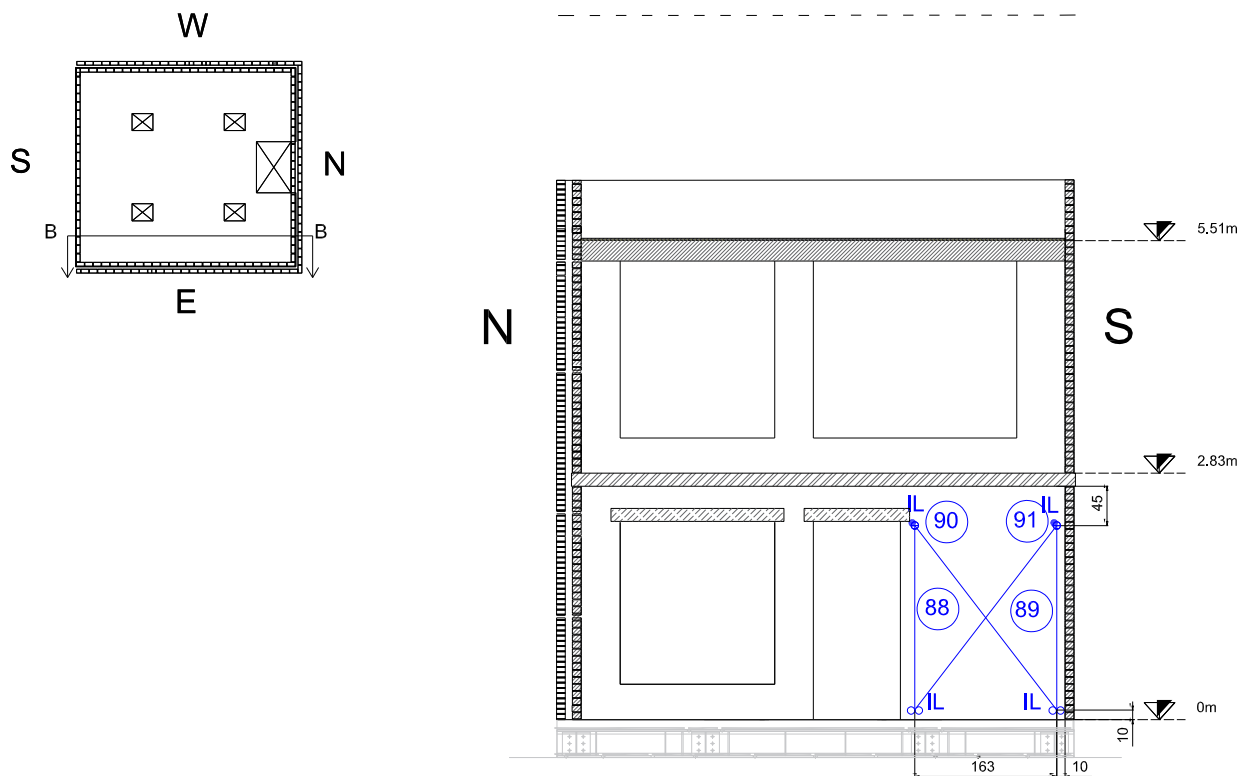


Figure 112 Wire potentiometer elevation: Section B-B.

Table 21 Linear potentiometer list.

Sensor ID	Location	Measured parameter
92	Ridge beam - North inner leaf (top of gable)	Displacement X
93	Ridge beam - South inner leaf (top of gable)	Displacement X
94	Timber diaphragm (North-West corner) - Rigid frame	Displacement X
95	Timber diaphragm (North-West corner) - Rigid frame	Displacement Y
96	Timber diaphragm (North-East corner) - Rigid frame	Displacement X
97	Timber diaphragm (North-East corner) - Rigid frame	Displacement Y
98	Timber diaphragm (South-East corner) - Rigid frame	Displacement X
99	Timber diaphragm (South-East corner) - Rigid frame	Displacement Y
100	Timber diaphragm (South-West corner) - Rigid frame	Displacement X
101	Timber diaphragm (South-West corner) - Rigid frame	Displacement Y
102	Timber diaphragm (South midspan) - Rigid frame	Displacement X
103	Timber diaphragm (South midspan) - South inner leaf	Displacement X
105	East outer leaf - East outer spreader beam	Displacement X
106	West inner leaf - West inner spreader beam	Displacement X
107	West outer leaf - West outer spreader beam	Displacement X
108*	North inner leaf - West inner spreader beam (North-West corner)	Displacement X
109	South inner leaf - West inner spreader beam (South-West corner)	Displacement X
110	South inner leaf - East inner spreader beam (South-East corner)	Displacement X
111	East inner leaf - East inner spreader beam	Displacement X
112*	North inner leaf - East inner spreader beam (North-East corner)	Displacement X
113	R.C. diaphragm (North-West corner) - Rigid frame	Displacement X
114	R.C. diaphragm (North-West corner) - Rigid frame	Displacement Y
115	R.C. diaphragm (North-East corner) - Rigid frame	Displacement X
116	R.C. diaphragm (South-East corner) - Rigid frame	Displacement X
117	R.C. diaphragm (South-East corner) - Rigid frame	Displacement Y
118	R.C. diaphragm (South-West corner) - Rigid frame	Displacement X
119	R.C. diaphragm (South midspan) - South inner leaf	Displacement X
120	R.C. diaphragm (North-West corner) - Inner leaf below	Displacement Z
121	R.C. diaphragm (North-East corner) - Inner leaf below	Displacement Z
122	R.C. Diaphragm - East inner leaf (first-storey squat pier top corner)	Displacement Z
123	R.C. diaphragm (South-East corner) - Inner leaf below	Displacement Z
124	East inner leaf (top of first-storey squat pier)	Displacement X
125	R.C. diaphragm (South-West corner) - Inner leaf below	Displacement Z
126	East inner leaf (first-storey squat pier mid-height)	Displacement X
127	West outer leaf - Foundation beam	Displacement X
128	West inner leaf - Foundation beam	Displacement X
129	East outer leaf - Foundation beam	Displacement X
130	West inner leaf - Foundation beam	Displacement X
131	East inner leaf (first-storey squat pier bott. corner) - Foundation beam	Displacement Z
132	East inner leaf (first-storey squat pier bott. corner) - Foundation beam	Displacement Z
133	Foundation beam - Shaking table (South-West corner)	Displacement X

Sensor ID	Location	Measured parameter
134	Foundation beam - Shaking table (South-East corner)	Displacement X
135	Shaking table - Laboratory strong floor	Displacement X
137	R.C. diaphragm - East inner leaf first-storey squat pier (top)	Displacement X

*removed after test #21.

- IL → inner leaf
OL → outer leaf
FB → foundation beam
T → shaking table
LAB → laboratory floor
RC → reinforced concrete diaphragm
TD → timber diaphragm
R → ridge beam
IS → inner spreader beam
OS → outer spreader beam
F → internal rigid frame

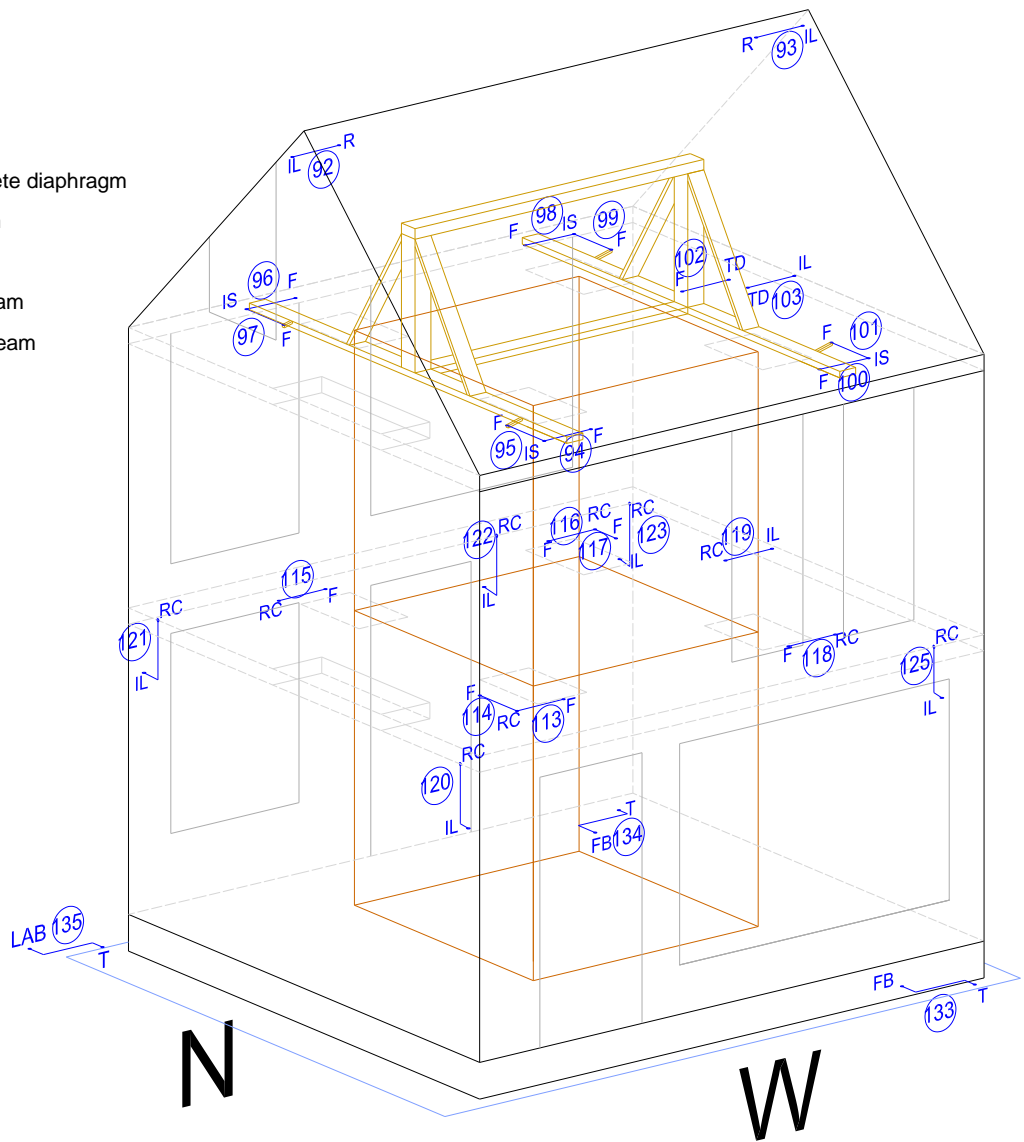


Figure 113 Linear potentiometer 3D view: foundation, first floor, second floor and roof diaphragms.

IL → inner leaf
OL → outer leaf
FB → foundation beam
T → shaking table
LAB → laboratory floor
RC → reinforced concrete diaphragm
TD → timber diaphragm
R → ridge beam
IS → inner spreader beam
OS → outer spreader beam
F → internal rigid frame

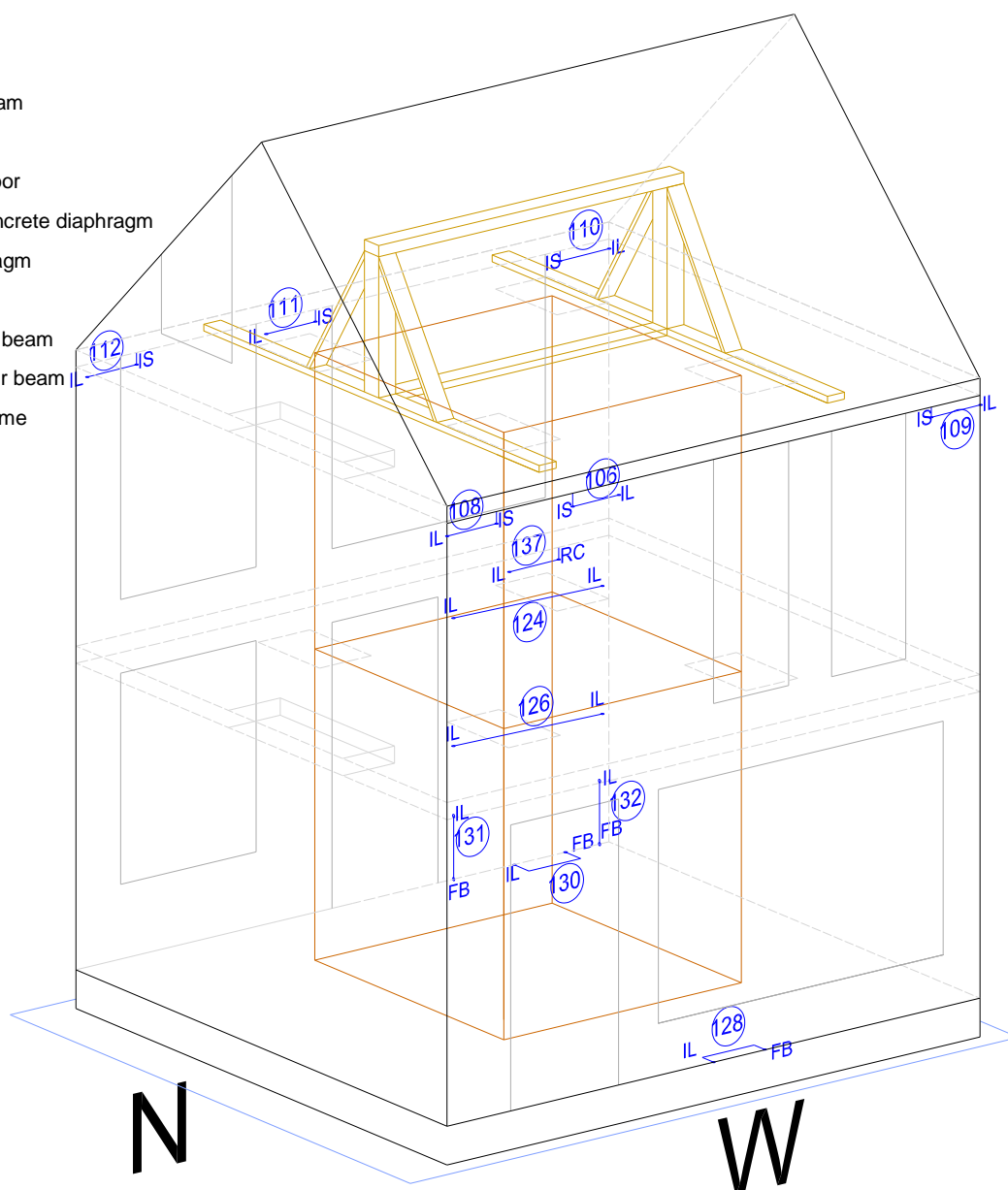


Figure 114 Linear potentiometer 3D view: calcium silicate inner leaves.

IL → inner leaf
 OL → outer leaf
 FB → foundation beam
 T → shaking table
 LAB → laboratory floor
 RC → reinforced concrete diaphragm
 TD → timber diaphragm
 R → ridge beam
 IS → inner spreader beam
 OS → outer spreader beam
 F → internal rigid frame

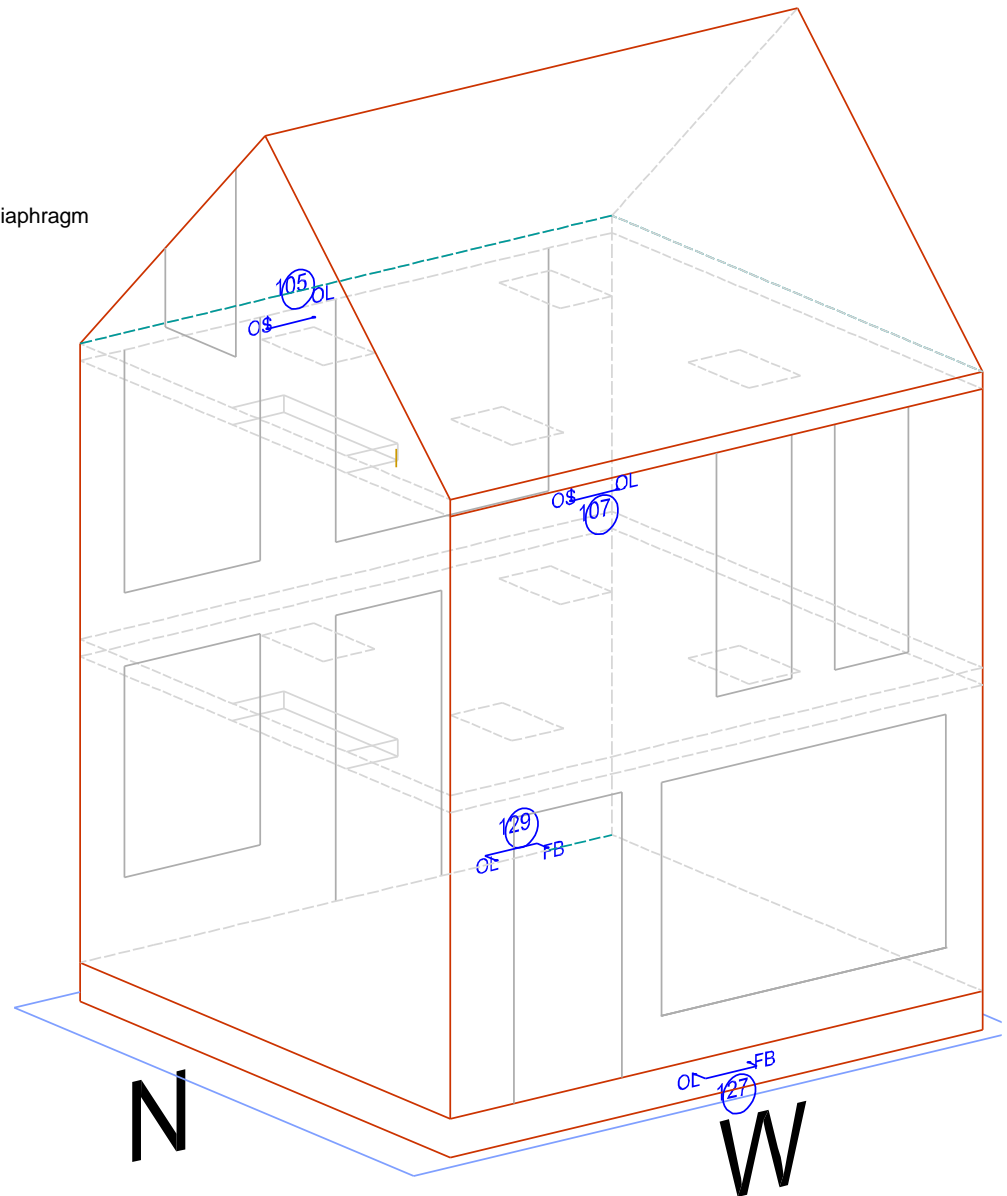


Figure 115 Linear potentiometer 3D view: clay outer leaves.

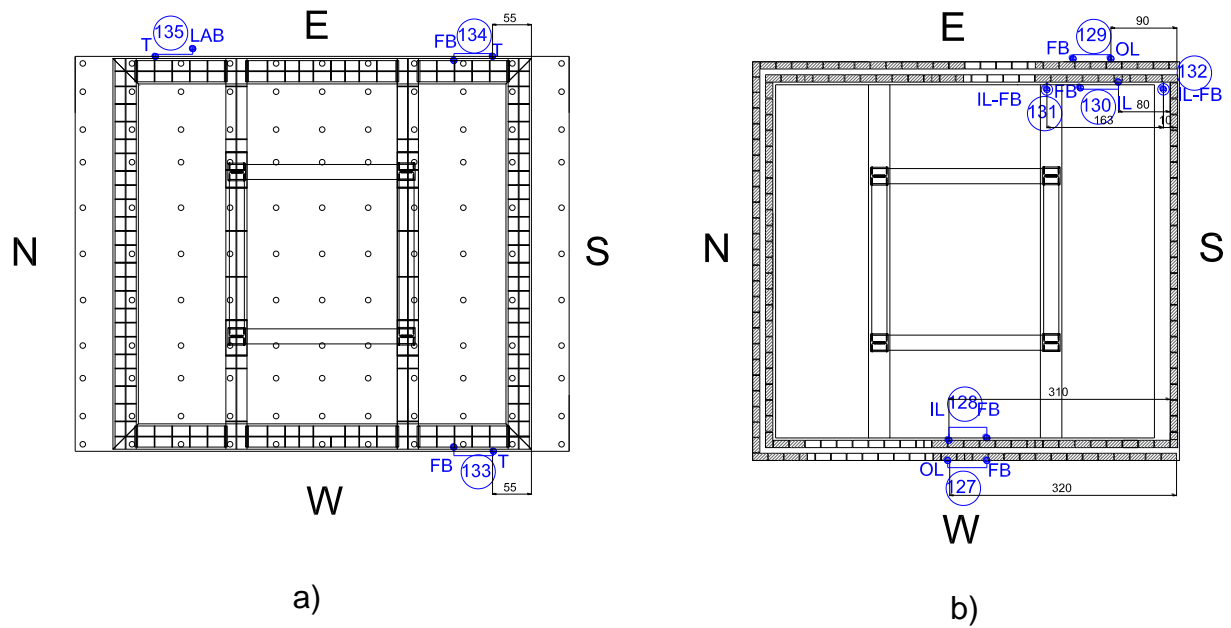


Figure 116 Linear potentiometer plan views: a) foundation level; b) ground-floor level.

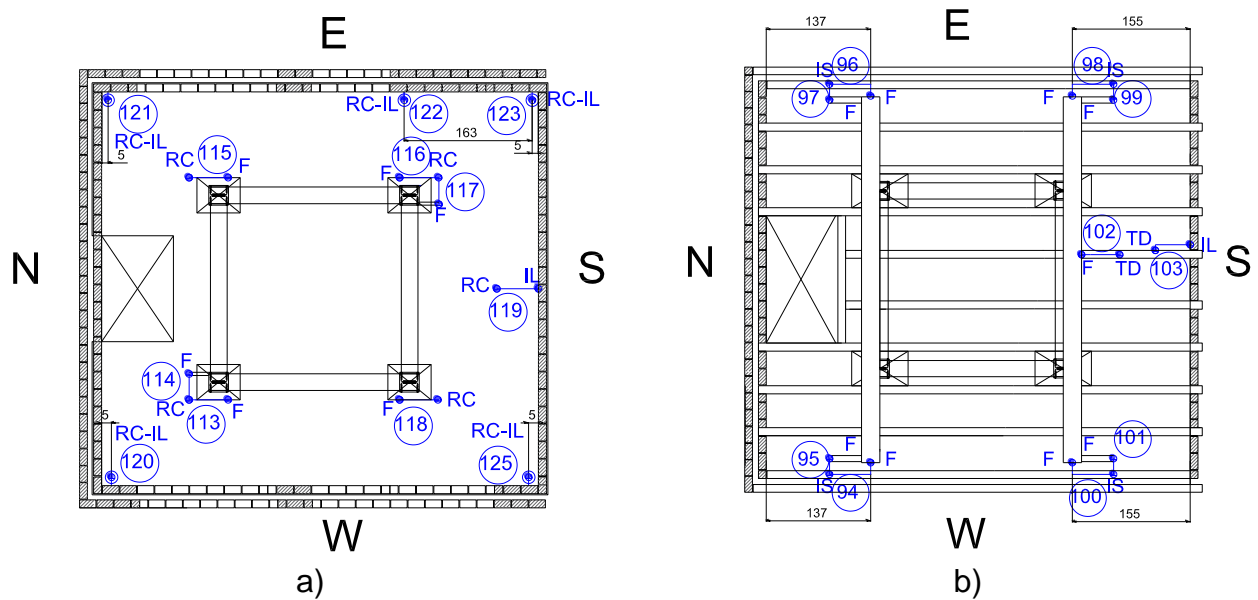


Figure 117 Linear potentiometer plan views: a) first-floor level (R.C. diaphragm); b) second-floor level (timber diaphragm).

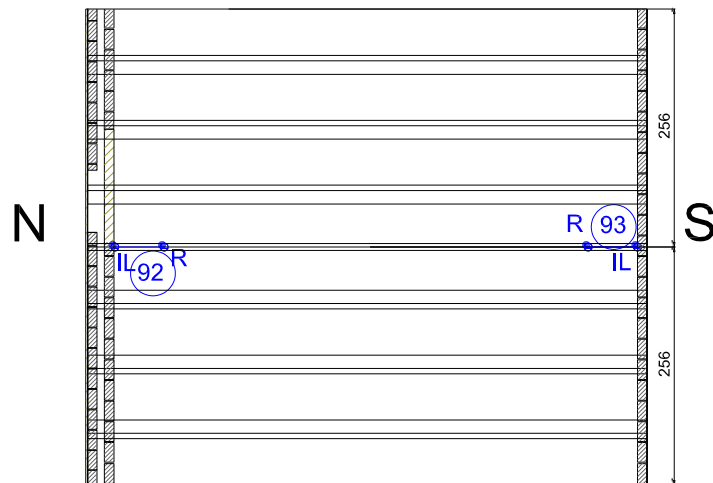


Figure 118 Linear potentiometer plan view: roof level.

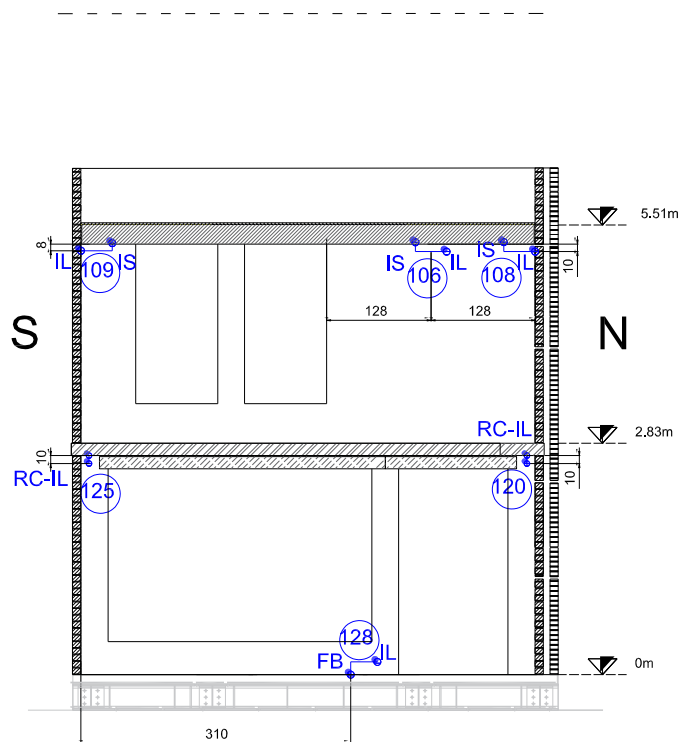
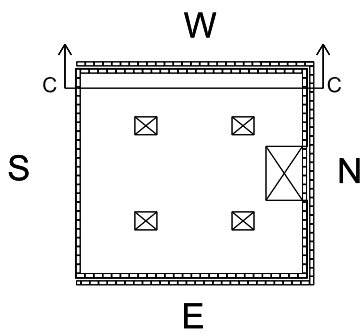


Figure 119 Linear potentiometer elevation: West calcium silicate inner leaf - Section C-C.

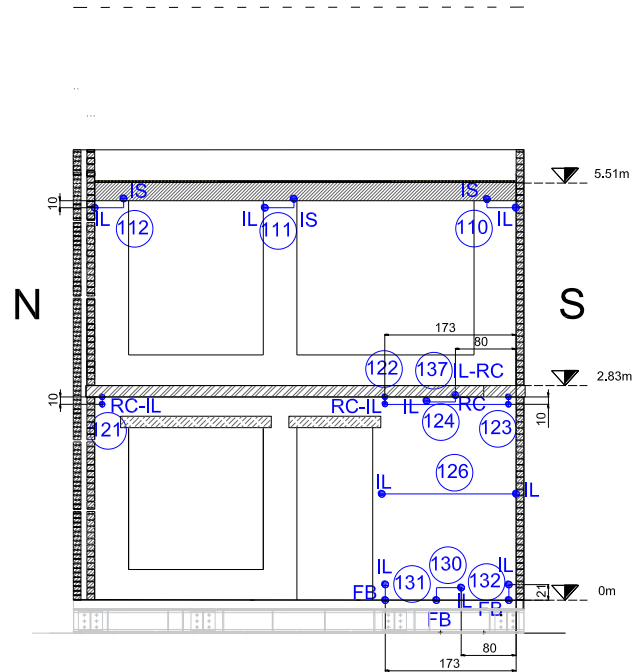
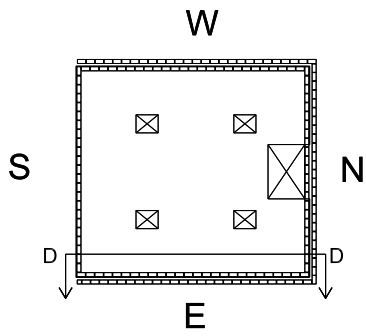


Figure 120 Linear potentiometer elevation: East calcium silicate inner leaf - Section D-D.

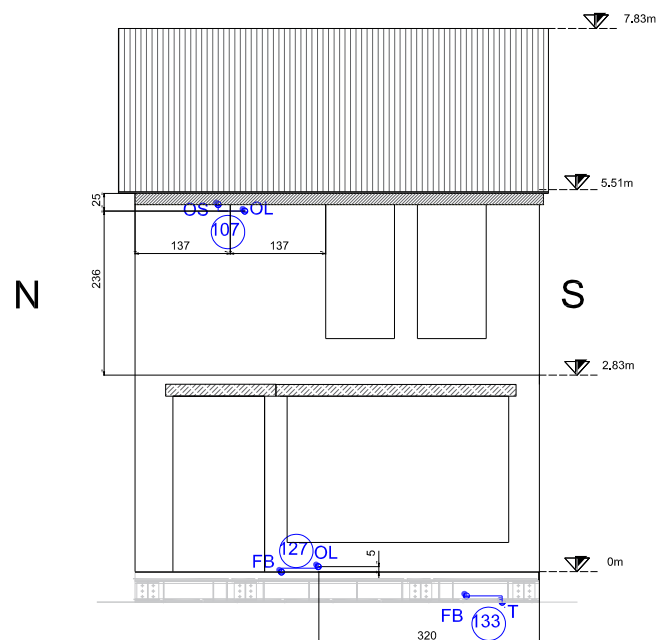


Figure 121 Linear potentiometer elevation: West clay outer leaf.

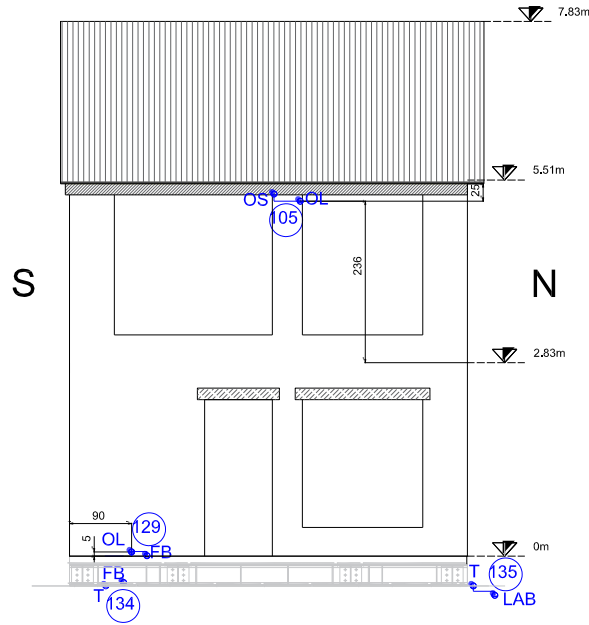


Figure 122 Linear potentiometer elevation: East clay outer leaf.

3.3 3D optical motion acquisition system

The 3D optical motion acquisition system consisted of passive reflective markers installed on the North, West, and South façades of the building (Figure 123). High-definition cameras recorded the trajectories of the corresponding points during the dynamic incremental tests. Figure 124, Figure 125 and Figure 126 show how these markers were distributed.

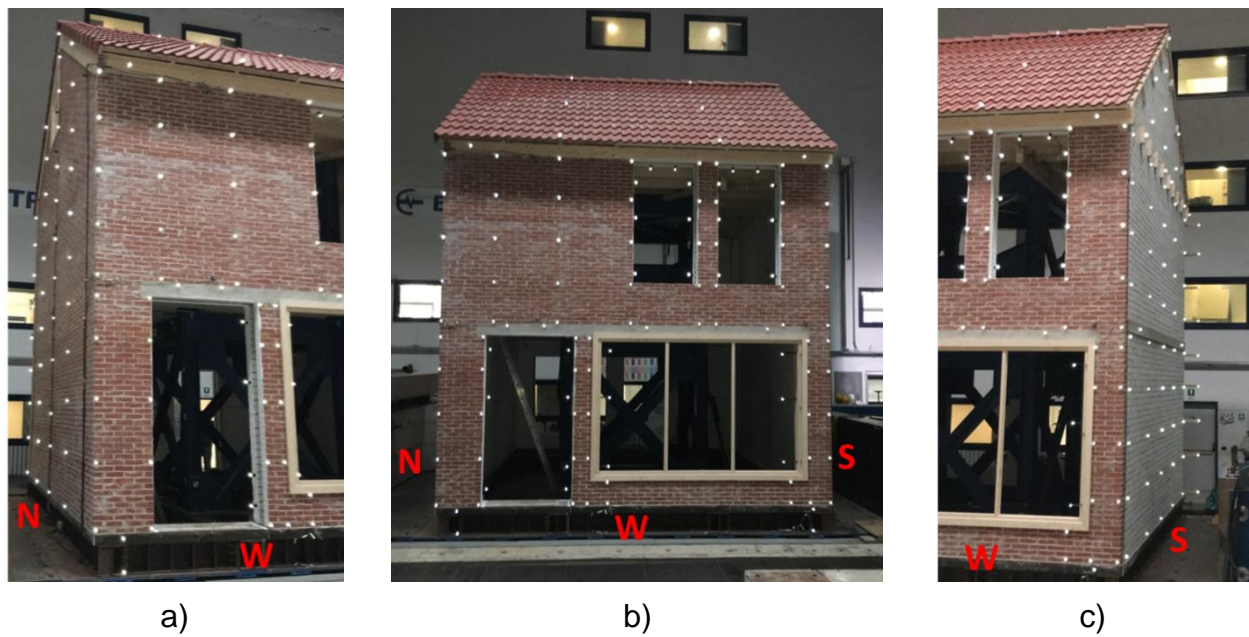


Figure 123 Reflective markers: a) North and West façades; b) West façade; c) West and South façades.

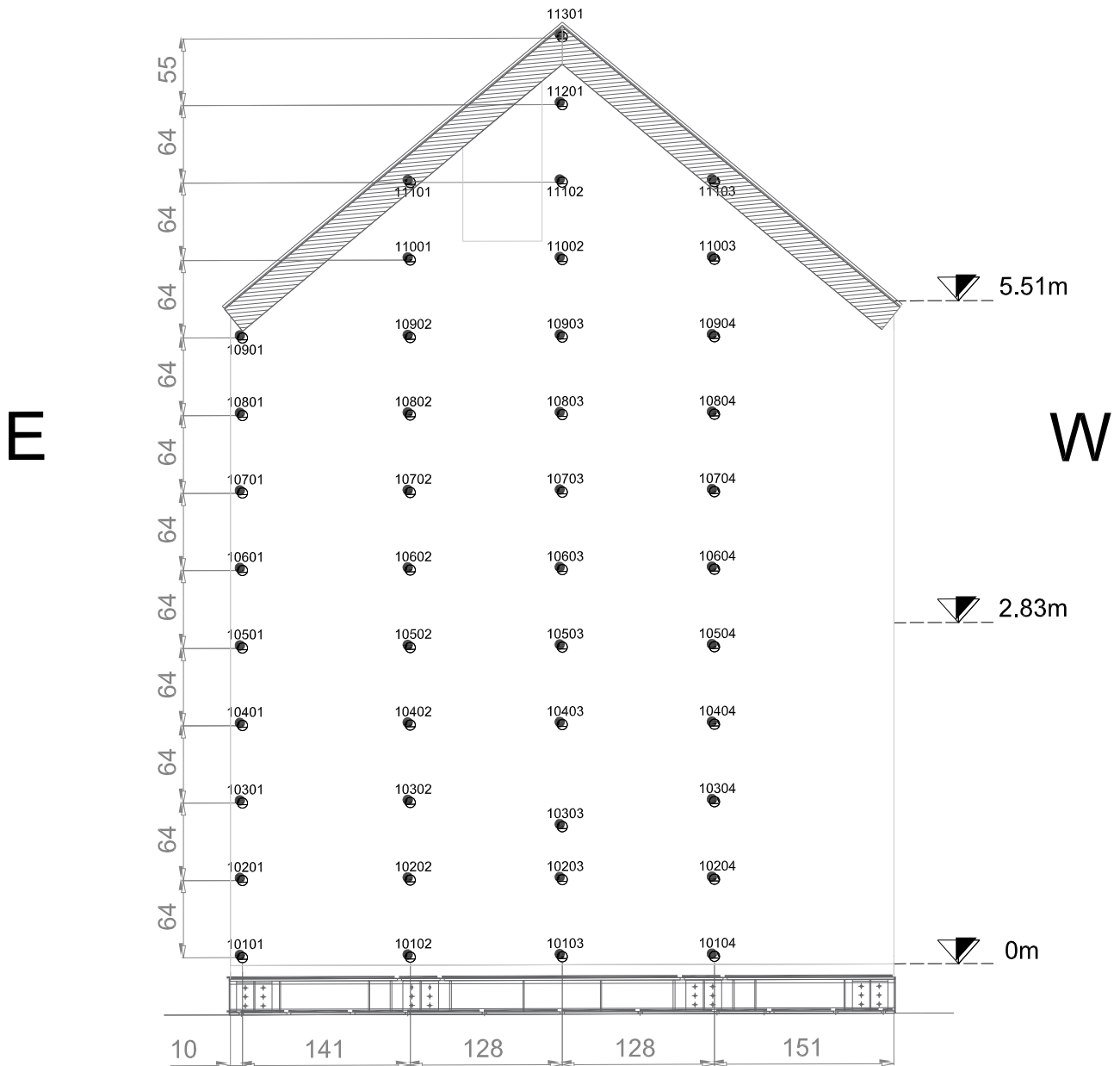


Figure 124 Reflective marker distribution: North façade.



Figure 125 Reflective marker distribution: South façade.



S

4. TEST PROCEDURE

The building specimen was subjected to an incremental dynamic test, applying to the shaking table a series of motions of increasing intensity, to assess damage evolution, failure modes, and ultimate capacity of the building. The input signal consisted of an acceleration time history representing a realistic ground motion for the Groningen region. The same acceleration history was then scaled in amplitude to obtain the desired incremental test protocol, consisting of eight main-shock events (Table 23 and Table 24).

4.1 Shake-table input signals

In order to perform the test, the specimen was subjected to 2 different typologies of ground motions (Table 22). The earthquake signal labelled EQ-NPR was used to generate the main events and the necessary table compensation tests. This ground motion is compatible with the uniform hazard spectrum with 2475-years return period for the Groningen region, according to the probabilistic seismic hazard assessment PSHA [8]. A random noise (RNDM) was also applied between the main shocks, for table calibration and structural dynamic identification purposes.

Figure 127 and Figure 128 show the acceleration time history of the earthquake signal and its acceleration and displacement elastic response spectra.

Table 22 Characteristics of the input signals.

Input	PGA [g]	Waveform name	5-75% significant duration [s]
RNDM	0.05	RNDM	180
EQ-NPR	0.32	EQ-NPR	1.37

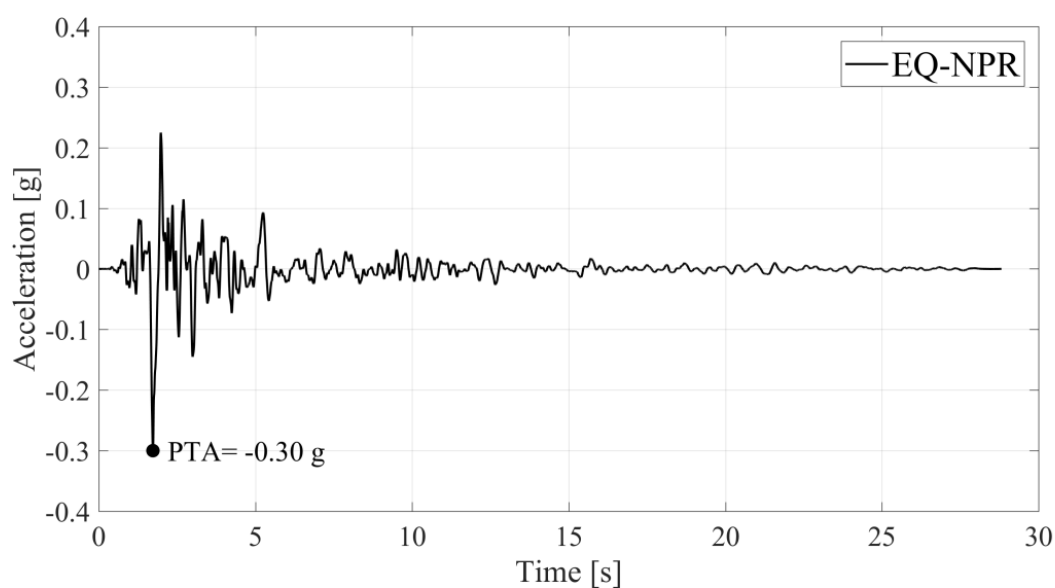


Figure 127 EQ-NPR acceleration time history (PTA = Peak table acceleration).

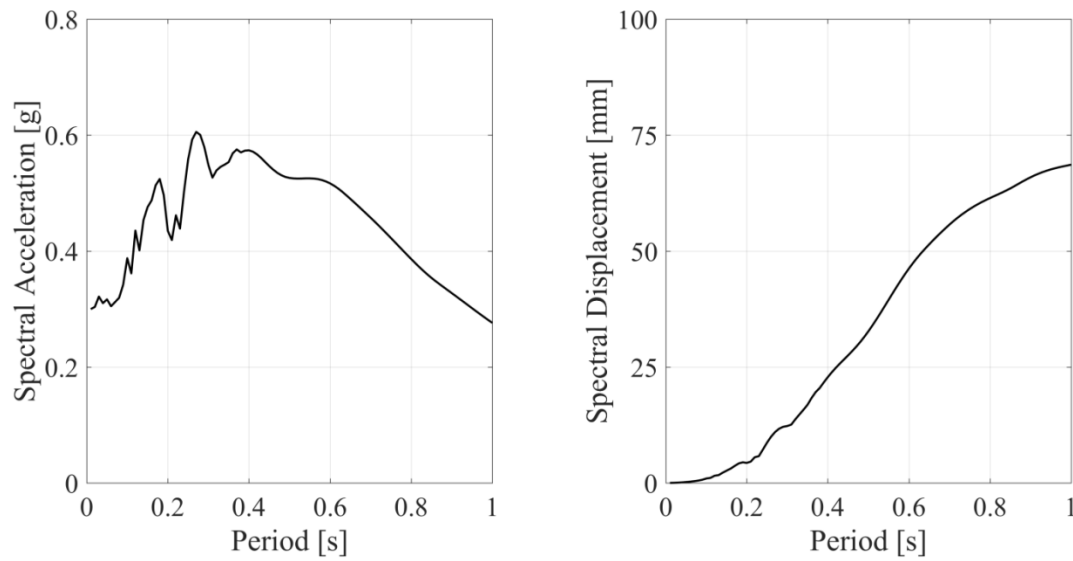


Figure 128 EQ-NPR elastic response spectra: acceleration (left), and displacement (right).

4.2 Applied input dynamic sequence

Table 23 summarises the testing sequence, providing for each record:

- date of execution;
- test sequential number;
- test ID;
- nominal PGA;
- recorded PGA.

Table 23 Testing sequence.

Date	Test #	Test ID	Nominal PGA [g]	Recorded PGA [g]
12/06/2018	1	RNDM	± 0.05	0.03
	2	EQ-NPR 20%	-0.06	-0.06
	3	EQ-NPR 33%	-0.10	-0.14
	4	RNDM	± 0.05	0.04
	5	EQ-NPR C	-	0.09
	6	EQ-NPR C	-	-0.12
	7	EQ-NPR C	-	-0.15
	8	EQ-NPR 50%	-0.15	-0.15
	9	RNDM	± 0.05	-0.03
	10	EQ-NPR 66%	-0.20	-0.22
	11	RNDM	± 0.05	0.04
13/06/2018	12	EQ-NPR C	-	-0.08
	13	EQ-NPR C	-	-0.12
	14	EQ-NPR C	-	-0.13
	15	EQ-NPR 85%	-0.25	-0.25
	16	RNDM	± 0.05	-0.05
	17	EQ-NPR C	-	-0.08
	18	EQ-NPR C	-	-0.12
	19	EQ-NPR C	-	-0.15
	20	EQ-NPR C	-	-0.15
	21	EQ-NPR 100%	-0.30	-0.3
	22	RNDM	± 0.05	0.04
14/06/2018	23	EQ-NPR IS C	-	+0.11
	24	EQ-NPR IS 100%	+0.30	+0.29
	25	EQ-NPR IS 133%	+0.40	+0.38
	26	RNDM	± 0.05	0.03

Bold rows contain the main shocks of the incremental dynamic test sequences.

Table 24 lists additional parameters for these main events. Compensations tests (EQ-NPR C) were performed before the main shocks using the same earthquake signal (EQ-NPR), to improve the matching between target and actual table motions. The period of the building prototype in undamaged conditions was $T_{und} = 0.17$ s.

The EQ-NPR signal is characterised by negative PGA and was applied with its normal polarity up to test #21 (EQ-NPR 100%). From that run onward, the table motions were applied with inverted polarity, in order to reduce the risk of structural collapse, being the specimen already heavily damaged with significant residual deformations. For this reason, the PGA of the last tests is positive and their ID includes the term “IS”, indicating “inverted signal”.

Table 24 Summary of the main-shock input parameters.

Test #	Test name	Scale factor	Nominal PGA [g]	Recorded PGA [g]	$T_{1,dam}$	$S_a(T_{1,und})$ [g]	$S_a(T_{1,dam})$ [g]
2	EQ-NPR 20%	20%	-0.058	-0.060	0.17	0.105	0.105
3	EQ-NPR 33%	33%	-0.099	-0.136	0.17*	0.210	0.210
8	EQ-NPR 50%	50%	-0.15	-0.151	0.21	0.264	0.227
10	EQ-NPR 66%	66%	-0.197	-0.218	0.23	0.346	0.312
15	EQ-NPR 85%	85%	-0.254	-0.255	0.24	0.428	0.423
21	EQ-NPR 100%	100%	-0.299	-0.303	0.31	0.518	0.509
24	EQ-NPR IS 100%	-100%	0.299	0.291	0.53	0.623	0.531
25	EQ-NPR IS 133%	-133%	0.398	0.385	0.53*	0.791	0.665

* no random input motion performed before the test, last computed value.

5. TEST RESULTS

In this chapter the seismic response of the building specimen is discussed in detail. First, the damage pattern evolution throughout all runs of the incremental shaking table test is discussed. Then, the building response is analysed in terms of force-displacement hysteresis, displacement profiles, interstorey drift ratio envelopes, and diaphragm deformations. Results from the 3D optical acquisition system are not discussed since they are currently under processing.

5.1 Damage pattern evolution

At the end of each stage of the shaking table test, the building was surveyed in detail and the crack patterns were accurately mapped to monitor the structural damage evolution. As emerged from these surveys, the in-plane flexural response of masonry piers of the East and West facades mainly governed the building behaviour. In particular, interior slender piers rocked at their ends, while corner slender piers behaved as flanges for the transverse walls and squatter corner piers rocked and partially detached from the perpendicular walls. Sliding of the second-floor timber spreader beams above the masonry piers was also observed.

In the following paragraphs, particular attention is devoted to crack development and activation of local failure mechanisms. For each significant run, four section views of the interior calcium-silicate walls (Figure 129 a) and three elevations profiles of clay walls are presented. Cracks marked in red were observed right after the test under examination, while those in black were previously detected (Figure 129 b).

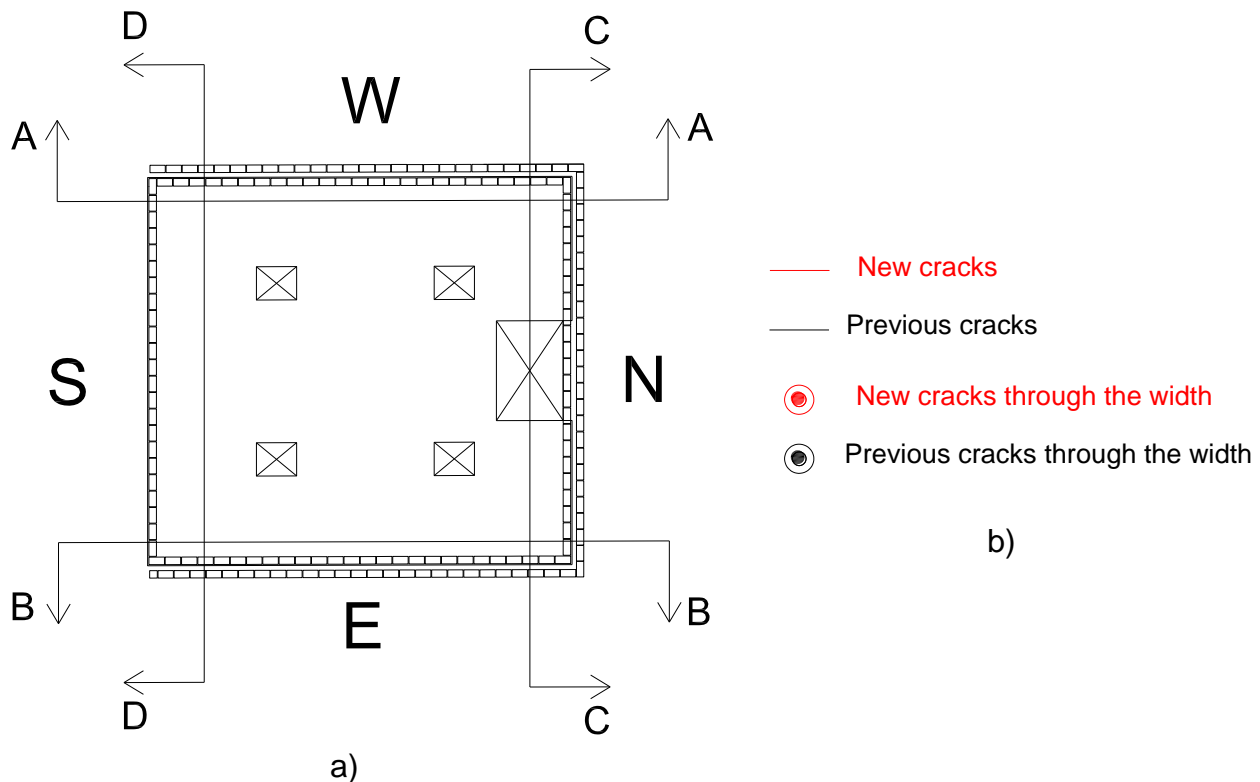


Figure 129 Damage evolution legend: a) location of the vertical sections to show inner calcium silicate walls; b) crack notations.

5.1.1 Observed damage after Test #2, EQ-NPR 20%, $PGA = 0.06 g$

The survey carried out immediately after testing did not show any visible damage. Only a few hairline cracks were detected at the interfaces of pocket connections between roof timber joist-to-perpendicular walls (North and South facades, Figure 131 and Figure 134 a) as well as at the second-floor plank-to-wall interfaces (Figure 131 and Figure 134 b); and at the base of the second-floor pier of the Southern corner of the West façade (Figure 130 and Figure 135).

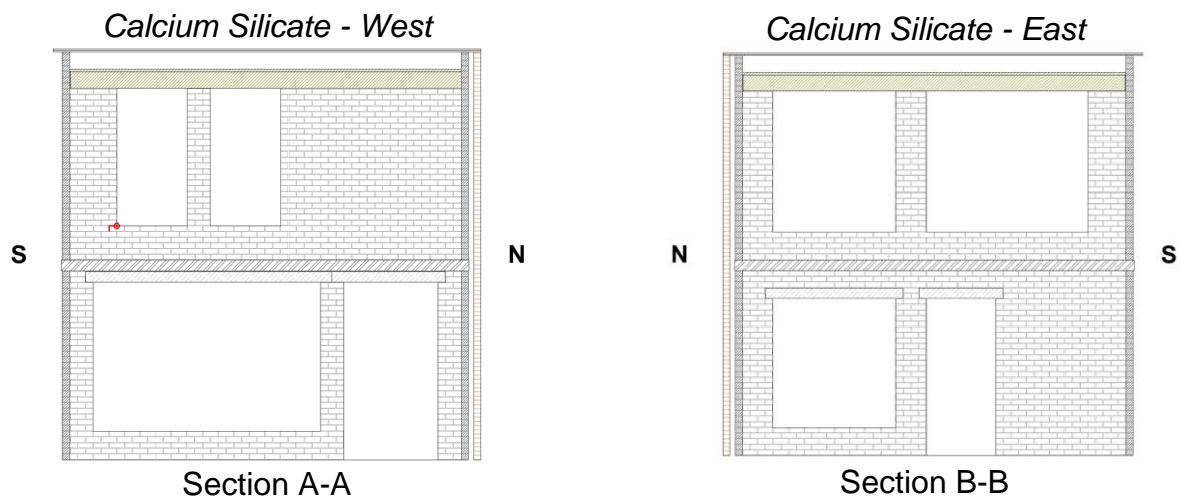


Figure 130 EQ-NPR 20% cracks - Calcium silicate longitudinal walls.

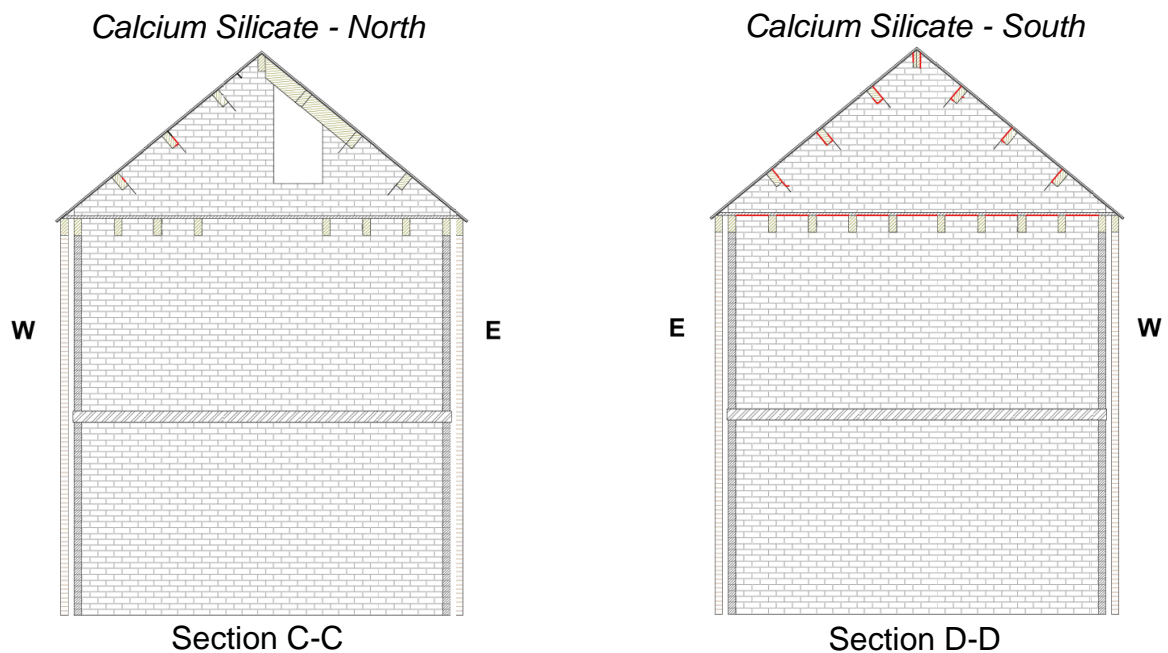


Figure 131 EQ-NPR 20% cracks - Calcium Silicate transversal walls.

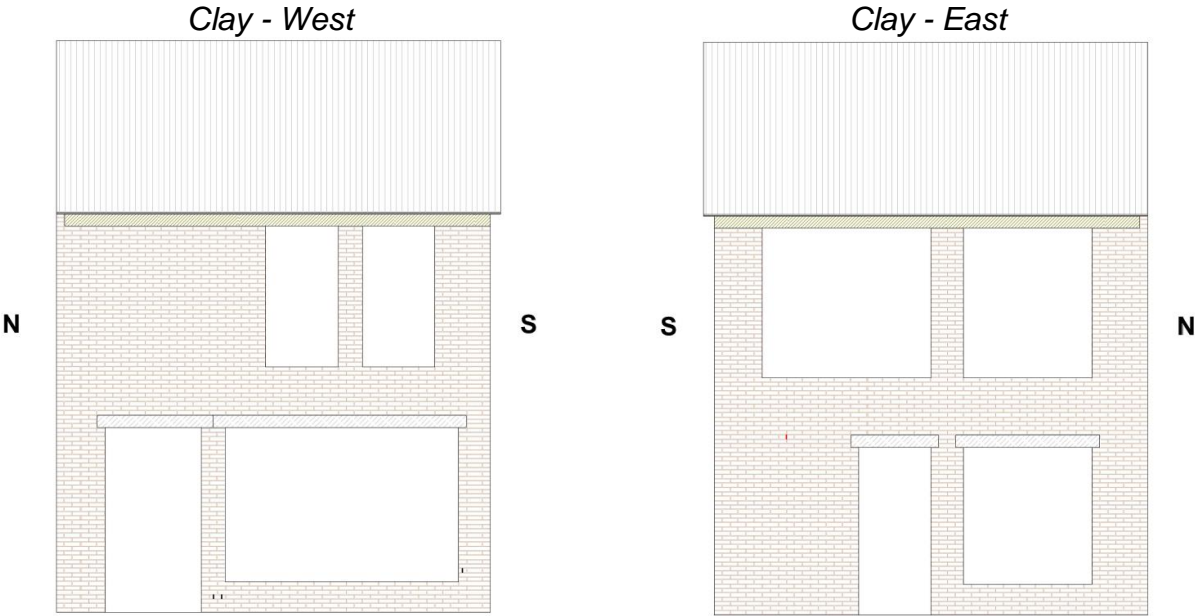


Figure 132 EQ-NPR 20% cracks – West and East clay façades.

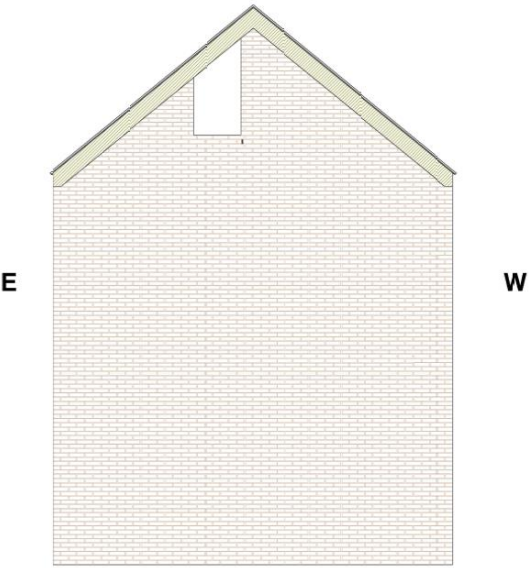


Figure 133 EQ-NPR 20% cracks – North clay façade.



Figure 134 EQ-NPR 20% Cracks view: a) South façade roof joist-to-wall connection; b) plank-to-wall interface.



Figure 135 EQ-NPR 20% Cracks on the West facade: a) overall view; b) window corner.

5.1.2 Observed damage after Test #3, EQ-NPR 33%, PGA = 0.1 g

At this stage, the building still did not experience any significant damage. No cracks were detected on the clay outer leaves (Figure 138 and Figure 139), while only minor extension of cracks (with residual width smaller than 0.1 mm) were observed at the interfaces between the calcium silicate inner leaf and the timber joist and planks (Figure 137, Figure 140 and Figure 141). Remarkably, small cracks were detected on the East and West façades between the roof spreader beams and the masonry walls (Figure 136 and Figure 142).

No appreciable extension of crack was found at the base of the first-floor pier of the West façade at its South corner (Figure 136 a).

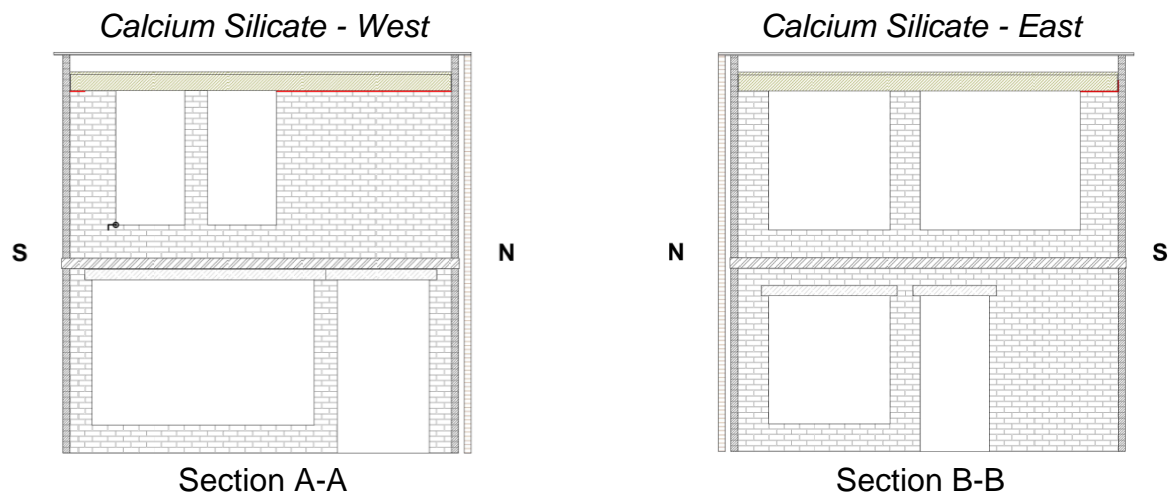


Figure 136 EQ-NPR 33% cracks - Calcium silicate longitudinal walls.

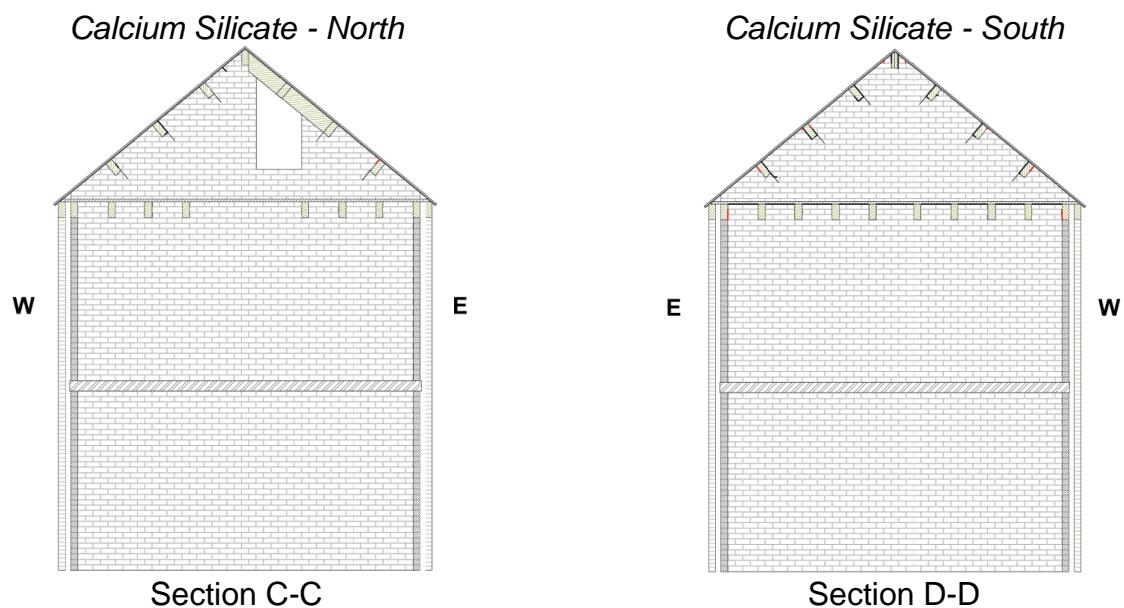


Figure 137 EQ-NPR 33% cracks - Calcium Silicate transverse walls.

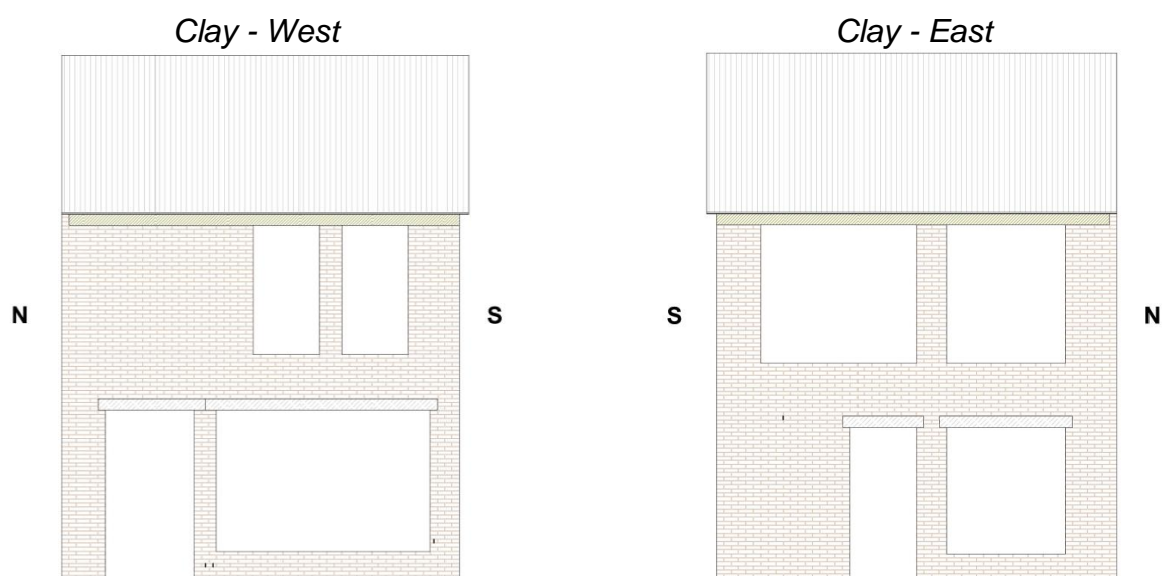


Figure 138 EQ-NPR 33% cracks – West and East clay façades.

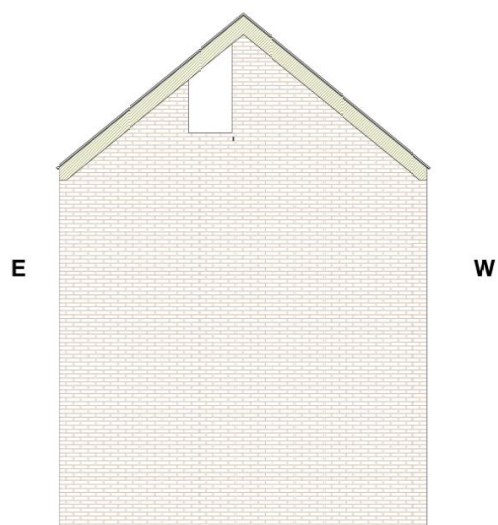


Figure 139 EQ-NPR 33% cracks – North clay façade.

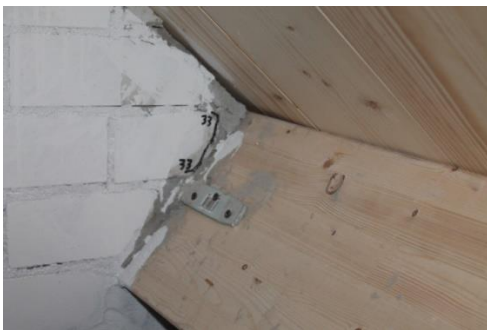


a)



b)

Figure 140 EQ-NPR 33% - Overall view of the cracks on the South gable wall: a) West side; b) East side.



a)



b)

Figure 141 EQ-NPR 33% - Zoom-in on the cracks of the South gable wall: a) West side; b) East side.



a)



b)

Figure 142 EQ-NPR 33% - West facade sliding cracks: a) overall view of the North side; b) zoom-in on the South side.

5.1.3 Observed damage after Test #8, EQ-NPR 50%, $PGA = 0.15 g$

After this test, the timber-to-masonry interface cracks of the inner leaves extended moderately. Sliding cracks on top of first floor piers, formed also on the outer leaves of East and West side (Figure 145 and Figure 149). Moreover, many other new cracks developed, denoting the onset of local failures mechanisms.

Several cracks (with residual widths smaller than 1 mm) formed throughout the width of walls at the base and top of the piers of the West and East façades, on both inner and outer leaves, especially at the first floor (Figure 143 and Figure 147, Figure 145 and Figure 148). Such evidences denoted the onset of uplift at the base of piers, meaning the activation of flexural mechanisms.

Moreover, some cracks developed at the interface between RC lintels and the calcium silicate inner leaf (Figure 143), as well as at the North and South façades roof joist-to-gable pocket connections (Figure 144).

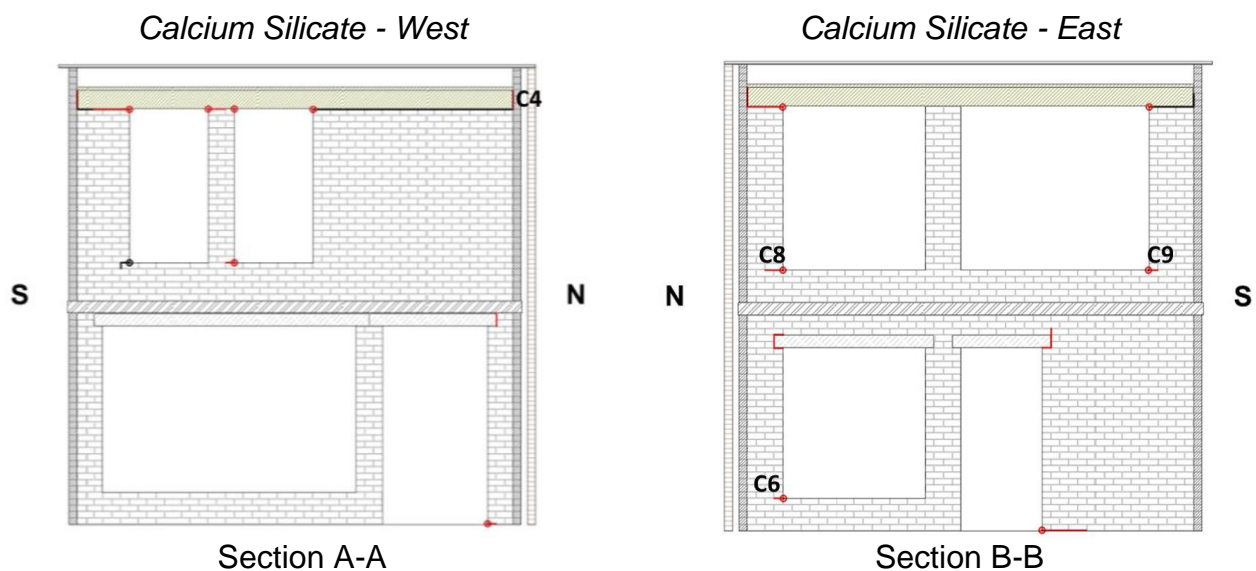


Figure 143 EQ-NPR 50% cracks - Calcium silicate longitudinal walls.

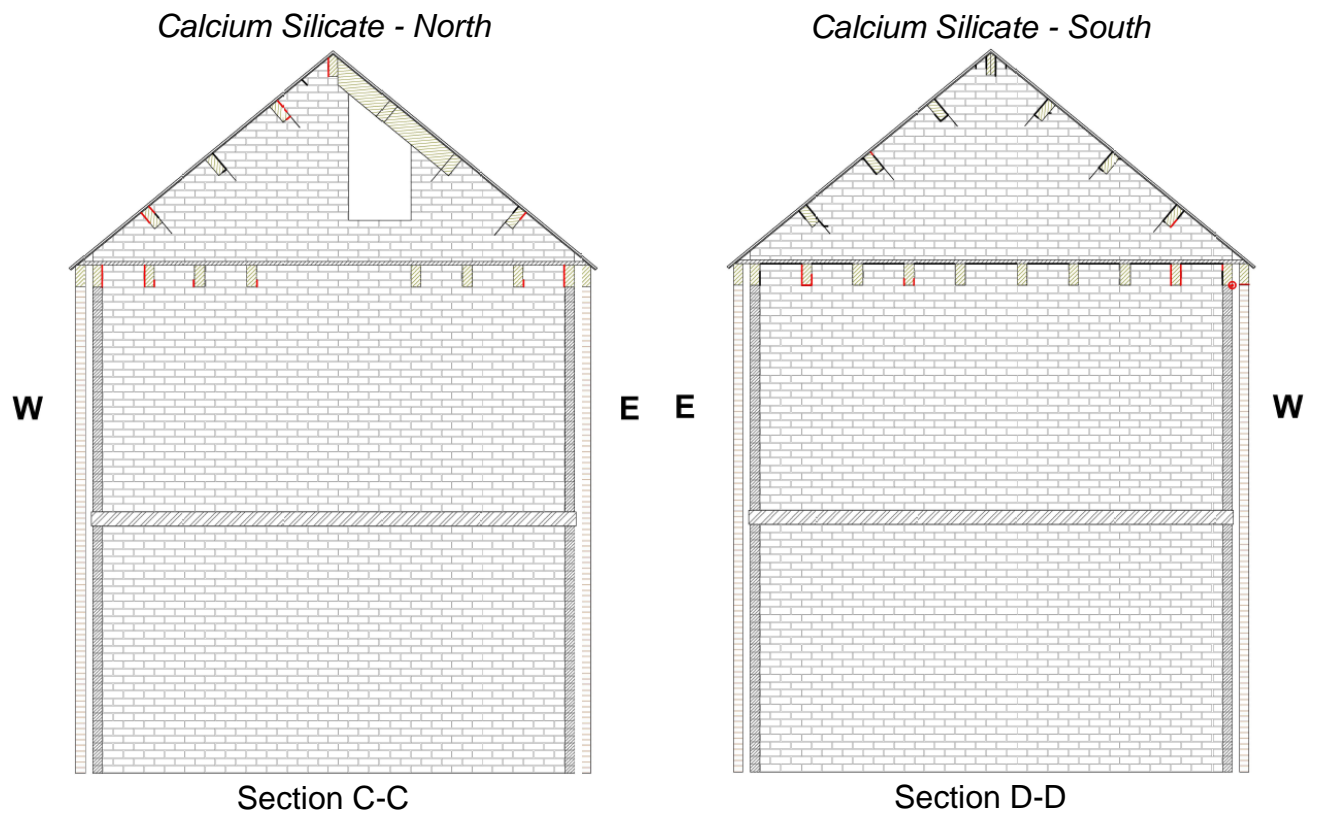


Figure 144 EQ-NPR 50% cracks - Calcium silicate transverse walls.

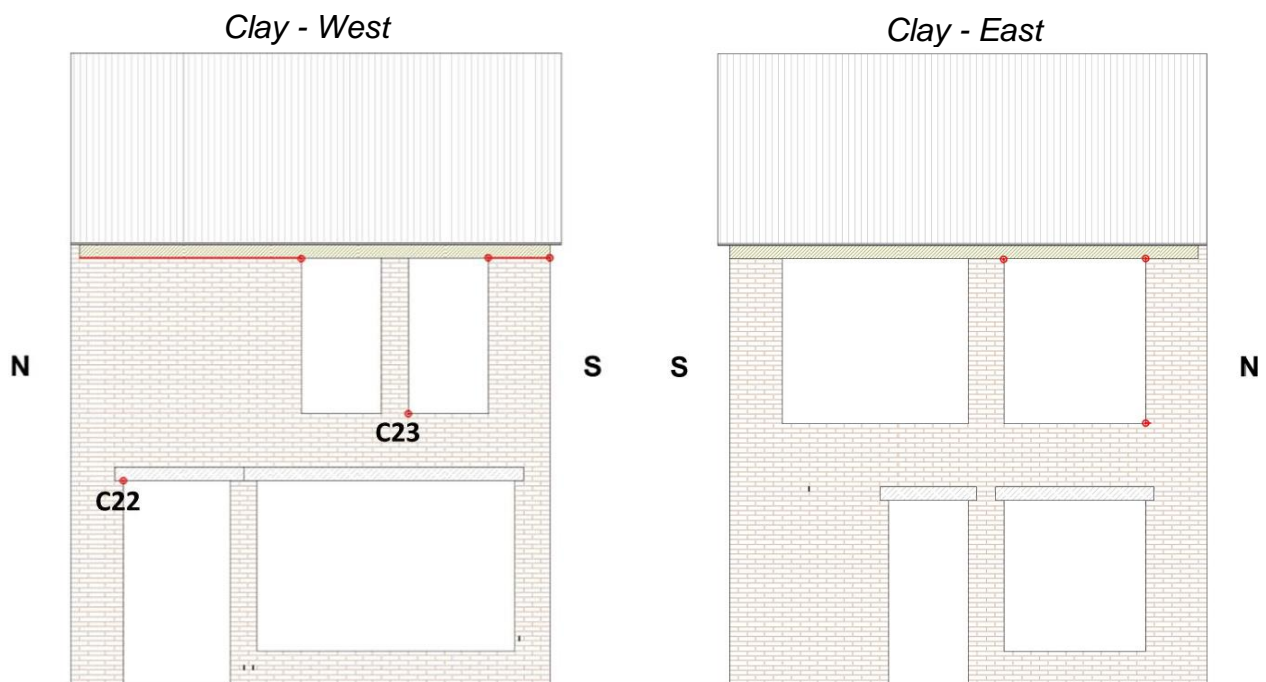


Figure 145 EQ-NPR 50% cracks – West and East clay façades.

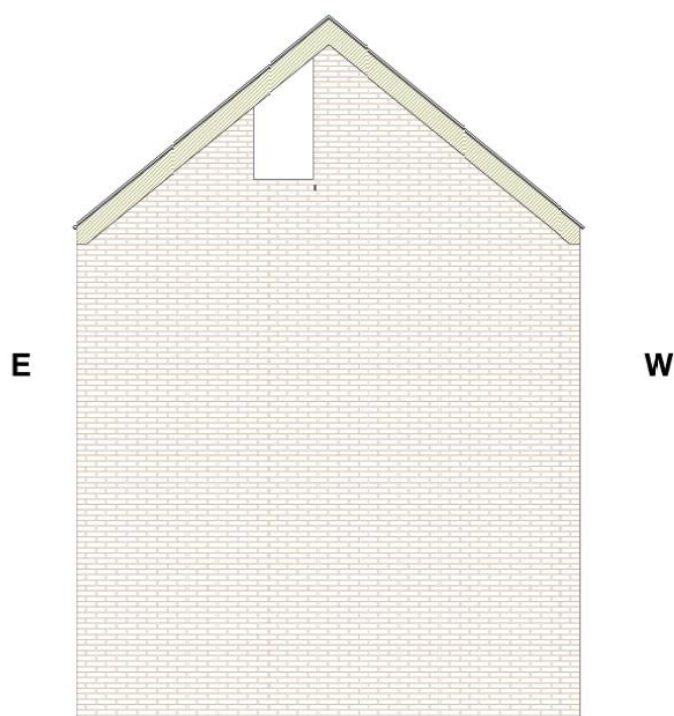


Figure 146 EQ-NPR 50% cracks – North clay façade.



a)



b)

Figure 147 EQ-NPR 50% pier base cracks on the inner leaf: a) C8; b) C9.

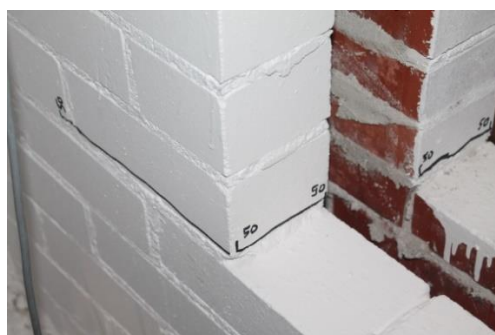


Figure 148 EQ-NPR 50% pier base cracks: C9 on the inner leaf and corresponding crack on the outer leaf.



Figure 149 EQ-NPR 50% sliding cracks: between timber spreader beam and West façade outer leaf: a) North end; b) mid-span.

5.1.4 Observed damage after Test #10, EQ-NPR 66%, PGA = 0.20 g

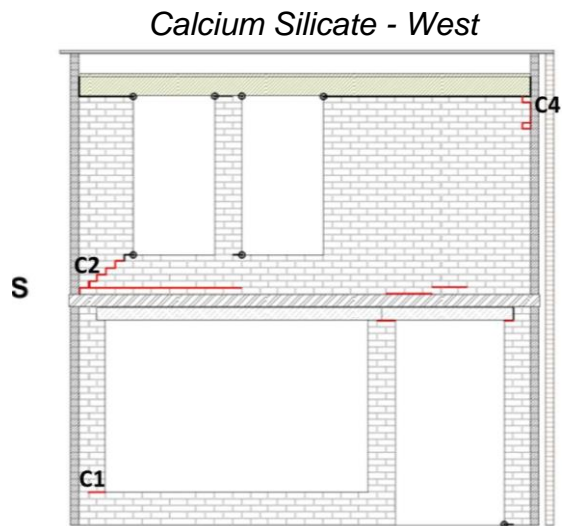
The survey revealed that several new cracks developed while the majority of pre-existing cracks extended significantly.

Looking at the transverse walls, the most remarkable damage was found at the Southern Calcium Silicate gable wall (Figure 151); while timber joist-to-masonry interface cracks extended throughout the whole perimeter (Figure 151 and Figure 154).

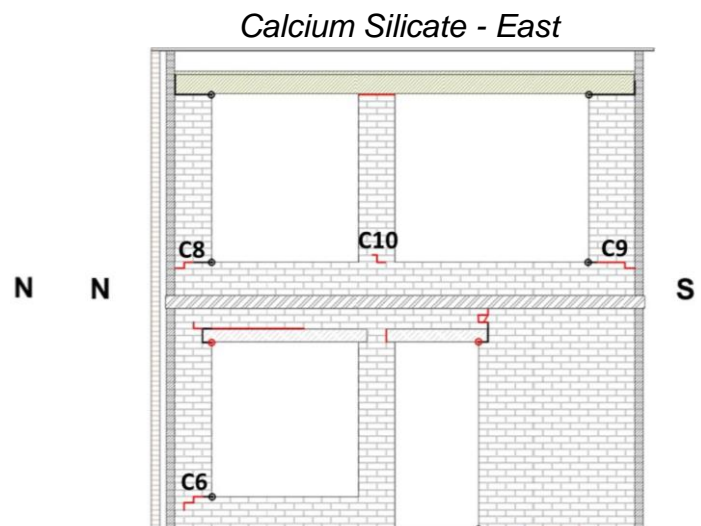
Focusing on the longitudinal facades (East and West), cracks highlighted the local response of structural elements, especially on the calcium silicate inner leaves. Looking at Figure 150, at the Southern end of the West section at the first floor, crack C2 evidenced that the pier tended to participate in the out-of-plane overturning mechanism of the South façade, behaving as a flange. At the opposite end of the same wall, the squat pier began to detach from the perpendicular North wall, without showing flange behaviour due to its geometrical characteristics (crack C4). Moreover, the onset of flange effect can be seen also at the ground floor of the calcium silicate East and West walls (crack C1 and C6, Figure 150 and Figure 155).

At the ground floor of the East side, the crack at the base of the calcium silicate squat pier extended, showing clearer evidence of rocking (Figure 150). At the second floor all piers were cracked at their top and bottom: the central piers rocked on their bases (C10, Figure 150 and Figure 156) while the spreader beams slid above them; the edge piers behaved as flanges of the transverse walls (C8, C9, Figure 150), with spreader beam sliding as well.

Similar cracks were observed on the outer clay leaves with lower extent (Figure 152 and Figure 157).

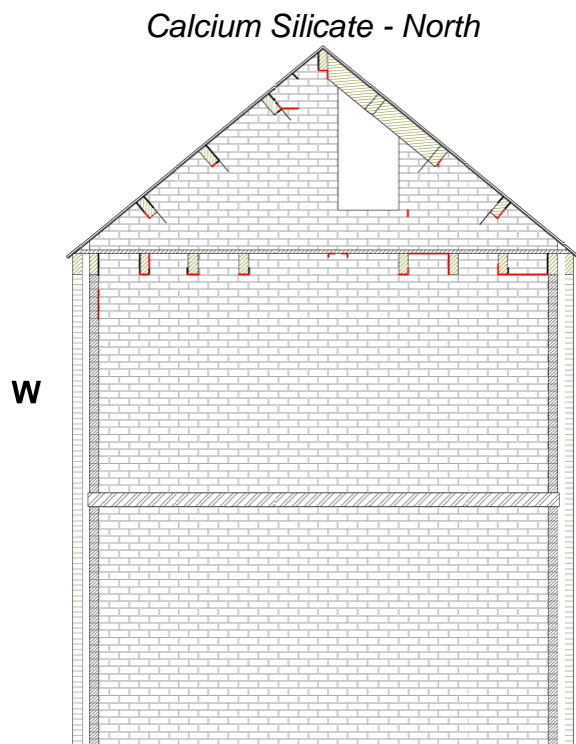


Section A-A

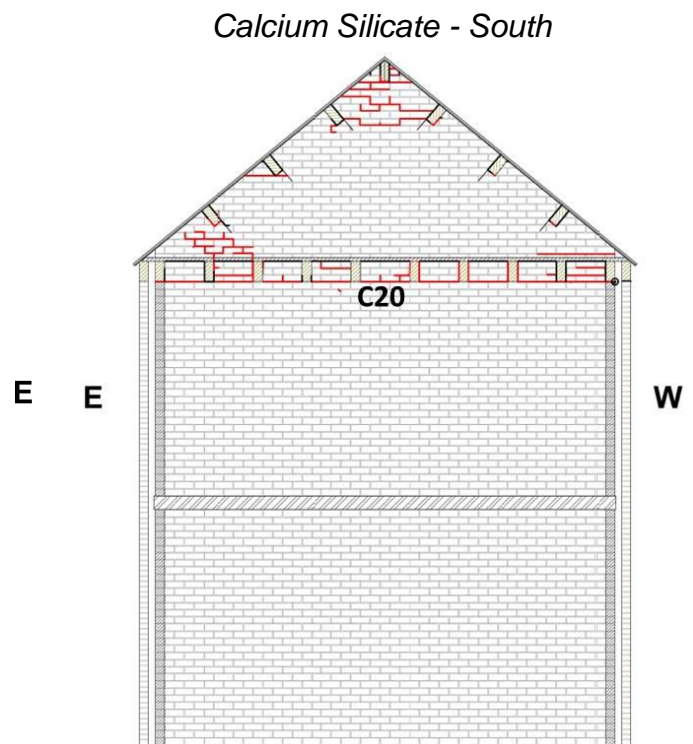


Section B-B

Figure 150 EQ-NPR 66% cracks - Calcium silicate longitudinal walls.



Section C-C



Section D-D

Figure 151 EQ-NPR 66% cracks - Calcium silicate transverse walls.

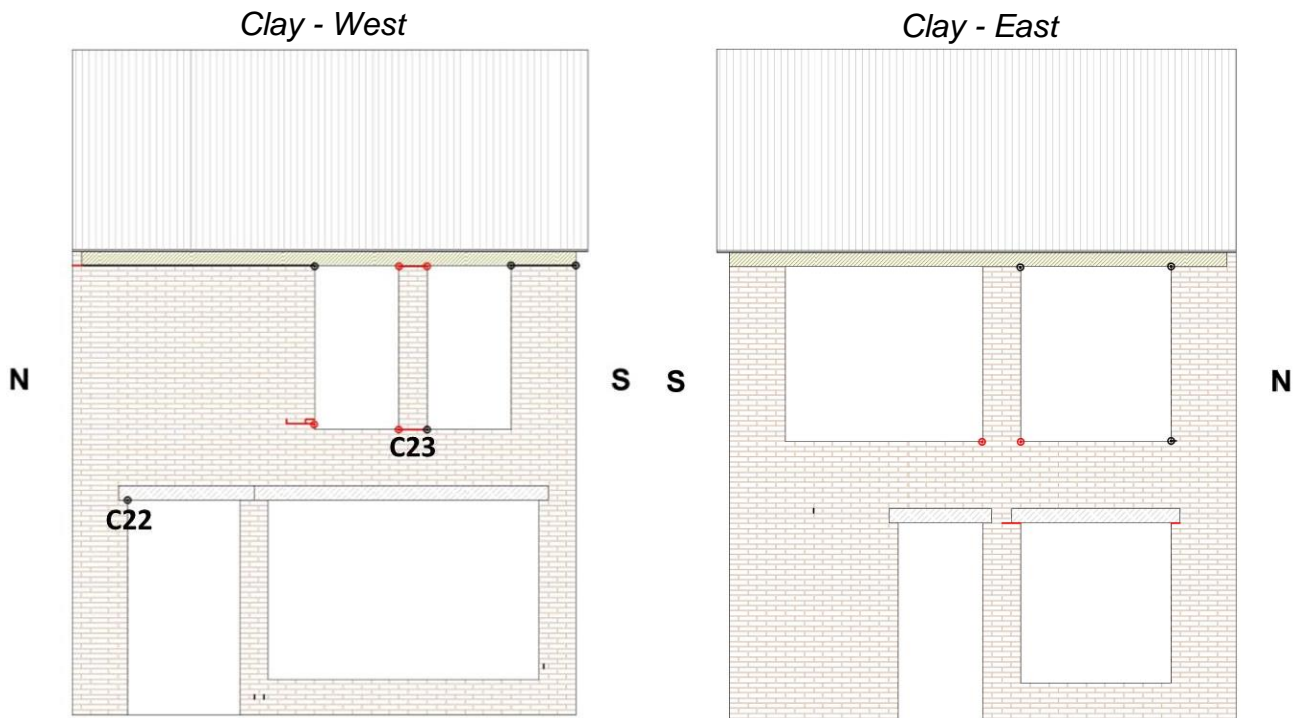


Figure 152 EQ-NPR 66% cracks – West and East clay façade.

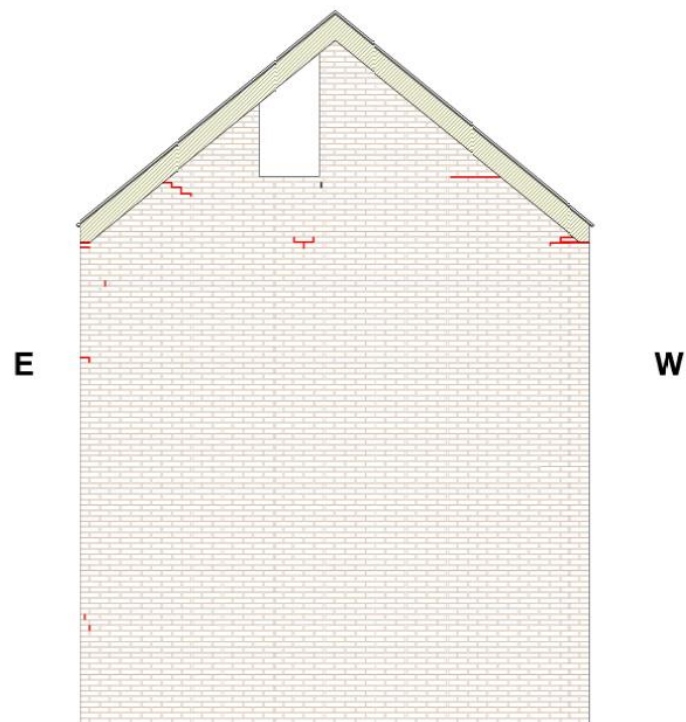
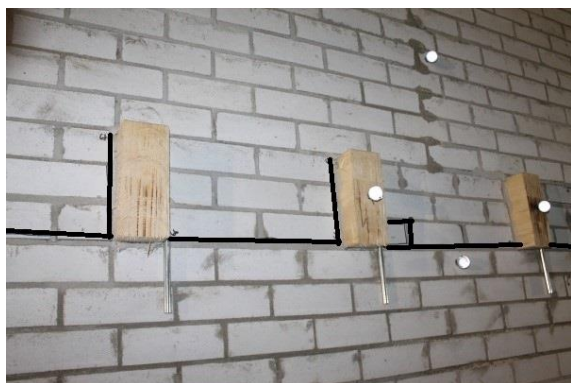
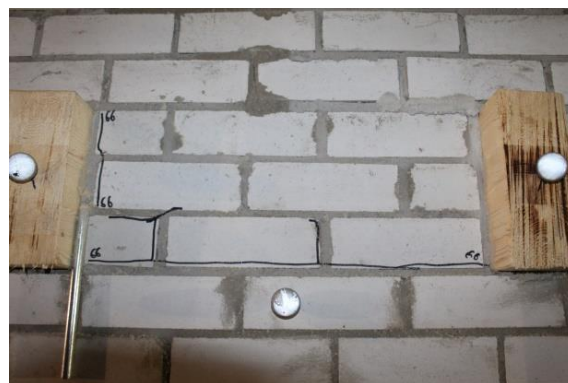


Figure 153 EQ-NPR 66% cracks – North clay façade.

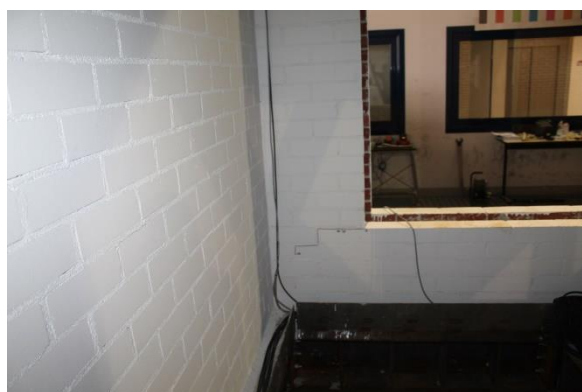


a)

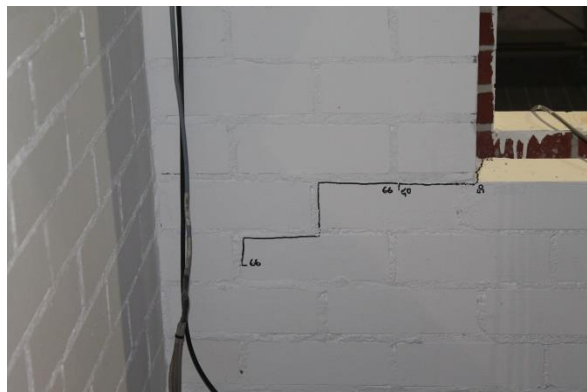


b)

Figure 154 EQ-NPR 66% cracks: a) C20 overview; b) C20 zoom in.



a)



b)

Figure 155 EQ-NPR 66% cracks: a) C6 overview; b) C6 zoom in.



Figure 156 EQ-NPR 66% cracks: C10 overview.



Figure 157 EQ-NPR 66% cracks: a) C23; b) C25.

5.1.5 Observed damage after Test #15, EQ-NPR 85%, PGA = 0.25 g

This test brought the specimen to a condition of widespread damage, with evident mechanism on the inner leaves of the East and West facades (Figure 158). At the ground floor slender piers were damaged at their top and bottom, denoting rocking behaviour of the central ones and flange effects on the ones connected to transverse walls (Figure 158); the squat pier tended to rock without following the perpendicular walls responses (Figure 158). The same considerations can be extended to the first floor of East and West facades: central slender piers rocked on their bases, while edge slender piers followed the transversal walls due to flange effect; the edge squat pier on the West facade tended to rock and slide without following the transverse North wall. Indeed, crack C4 extended (Figure 158 a), highlighting the detachment between the pier and the transverse wall. The same conclusions can be extended to the outer leaves of the East and West façades (Figure 160).

Focusing on the calcium silicate transverse walls, new cracks concentrated at the first floor of the North and South facades, resulting from the activation of the out-of-plane flexural response of the walls. Each wall developed a horizontal crack at about one third of the storey height throughout almost their entire length (Figure 159, Figure 162 and Figure 163), as well as inclined stepped cracks at the corners (Figure 159 and Figure 163). Again, similar observations can be extended to the North clay outer leaf (Figure 161, Figure 164 and Figure 165), with some differences probably due to the connection between the calcium silicate walls and timber floor joists, which resulted in different boundary conditions.

Residual cracks widths after the test were negligible except for crack C24 (Figure 160 and Figure 164), which accumulated around 1 mm.

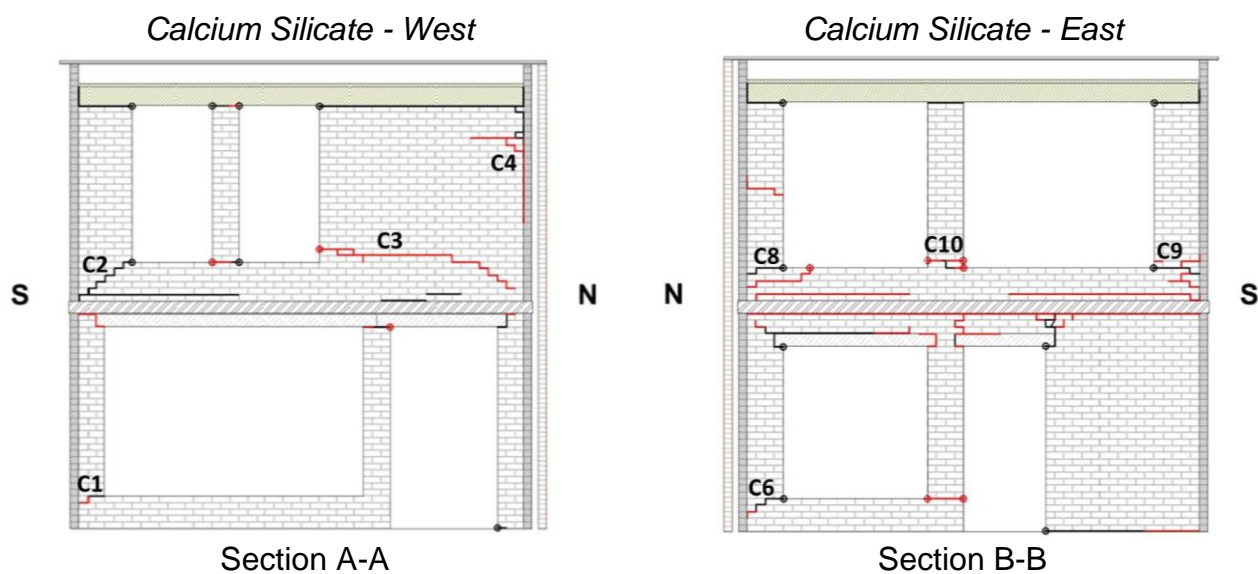


Figure 158 EQ-NPR 85% cracks - Calcium silicate longitudinal walls.

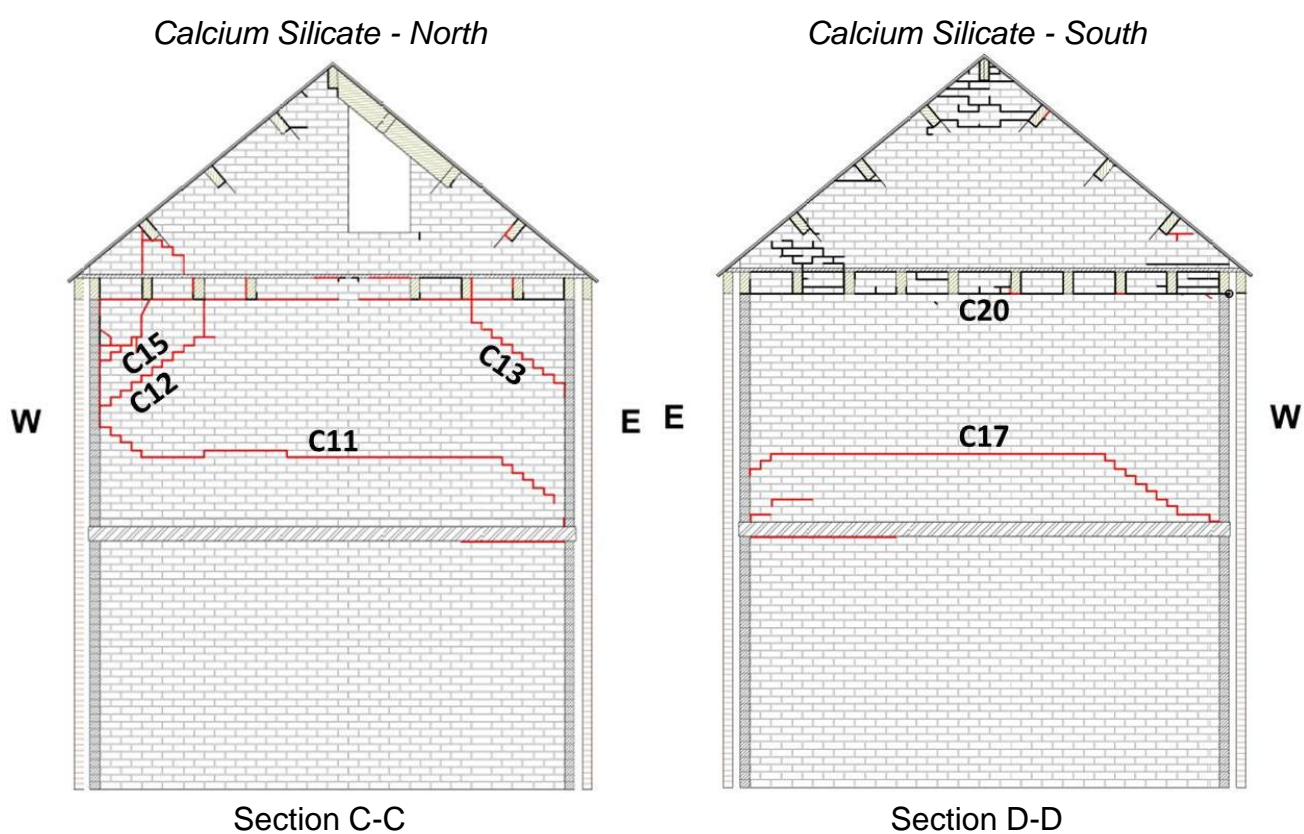


Figure 159 EQ-NPR 85% cracks - Calcium silicate transversal walls.

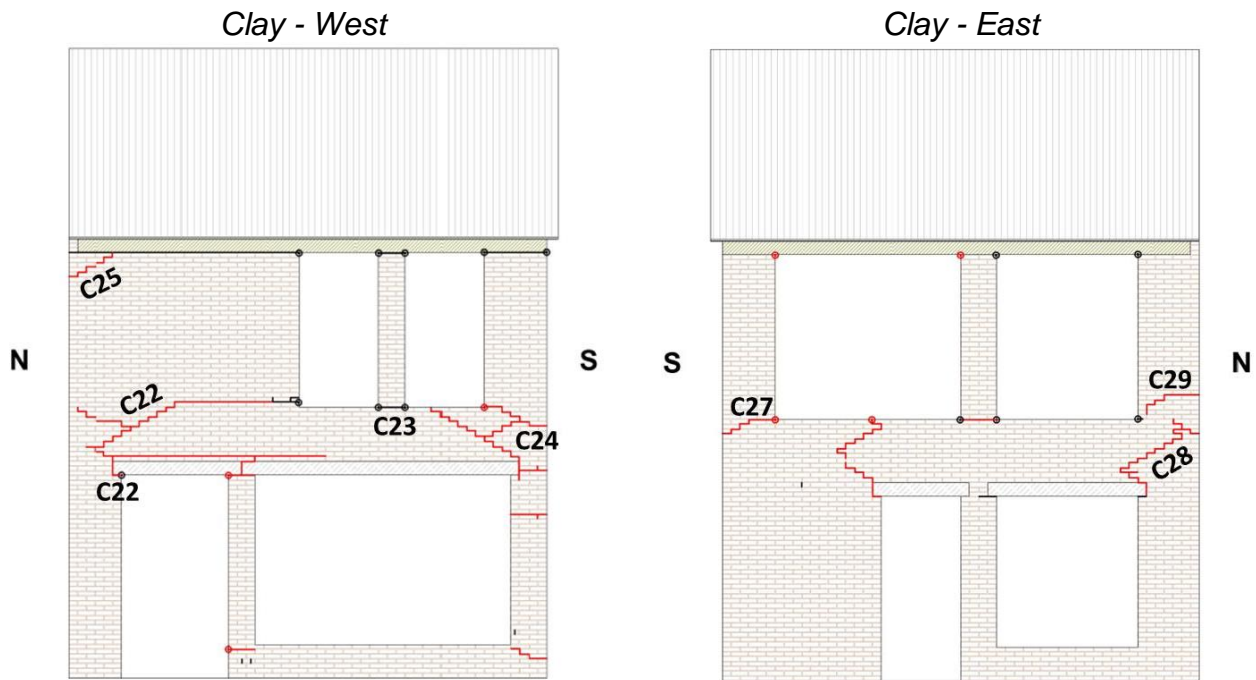


Figure 160 EQ-NPR 85% cracks – West and East clay façades.

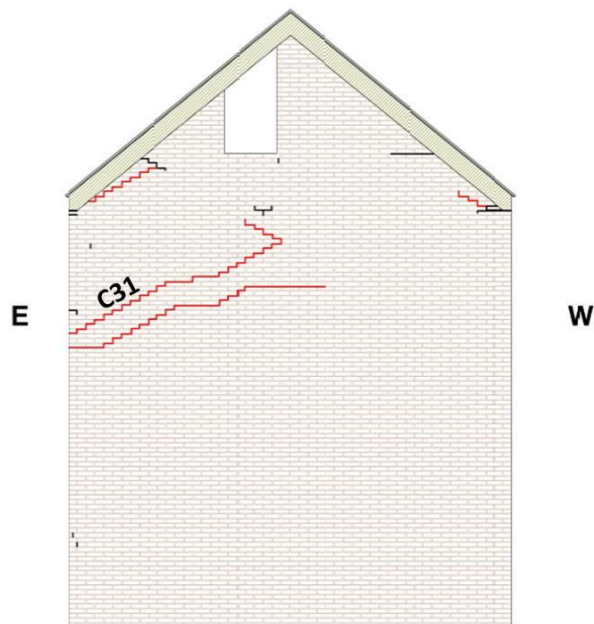
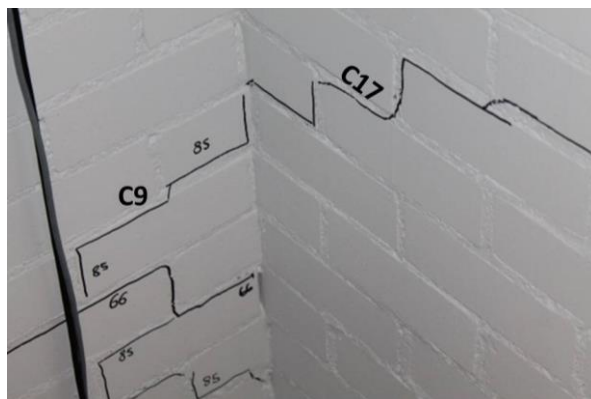


Figure 161 EQ-NPR 85% cracks – North clay façade.

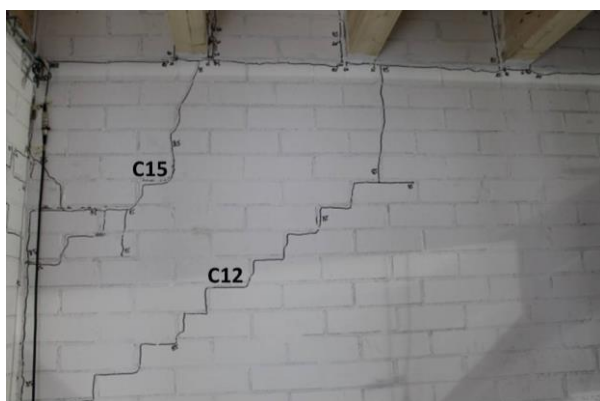


a)



b)

Figure 162 EQ-NPR 85% cracks: a) C9 and C17 overview ; b) C9 and C17 Zoom in.



a)



b)

Figure 163 EQ-NPR 85% cracks: a) C12 and C15; b) C13.



a)



b)

Figure 164 EQ-NPR 85% cracks: a) C24; b) C31.



Figure 165 EQ-NPR 85% cracks: a) C25; b) C22.

5.1.6 Observed damage after Test #21, EQ-NPR 100%, PGA = 0.30 g

At this stage of the shaking table test, the building prototype reached a condition of extensive damage. On the longitudinal facades (East and West, Figure 166), all slender piers connected to the transverse walls were interested by the flange effect, the central ones rocked, while the squat piers connected to the transverse walls rocked and slid detaching from them. The only exception was for the clay squat pier at the ground floor of the West side (Figure 168), that showed the onset of rocking at its base but no remarkable cracks at its top, being unloaded and not connected to any perpendicular wall.

North and South facades (Figure 167 and Figure 169) showed a significant extension and increase in the amount of cracks, especially on the clay outer leaf (Figure 169 to Figure 172). Diagonal stepped cracks originated from each corner of the wall and linked to each other through horizontal cracks in the central part, in a sort of two-way bending mechanism (cracks C31, C32, C33, C34, Figure 169, Figure 172, Figure 173 and Figure 174).

After this test, residual cracks widths became significant: C29 (Figure 168 and Figure 174) C4 (Figure 166 and Figure 171) reached around 1.2 cm; C8 (Figure 166 and Figure 170), C13 (Figure 167 and Figure 170) and C31 (Figure 169, Figure 173 and Figure 174), accumulated 2 cm, 1.5 cm and 1.5 cm respectively, in their out-of-plane directions.

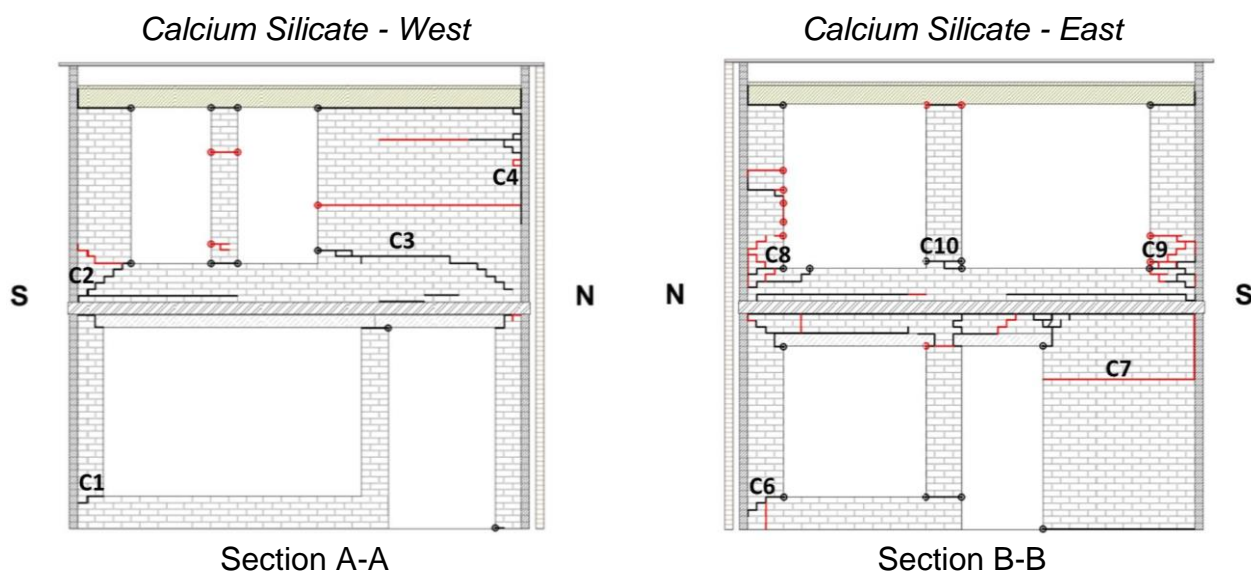


Figure 166 EQ-NPR 100% cracks - Calcium silicate longitudinal walls.

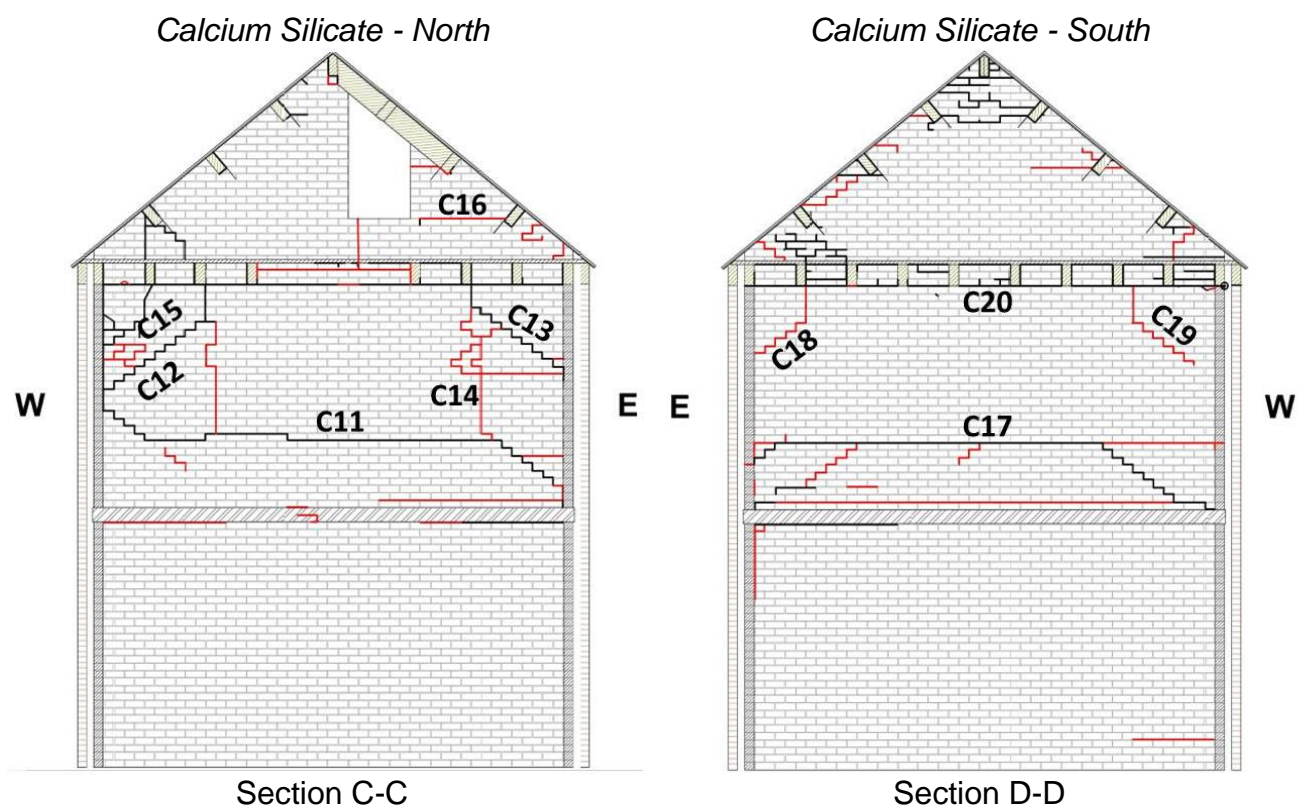


Figure 167 EQ-NPR 100% cracks - Calcium silicate transversal walls.

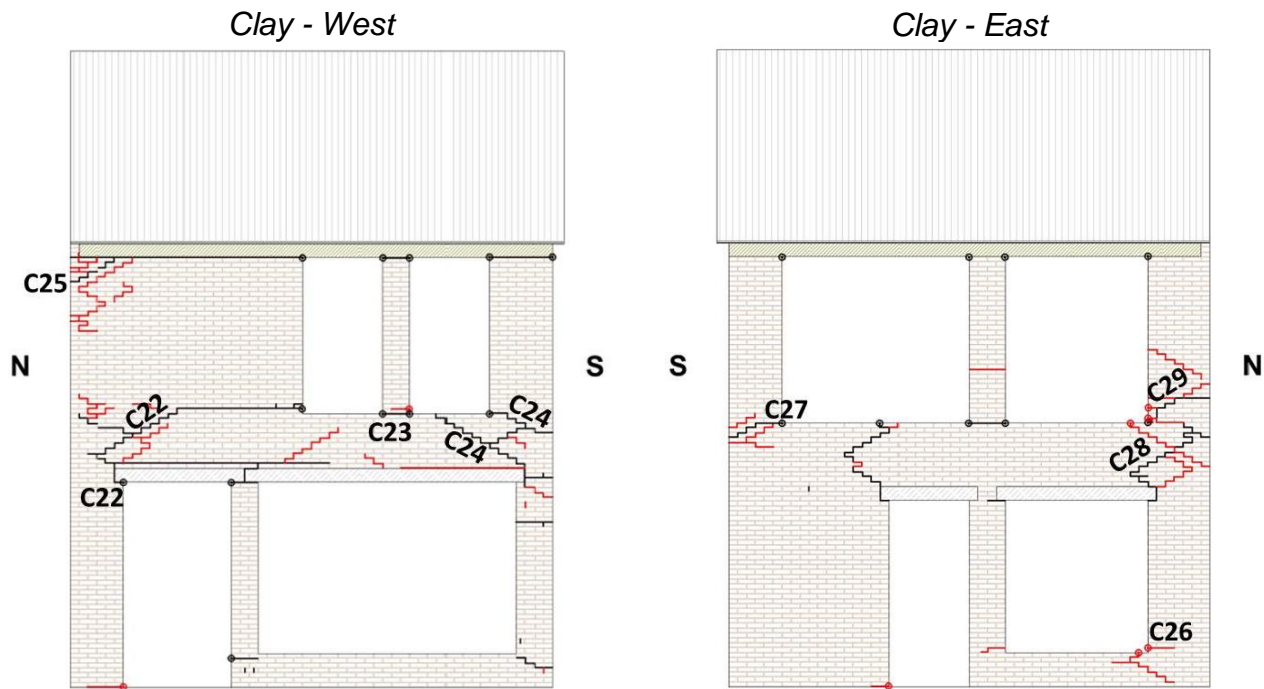


Figure 168 EQ-NPR 100% cracks – West and East clay façades

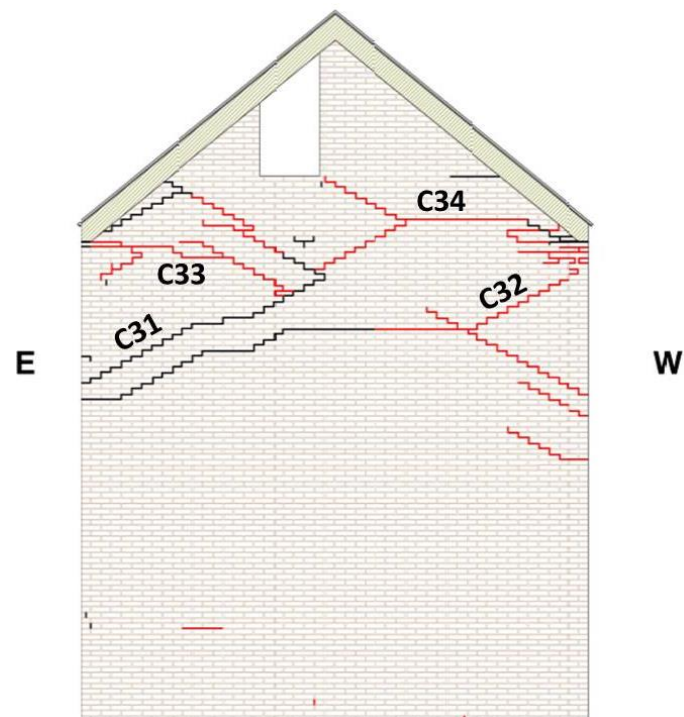
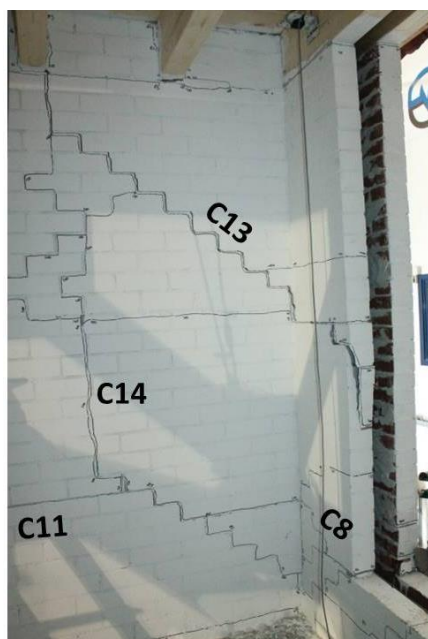


Figure 169 EQ-NPR 100% cracks – North clay façade.

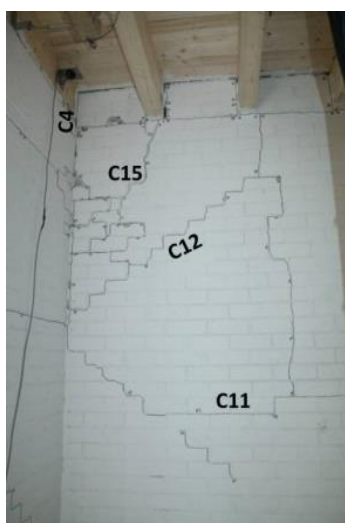


a)



b)

Figure 170 EQ-NPR 100% cracks: a) C8, C11, C13 and C14 overview; b) C13 zoom in.



a)



b)

Figure 171 EQ-NPR 100% cracks: a) C4, C11, C12 and C15 overview; b) C4 and C15 zoom in.



Figure 172 EQ-NPR 100% cracks: a) C33; b) C34.

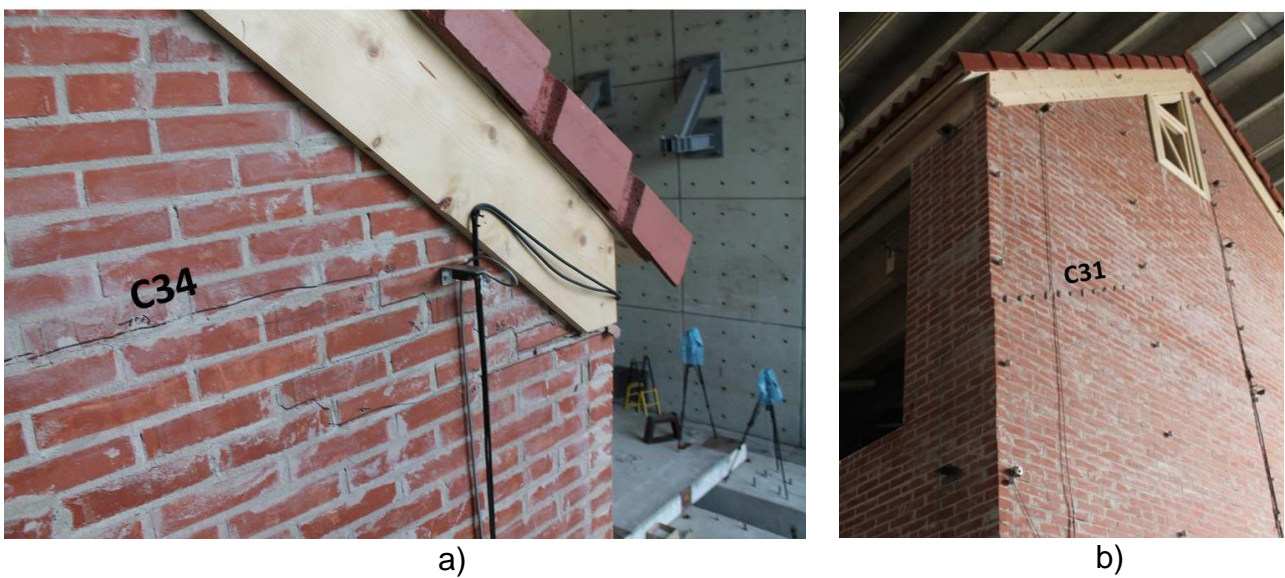


Figure 173 EQ-NPR 100% cracks: a) C34; b) C31.



Figure 174 EQ-NPR 100% cracks: a) C29, C31 overview; b) C29 zoom in.

5.1.7 Observed damage after Test #24, EQ-NPR IS 100%, PGA = 0.30 g (inverted sign)

A quick visual survey after this run with inverted input signal did not revealed any significant damage evolution in terms of new cracks, but only minor changes of crack residual widths. For this reason, a detailed survey was not performed.

5.1.8 Observed damage after Test #25, EQ-NPR IS 133%, PGA = 0.40 g (inverted sign)

The final survey detected extension of existent cracks, loss of some portions of masonry, and accumulation of significant residual crack widths, but no activation of new local failure mechanisms. The specimen was extensively damaged, all masonry elements in the building were cracked at several locations and very large residual displacements could be observed.

Considering the calcium silicate walls, on the West façade (Figure 175), crack C4 showed 3 cm of residual width (Figure 179); crack C13, on the North façade (Figure 176), led to loss of bricks on the East façade (Figure 181 and Figure 182); crack C14 on the North side (Figure 176) accumulated 3.5 cm (Figure 176, Figure 181 and Figure 183). Considering the clay walls (Figure 177 and Figure 178), the most significant damage was observed on the North façade: cracks C31 and C33 ended with about 3 cm of residual width (Figure 186, Figure 187). Moreover, other cracks (such as C22, Figure 177 and Figure 184; C24 and C25, Figure 177 and Figure 185) showed residual displacements around 1 cm (see Table 25).

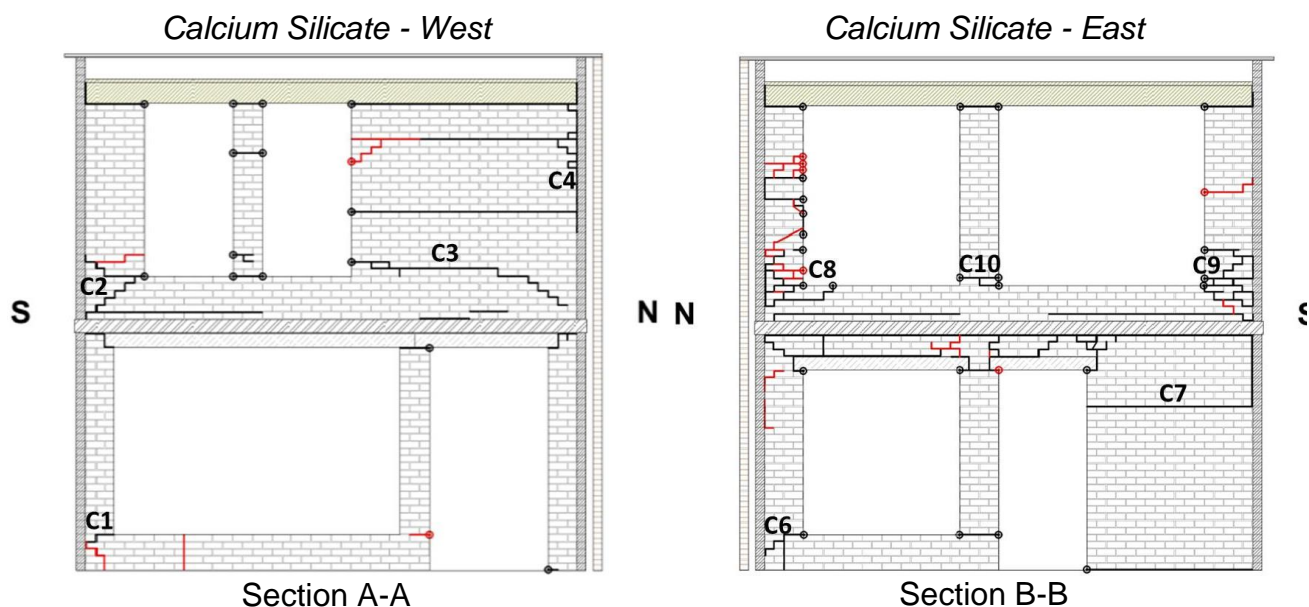


Figure 175 EQ-NPR IS 133% cracks - Calcium silicate longitudinal walls.

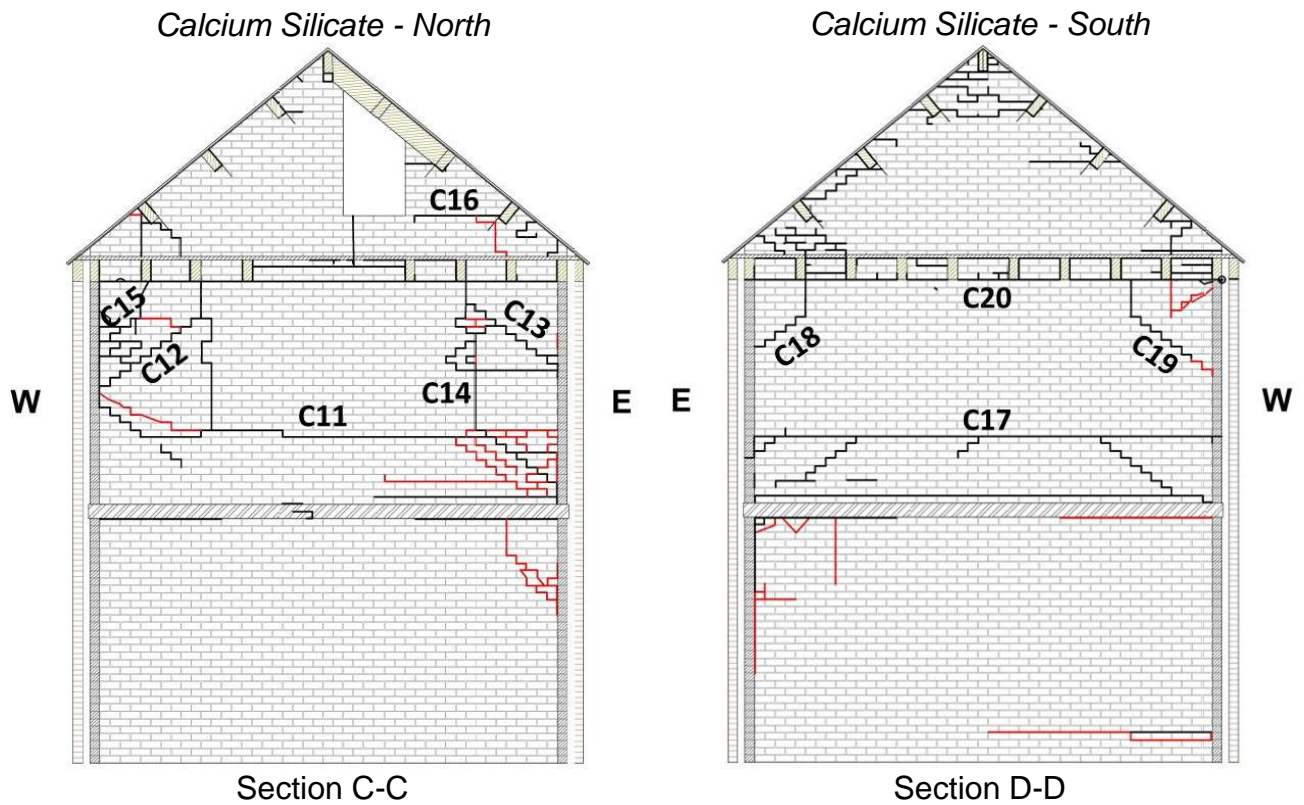


Figure 176 EQ-NPR IS 133% cracks - Calcium silicate transversal walls.

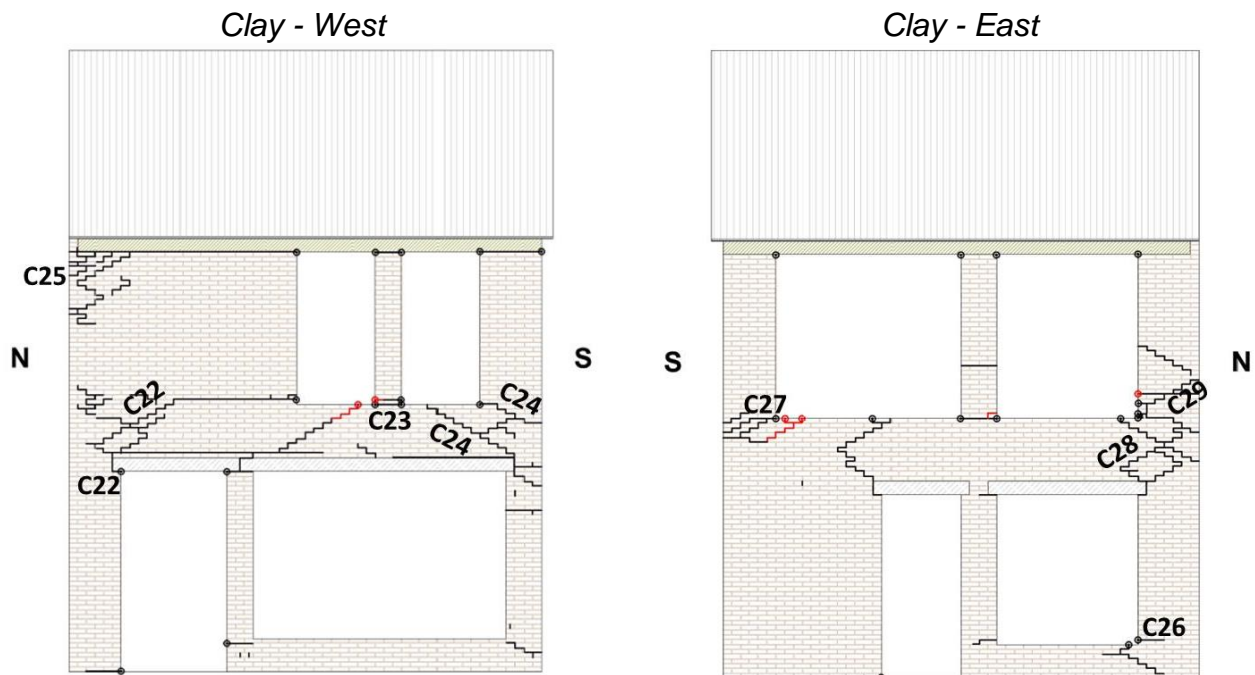


Figure 177 EQ-NPR IS 133% cracks - West and East clay façades.

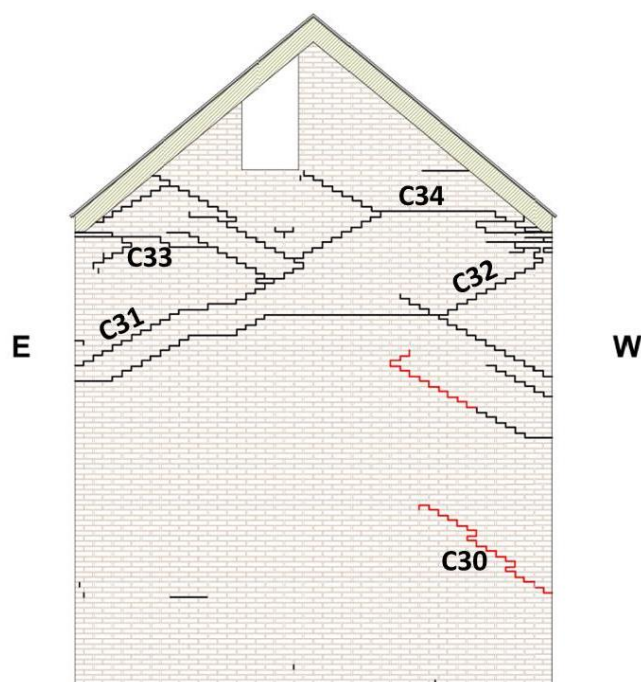


Figure 178 EQ-NPR IS 133% cracks - North clay façade.

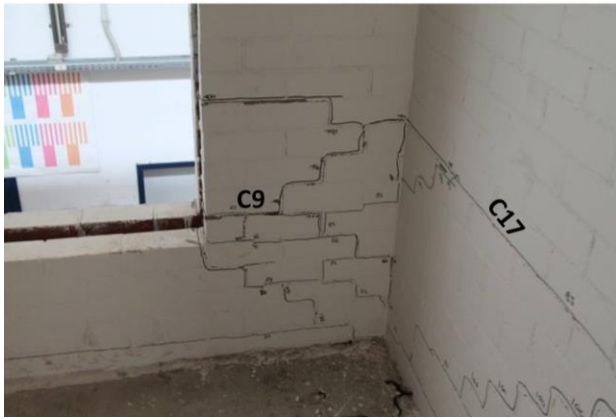


a)

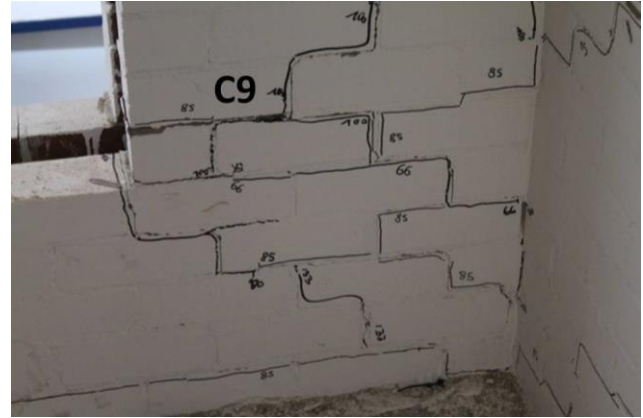


b)

Figure 179 EQ-NPR IS 133% cracks: a) C4 and C15 overview; b) C4 zoom in.



a)



b)

Figure 180 EQ-NPR IS 133% cracks: a) C9 and C17 overview; b) C9 zoom in.

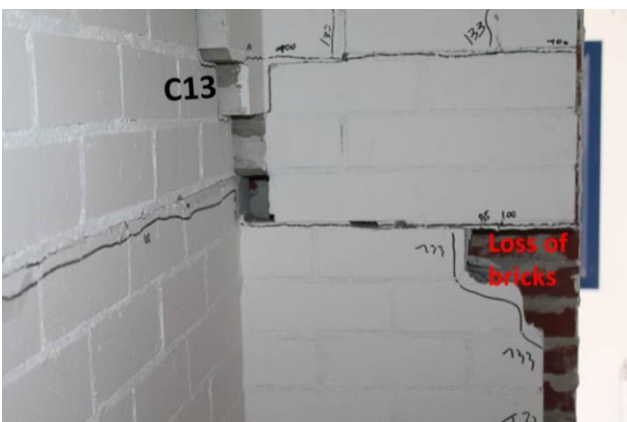


a)

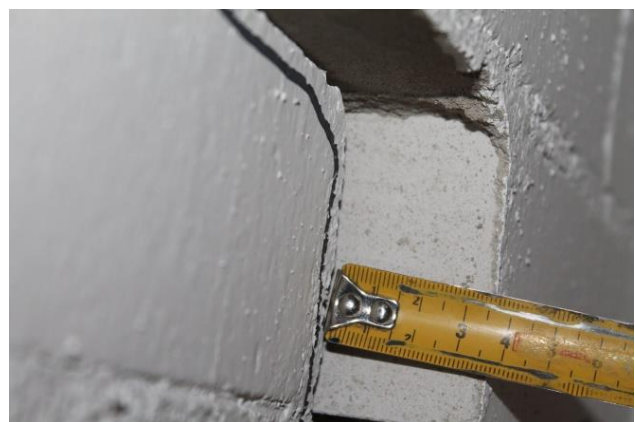


b)

Figure 181 EQ-NPR IS 133% cracks: a) C8, C11 and C14; b) C13.

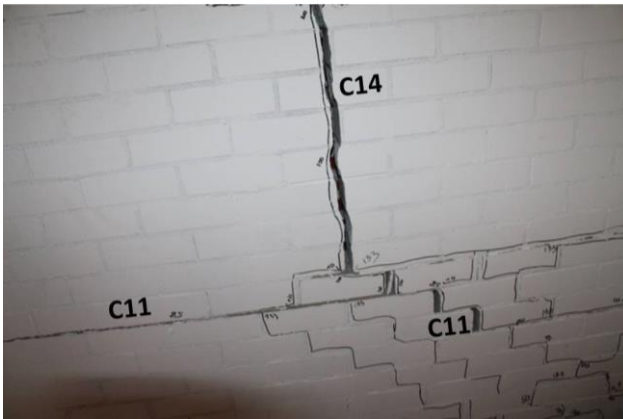


a)

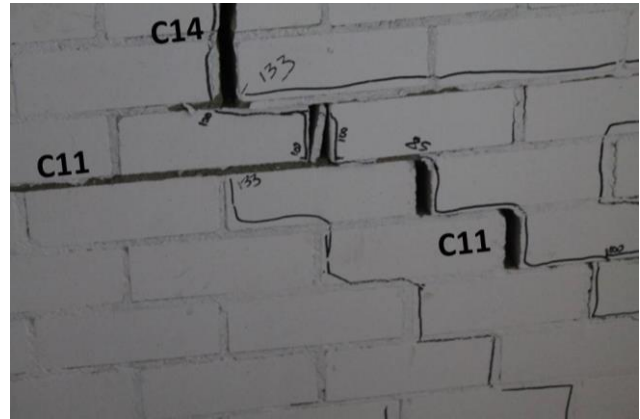


b)

Figure 182 EQ-NPR IS 133% cracks: a) C13; b) C13 zoom-in.

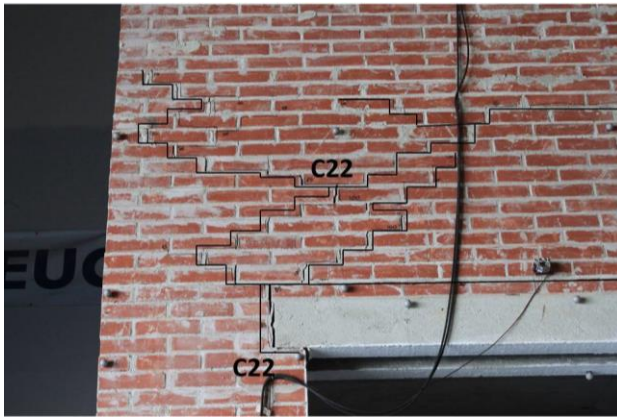


a)



b)

Figure 183 EQ-NPR IS 133% cracks: a) C11 and C14 overview; b) C11 zoom in.



a)

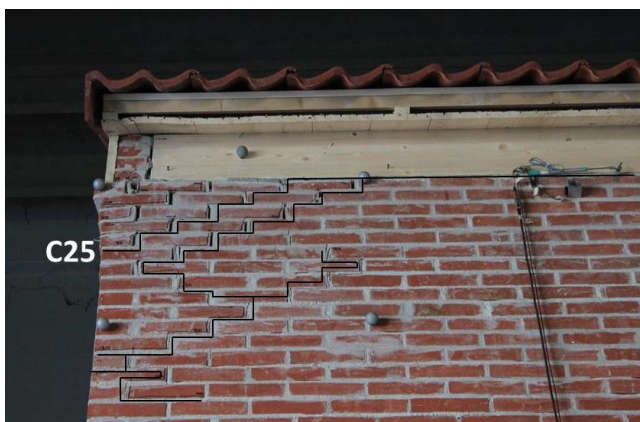


b)

Figure 184 EQ-NPR IS 133% cracks: a) C22 overview; b) C22 zoom in.



a)



b)

Figure 185 EQ-NPR IS 133% cracks: a) C24; b) C25.

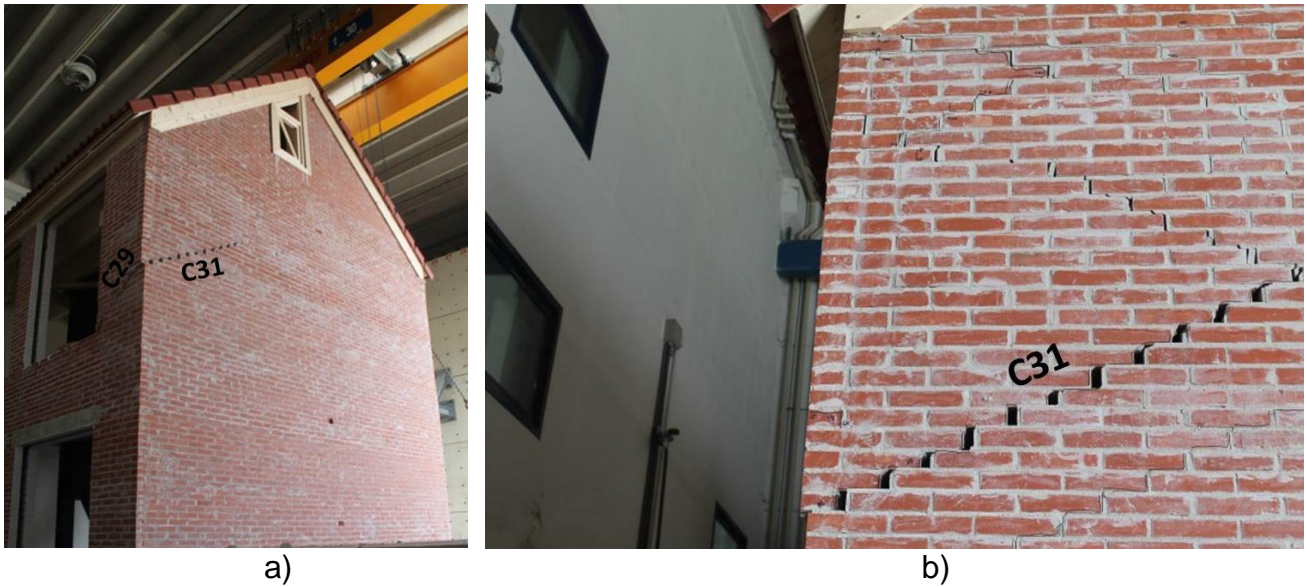


Figure 186 EQ-NPR IS 133% cracks: a) C29 and C31 overview; b) C31 zoom in.

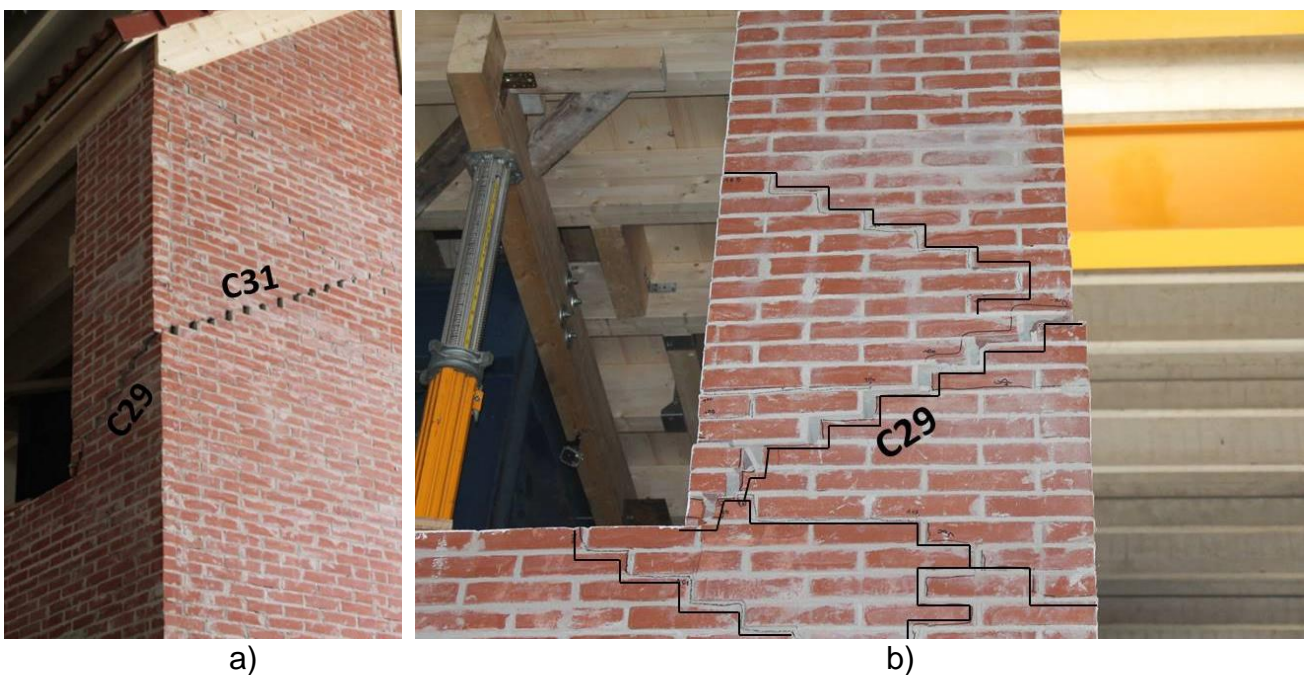


Figure 187 EQ-NPR IS 133% cracks: a) C29, C31 overview; b) C29 zoom in.

5.1.9 Crack width evolution

Table 25 summarizes the residual crack widths after each test based on the crack labels used in par. from 5.1.2 to 5.1.8. As already noted, several cracks reached a significant residual width, up to more than 3 cm at the end of the sequence. After Table 25, a detailed residual width evolution is reported for a number of selected cracks (i.e. C4, C13, C24 and C31)

Table 25 reports two values of residual displacement for the test runs at 100% and 133% of EQ-NPR: the first one is measured in the in-plane direction of the structural element where the crack is located, the second one in its out-of-plane direction. Note that no cracks width is reported for test #24 since cracks were not surveyed.

Table 25 Crack widths evolution

Residual width of cracks [mm]										
Crack Name	Location	test # 2	test # 3	test # 8	test # 10	test # 15	test # 21		test # 25	
		EQ-NPR	EQ-NPR	EQ-NPR	EQ-NPR	EQ-NPR	EQ-NPR		EQ-NPR	
		20%	33%	50%	66%	85%	100%		IS 133%	
		In-plane	In-plane	In-plane	In-plane	In-plane	In-plane	OOP	In-plane	OOP
C1	West CS	/	/	/	0.05	0.1	0.1	/	0.7	/
C2	West CS	0.05	0.05	0.05	0.1	0.1	0.6	/	1	/
C3	West CS	/	/	/	/	0.05	0.1	/	0.1	/
C4	West CS	/	/	0.1	0.1	0.5	12	2	30	10
C5	West CS	/	/	0.05	0.05	0.1	0.1	/	0.1	/
C6	East CS	/	/	/	0.05	0.1	0.5	/	1.5	/
C7	East CS	/	/	/	/	/	0.05	/	0.05	/
C8	East CS	/	/	0.05	0.05	0.1	1.5	20	50	20 + bricks loss
C9	East CS	/	/	0.05	0.05	0.1	2	/	2	/
C10	East CS	/	/	/	0.1	0.1	0.5	/	0.5	/
C11	North CS	/	/	/	/	0.2	3	/	10	20
C12	North CS	/	/	/	/	0.1	0.1	/	0.1	/
C13	North CS	/	/	/	/	0.1	0.6	15	10	40
C14	North CS	/	/	/	/	/	3	/	35	/
C15	North CS	/	/	0.05	0.05	0.1	3	/	10	/
C16	North CS	/	0.05	0.05	0.05	0.1	0.1	/	1.5	/
C17	South CS	/	/	/	/	0.05	0.1	2	0.1	2
C18	South CS	/	/	/	/	/	0.1	/	1.5	/
C19	South CS	/	/	/	/	/	0.1	/	0.2	/
C20	South CS	/	/	/	0.05	0.1	0.1	/	0.1	/
C21	West CL	/	/	/	/	0.05	0.05	/	0.1	/
C22	West CL	/	/	/	/	0.05	0.1	/	0.1	/
C23	West CL	/	/	0.05	0.05	0.2	5	/	5	/
C24	West CL	/	/	/	/	1	3	/	10	/
C25	West CL	/	/	0.05	0.05	0.1	12	7	14	7
C26	East CL	/	/	/	/	/	0.05	/	0.4	/
C27	East CL	/	/	/	/	/	4	/	13	/
C28	East CL	/	/	/	/	0.1	0.1	/	5	/
C29	East CL	/	/	/	/	0.1	20	/	22	24
C30	North CL	/	/	/	/	/	/	/	0.6	/
C31	North CL	/	/	/	/	0.1	10	15	28	25
C32	North CL	/	/	/	/	/	0.3	/	4	/
C33	North CL	/	/	/	/	/	0.3	/	10	35
C34	North CL	/	/	/	/	/	0.1	/	1	4

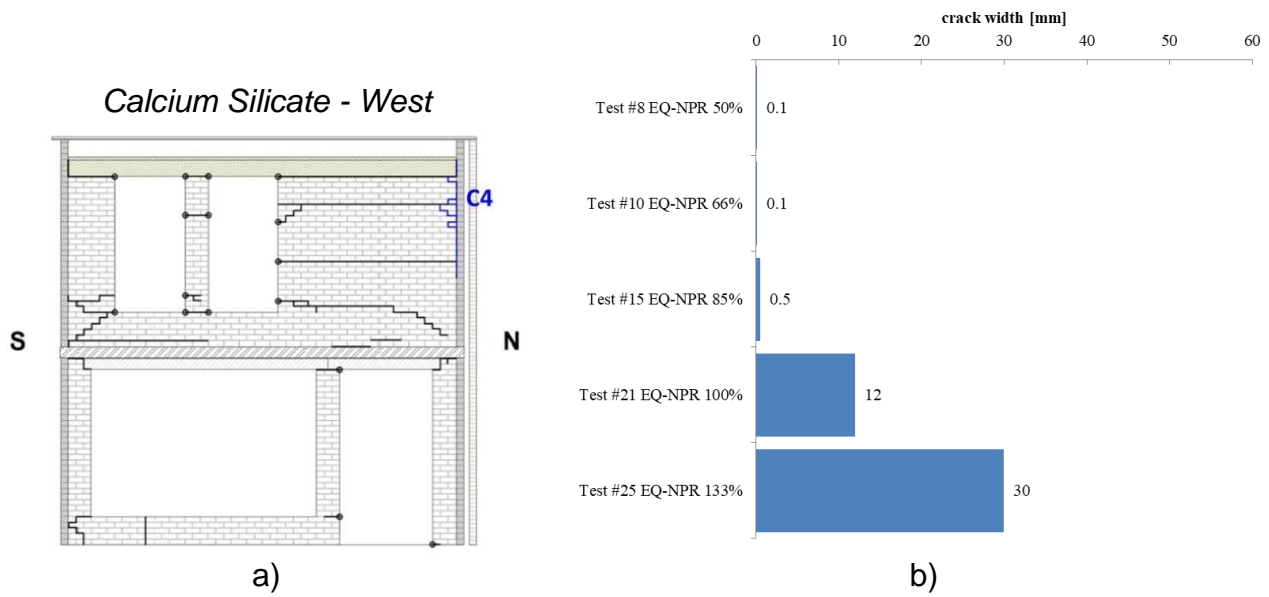


Figure 188 Crack C4 evolution: a) location; b) in-plane residual widths.



Figure 189 Crack C4 after EQ-NPR 100%: a) overview; b) zoom in.

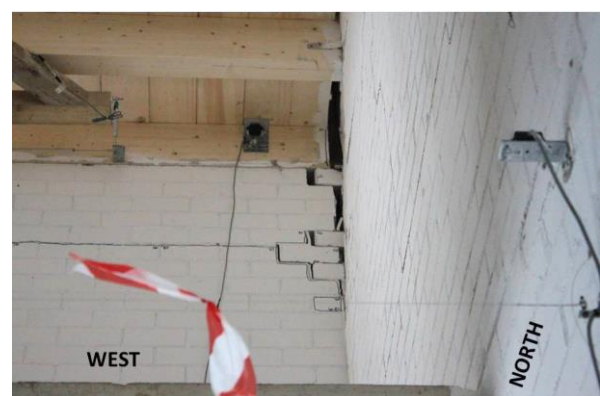
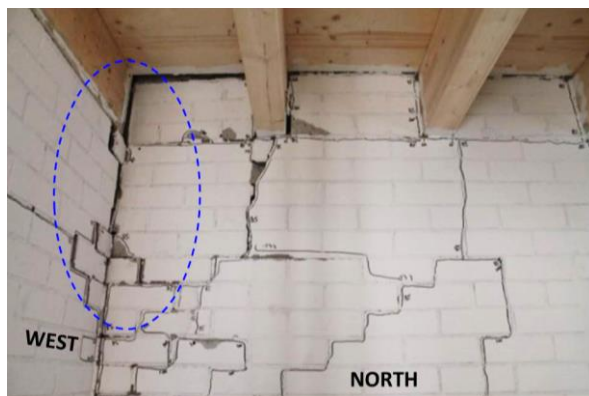


Figure 190 Crack C4 after EQ-NPR IS 133%: a) looking North; b) looking West.

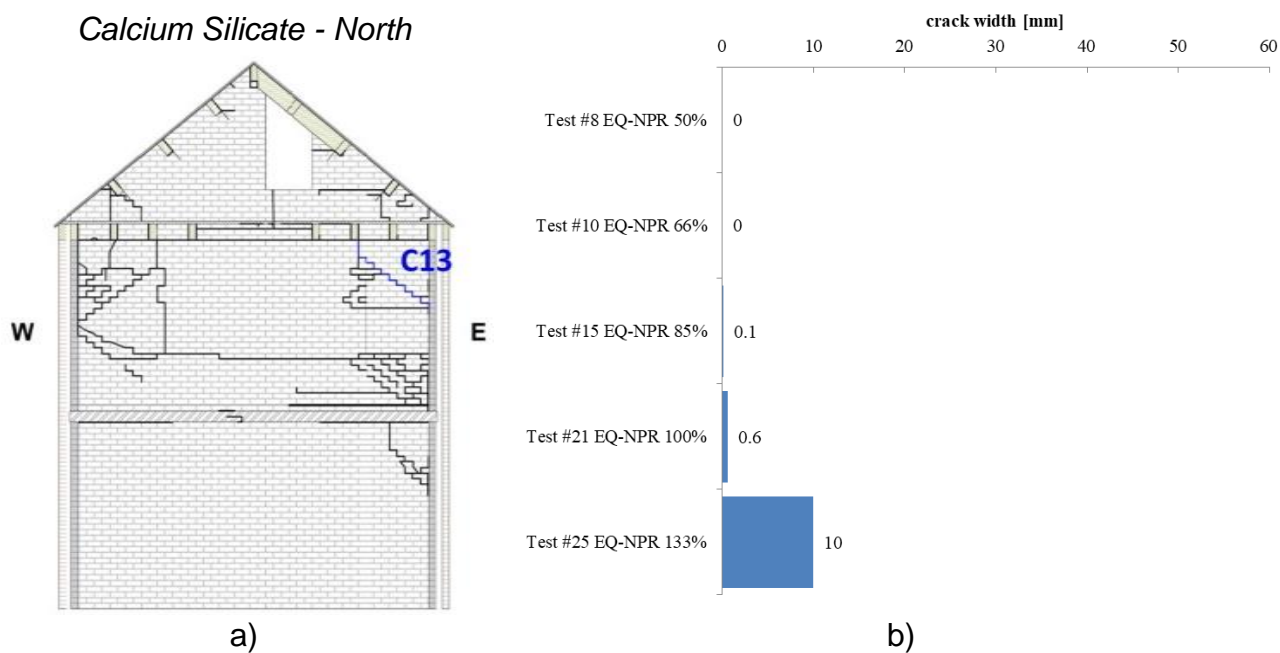


Figure 191 Cracks C4, C13 evolution: a) location; b) in-plane residual widths.

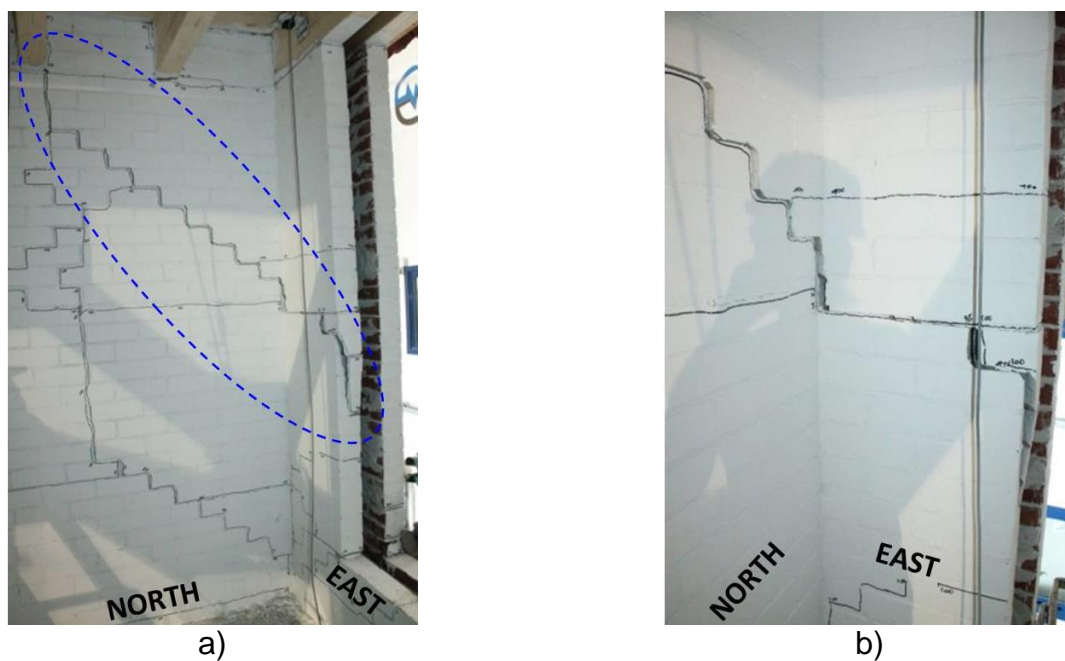


Figure 192 Crack C13 after EQ-NPR 100%: a) overview; b) North-East walls intersection.

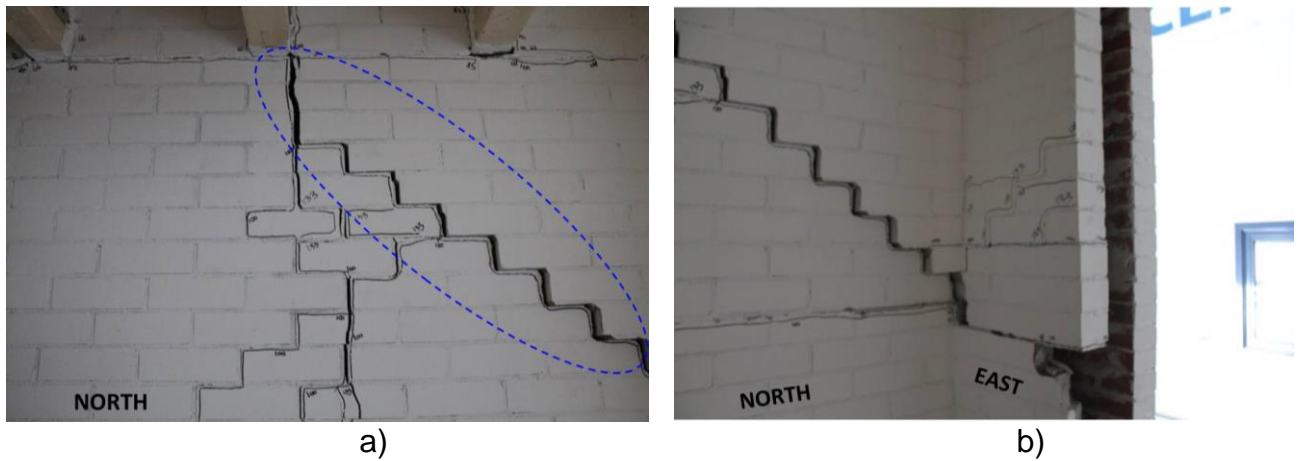


Figure 193 Crack C13 after EQ-NPR IS 133%: a) looking North; b) North-East walls intersection.



Figure 194 Cracks C13 after EQ-NPR IS 133%: a) looking East; b) Out-of-plane residual width zoom in.

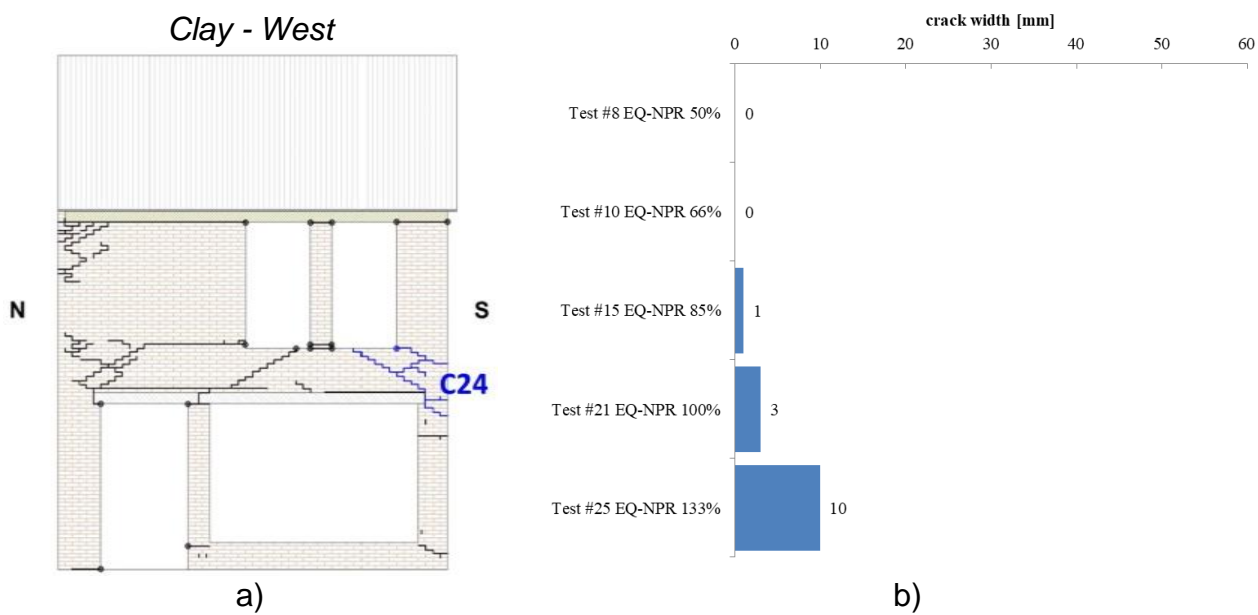


Figure 195 Cracks C24 evolution: a) location; b) in-plane residual widths.



a)



b)

Figure 196 Crack C24: a) after EQ-NPR 85%; b) after EQ-NPR IS 133%.

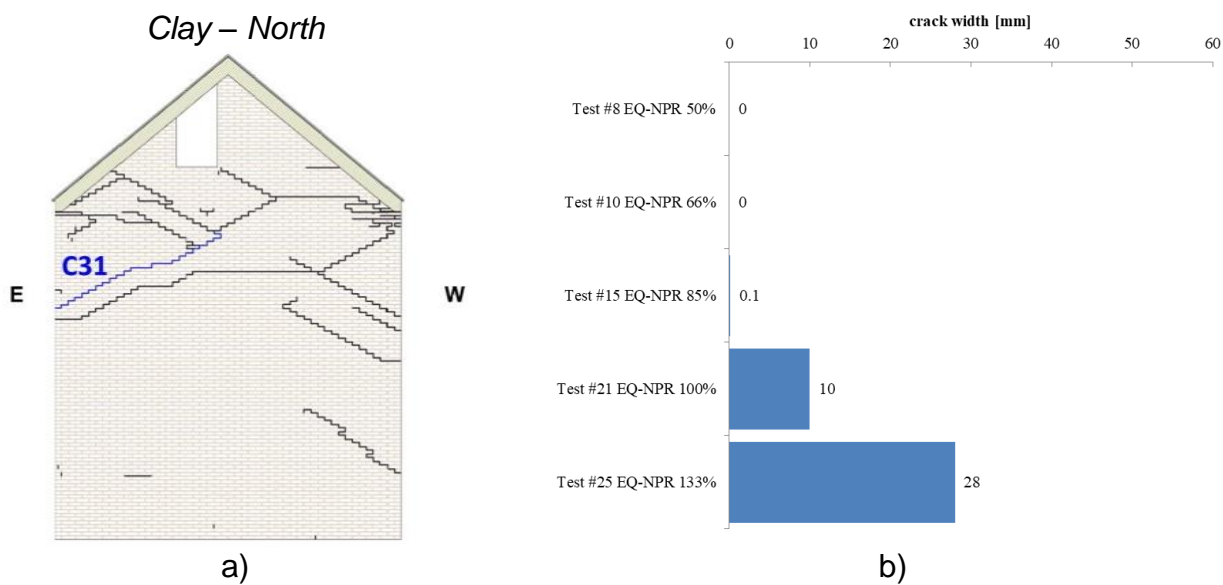


Figure 197 Crack C31 evolution: a) location; b) in-plane residual widths.



Figure 198 Crack C31: a) after EQ-NPR 85%; b) after EQ-NPR 100%.

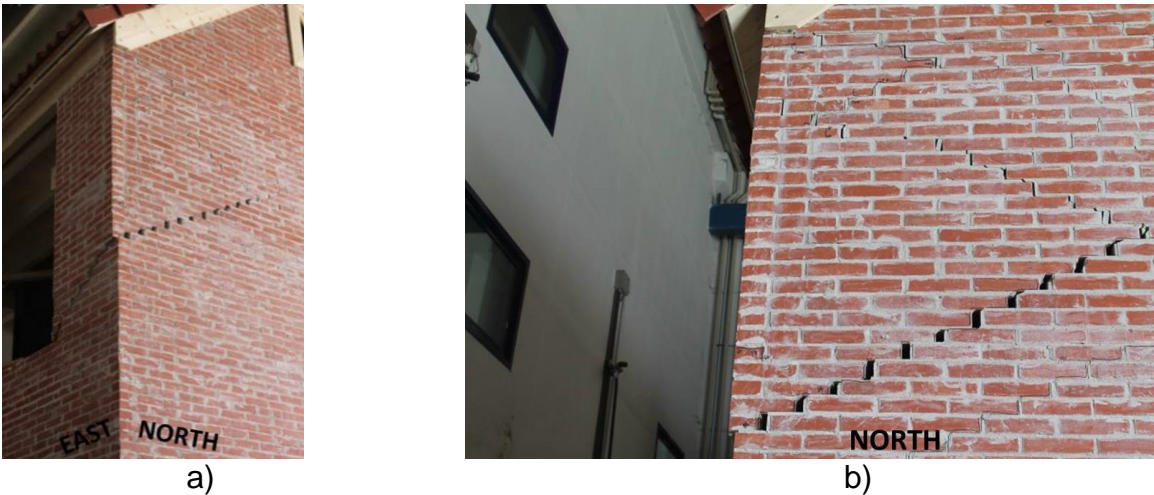


Figure 199 Crack C31 after EQ-NPR IS 133%: a) overview; b) zoom in.

5.2 Analysis of the building response

The following section analyses the experimental response of the specimen under each input motion. First the response spectrum of the foundation acceleration history is compared with the target spectrum. Then force-displacement hysteretic curves, displacement profiles, interstorey drift ratio envelopes, and floor diaphragm deformed shapes are plotted for each run. The procedures to obtain these quantities are described below. An explanation of the format of the published data is given in Appendix A1. Results file format.

- **Response spectra comparison**

The experimental acceleration time history is the average of those recorded on the specimen foundation by accelerometers #2 and #3 (Table 5, Figure 51 and Figure 54).

- **Hysteretic force-displacement response**

The hysteretic response of the building is expressed in terms of base shear or base shear coefficient (BSC) and second-floor diaphragm displacement or global drift ratio.

The base shear was obtained by summing the product of each recorded acceleration history times its associated mass. The base shear coefficient is the base shear divided by the specimen total mass (47.5 t).

The second-floor diaphragm displacement was computed as the average of the displacements recorded at the East and West sides of the timber diaphragm. The former is the average of the displacements from potentiometers #94, #100 (Table 21, Figure 113 and Figure 117) and the latter the average of those from potentiometers #96, #98 (Table 21, Figure 113 and Figure 117). The global drift ratio is the ratio of the average second-floor displacement to the height of the second floor above the foundation.

Note that up to the Test #10 EQ-NPR 66% global drift ratios are not reported since values are below 0.1%.

- **Displacements profiles**

This plot is taken at the instant where the maximum displacement of the second-floor timber diaphragm (computed as above) was recorded. The reported values are taken at midspan of the walls perpendicular to the direction of shaking.

All the OOP displacements of the North façade (inner and outer leaves) and the ones at mid-floor height of the South façade were measured by wire potentiometers (#73 through #87, Table 6, Figure 64 and Figure 65). The value reported at the first-floor height (2.75 m above ground) on the south façade was obtained as the average of the displacements from potentiometers #113, #115, #116 and #118 (Table 7, Figure 67 and Figure 71). The value indicated at the second-floor height (5.4 m above ground) is the sum of the readings of potentiometers #102 and #103 (Table 7, Figure 67 and Figure 71).

The deflected shapes are magnified by the scaling factor indicated below each plot.

- **Interstorey drift ratio envelopes**

As for the displacement profiles, the reported values are taken at midspan of the walls perpendicular to the direction of shaking. They are the maximum in absolute value.

The first-storey drift ratio was obtained as the average first-floor displacement (from potentiometers #113, #115, #116, #118 - Table 7, Figure 67 and Figure 71) divided by the first-storey height (2.75 m). The second-storey drift ratio was computed as the difference between the average second-floor diaphragm displacement (from potentiometers #94, #96, #98, #100, Table 7, Figure 67 and

Figure 71) and the average first-floor diaphragm displacement, divided by the second-storey height (2.65 m).

For the roof, the in-plane shear deformation γ of the diaphragm was calculated, taking into account its inclined length. The reported value is obtained as the difference between the ridge beam displacement (from potentiometer #74, Table 7, Figure 64 and Figure 65) and the average second-floor diaphragm displacement, divided by the roof pitch length ($L = 3.56$ m).

- **Floor diaphragms deformed shapes**

In-plane deformed shapes were computed by post-processing data recorded from pairs of potentiometers at the first-floor diaphragm (potentiometers #113, 114 and #116, 117) and second-floor diaphragm (potentiometers #94, 95; #96, 97; #98, 99; and #100, 101). Using pairs of potentiometers in two orthogonal directions was dictated by the need of capturing in-plane rotations. A pair instruments connected to a point on the floor monitors its trajectory, and the position at each instant can be determined as the intersection of two conferences centred at each individual instrument origin with radius equal to the instantaneous instrument length.

The diaphragm deformed shapes are presented at two instants: the one at maximum average first-floor diaphragm displacement (RC diaphragm only), and the one at maximum average second-floor diaphragm displacement (both diaphragms).

5.2.1 Test #2 EQ-NPR 20%, PGA = 0.06 g

Figure 200 shows a good match in terms of spectral accelerations and displacements at the current specimen fundamental period of vibration.

Figure 201 shows the hysteretic response of the building: at this stage the specimen is within its elastic range.

Displacement profiles and interstorey drift envelopes show lateral deformation increasing with the height above ground.

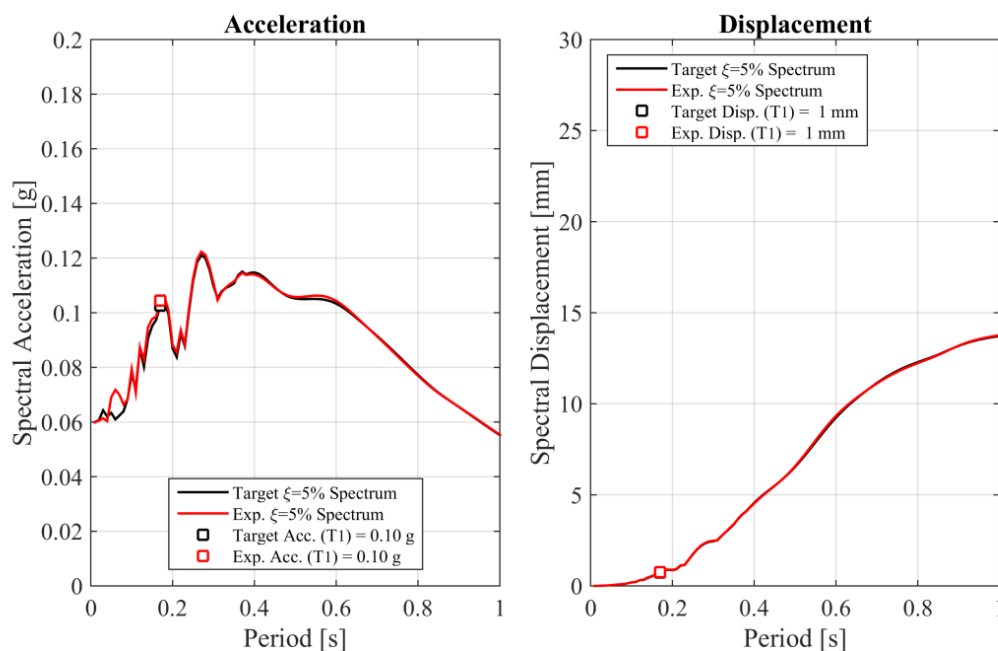


Figure 200 Test #2 EQ-NPR 20% - Target and experimental elastic response spectra.

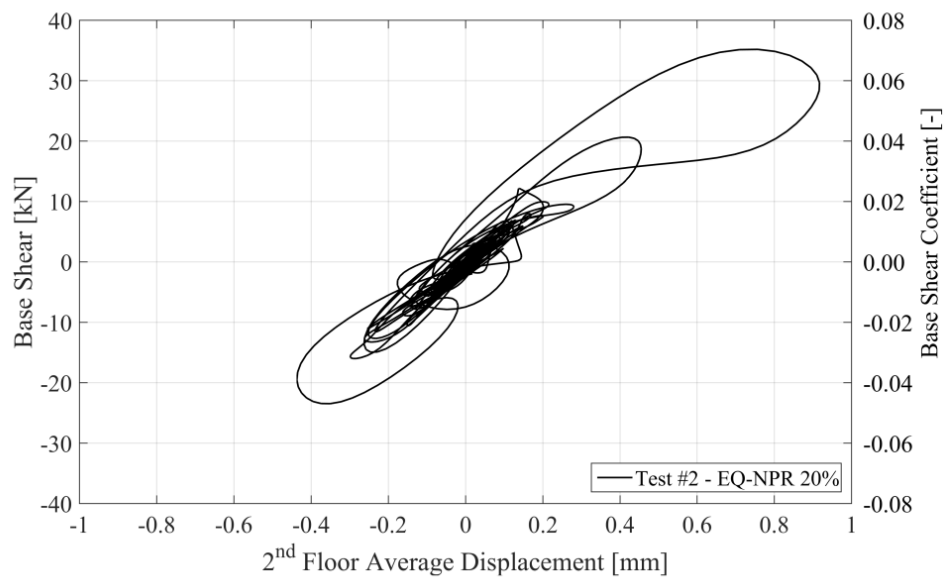


Figure 201 Test #2 EQ-NPR 20% - Hysteretic force-displacement response.

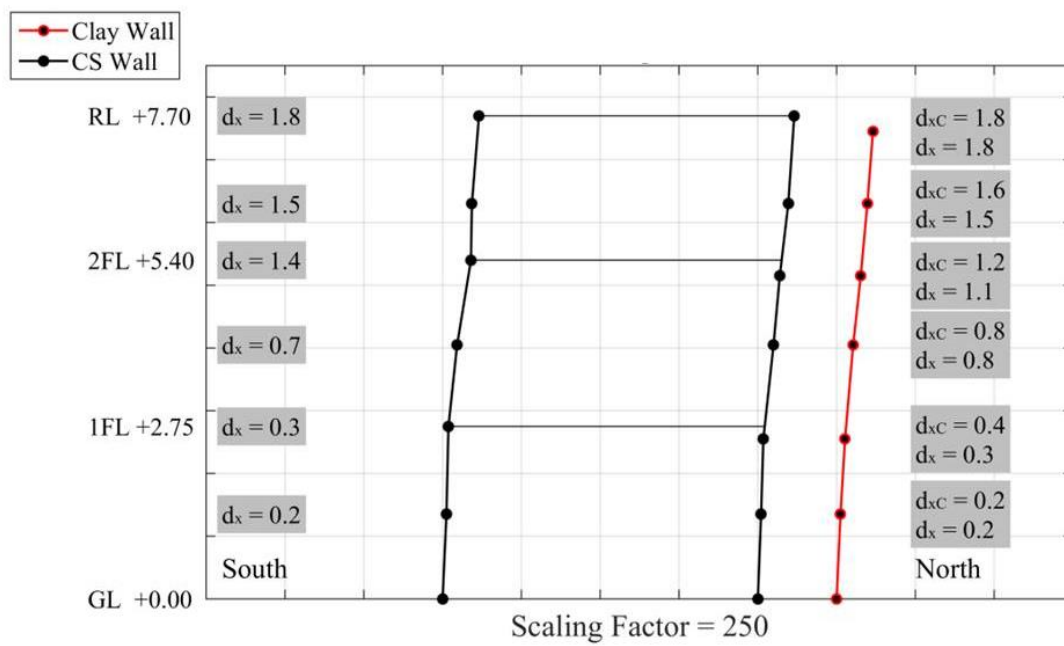


Figure 202 Test #2 EQ-NPR 20% - Displacement profile at maximum second-floor displacement.

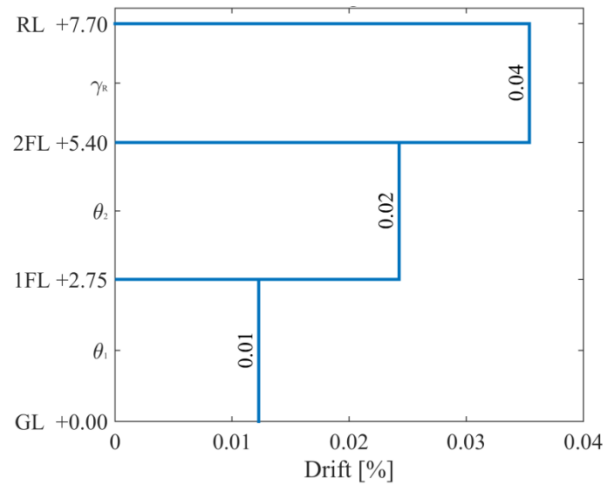


Figure 203 Test #2 EQ-NPR 20% - Interstorey drift ratio envelope.

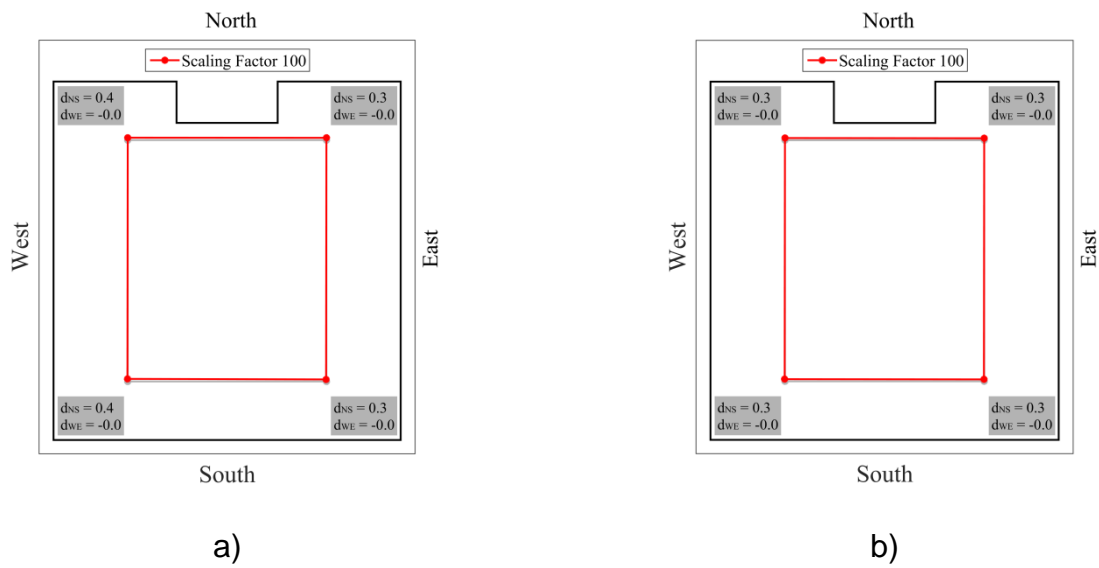


Figure 204 Test #2 EQ-NPR 20% - First-floor diaphragm deformed shapes: a) at maximum first-floor displacement; b) at maximum average second-floor displacement.

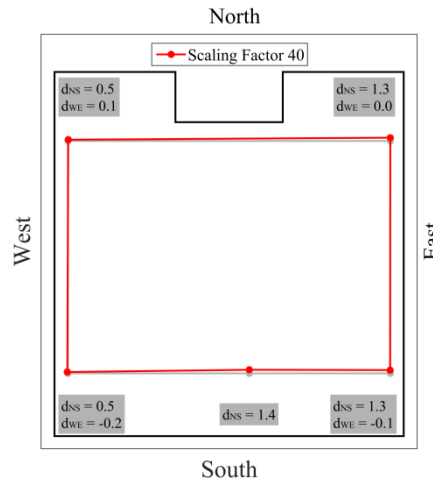


Figure 205 Test #2 EQ-NPR 20% - Second-floor diaphragm deformed shape at maximum average second-floor displacement.

5.2.2 Test #3 EQ-NPR 33%, PGA = 0.1 g

Figure 206 shows that the actual input overshoots the spectral accelerations at short periods, probably due to difficulties for the controller to replicate the input spectra when the fundamental period of the structure is very close to the one of the actuator oil column. However, the difference was only about 0.04 g.

Figure 207 shows the hysteretic response of the building, overlapped with results of the previous run: the behaviour is still elastic.

Displacement profiles and interstorey drift envelopes show lateral deformation increasing with the height above ground.

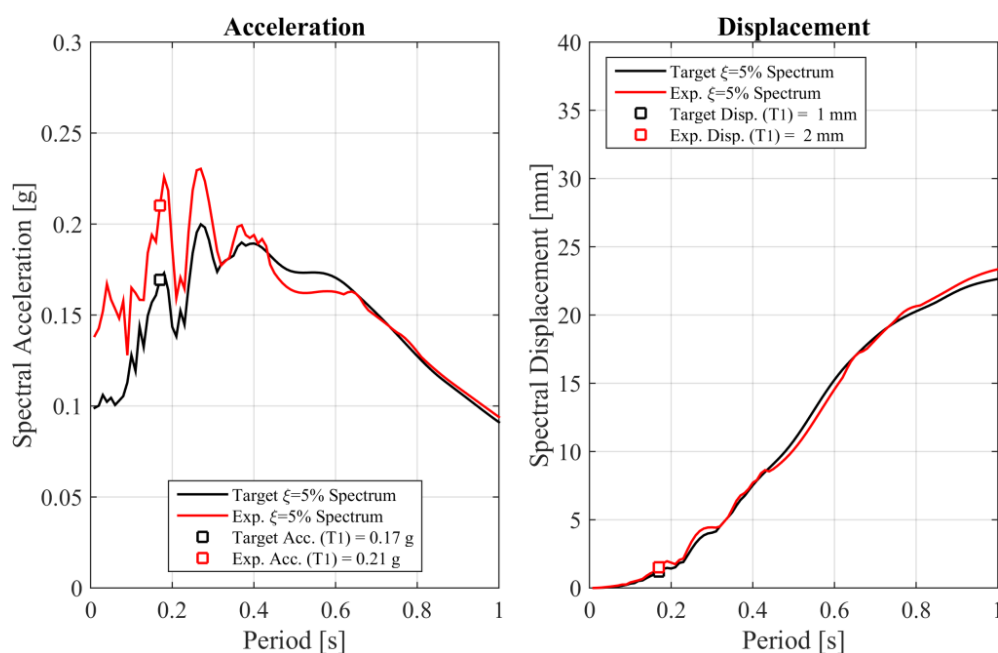


Figure 206 Test #3 EQ-NPR 33% - Target and experimental elastic response spectra.

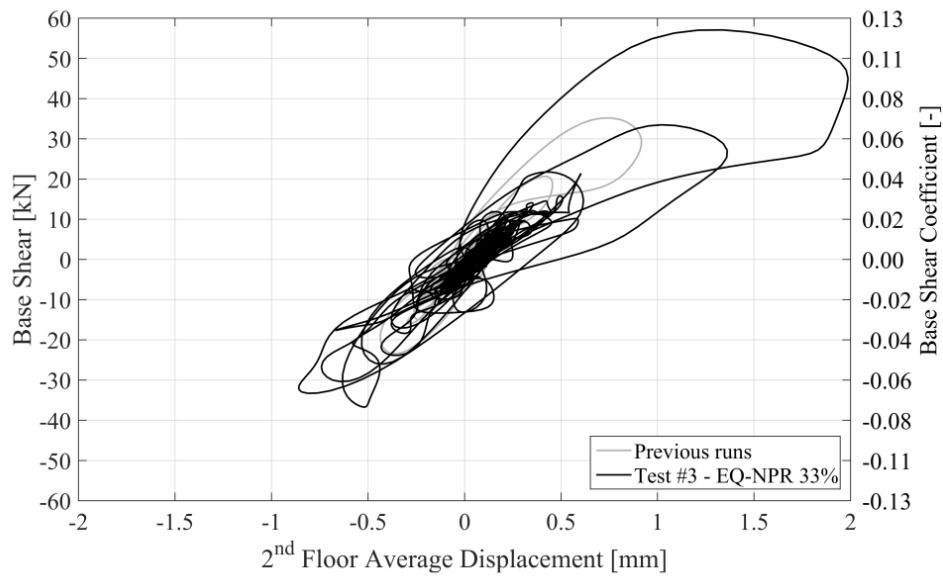


Figure 207 Test #3 EQ-NPR 33% - Hysteretic force-displacement response.

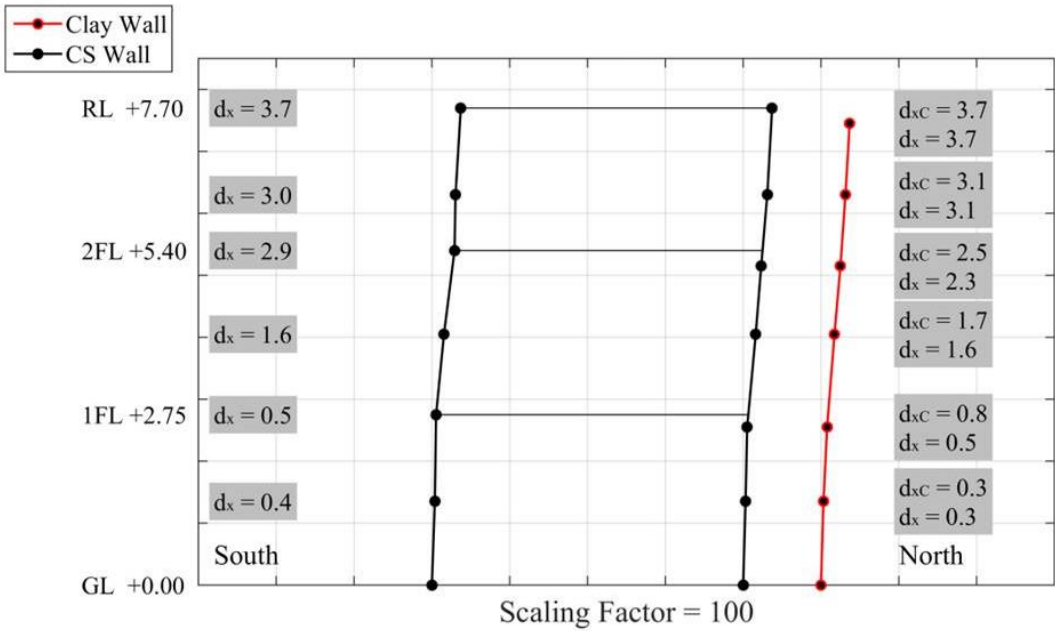


Figure 208 Test #3 EQ-NPR 33% - Displacement profile at maximum second-floor displacement.

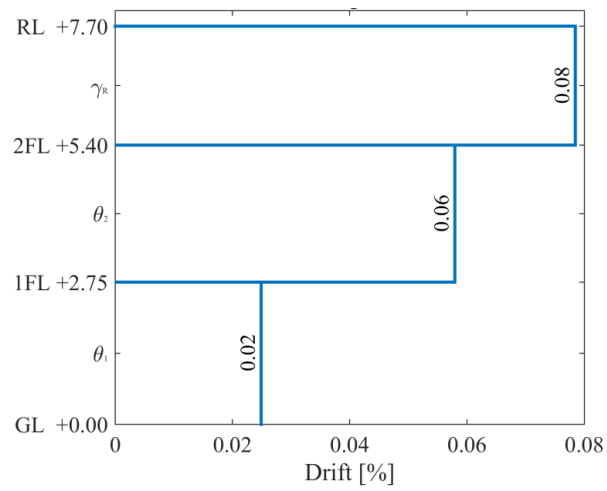


Figure 209 Test #3 EQ-NPR 33% - Interstorey drift ratio envelope.

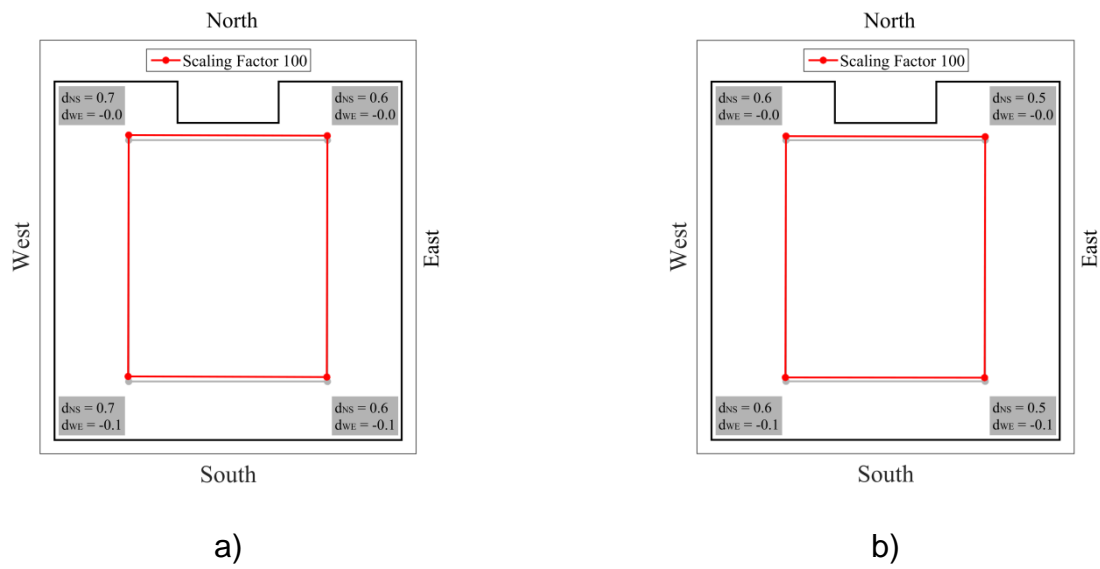


Figure 210 Test #3 EQ-NPR 33% - First-floor diaphragm deformed shapes: a) at maximum first-floor displacement; b) at maximum average second-floor displacement.

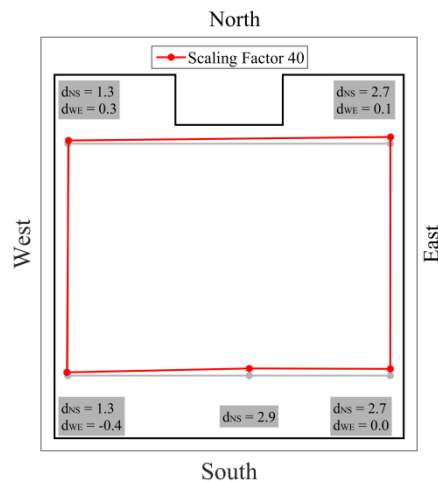


Figure 211 Test #3 EQ-NPR 33% - Second-floor diaphragm deformed shape at maximum average second-floor displacement.

5.2.3 Test #8 EQ-NPR 50%, PGA = 0.15 g

Figure 212 shows a good match in terms of spectral accelerations and displacements at the current specimen fundamental period of vibration.

The force-displacement curve shows elastic behaviour (Figure 213).

Displacement profiles and interstorey drift envelopes show lateral deformation increasing with the height above ground.

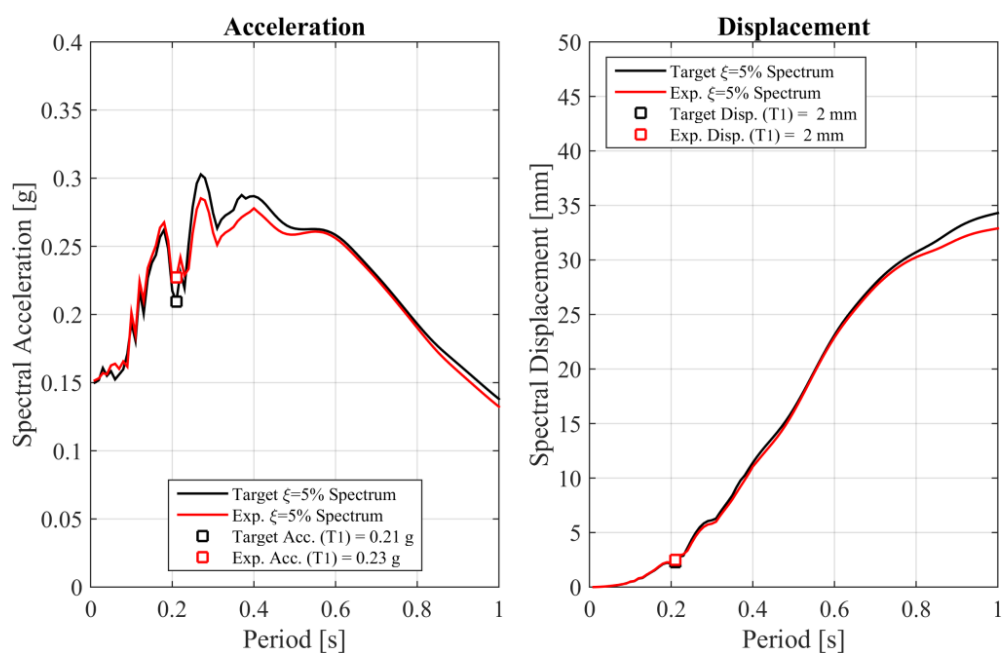


Figure 212 Test #8 EQ-NPR 50% - Target and experimental elastic response spectra.

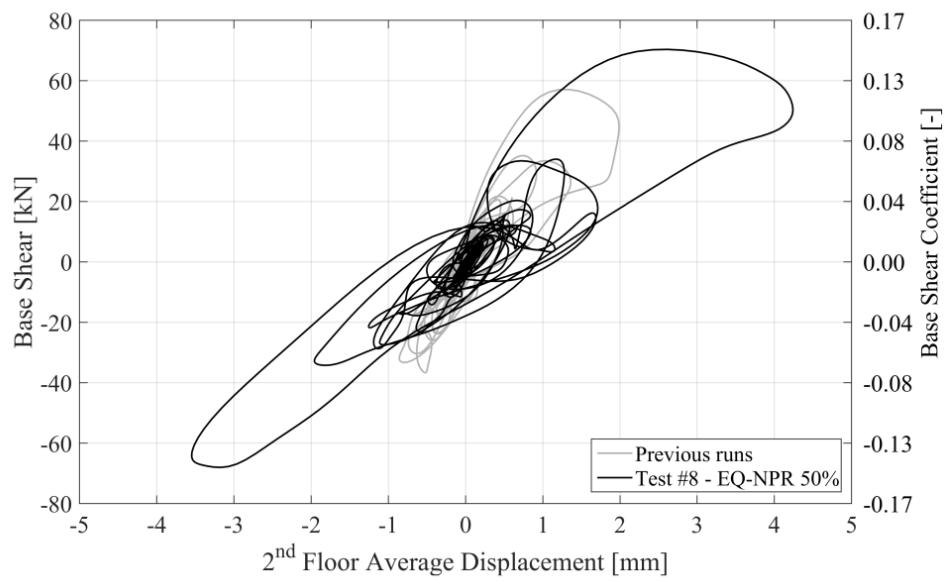


Figure 213 EQ-NPR 50% - Hysteretic force-displacement response.

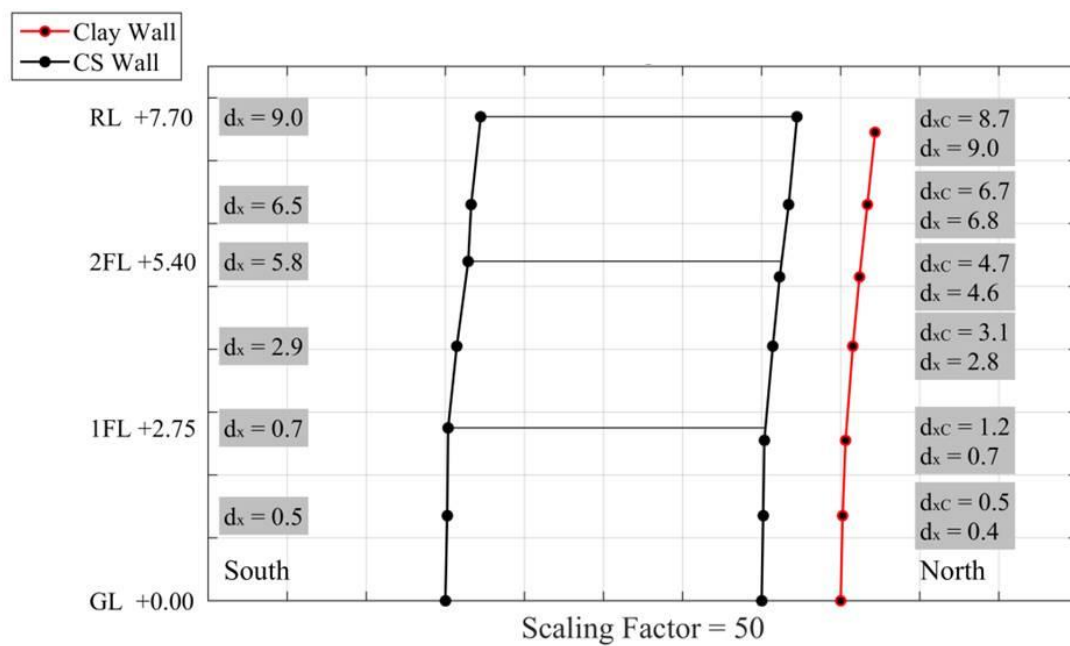


Figure 214 Test #8 EQ-NPR 50% - Displacement profile at maximum second-floor displacement.

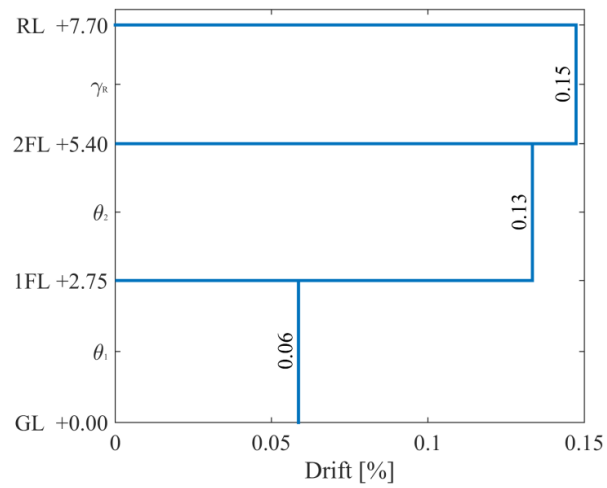


Figure 215 Test #8 EQ-NPR 50% - Interstorey drift ratio envelope.

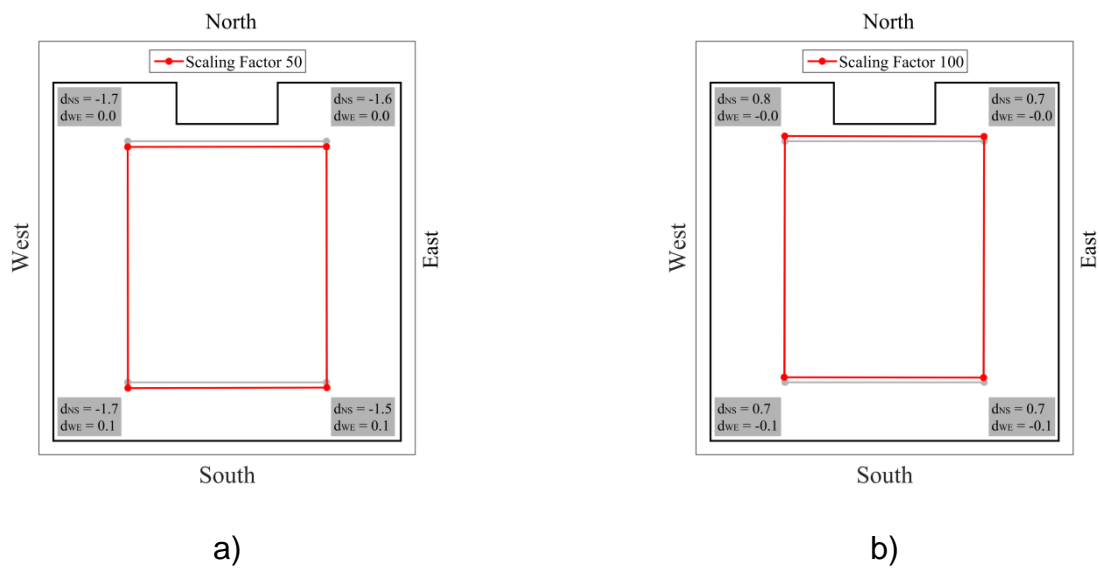


Figure 216 Test #8 EQ-NPR 50% - First-floor diaphragm deformed shapes: a) at maximum first-floor displacement; b) at maximum average second-floor displacement.

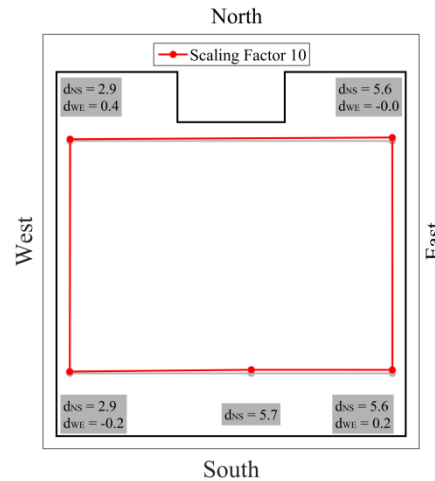


Figure 217 Test #8 EQ-NPR 50% - Second-floor diaphragm deformed shape at maximum average second-floor displacement.

5.2.4 Test #10 EQ-NPR 66%, PGA = 0.20 g

Figure 218 shows that the theoretical and experimental spectral accelerations at the current fundamental period of vibration are similar: they differ only by 0.02 g, despite some undershooting at longer periods.

Figure 219 shows some excursions into the inelastic range of response, especially in the widest positive and negative cycles.

Displacement profiles and interstorey drift envelopes show that deformations started concentrating at the second storey.

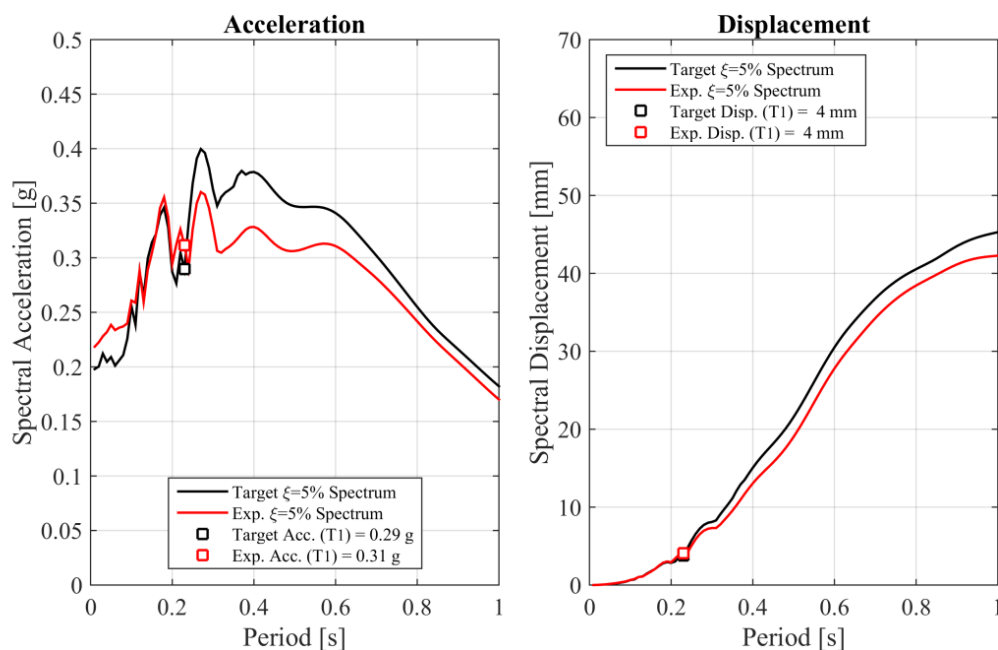


Figure 218 Test #10 EQ-NPR 66% - Target and experimental elastic response spectra.

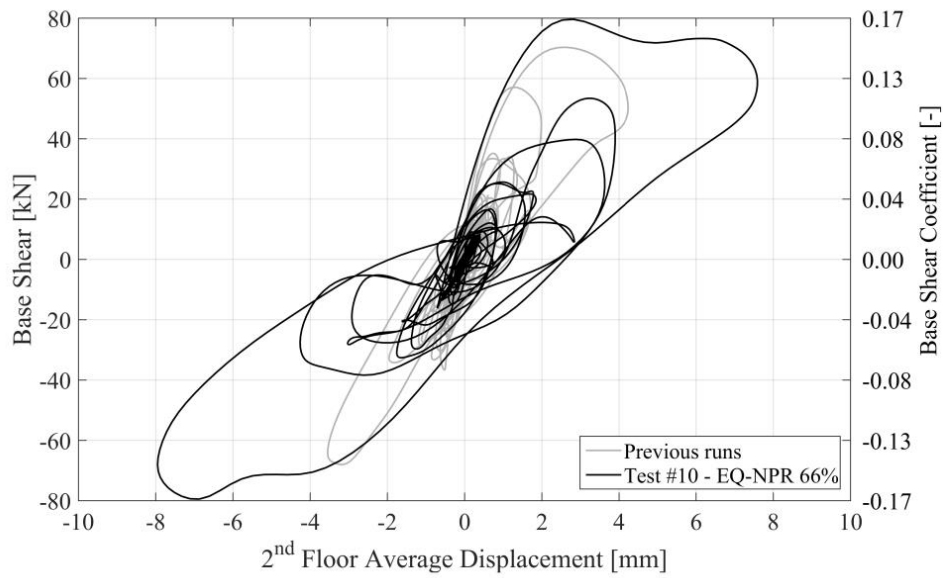


Figure 219 Test #10 EQ-NPR 66% - Hysteretic force-displacement response.

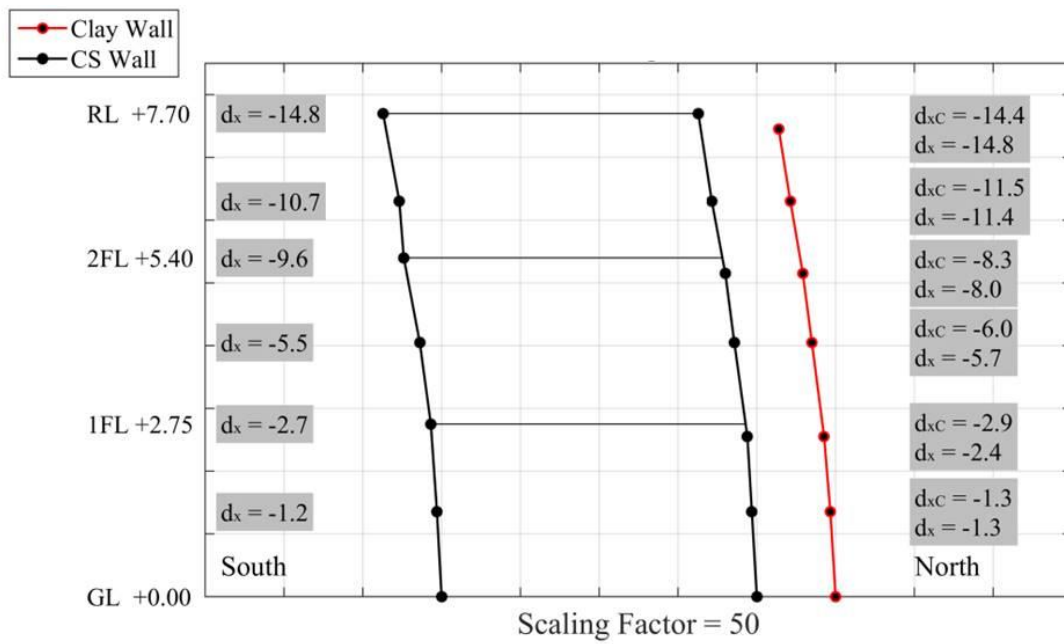


Figure 220 Test #10 EQ-NPR 66% - Displacement profile at maximum second-floor displacement.

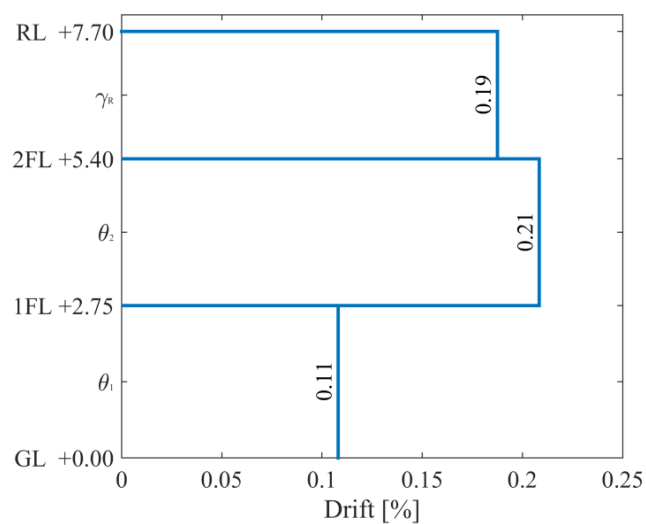


Figure 221 Test #10 EQ-NPR 66% - Interstorey drift ratio envelope.

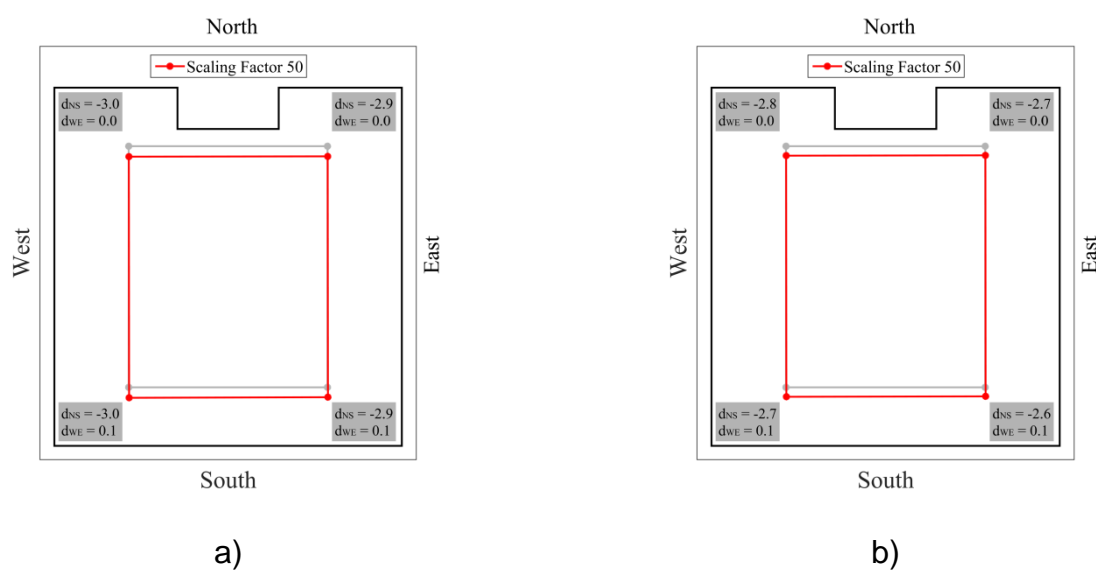


Figure 222 Test #10 EQ-NPR 66% - First-floor diaphragm deformed shapes: a) at maximum first-floor displacement; b) at maximum average second-floor displacement.

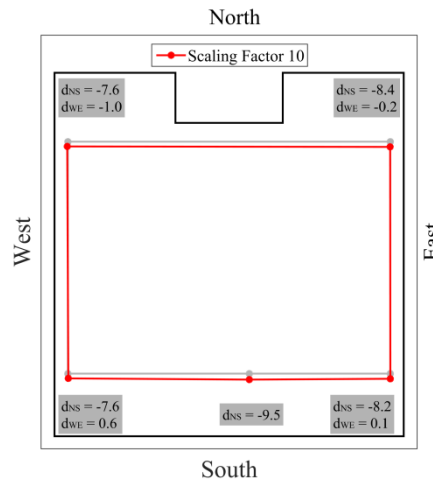


Figure 223 Test #10 EQ-NPR 66% - Second-floor diaphragm deformed shape at maximum average second-floor displacement.

5.2.5 Test #15 EQ-NPR 85%, PGA = 0.25 g

A very good match is obtained in terms of spectral acceleration at the current fundamental period of vibration (Figure 224), despite some undershooting at longer periods.

The hysteretic response clearly shows inelastic response of the building prototype (Figure 225). Global drift ratios are also reported on the hysteretic diagrams, since they reached appreciable amounts.

The displacement profile (Figure 226) and interstorey drift ratio envelopes (Figure 227) show significant deformation concentration at the second storey, which reached a drift ratio nearly four times the first-story one.

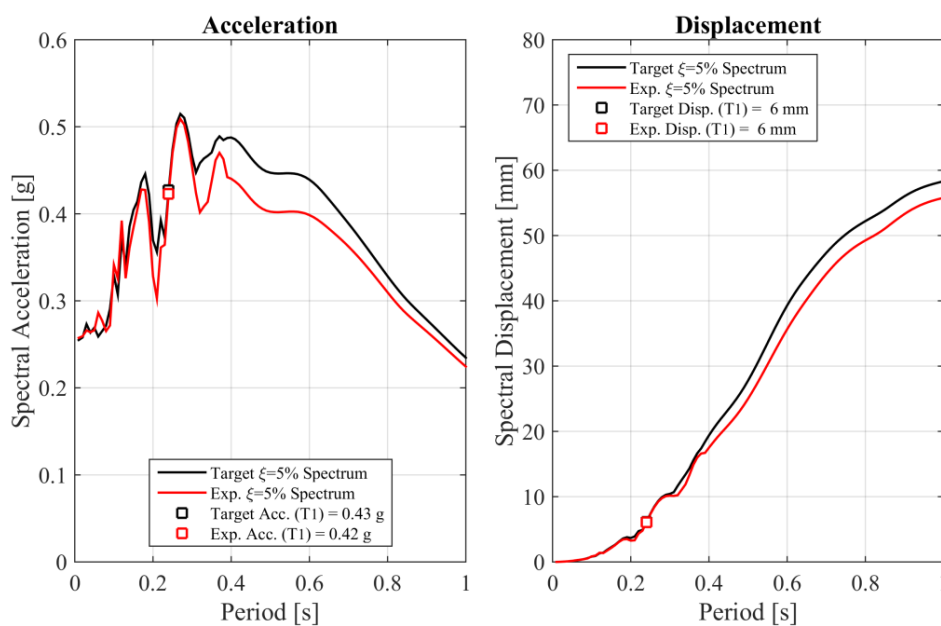


Figure 224 Test #15 EQ-NPR 85% - Target and experimental elastic response spectra.

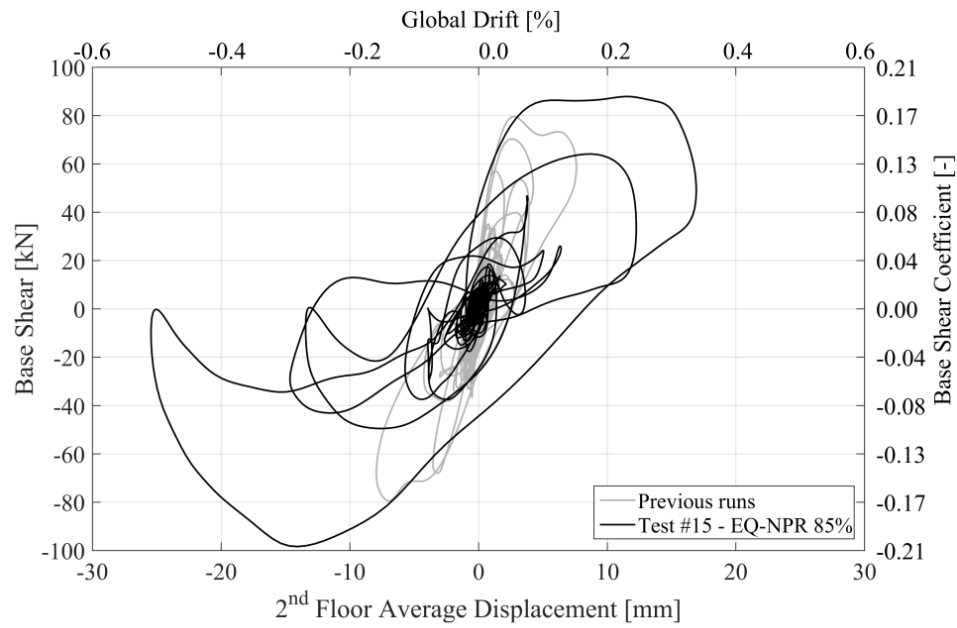


Figure 225 Test #15 EQ-NPR 85% - Hysteretic force-displacement response.

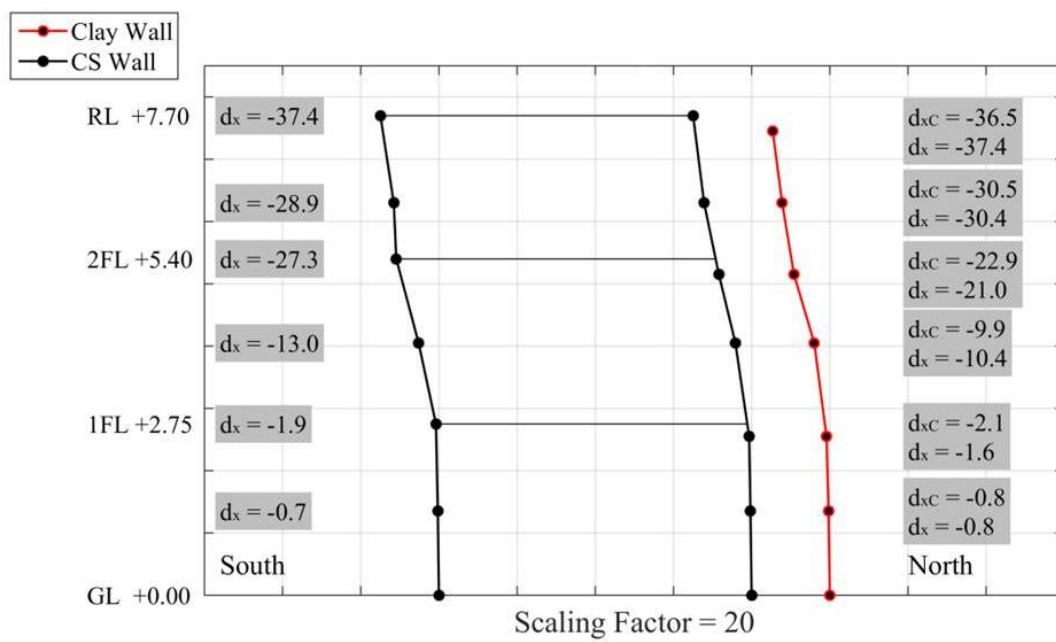


Figure 226 Test #15 EQ-NPR 85% - Displacement profile at maximum second-floor displacement.

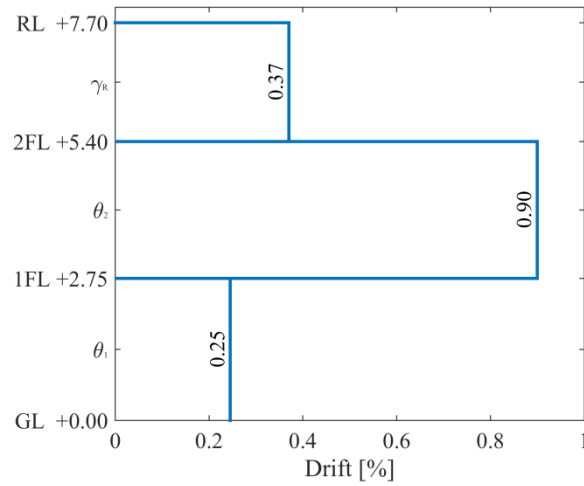


Figure 227 Test #15 EQ-NPR 85% - Interstorey drift ratio envelope.

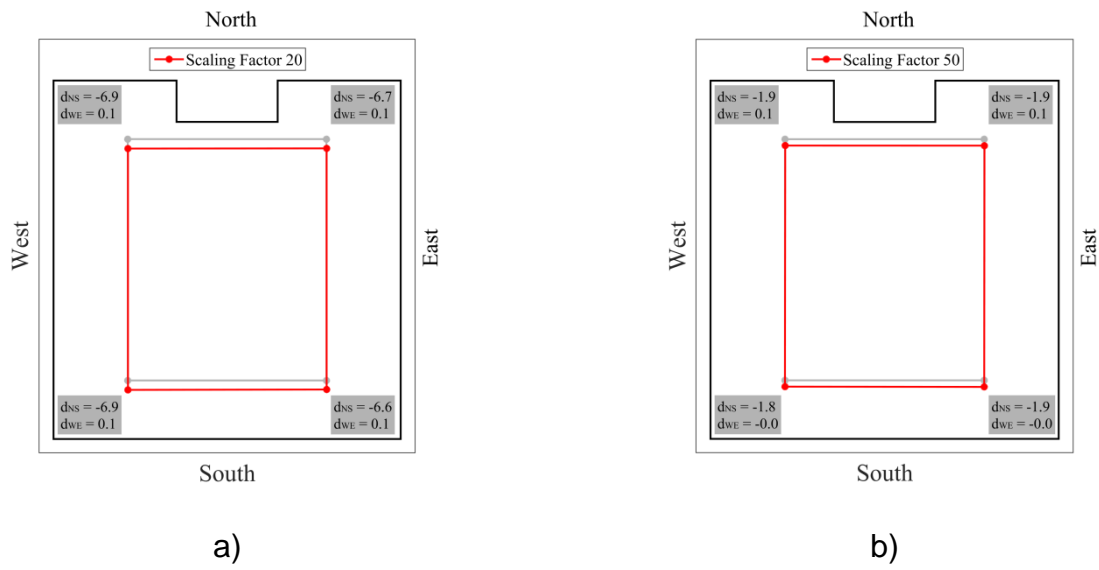


Figure 228 Test #15 EQ-NPR 85% - First-floor diaphragm deformed shapes: a) at maximum first-floor displacement; b) at maximum average second-floor displacement.

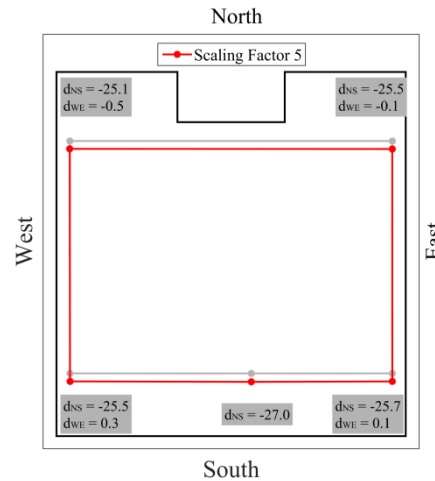


Figure 229 Test #15 EQ-NPR 85% - Second-floor diaphragm deformed shape at maximum average second-floor displacement.

5.2.6 Test #21 EQ-NPR 100%, PGA = 0.30 g

A very good match is obtained in terms of spectral acceleration at the current fundamental period of vibration (Figure 230), despite some undershooting at longer periods.

The specimen behaved inelastically and significant residual displacement was accumulated (Figure 231). The significant base-shear drop during the wide cycle in the third quadrant may be a sign of incipient loss of global stability.

Compared to the previous run, deformation concentration at the second storey became more evident (Figure 232 and Figure 233), with a second-storey drift ratio about five times the first-storey one.

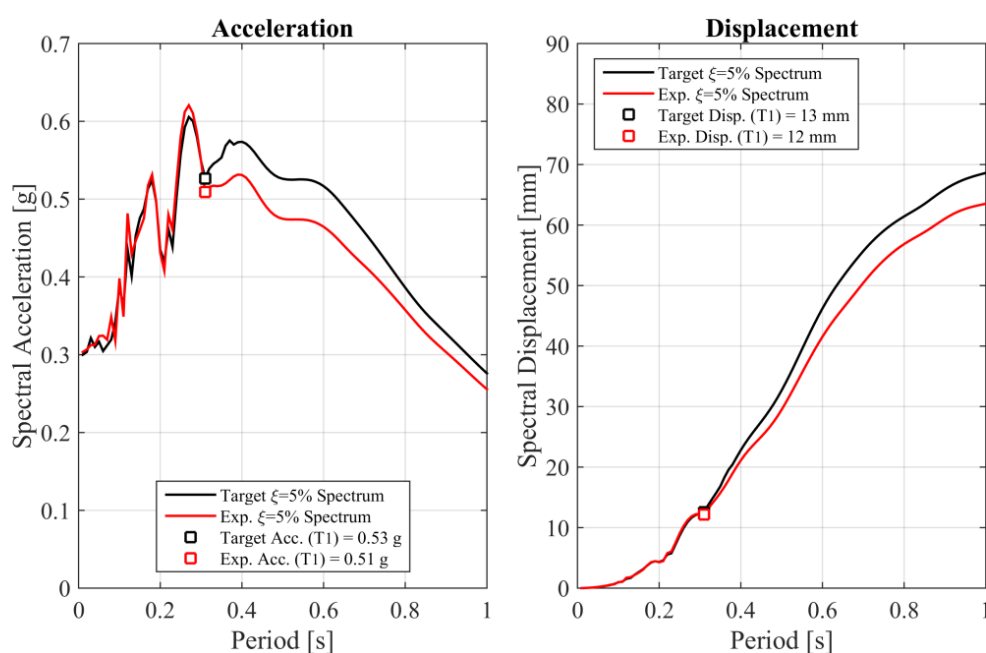


Figure 230 Test #21 EQ-NPR 100% - Target and experimental elastic response spectra.

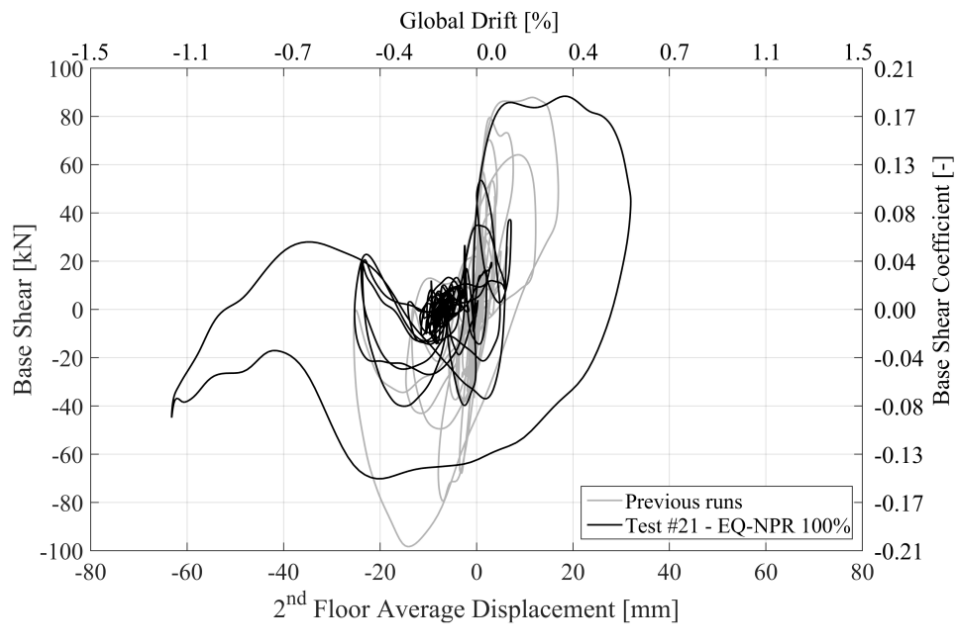


Figure 231 Test #21 EQ-NPR 100% - Hysteretic force-displacement response.

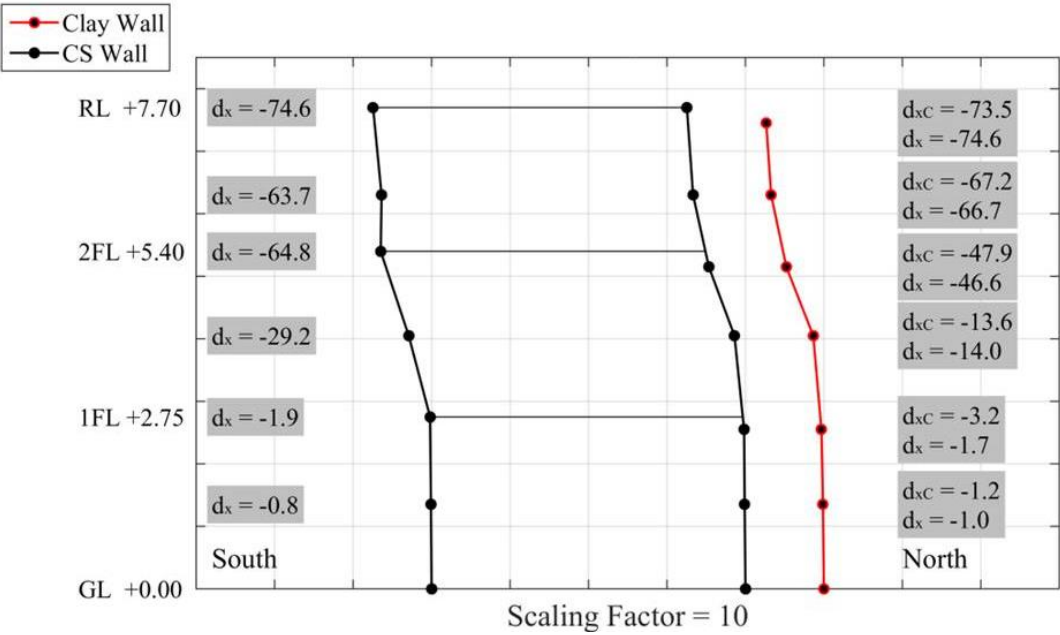


Figure 232 Test #21 EQ-NPR 100% - Displacement profile at maximum second-floor displacement.

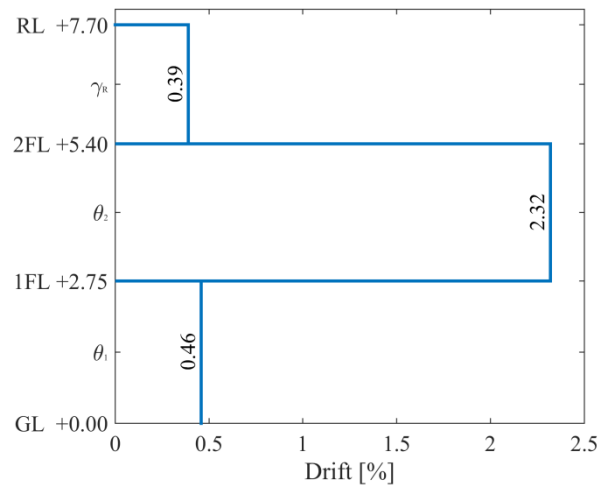


Figure 233 Test #21 EQ-NPR 100% - Interstorey drift ratio envelope.

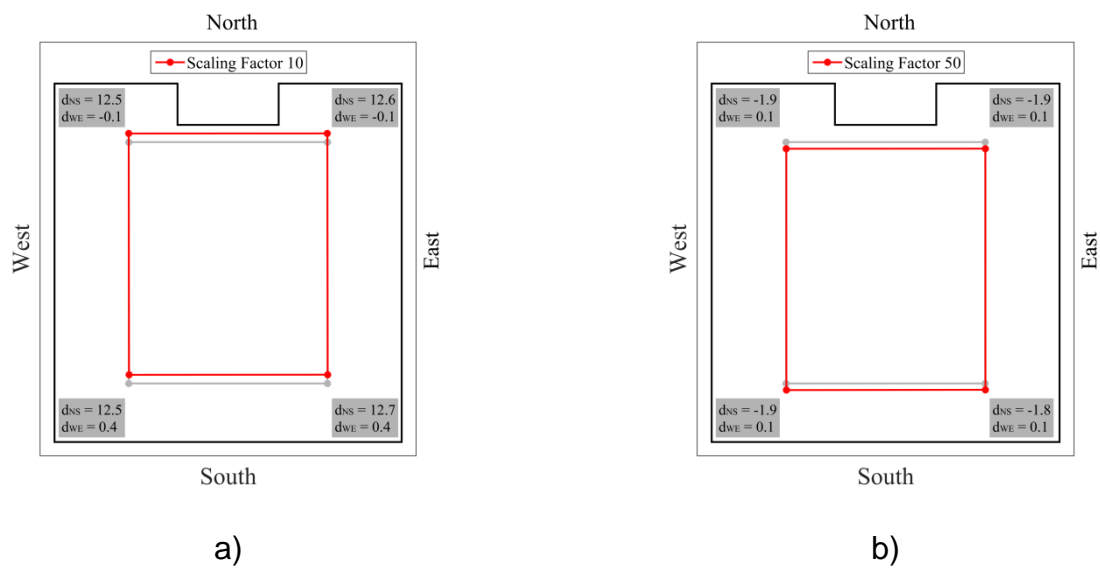


Figure 234 Test #21 EQ-NPR 100% - First-floor diaphragm deformed shapes: a) at maximum first-floor displacement; b) at maximum average second-floor displacement.

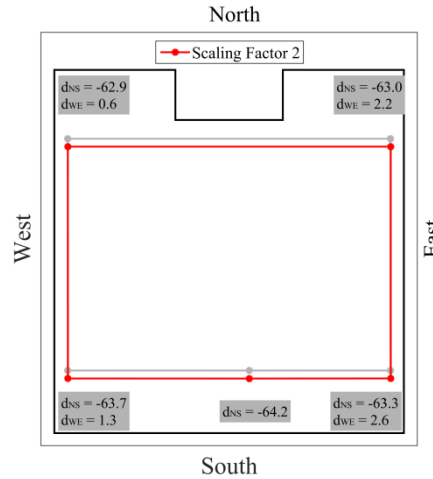


Figure 235 Test #21 EQ-NPR 100% - Second-floor diaphragm deformed shape at maximum average second-floor displacement.

5.2.7 Test #24 EQ-NPR IS 100%, PGA = 0.30 g (inverted sign)

Figure 236 shows that the theoretical and experimental spectral accelerations at the current fundamental period of vibration are very close to each other, despite some limited overshooting at very short periods.

The hysteretic response (Figure 237) shows an excursion into the fourth quadrant with increasing negative displacement, which denotes loss of global static stability. However, dynamic effects prevented total loss of equilibrium, allowing exploration of near-collapse conditions. Further increase of residual displacement was also recorded.

Concentration of deformations at the second storey (Figure 238 and Figure 239) resulted in an interstorey drift more than six times the first-storey one. Please note that Figure 238 shows only the calcium silicate inner leaf displacement profiles, as the wire potentiometers connected to the clay outer leaf North façade had been removed (see par. 3.1 and 3.2).

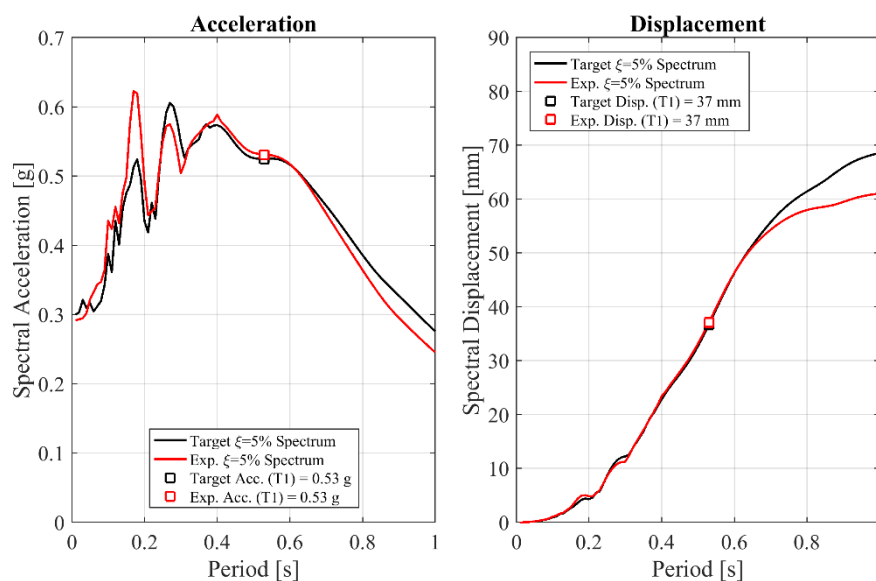


Figure 236 Test #24 EQ-NPR IS 100% - Target and experimental elastic response spectra.

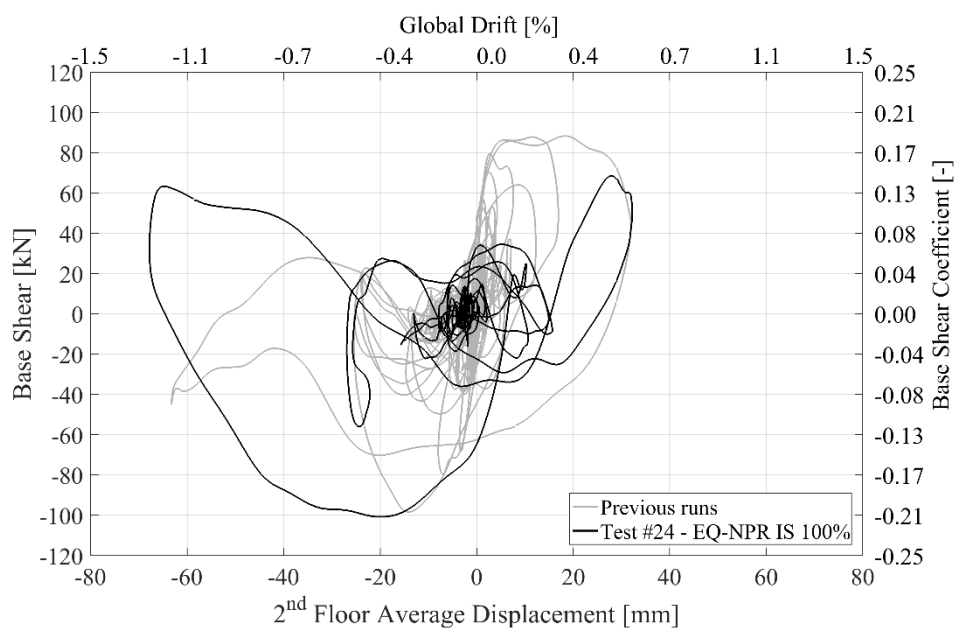


Figure 237 Test #24 EQ-NPR IS 100% - Hysteretic force-displacement response.

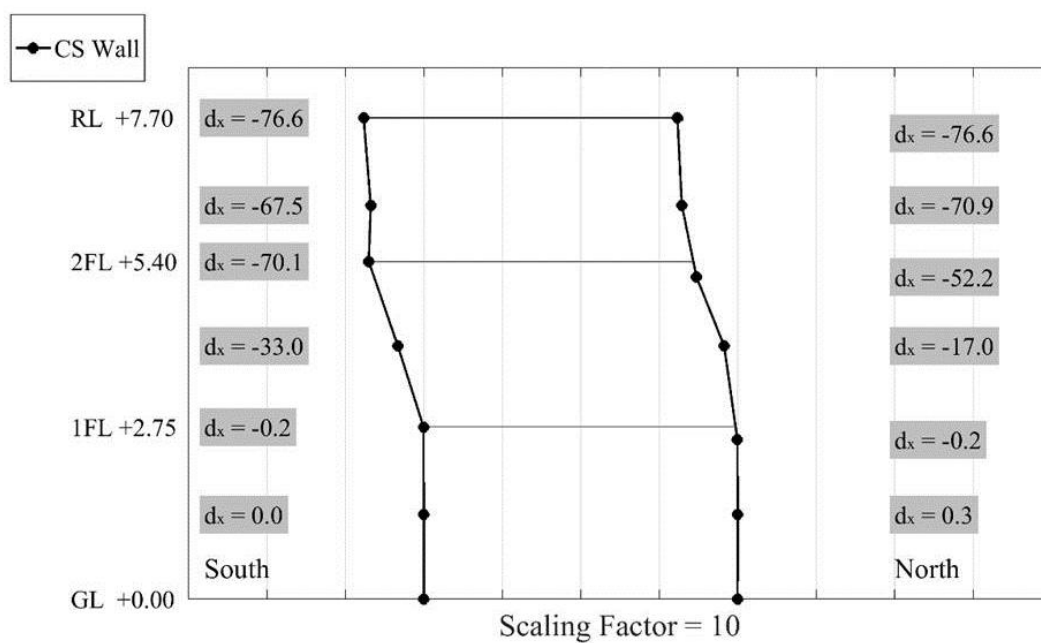


Figure 238 Test #24 EQ-NPR IS 100% - Displacement profile at maximum second-floor displacement.

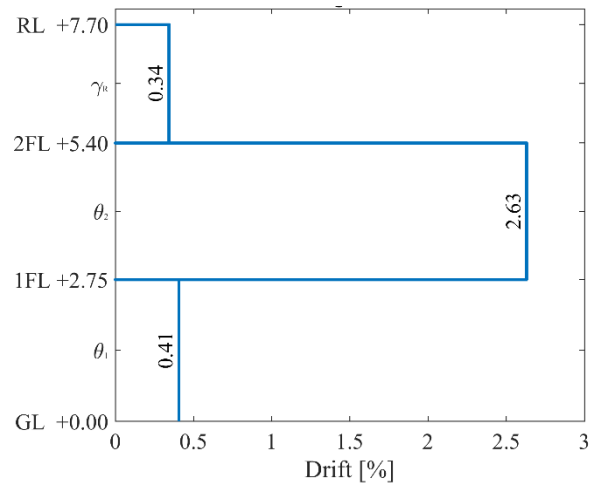


Figure 239 Test #24 EQ-NPR IS 100% - Interstorey drift ratio envelope.

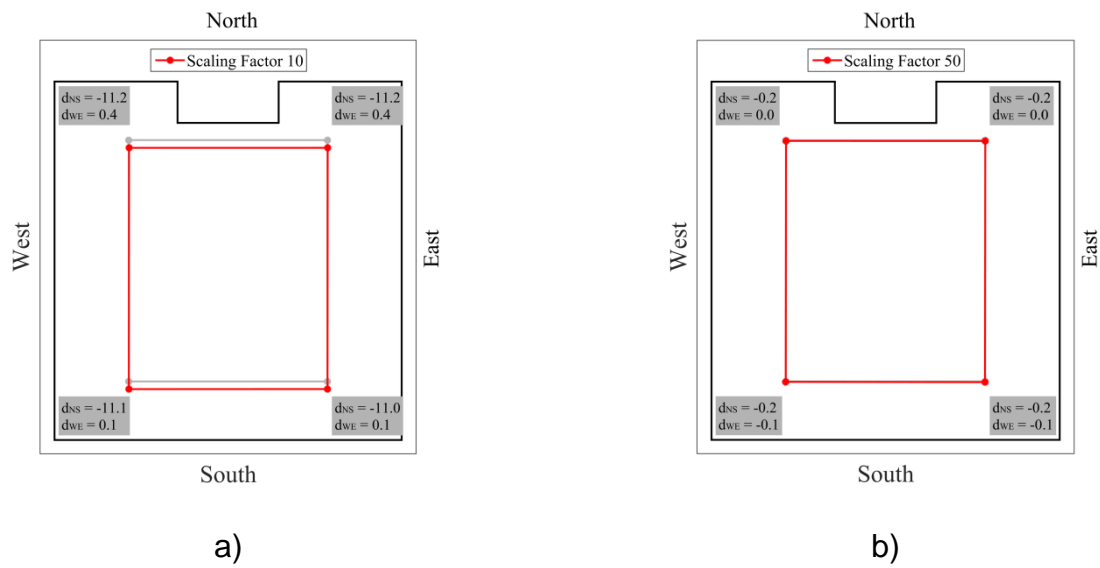


Figure 240 Test #24 EQ-NPR IS 100% - First-floor diaphragm deformed shapes: a) at maximum first-floor displacement; b) at maximum average second-floor displacement.

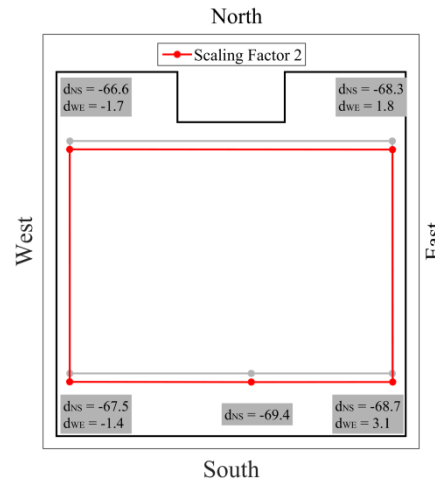


Figure 241 Test #24 EQ-NPR IS 100% - Second-floor diaphragm deformed shape at maximum average second-floor displacement.

5.2.8 Test #25 EQ-NPR IS 133%, $PGA = 0.40\text{ g}$ (inverted sign)

Figure 242 shows an overshoot for periods lower than 0.25 and an undershoot for periods higher than that can be seen. The experimental and analytical spectral acceleration at the current fundamental period of vibration are very similar.

Figure 243 shows again a statically unstable global response balanced by dynamic effects, resulting in a near-collapse state of the specimen.

Figure 244 and Figure 245 confirm the concentration of deformations at the second storey. Please note that Figure 244 shows only the calcium silicate inner leaf displacement profiles, as the wire potentiometers connected to the clay outer leaf North façade had been removed (see par. 3.1 and 3.2).

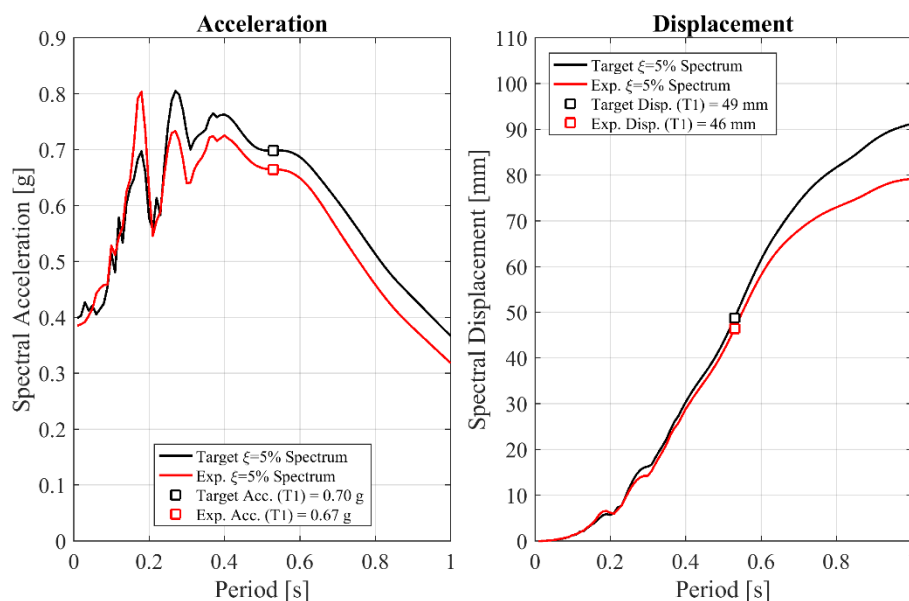


Figure 242 Test #25 EQ-NPR IS 133% - Target and experimental elastic response spectra.

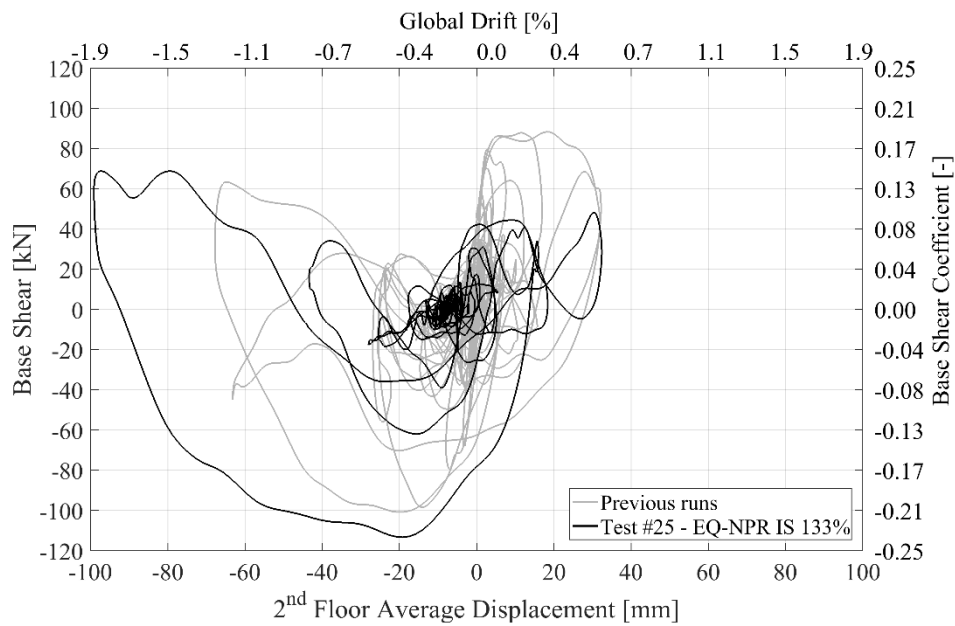


Figure 243 Test #25 EQ-NPR IS 133% - Hysteretic force-displacement response.

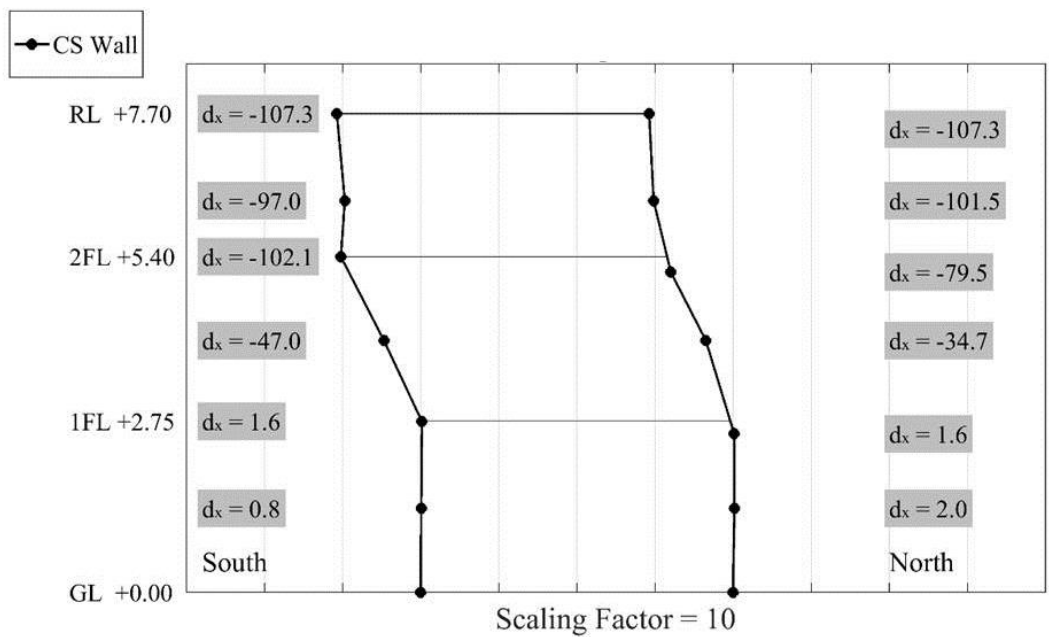


Figure 244 Test #25 EQ-NPR IS 133% - Displacement profile at maximum second-floor displacement.

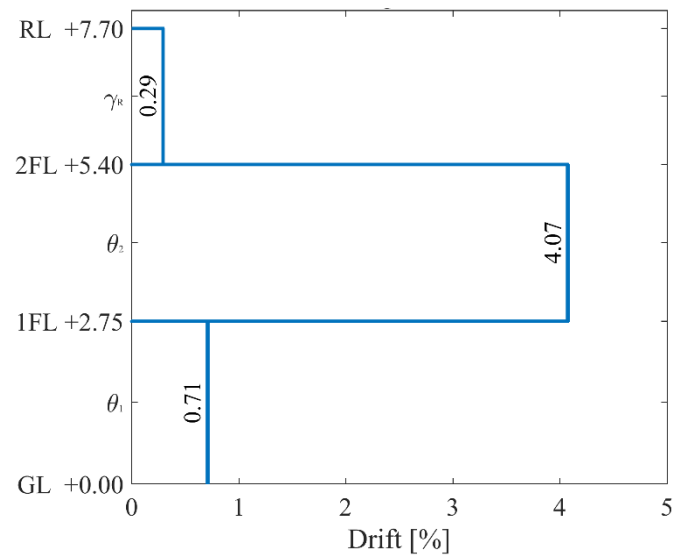


Figure 245 Test #25 EQ-NPR IS 133% - Interstorey drift ratio envelope.

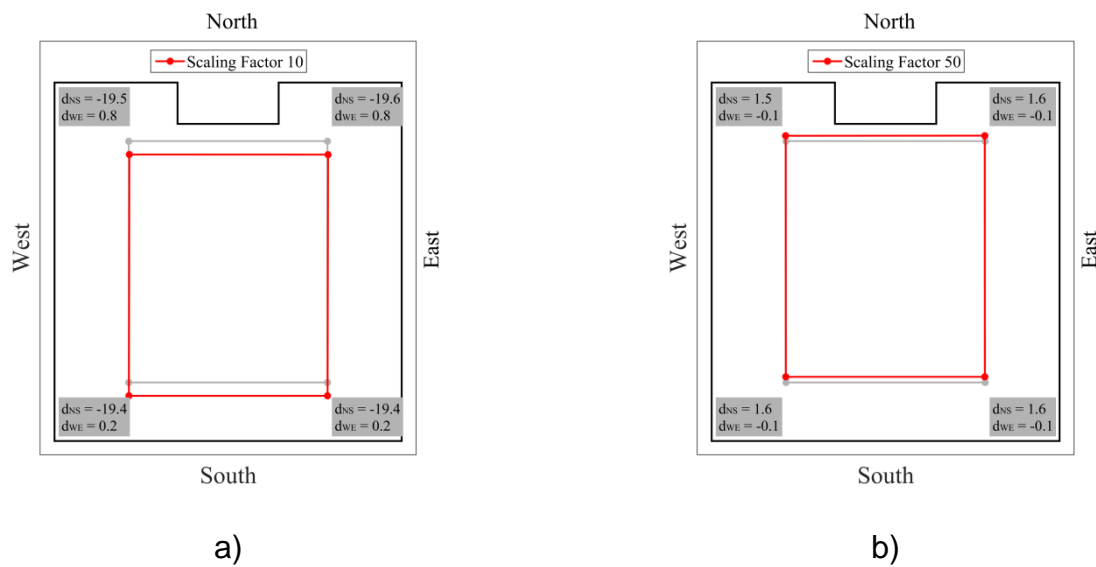


Figure 246 Test #25 EQ-NPR IS 133% - First-floor diaphragm deformed shapes: a) at maximum first-floor displacement; b) at maximum average second-floor displacement.

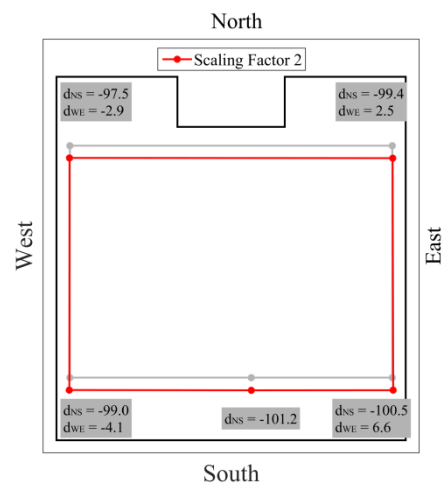


Figure 247 Test #25 EQ-NPR IS 133% - Second-floor diaphragm deformed shape at maximum average second-floor displacement.

5.3 Summary of the results

Figure 248 shows the computed backbone curve in terms of base shear (or base shear coefficient) and second-floor displacement (or global drift ratio). Grey lines represent the derived hysteretic response for each dynamic test run, while the black curve is the resulting backbone curve. The negative-side response shows clearly a loss of static stability, compensated by dynamic effects. For the derivation of the backbone curve, all test responses were plotted removing the accumulated residual displacements of preceding tests.

Figure 249 shows the evolution of the building prototype response during the incremental dynamic test. It includes:

- peak displacements of the first and second floor (average, East and West) and of the roof, relative to the foundation;
- peak and residual interstorey drift ratios (IDR) for the first and second storeys (average, East and West);
- peak and residual shear deformation of the roof;
- acceleration amplification factors (AMP) for the first and second floor and for the roof;
- fundamental period evolution.

The subscript associated with the fundamental period on the figure indicates the test number of the random motion used for dynamic identification, applied right after the main test on the x-axis. No random noise was applied after test #24 EQ-NPR IS 100%, so the same period obtained after test #21 EQ-NPR 100% is reported on the figure.

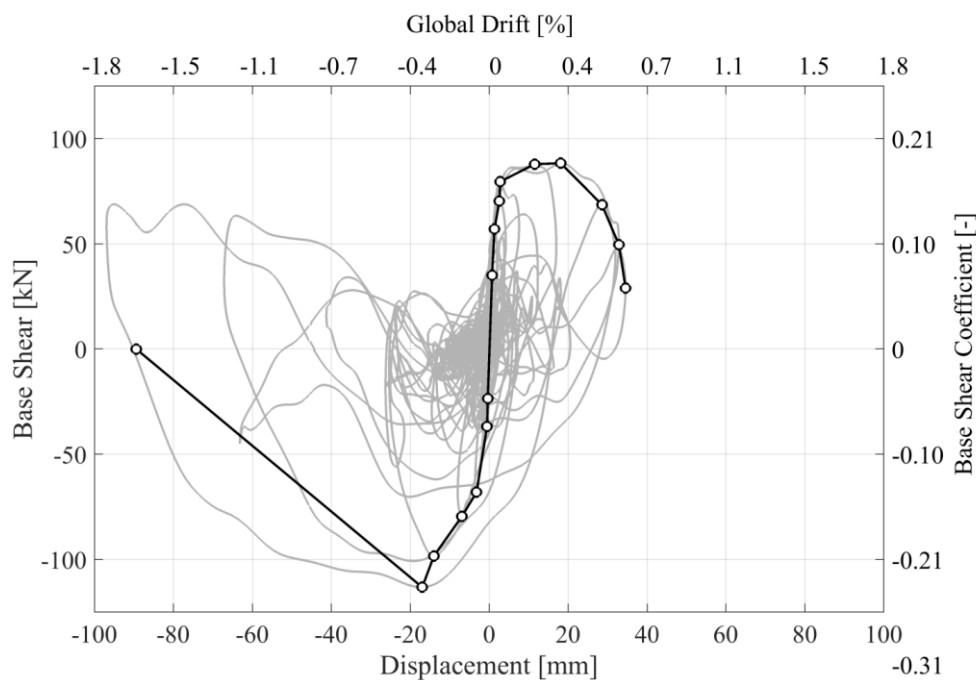


Figure 248 Backbone force-displacement curve.

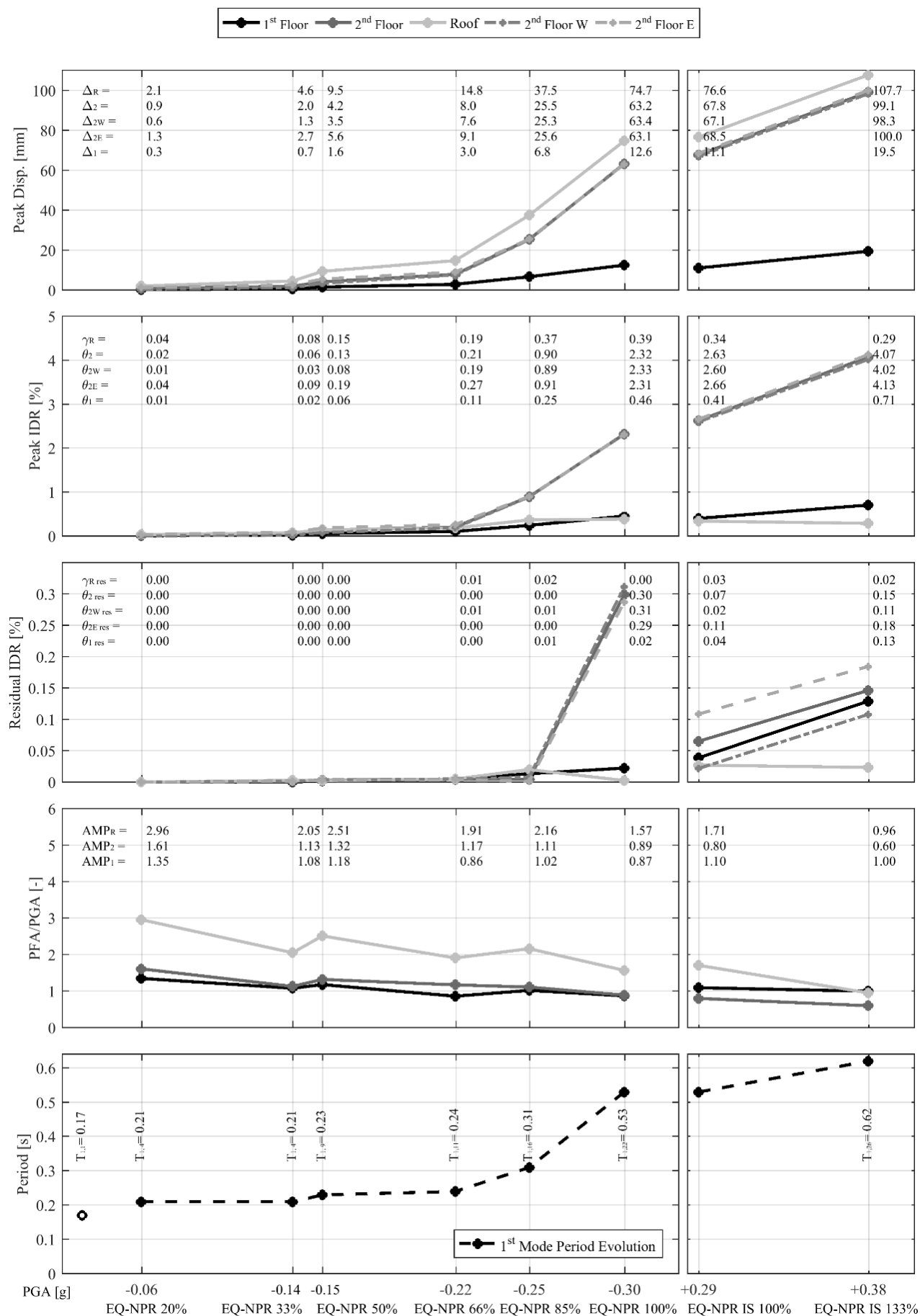


Figure 249 Evolution of the building specimen response.

REFERENCES

- [1]. Graziotti, F., Tomassetti, U., Rossi, A., Kallioras, S., Mandirola, M., Cenja, E., Penna, A., Magenes, G. (2015). *Experimental Campaign on Cavity-Wall Systems Representative of the Groningen Building Stock*. Technical Report EUC318/2015U, EUCENTRE, Pavia, Italy. Available at: <http://www.eucentre.it/project-nam/>
- [2]. Graziotti, F., Tomassetti, U., Kallioras, S., Penna, A., & Magenes, G. (2017). Shaking table test on a full scale URM cavity wall building. *Bulletin of Earthquake Engineering*, 15(12):5329-5364.
- [3]. CEN (2011). *Methods of test for masonry units. Part 1: Determination of compressive strength*. European Standard EN 772-1. CEN/TC, Brussels, Belgium.
- [4]. CEN (2006). *Methods of test for mortar for masonry. Part 11: Determination of flexural and compressive strength of hardened mortar*. European Standard EN 1015-11. CEN/TC, Brussels, Belgium.
- [5]. CEN (1998). *Methods of test for masonry. Part 1: Determination of compressive strength*. European Standard EN 1052-1. CEN/TC, Brussels, Belgium.
- [6]. CEN (2005). *Methods of test for masonry. Part 5: Determination of bond strength by the Bond Wrench method*. European Standard EN 1052-5. CEN/TC, Brussels, Belgium.
- [7]. CEN (2007). *Methods of test for masonry units. Part 3: Determination of initial shear strength*. European Standard EN 1052-3. CEN/TC, Brussels, Belgium.
- [8]. Bommer, J.J., Dost, B., Edwards, B., Kruiver, P.P., Meijers, P., Ntinalexis, M., Rodriguez-Marek, A., Ruigrok, E., Spetzler, J., Stafford, P.J. (2017). *V4 Ground-Motion Model (GMM) for Response Spectral Accelerations, Peak Ground Velocity, and Significant Durations in the Groningen Field*. Report submitted to NAM.

APPENDIX

A1. RESULTS FILE FORMAT

Results obtained for each run are collected in dedicated .txt files (one per test), labelled with the test name as reported in section 4.2. The following tables provide information of the quantities reported in every column of the published data.

The experimental time histories of each instrument are provided in the following scheme:

- Accelerometers;
- Wire potentiometers;
- Linear potentiometers;
- Derived data.

Referring to chapter 3, column numbers with * indicate instruments removed after test #21. These columns are zero-padded after removal of the sensors.

Columns from 155 to 168 contain the derived trajectories (X and Y displacement histories) of the diaphragm corners, where two orthogonal potentiometers were provided. X and Y displacements were calculated instant by instant from the intersection of the two circles centred at the single potentiometer origin (on the rigid frame) with radii taken in the displaced configuration.

Table 26 Results file format: accelerometers

ACCELEROMETERS				
Column #	Location	Measured parameter	Mass (X dir.) [kg]	Mass after test #21 (X dir.) [kg]
1	-	time	-	-
2	Foundation beam (West side)	Acceleration X	2929	2929
3	Foundation beam (East side)	Acceleration X	3572	3572
4	R.C. diaphragm (centre)	Acceleration Z	0	0
5	R.C. diaphragm (North-East corner)	Acceleration X	3363.5	3363.5
6	R.C. diaphragm (North-East corner)	Acceleration Y	0	0
7	R.C. diaphragm (North-East corner)	Acceleration Z	0	0
8	R.C. diaphragm (South-East corner)	Acceleration X	3242	3242
9	R.C. diaphragm (South-East corner)	Acceleration Y	0	0
10	R.C. diaphragm (South-East corner)	Acceleration Z	0	0
11	R.C. diaphragm (South-West corner)	Acceleration X	3760	3760
12	R.C. diaphragm (South-West corner)	Acceleration Y	0	0
13	R.C. diaphragm (South-West corner)	Acceleration Z	0	0
14	Timber diaphragm (North-West corner)	Acceleration X	651	651
15	Timber diaphragm (North-West corner)	Acceleration Y	0	0
16	Timber diaphragm (North-West corner)	Acceleration Z	0	0
17	Timber diaphragm (North-East corner)	Acceleration X	958	958
18	Timber diaphragm (North-East corner)	Acceleration Y	0	0
19	Timber diaphragm (North-East corner)	Acceleration Z	0	0
20	Timber diaphragm (South-East corner)	Acceleration X	888	888
21	Timber diaphragm (South-East corner)	Acceleration Y	0	0
22	Timber diaphragm (South-East corner)	Acceleration Z	0	0

23	Timber diaphragm (South-West corner)	Acceleration X	1071	1337
24	Timber diaphragm (South-West corner)	Acceleration Y	0	0
25	Timber diaphragm (South-West corner)	Acceleration Z	0	0
26	Timber diaphragm (centre)	Acceleration X	455	455
27	Timber diaphragm (centre)	Acceleration Z	0	0
28	North outer leaf (top of gable)	Acceleration X	136	392
29	Ridge beam (South end)	Acceleration X	692	692
30	Ridge beam (South end)	Acceleration Y	0	0
31	Ridge beam (South end)	Acceleration Z	0	0
32	Ridge beam (midspan)	Acceleration Z	0	0
33	North inner leaf (centre of gable)	Acceleration X	571	571
34	North inner leaf (second storey mid-height)	Acceleration X	1131	1131
35	North inner leaf (first storey mid-height)	Acceleration X	709	709
36	South inner leaf (centre of gable)	Acceleration X	1106	1106
37	South inner leaf (second-floor level)	Acceleration X	668	668
38	South inner leaf (second storey mid-height)	Acceleration X	162	1628
39	South inner leaf (first storey mid-height)	Acceleration X	1274	1274
40	West inner leaf (top of second-storey squat pier)	Acceleration X	535	535
41	East inner leaf (top of first-storey squat pier)	Acceleration X	560	560
42*	North outer leaf (centre of gable)	Acceleration X	390	0
43	North outer leaf (second-floor level)	Acceleration X	615	1015
44	North-East outer leaf corner (second-floor level, North side)	Acceleration X	501	1442
45	North-West outer leaf corner (second-floor level)	Acceleration X	501	576
46*	North outer leaf (second storey mid-height)	Acceleration X	744	0
47	North outer leaf (first-floor level)	Acceleration X	664	4292
48*	North-East outer leaf corner (first-floor level, North side)	Acceleration X	1079	0
49*	North-West outer leaf corner (first-floor level)	Acceleration X	1338	0
50*	North outer leaf (first storey mid-height)	Acceleration X	1135	0
51*	South-West outer leaf corner (second-floor level)	Acceleration X	187	0
52	South-West outer leaf corner (first-floor level)	Acceleration X	728	728
53	West outer leaf (top of second-storey squat pier)	Acceleration X	611	611
54	West outer leaf (bott. of second-storey squat pier)	Acceleration X	780	1163
55	South-East outer leaf corner (second-floor level)	Acceleration X	160	160
56	South-East outer leaf corner (first-floor level)	Acceleration X	1042	1042
57	North inner leaf (first-floor level)	Acceleration X	1148	1148
58	Shaking table	Acceleration X	0	0
59	R.C. diaphragm (North-West corner)	Acceleration X	3245	3245
60	R.C. diaphragm (North-West corner)	Acceleration Y	0	0
61	R.C. diaphragm (North-West corner)	Acceleration Z	0	0
62	Rigid frame (second-floor level)	Acceleration X	0	0
63	Ridge beam (North end)	Acceleration X	692	692
64	Ridge beam (North end)	Acceleration Y	0	0
65	Ridge beam (North end)	Acceleration Z	0	0
66	North inner leaf (second-floor level)	Acceleration X	957	957
67*	North-East outer leaf corner (second-floor level, East side)	Acceleration X	159	0
68*	North-East outer leaf corner (first-floor level, East side)	Acceleration X	879	0

Table 27 Results file format: wire potentiometers.

WIRE POTENTIOMETERS		
Column #	Location	Measured parameter
73*	Ridge beam - North outer leaf (top of gable)	Displacement X
74	Ridge beam - Rigid frame	Displacement X
75	North inner leaf (centre of gable) - Rigid frame	Displacement X
76*	North outer leaf (centre of gable) - Rigid frame	Displacement X
77	South outer leaf (centre of gable) - Rigid frame	Displacement X
78*	North outer leaf (second-floor level) - Rigid frame	Displacement X
79	North inner leaf (second-floor level) - Rigid frame	Displacement X
80	North inner leaf (second storey mid-height) - Rigid frame	Displacement X
81*	North outer leaf (second storey mid-height) - Rigid frame	Displacement X
82	South inner leaf (second storey mid-height) - Rigid frame	Displacement X
83	North inner leaf (first-floor level) - Rigid frame	Displacement X
84*	North outer leaf (first-floor level) - Rigid frame	Displacement X
85	North inner leaf (first storey mid-height) - Rigid frame	Displacement X
86*	North outer leaf (first storey mid-height) - Rigid frame	Displacement X
87	South inner leaf (first storey mid-height) - Rigid frame	Displacement X
88	East inner leaf (first-storey squat pier)	Displacement Z
89	East inner leaf (first-storey squat pier)	Displacement Z
90	East inner leaf (first-storey squat pier)	Displacement along the diagonal
91	East inner leaf (first-storey squat pier)	Displacement along the diagonal

Table 28 Results file format: linear potentiometers.

LINEAR POTENTIOMETERS		
Column #	Location	Measured parameter
92	Ridge beam - North inner leaf (top of gable)	Displacement X
93	Ridge beam - South inner leaf (top of gable)	Displacement X
94	Timber diaphragm (North-West corner) - Rigid frame	Displacement X
95	Timber diaphragm (North-West corner) - Rigid frame	Displacement Y
96	Timber diaphragm (North-East corner) - Rigid frame	Displacement X
97	Timber diaphragm (North-East corner) - Rigid frame	Displacement Y
98	Timber diaphragm (South-East corner) - Rigid frame	Displacement X
99	Timber diaphragm (South-East corner) - Rigid frame	Displacement Y
100	Timber diaphragm (South-West corner) - Rigid frame	Displacement X
101	Timber diaphragm (South-West corner) - Rigid frame	Displacement Y
102	Timber diaphragm (South midspan) - Rigid frame	Displacement X
103	Timber diaphragm (South midspan) - South inner leaf	Displacement X
105	East outer leaf - East outer spreader beam	Displacement X
106	West inner leaf - West inner spreader beam	Displacement X

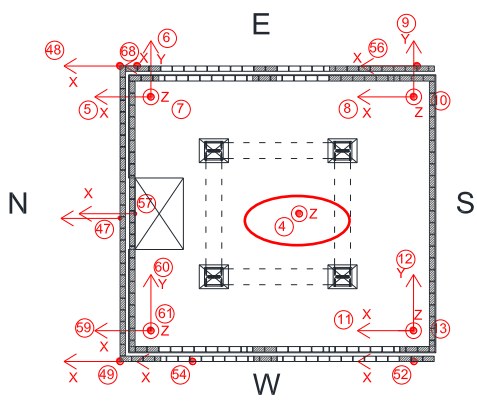

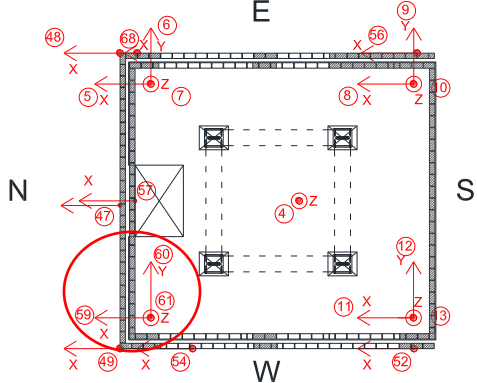
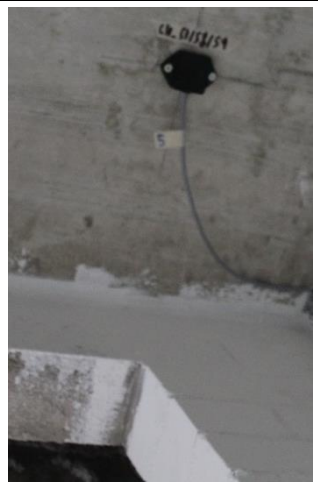
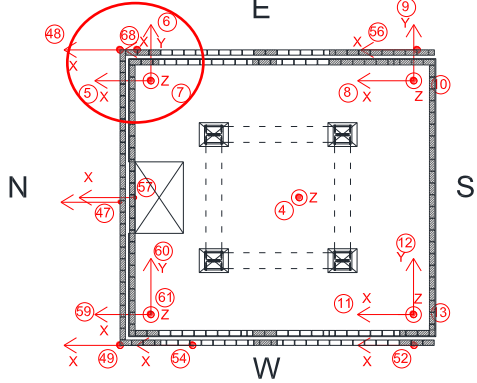

107	West outer leaf - West outer spreader beam	Displacement X
108*	North inner leaf - West inner spreader beam (North-West corner)	Displacement X
109	South inner leaf - West inner spreader beam (South-West corner)	Displacement X
110	South inner leaf - East inner spreader beam (South-East corner)	Displacement X
111	East inner leaf - East inner spreader beam	Displacement X
112*	North inner leaf - East inner spreader beam (North-East corner)	Displacement X
113	R.C. diaphragm (North-West corner) - Rigid frame	Displacement X
114	R.C. diaphragm (North-West corner) - Rigid frame	Displacement Y
115	R.C. diaphragm (North-East corner) - Rigid frame	Displacement X
116	R.C. diaphragm (South-East corner) - Rigid frame	Displacement X
117	R.C. diaphragm (South-East corner) - Rigid frame	Displacement Y
118	R.C. diaphragm (South-West corner) - Rigid frame	Displacement X
119	R.C. diaphragm (South midspan) - South inner leaf	Displacement X
120	R.C. diaphragm (North-West corner) - Inner leaf below	Displacement Z
121	R.C. diaphragm (North-East corner) - Inner leaf below	Displacement Z
122	R.C. Diaphragm - East inner leaf (first-storey squat pier top corner)	Displacement Z
123	R.C. diaphragm (South-East corner) - Inner leaf below	Displacement Z
124	East inner leaf (top of first-storey squat pier)	Displacement X
125	R.C. diaphragm (South-West corner) - Inner leaf below	Displacement Z
126	East inner leaf (first-storey squat pier mid-height)	Displacement X
127	West outer leaf - Foundation beam	Displacement X
128	West inner leaf - Foundation beam	Displacement X
129	East outer leaf - Foundation beam	Displacement X
130	West inner leaf - Foundation beam	Displacement X
131	East inner leaf (first-storey squat pier bott. corner) - Foundation beam	Displacement X
132	East inner leaf (first-storey squat pier bott. corner) - Foundation beam	Displacement X
133	Foundation beam - Shaking table (South-West corner)	Displacement X
134	Foundation beam - Shaking table (South-East corner)	Displacement X
135	Shaking table - Laboratory strong floor	Displacement X
137	R.C. diaphragm - East inner leaf first-storey squat pier (top)	Displacement X

Table 29 Results file format: derived data.

PROCESSED DATA		
Column #	Computed parameter	Description
138	Ground X Acceleration	Average of col. 2, 3
139	First Floor X Acceleration	Average of col. 5, 8, 11, 59
140	Second Floor X Acceleration (Mean East-West-Centre)	Average of col. 145, 146, 26
141	Roof X Acceleration	Average of col. 29, 63
142	First Floor Y Acceleration	Average of col. 6, 9, 12, 60
143	Second Floor Y Acceleration (Mean North-South)	Average of col. 15, 18, 21, 24
144	Roof Y Acceleration	Average of col. 30, 64
145	Second Floor X Acceleration (Mean East)	Average of col. 17, 20
146	Second Floor X Acceleration (Mean West)	Average of col. 14, 23
147	Average X Disp. 1st Floor (RC)	Average of col. 155, 115, 157, 118
148	Average X Disp. 2nd Floor (Timber)	Average of col. 152, 153
149	X Disp. Roof	Col. 74
150	Average X Disp. 1st Floor East (RC)	Average of col. 155, 118
151	Average X Disp. 1st Floor East (RC)	Average of col. 115, 157
152	Average X Disp. 2nd Floor West Timber	Average of col. 159, 165
153	Average X Disp. 2nd Floor East Timber	Average of col. 161, 163
154	Base Shear [kN]	sum (acceleration x mass)
155	RC diaphragm N-W – X dir.	Circle intersection, col. 113 & 114
156	RC diaphragm N-W – Y dir.	Circle intersection, col. 113 & 114
157	RC diaphragm S-E – X dir.	Circle intersection, col. 116 & 117
158	RC diaphragm S-E – Y dir.	Circle intersection, col. 116 & 117
159	Timber diaphragm N-W – X dir.	Circle intersection, col. 94 & 95
160	Timber diaphragm N-W – Y dir.	Circle intersection, col. 94 & 95
161	Timber diaphragm N-E – X dir.	Circle intersection, col. 96 & 97
162	Timber diaphragm N-E – Y dir.	Circle intersection, col. 96 & 97
163	Timber diaphragm S-E – X dir.	Circle intersection, col. 98 & 99
164	Timber diaphragm S-E – Y dir.	Circle intersection, col. 98 & 99
165	Timber diaphragm S-W – X dir.	Circle intersection, col. 100 & 101
166	Timber diaphragm S-W – Y dir.	Circle intersection, col. 100 & 101

A2. ORGANIZATION OF THE INSTRUMENTATION: ACCELEROMETERS

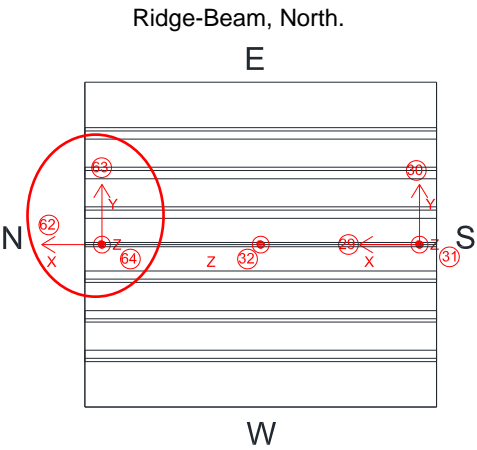

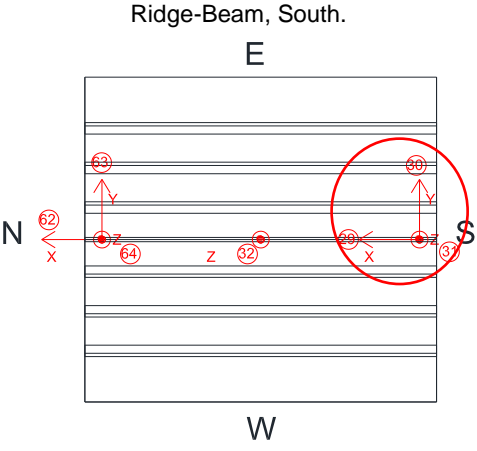

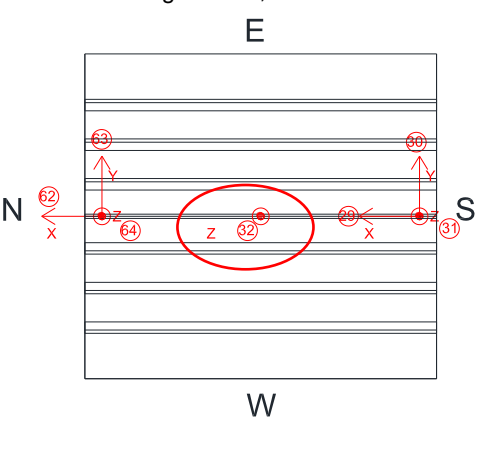

Column #	Type of Instrument	Orientation	Mass [kg]	Mass after test #21 [kg]	Polarity	Location	Photo
2	Uniaxial	Dir. X	1517.03	2652	+ 1	<p>Foundation, west side.</p>	
3	Uniaxial	Dir. X	2197.09	4266	+ 1	<p>Foundation, east side.</p>	
58	Uniaxial	Dir. X	-	-	+ 1	<p>Shake Table.</p>	

4	Uniaxial	Dir. Z	-	-	+1	<p>Centered on Reinforced Concrete Diaphragm.</p> 	
59	Triaxial	Dir. X	3296.27	3296.27	+1	<p>Reinforced Concrete Diaphragm, North-West corner.</p> 	
60	Triaxial	Dir. Y	-	-	+1		
61	Triaxial	Dir. Z	-	-	+1		
5	Triaxial	Dir. X	3200	3200	+1	<p>Reinforced Concrete Diaphragm, North-East corner.</p> 	
6	Triaxial	Dir. Y	-	-	+1		
7	Triaxial	Dir. Z	-	-	+1		

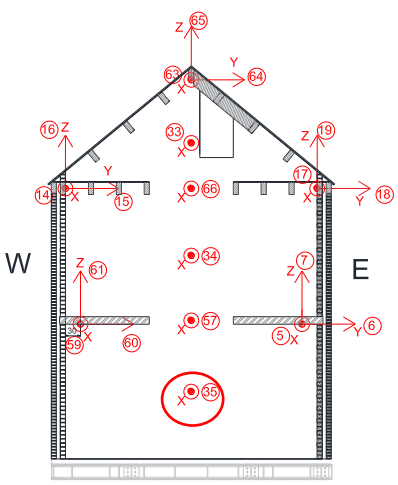

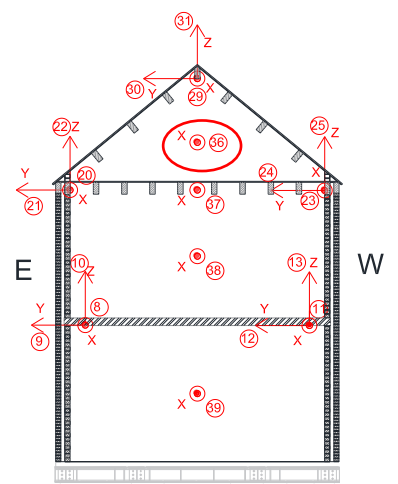

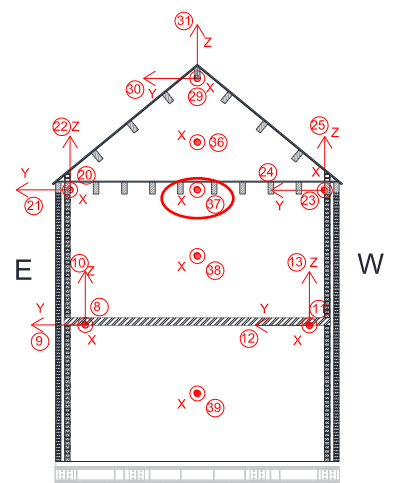

8	Triaxial	Dir. X	3367	3367	+1	<p>Timber Diaphragm, North-East corner.</p>	
9	Triaxial	Dir. Y	-	-	+1		
10	Triaxial	Dir. Z	-	-	+1		
11	Triaxial	Dir. X	3515	3515	+1	<p>Timber Diaphragm, South-East corner.</p>	
12	Triaxial	Dir. Y	-	-	+1		
13	Triaxial	Dir. Z	-	-	+1		
14	Triaxial	Dir. X	650	650	+1	<p>Timber Diaphragm, South-West corner.</p>	
15	Triaxial	Dir. Y	-	-	+1		
16	Triaxial	Dir. Z	-	-	+1		

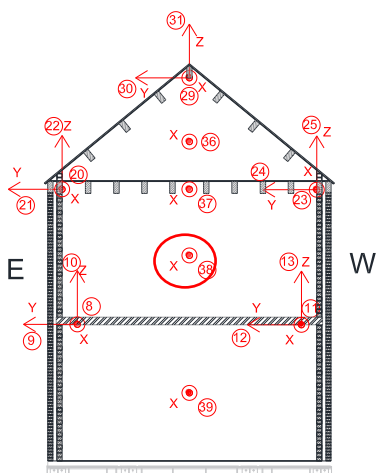

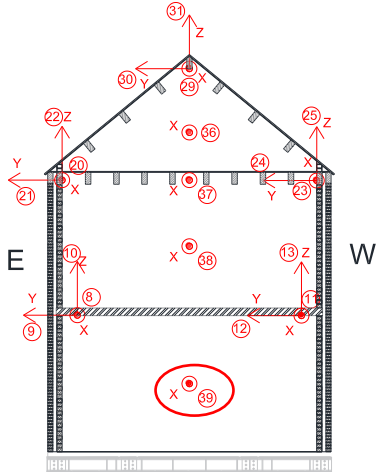

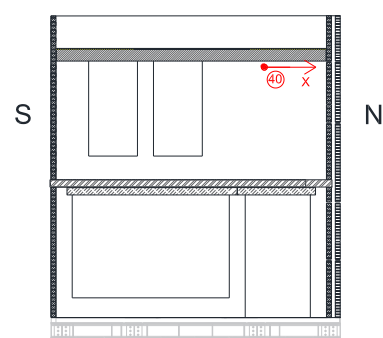

17	Triaxial	Dir. X	650	650	+1	<p>Timber Diaphragm, North-East corner.</p>	
18	Triaxial	Dir. Y	-	-	+1		
19	Triaxial	Dir. Z	-	-	+1		
20	Triaxial	Dir. X	650	650	+1	<p>Timber Diaphragm, South-East corner.</p>	
21	Triaxial	Dir. Y	-	-	+1		
22	Triaxial	Dir. Z	-	-	+1		
23	Triaxial	Dir. X	650	650	+1	<p>Timber Diaphragm, South-West corner.</p>	
24	Triaxial	Dir. Y	-	-	+1		
25	Triaxial	Dir. Z	-	-	+1		

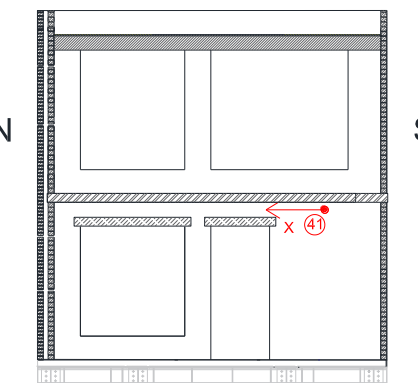
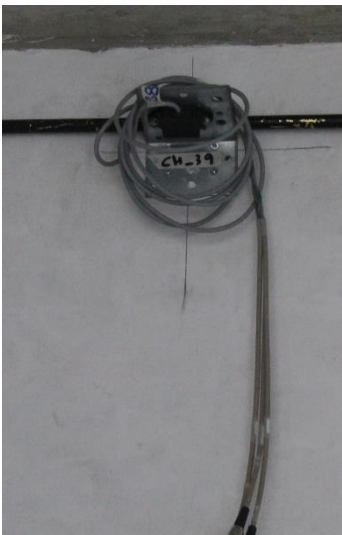
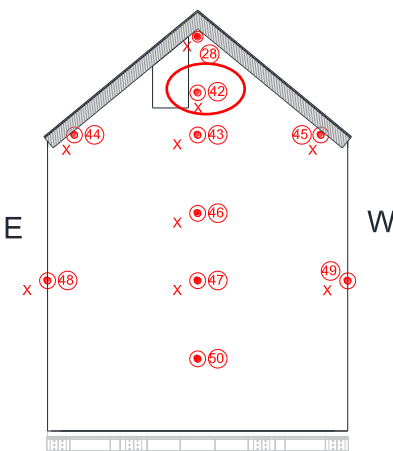
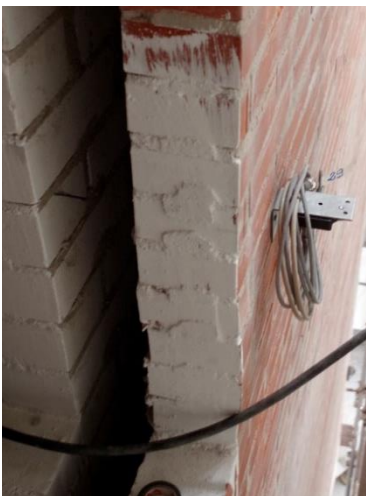
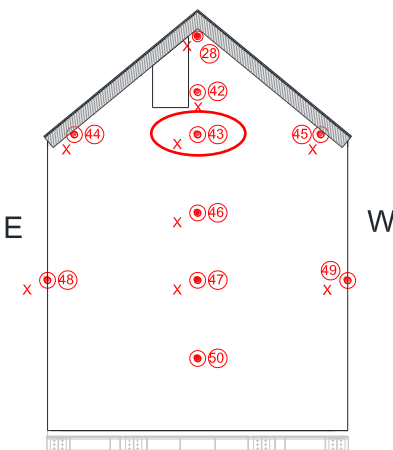

26	Biaxial	Dir. X	479	479	+1	<p>Timber Diaphragm, center.</p>	
27	Biaxial	Dir. Z	-	-	+1		
28	Uniaxial	Dir. X	156	376	+1	<p>Top of the North Gable, Clay.</p>	
62	Uniaxial	Dir. X	-	-	+1	<p>Steel Frame.</p>	

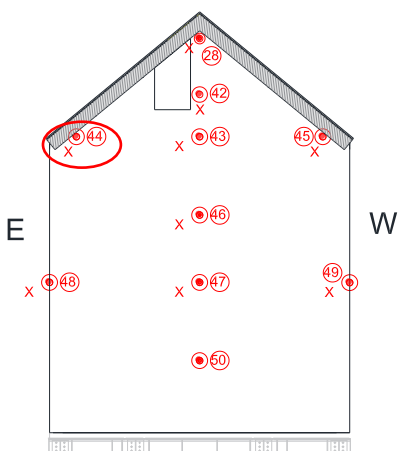
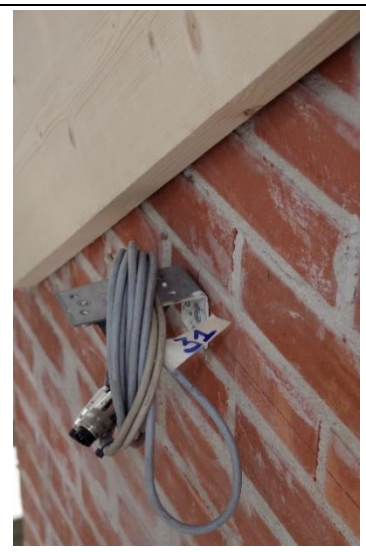
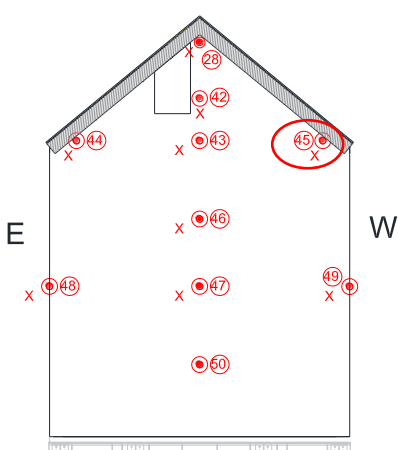

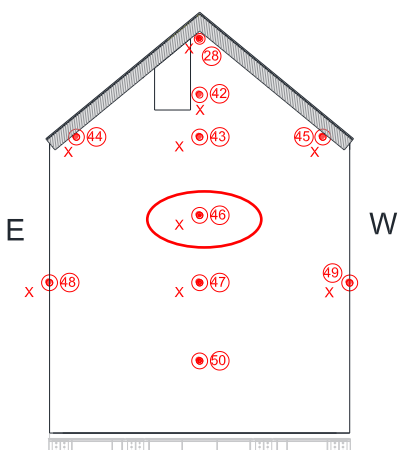
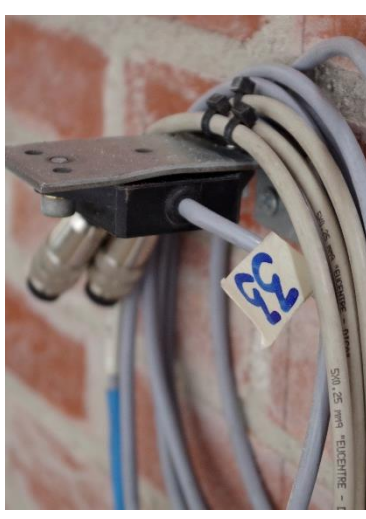
63	Triaxial	Dir. X	692	692	+1	<p>Ridge-Beam, North.</p> 	
64	Triaxial	Dir. Y	-	-	+1		
65	Triaxial	Dir. Z	-	-	+1		
29	Triaxial	Dir. X	692	692	+1	<p>Ridge-Beam, South.</p> 	
30	Triaxial	Dir. Y	-	-	+1		
31	Triaxial	Dir. Z	-	-	+1		
32	Uniaxial	Dir. Z	-	-	+1	<p>Ridge-Beam, Center.</p> 	

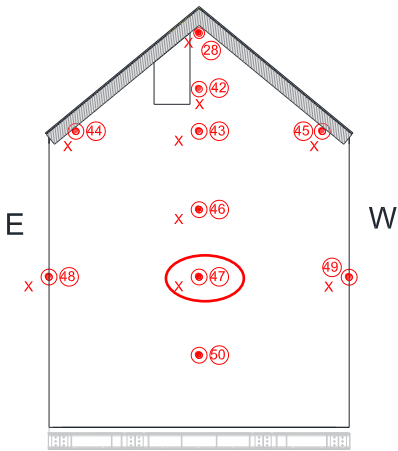

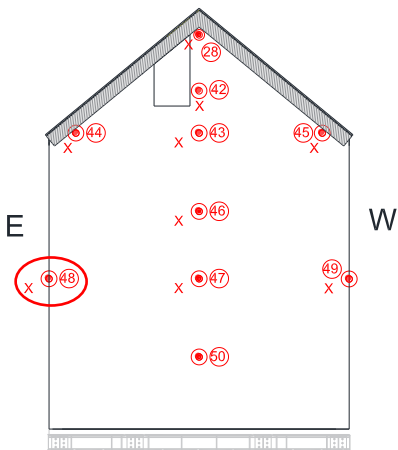

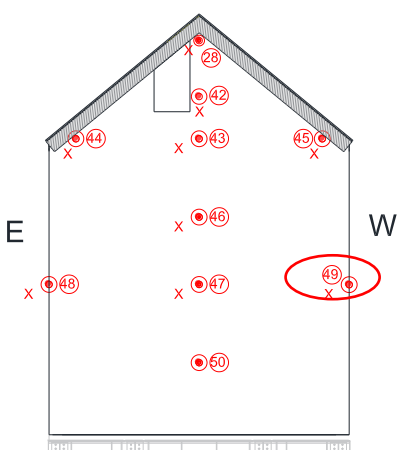

33	Uniaxial	Dir. X	663	663	+1	<p>Center of the North Gable, Calcium Silicate.</p>	
66	Uniaxial	Dir. X	1030	1030	+1	<p>North Facade, Timber Diaphragm Height, Calcium Silicate.</p>	
34	Uniaxial	Dir. X	1247	1247	+1	<p>North Facade, Half Height of the 2nd Floor, Calcium Silicate.</p>	

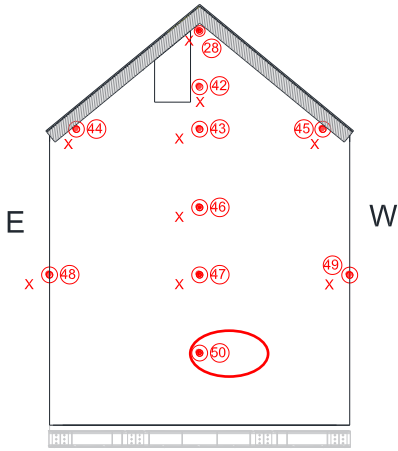

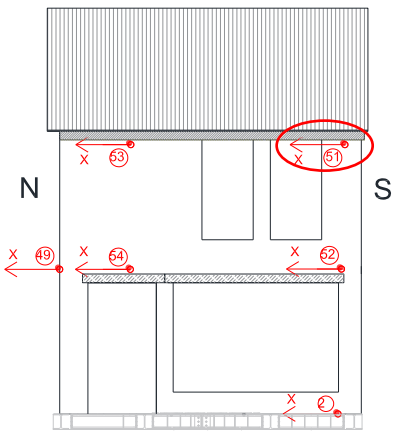

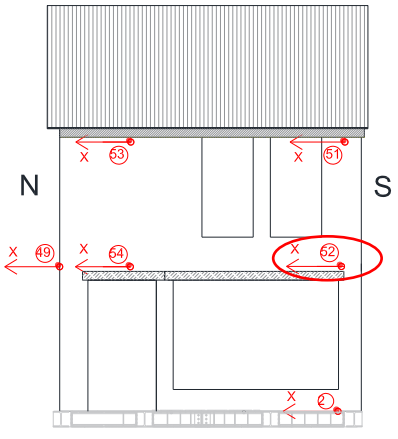

35	Uniaxial	Dir. X	1924	1924	+1	<p>North Facade, Half Height of the 1st Floor, Calcium Silicate.</p> 	
36	Uniaxial	Dir. X	1126	1126	+1	<p>Center of the South Gable, Calcium Silicate.</p> 	
37	Uniaxial	Dir. X	930	930	+1	<p>South Facade, Timber Diaphragm Height, Calcium Silicate.</p> 	

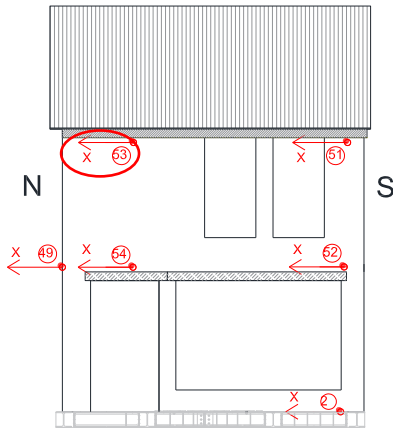

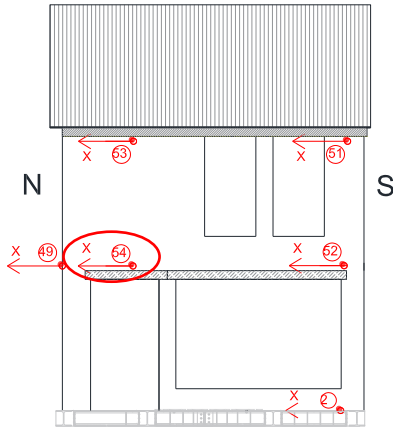

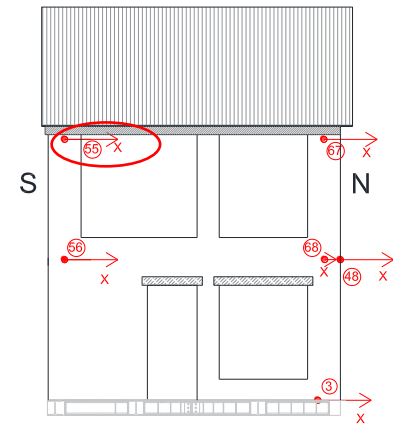

38	Uniaxial	Dir. X	1740	1740	+1	<p>South Facade, Half Height of the 2nd Floor, Calcium Silicate.</p> 	
39	Uniaxial	Dir. X	2491	2491	+1	<p>South Facade, Half Height of the 1st Floor, Calcium Silicate.</p> 	
40	Uniaxial	Dir. X	572	572	+1	<p>West Facade, 2nd Floor Height, Calcium Silicate.</p> 	

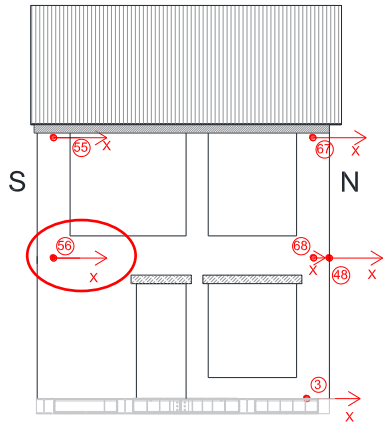

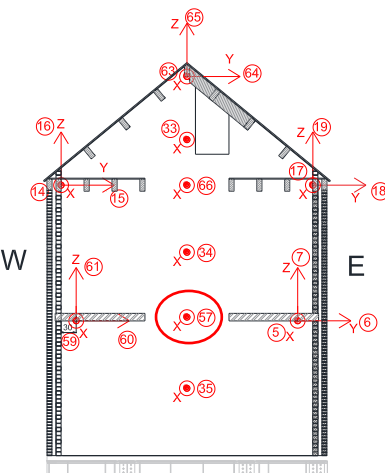

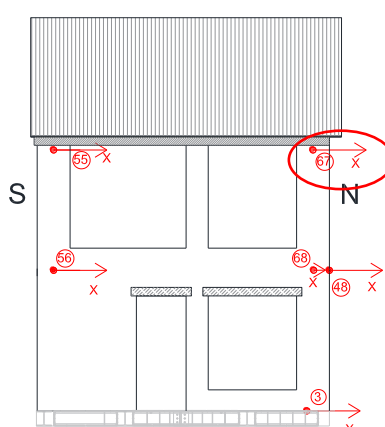

41	Uniaxial	Dir. X	560	560	+1	<p>East Facade, 1st Floor Height, Calcium Silicate</p> 	
42	Uniaxial	Dir. X	410	-	+1	<p>Center of the North Gable, Clay.</p> 	
43	Uniaxial	Dir. X	635	819	+1	<p>North Facade, centered at the 2nd Floor Height, Clay.</p> 	

44	Uniaxial	Dir. X	599	2150	+1	<p>North Facade, 2nd Floor Height, North-East, Clay.</p> 	
45	Uniaxial	Dir. X	599	1054	+1	<p>North Facade, 2nd Floor Height, North-West, Clay.</p> 	
46	Uniaxial	Dir. X	764	-	+1	<p>North Facade, centered at the Half Height of the 2nd Floor Height, Clay.</p> 	

47	Uniaxial	Dir. X	762	958	+1	<p>North Facade, centered at the 1st Floor Height, Clay.</p> 	
48	Uniaxial	Dir. X	1098	-	+1	<p>North Facade, 1st Floor Height, North-East, Clay.</p> 	
49	Uniaxial	Dir. X	1357	-	+1	<p>North Facade, 1st Floor Height, North-West, Clay.</p> 	

50	Uniaxial	Dir. X	1154	-	+1	<p>North Facade, centered at the Half Height of the 1st Floor Height, Clay.</p> 	
51	Uniaxial	Dir. X	187	187	+1	<p>West Facade, 2nd Floor Height, South-West, Clay.</p> 	
52	Uniaxial	Dir. X	862	862	+1	<p>West Facade, 1st Floor Height, South-West, Clay.</p> 	

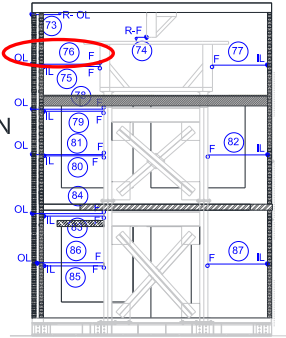

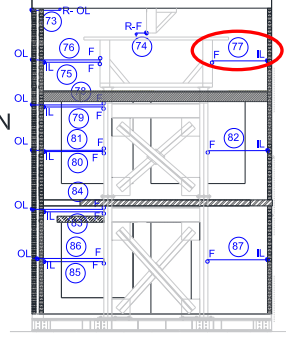

53	Uniaxial	Dir. X	670	670	+1	<p>North Facade, centered at the Half Height of the 1st Floor Height, Clay.</p> 	
54	Uniaxial	Dir. X	780	780	+1	<p>West Facade, 2nd Floor Height, South-West, Clay.</p> 	
55	Uniaxial	Dir. X	160	160	+1	<p>West Facade, 1st Floor Height, South-West, Clay.</p> 	

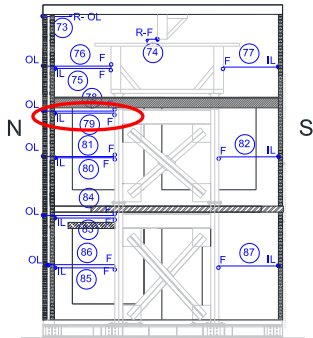

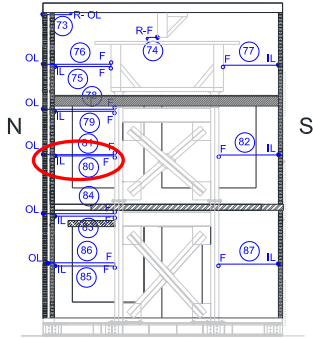

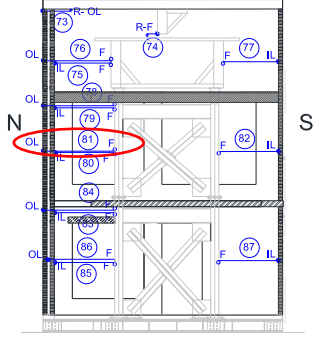

56	Uniaxial	Dir. X	1042	1210	+1	<p>East Facade, 1st Floor Height, South-East, Clay.</p> 	
57	Uniaxial	Dir. X	1167	1167	+1	<p>North Facade, Reinforced Concrete Diaphragm Height, Calcium Silicate.</p> 	
67	Uniaxial	Dir. X	159	-	+1	<p>East Facade, 2nd Floor Height, North-East, Clay.</p> 	

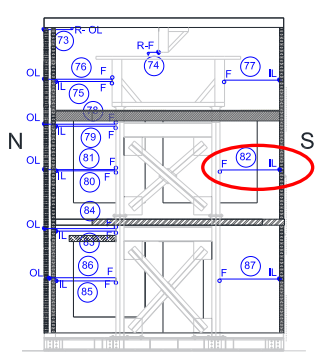

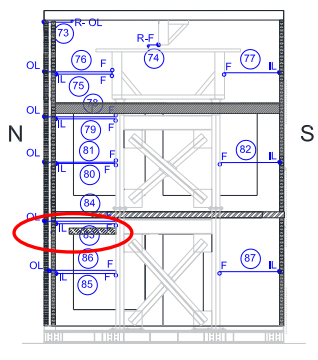

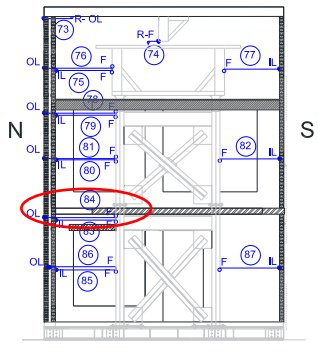

68	Uniaxial	Dir. X	1035	-	+1	<div>East Facade, 1st Floor Height, North-East, Clay.</div> <div></div>	<div></div>
----	----------	--------	------	---	----	--	-------------

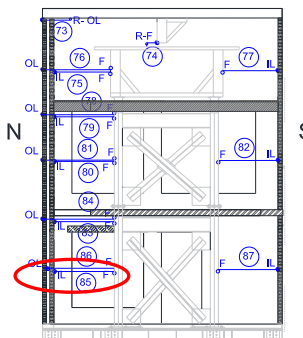

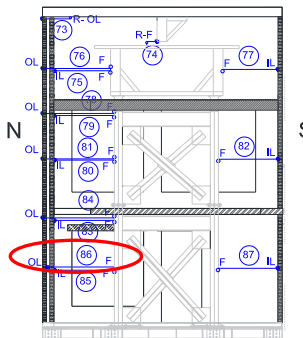

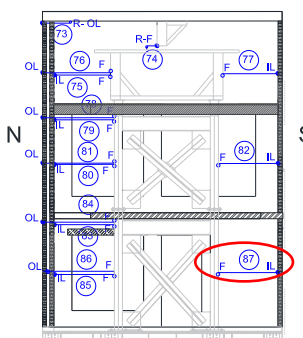
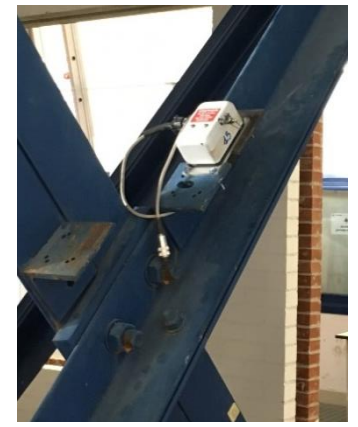
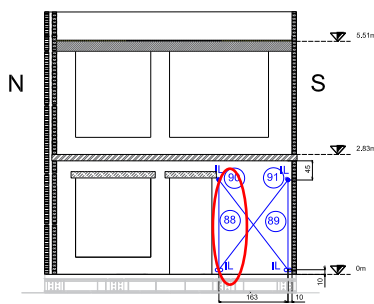
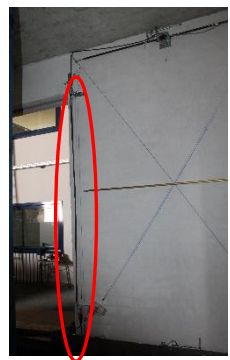
A3. ORGANIZATION OF THE INSTRUMENTATION: POTENTIOMETERS

Column #	Type of instr. & range	Orientation	Polarity	Location	Photo
73	Wire Pot. 250 mm	R - OL Direction X	+1	Ridge Beam/Outer Leaf. 	
74	Wire Pot. 250 mm	R - F Direction X	-1	Ridge Beam/Rigid Frame. 	
75	Wire Pot. 250 mm	F - IL Direction X	+1	Steel Frame/Inner Leaf. 	

76	Wire Pot. 250 mm	F - OL Direction X	+1	<p>Steel Frame/Outer Leaf.</p> 	
77	Wire Pot. 250 mm	F - IL Direction X	-1	<p>Steel Frame/Inner Leaf.</p> 	
78	Wire Pot. 250 mm	F - OL Direction X	+1	<p>Steel Frame/Outer Leaf.</p>	

79	Wire Pot. 250 mm	F - IL Direction X	+1	<p>Steel Frame/Inner Leaf.</p> 	
80	Wire Pot. 250 mm	F - IL Direction X	+1	<p>Steel Frame/Inner Leaf.</p> 	
81	Wire Pot. 250 mm	F - OL Direction X	+1	<p>Steel Frame/Outer Leaf.</p> 	

82	Wire Pot. 250 mm	F - IL Direction X	-1	<p>Steel Frame/Inner Leaf.</p> 	
83	Wire Pot. 125 mm	F - IL Direction X	+1	<p>Steel Frame/Inner Leaf.</p> 	
84	Wire Pot. 250 mm	F - OL Direction X	+1	<p>Steel Frame/Outer Leaf.</p> 	

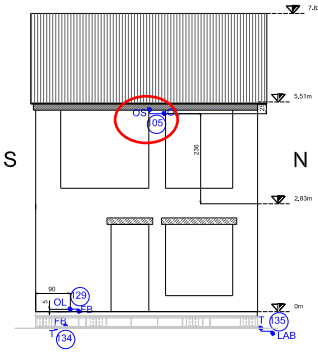

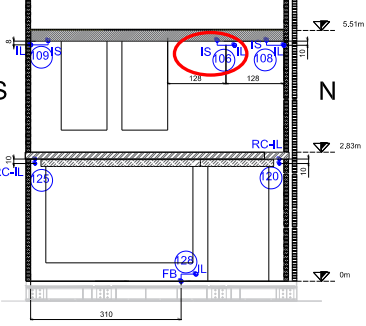

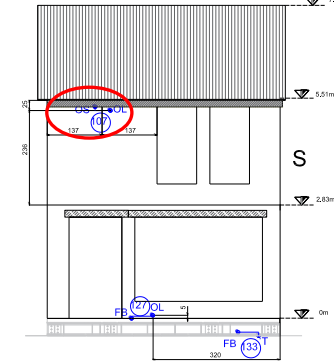

85	Wire Pot. 125 mm	F - IL Direction X	+1	<p>Steel Frame/Inner Leaf.</p> 	
86	Wire Pot. 250 mm	F - OL Direction X	+1	<p>Steel Frame/Outer Leaf.</p> 	
87	Wire Pot. 125 mm	F - IL Direction X	-1	<p>Steel Frame/Inner Leaf.</p> 	
88	Wire Pot. 125 mm	IL-IL Direction Z	+1	<p>East Wall.</p> 	

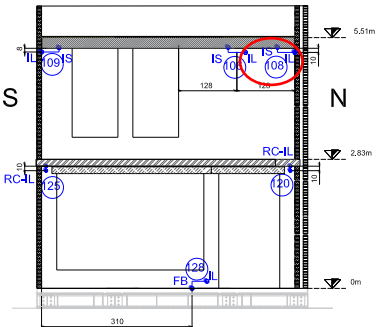

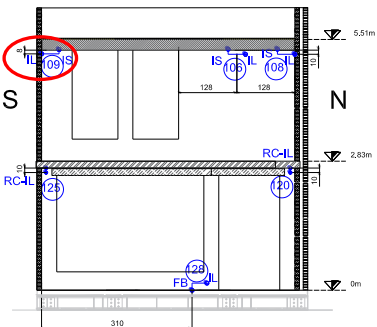

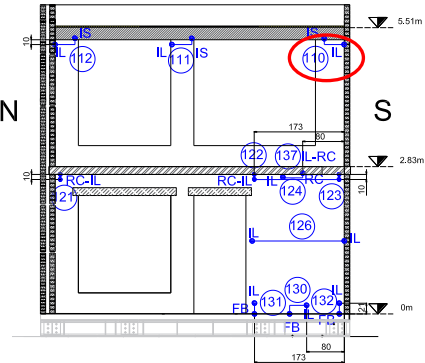

89	Wire Pot. 125 mm	IL-IL Direction Z	+1	<p>East Wall.</p>	
90	Wire Pot. 125 mm	IL-IL Direction Oblique	+1	<p>East Wall.</p>	
91	Wire Pot. 125 mm	IL-IL Direction Oblique	+1	<p>East Wall.</p>	

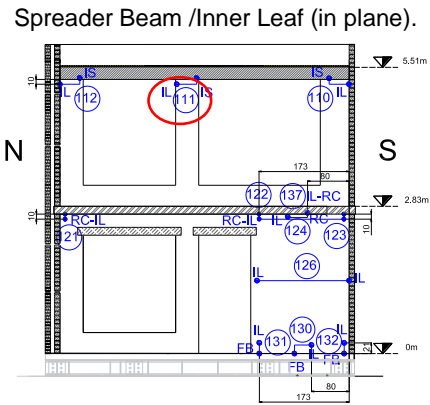

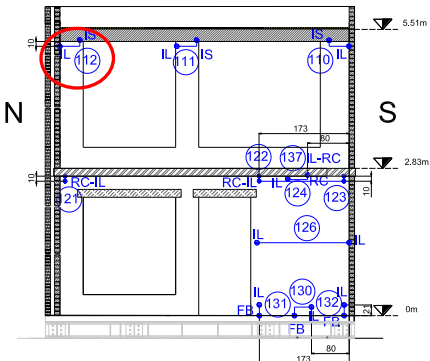
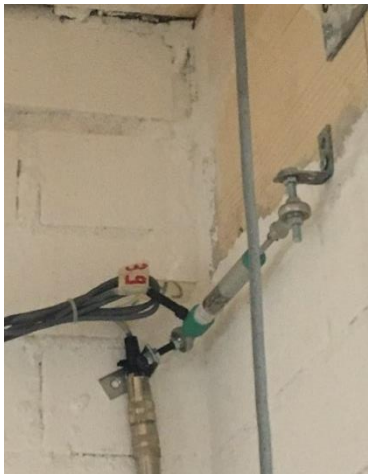
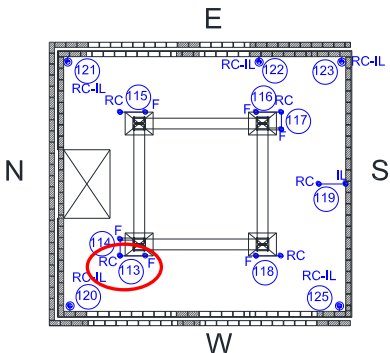

92	Pot. 250 mm	R - IL Direction X	+1	<p>Ridge Beam/Inner Leaf.</p>	
93	Pot. 250 mm	R - IL Direction X	+1	<p>Ridge Beam/Inner Leaf.</p>	
94	Pot. 250 mm	F - TD Direction X	+1	<p>Rigid Frame/Timber Diaphragm.</p>	

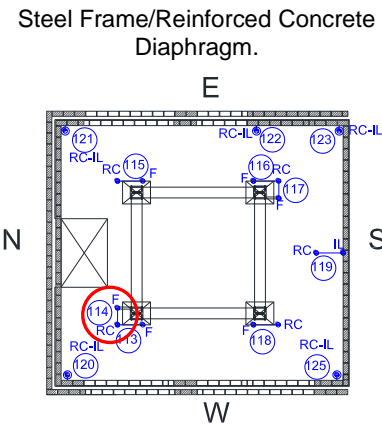

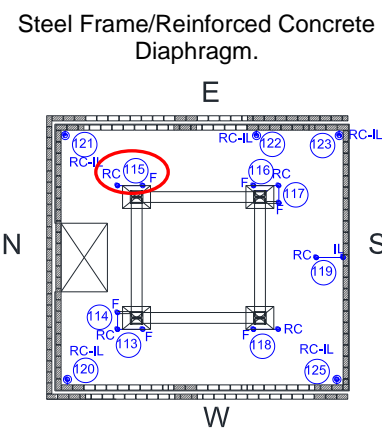

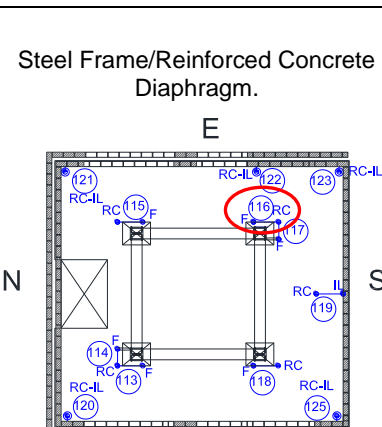
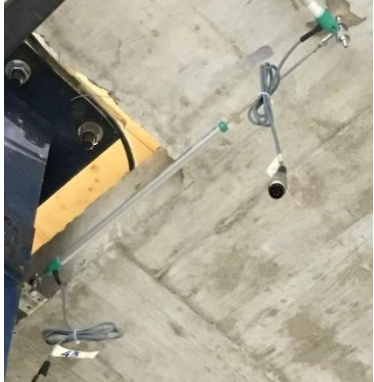
95	Pot. 100 mm	F - TD Direction Y	-1	<p>Rigid Frame/Timber Diaphragm.</p>	
96	Pot. 250 mm	F - TD Direction X	+1	<p>Rigid Frame/Timber Diaphragm.</p>	
97	Pot. 100 mm	F - TD Direction Y	+1	<p>Rigid Frame/Timber Diaphragm.</p>	

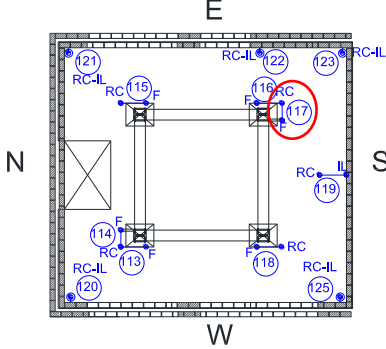

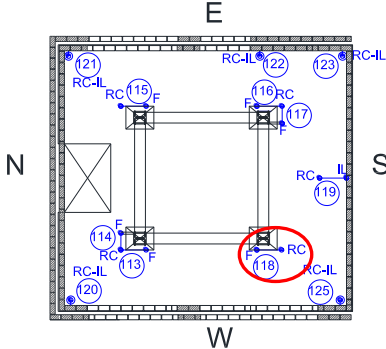
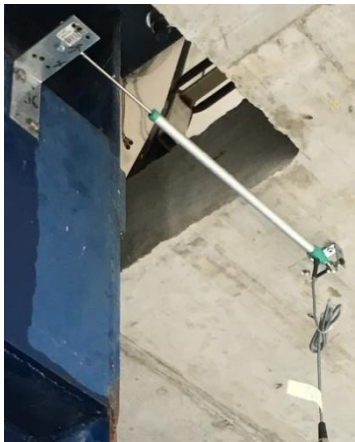
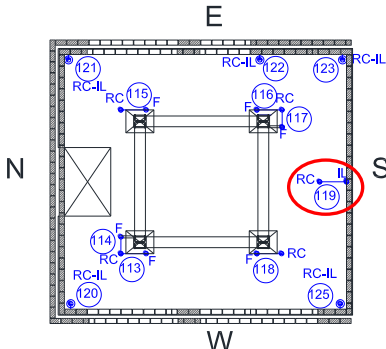

98	Pot. 250 mm	F - TD Direction X	-1	<p>Rigid Frame/Timber Diaphragm.</p>	
99	Pot. 100 mm	F - TD Direction Y	+1	<p>Rigid Frame/Timber Diaphragm.</p>	
100	Pot. 250 mm	F - TD Direction X	-1	<p>Rigid Frame/Timber Diaphragm.</p>	

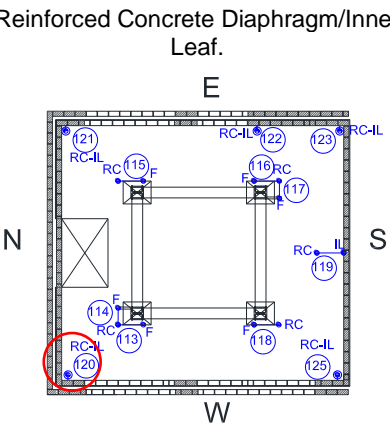

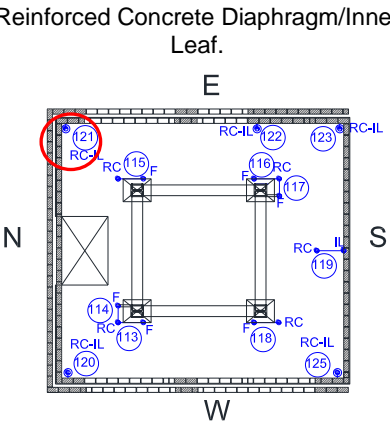

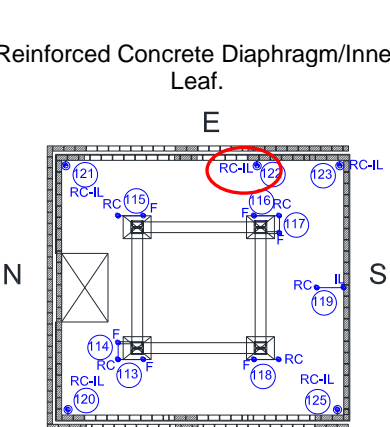

105	Pot. 100 mm	S - OL Direction X	+1	<p>Spreader Beam/Outer Leaf (in plane).</p> 	
106	Pot. 50 mm	S - IL Direction X	+1	<p>Spreader Beam/Inner Leaf (in plane).</p> 	
107	Pot. 100 mm	S - OL Direction X	+1	<p>Spreader Beam /Outer Leaf (in plane).</p> 	

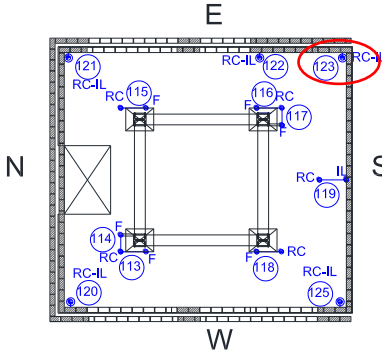

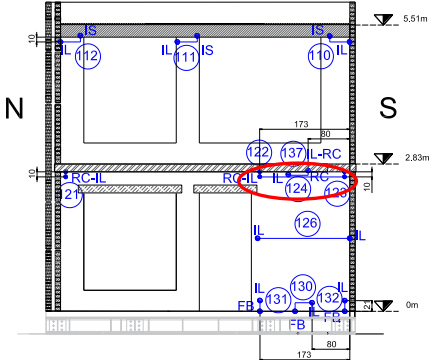
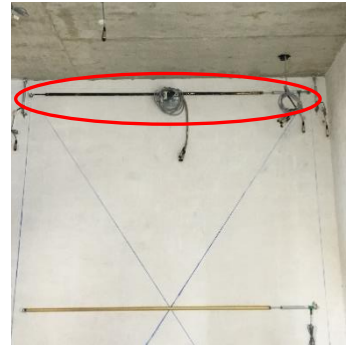
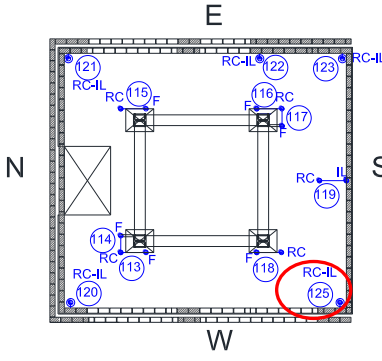

108	Pot. 50 mm	S - IL Direction X	+1	<p>Spreader Beam /Inner Leaf (out of plane).</p> 	
109	Pot. 50 mm	S - IL Direction X	+1	<p>Spreader Beam /Inner Leaf (out of plane).</p> 	
110	Pot. 50 mm	S - IL Direction X	+1	<p>Spreader Beam /Outer Leaf (out of plane).</p> 	

111	Pot. 50 mm	S - IL Direction X	+1	<p>Spreader Beam /Inner Leaf (in plane).</p> 	
112	Pot. 50 mm	S - IL Direction X	+1	<p>Spreader Beam /Inner Leaf (out of plane).</p> 	
113	Pot. 250 mm	F - RC Direction X	+1	<p>Steel Frame/Reinforced Concrete Diaphragm.</p> 	

114	Pot. 100 mm	F - RC Direction Y	-1	<p>Steel Frame/Reinforced Concrete Diaphragm.</p> 	
115	Pot. 250 mm	F - RC Direction X	+1	<p>Steel Frame/Reinforced Concrete Diaphragm.</p> 	
116	Pot. 250 mm	F - RC Direction X	-1	<p>Steel Frame/Reinforced Concrete Diaphragm.</p> 	

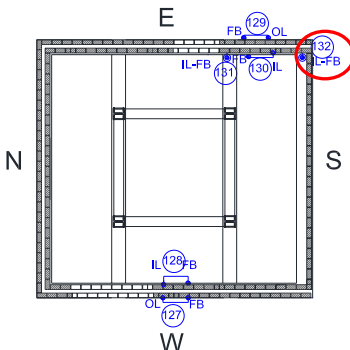

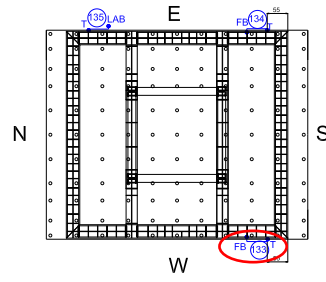

117	Pot. 100 mm	F - RC Direction Y	+1	<p>Steel Frame/Reinforced Concrete Diaphragm.</p> 	
118	Pot. 250 mm	F - RC Direction X	-1	<p>Steel Frame/Reinforced Concrete Diaphragm.</p> 	
119	Pot. 100 mm	RC - IL Direction X	+1	<p>Reinforced Concrete Diaphragm/Inner Leaf.</p> 	

120	Pot. 50 mm	RC - IL Direction Z	+1	<p>Reinforced Concrete Diaphragm/Inner Leaf.</p> 	
121	Pot. 50 mm	RC - IL Direction Z	+1	<p>Reinforced Concrete Diaphragm/Inner Leaf.</p> 	
122	Pot. 50 mm	RC - IL Direction Z	+1	<p>Reinforced Concrete Diaphragm/Inner Leaf.</p> 	

123	Pot. 50 mm	RC - IL Direction Z	+1	<p>Reinforced Concrete Diaphragm/Inner Leaf.</p> 	
124	Pot. 100 mm	IL - IL Direction X	+1	<p>Inner Leaf/Inner Leaf.</p> 	
125	Pot. 50 mm	RC - IL Direction Z	+1	<p>Reinforced Concrete Diaphragm/Inner Leaf.</p> 	

126	Pot. 100 mm	IL - IL Direction X	+1	<p>Inner Leaf/Inner Leaf.</p>	
127	Pot. 50 mm	FB - OL Direction X	-1	<p>Foundation Beam/Outer Leaf.</p>	
128	Pot. 50 mm	FB - IL Direction X	-1	<p>Foundation Beam/Inner Leaf.</p>	

129	Pot. 50 mm	FB - OL Direction X	-1	<p>Foundation Beam/Outer Leaf.</p>	
130	Pot. 50 mm	FB - IL Direction X	-1	<p>Foundation Beam/Inner Leaf.</p>	
131	Pot. 50 mm	FB - IL Direction Z	+1	<p>Foundation Beam/Inner Leaf.</p>	

132	Pot. 50 mm	FB - IL Direction Z	+1	<p>Foundation Beam/Inner Leaf.</p> 	
133	Pot. 50 mm	FB - T Direction X	+1	<p>Foundation Beam/Shaking Table.</p> 	
134	Pot. 50 mm	FB - T Direction X	+1	<p>Foundation Beam/Shaking Table.</p> 